

## Directed evolution of potassium channels for the understanding of neuronal activity including mechanisms of sleep and anaesthesia

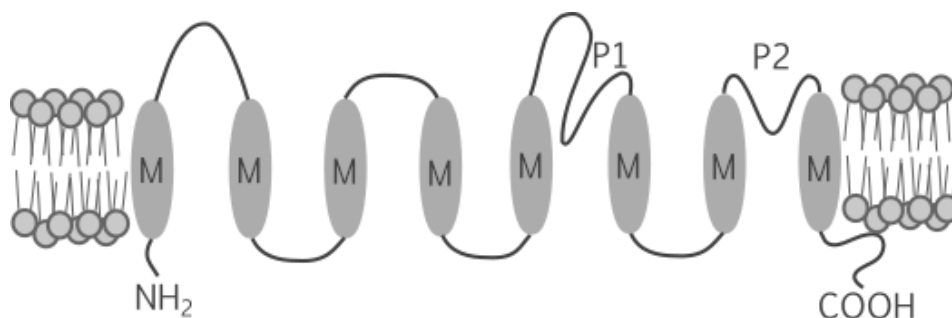
Degree level submission MPhil

Date June 2019

Author Lily Wong Le, CID 00606351

Supervisors Prof. Nick Franks & Prof. Bill Wisden

Affiliation Biophysics, Division of Cell and Molecular Biology,  
Department of Life Sciences,  
Imperial College London





## Declaration of originality

All work in this thesis was done by the named author except where appropriately referenced.

## Copyright declaration

The copyright of this thesis rests with the author. Unless otherwise indicated, its contents are licensed under a Creative Commons Attribution-Non Commercial 4.0 International Licence (CC BY-NC). Under this licence, you may copy and redistribute the material in any medium or format. You may also create and distribute modified versions of the work. This is on the condition that: you credit the author and do not use it, or any derivative works, for a commercial purpose. When reusing or sharing this work, ensure you make the licence terms clear to others by naming the licence and linking to the licence text. Where a work has been adapted, you should indicate that the work has been changed and describe those changes. Please seek permission from the copyright holder for uses of this work that are not included in this licence or permitted under UK Copyright Law.

## Word count

24,246

- excluding cover page, Declaration of originality, Copyright declaration, Abstract, Acknowledgements, Dedication, Contents, Abbreviations, figures, tables, graphs, captions, Appendix, and References.

## Abstract

Directed evolution is a technique able to modify functions on existing proteins which won the Noble Prize for Chemistry in 2018. It is based on diversifying the DNA coding sequence of the target protein, expression in a biological platform, and applying a selection pressure for screening. This is repeated for several rounds, each time generating incremental mutations directing the protein towards carrying out the desired function. Directed evolution has led to the production of molecules which have contributed to the understanding of neuronal activity underlying a range of physiological phenomena including loss of consciousness during sleep and anaesthesia. This thesis includes a short review of optogenetic tools developed by the technique including genetically-encoded calcium indicators which fluoresce upon detecting intracellular calcium ion influx and genetically-encoded voltage indicators which fluoresce upon detecting change in membrane potential of neurons. An additional short review covers the handful of metabotropic designer receptors exclusively activated by designer drugs also developed by the same technique. In an endeavour to further contribute to this field, we have conducted preliminary studies on ionotropic channels 5HT<sub>3A</sub>, and tandem two-pore potassium channels TASK3, TREK1, and TOK1 onto which directed evolution could be applied to add to this molecular toolbox. Parallel preliminary experiments, also preparing for directed evolution, investigate the binding site of halothane anaesthetic on TOK1 in order to better understand the activation mechanism of halothane on tandem two-pore potassium channels. Further work suggests experiments on TOK1 to conduct directed evolution and future perspectives for the developed molecules: a TOK1 receptor hypersensitive to halothane and a TOK1 receptor exclusively activated by Compound 21, a designer drug with no physiological targets.

## Acknowledgements

I would like to thank my supervisors Prof. Bill Wisden and Prof. Nick Franks as well as my fellow colleagues, especially Raquel Yustos and Ed Harding who have advised me on laboratory techniques. The postgraduate review panel, Dr. Geoff Baldwin Dr. Tony Southall, offered significant feedback and critique which has helped me progress on my work. I am thankful for the BBSRC for funding my time as a postgraduate student at Imperial College London.

I would also like to thank Dr. Tom Ellis and his students Robert Chen, Will Shaw, and Charlie Gilbert for donating parts of the Yeast Tool Kit and their advice on Golden Gate cloning and yeast technique. I am grateful for the Greta Stevenson Fund for enabling me to carry out a placement under the supervision of Professor Susan Ferro-Novick at the University of California San Diego to learn more thoroughly about working with *Saccharomyces cerevisiae*, and for the scientists who advised me there including Dr. Saralin Davis, Dr. Juan Wang, and Dr. Yuixin Cui. Undergraduate and Masters level students who helped to facilitate the progress of this work are: Farah Hadj-Idris, Katharina Wissmiller, Thomas Dofredo, Solweig Schumberg, and Wen Yin.

Yeast strains were also donated from Prof. Stephen Tucker of the University of Oxford and Prof. Per O Ljungdahl and his technician Kicki Ryman at the Wenner-Gren Institute. Advice on constructing airtight boxes was received from Dr. Robert Dickinson and Dr. Philip Aitken. Advice on yeast growth was offered by Dr. Luitpold Maximilian Reuter from the research group of Prof. Christian Speck. I received some microscopy training from Stephen Rothery of FILM at Imperial.

I would also like to acknowledge the support of the Life Sciences postgraduate administration office, Director of Postgraduate Studies, and the Graduate School. My work would also not have been possible without the welfare services provided at Imperial including the Chaplaincy Multi-Faith Centre, Student Counselling Service, Imperial Union Advice Centre, Imperial College Health Centre, College Tutors, and Faculty Tutor who play vital roles in supporting the welfare of students.

## Dedication

To C.M.M.

# Contents

Page  
number

<b>Abstract</b>	<b>1</b>
<b>Abbreviations</b>	<b>10</b>
<b>Chapter I: Introduction</b>	<b>11</b>
1.11 Electrophysiology reveals electrical activity of neurons	11
1.12 Genetic approaches link neuronal activity to physiological phenomena	11
Box 1.1 Understanding brain activity	12
1.2 Understanding neuronal plasma membrane protein channel activity is key to understanding neuronal activity	13
1.21 Directed evolution is a useful tool when little is known about the target protein	13
1.3 Introduction to the literature review of methods used to develop optogenetic and chemogenetic molecules	13
Box 1.3 Genetic approaches reveal sleep-wake circuits with potential therapeutic targets	14
1.31 Introduction to the development of optogenetic molecules	15
1.32 Introduction to the development of chemogenetic molecules (DREADDs)	15
1.4 An empirical case study using directed evolution to understand neural mechanisms of sleep and anaesthesia	16
1.41 Initial experiments to evolve an ionotropic DREADD were based on 5HT <sub>3A</sub>	16
1.42 The use of directed evolution to understand the action of halothane anaesthetic on potassium channels	16
1.43 Potassium channel activation contributes to loss of consciousness under halothane anaesthesia	17
1.44 TASK3 is a target of halothane	18
1.45 TREK1 is a target of halothane	18
1.46 Yeast TOK1 is related to tandem two-pore potassium channels	18
<b>Chapter II Literature Review: The use of directed evolution to develop biological molecules contributing to the understanding of neuronal activity</b>	<b>20</b>
2.1 Types of optogenetic molecules	20
Box 2.1 Lessons learned from reviewing methods used to generate optogenetic molecules	21
2.2 Methods used to develop genetically-encoded calcium indicators	23
2.21 Chameleon was the basis of the first GECI	23
2.22 Circularly permutating fluorescent proteins led to Camgaroo	23
2.23 Pericam was developed by rational design	24
2.24 GCaMP requires the modification of motifs deregulating endogenous protein function	24
2.3 Genetically-encoded calcium indicators based on FRET	26
2.31 Targeting sequence diversification was efficient for evolving Twitches	26
2.4 The use of directed evolution to develop genetically-encoded voltage indicators	27

2.41 A library of Archaelrhodopsin 3 variants were screened to develop QuasArs	27
2.42 Targeted saturation mutagenesis was efficient for evolving GRb(lue)3 and GRr(ed)3	28
2.43 Targeted saturation mutagenesis, error-prone PCR, and DNA shuffling produced FlicR1	29
2.44 Targeted saturation mutagenesis was efficient for evolving Marina	29
2.45 Automated screening allowed for unprecedented high throughput evolution of Archon1	30
2.5 The use of DREADDs and comparison to optogenetics	31
2.51 Expression and drug screening of library variants in yeast evolved HM3Dq	31
2.52 Transferring mutations discovered by directed evolution of HM3Dq led to a family of DREADDs	32
2.53 Directed evolution was unsuccessful during attempts to develop hKORD	32
Box 2.5 Lessons learned since the development of DREADDs	33
<b>Chapter III: Materials and Methods</b>	<b>34</b>
3.1 Experimental design	34
3.11 Aims	34
3.12 Objectives	34
3.13 Experimental procedure	34
3.2 Materials and Methods	36
3.21 Golden Gate Part Plasmid Cloning	36
3.22 Golden Gate cassette plasmid cloning	37
3.23 Digestion/ligation cloning	40
3.24 Colony PCR for yeast transformation-associated recombination	41
3.25 Yeast growth	41
3.26 Yeast transformations	41
3.27 Fluorescence microscopy	42
3.28 Spotting assays	42
3.29 Halothane exposure chamber	43
3.210 Yeast growth with agonists	43
3.211 Statistical Analysis	43
<b>Chapter IV: Results</b>	<b>44</b>
4.11 Understanding yeast growth rates contributes to more efficient preparation of transformations	44
4.12 Mammalian potassium channels fused to Venus-YFP at the N terminus are not translocated to the plasma membrane in $\Delta TRK1 \Delta TRK2 \Delta TOK1$ PLY246	47
4.13 An expression of 5HT <sub>3A</sub> at the plasma membrane of yeast strain $\Delta TRK1 \Delta TRK2 \Delta TOK1$ PLY246 was a false positive result	50
4.14 Mammalian potassium channels fused to Venus-YFP at the C-terminus are not translocated to the plasma membrane in $\Delta TRK1 \Delta TRK2 \Delta TOK1$ PLY246	52
4.15 Several yeast strains are unable to translocate TASK3, TREK1, and 5HT <sub>3A</sub> to the plasma membrane	53
4.16 Previous experiments expressing human TASK3 in <i>Saccharomyces cerevisiae</i> were unable to be replicated	54
4.17 TOK1:Venus-YFP is successfully translocated to the plasma membrane of <i>Saccharomyces cerevisiae</i>	55
4.18 The transexpression of TOK1 may be able to compensate for yeast potassium transporters and channel deletions	57

4.19 Arachidonic acid is able to enhance the growth of <i>Saccharomyces cerevisiae</i>	58
4.2 <i>Saccharomyces cerevisiae</i> colonies show growth variation in the presence of arachidonic acid	62
4.21 A halothane incubation chamber was set up to verify the effect of halothane gas on the growth of <i>Saccharomyces cerevisiae</i>	63
4.22 Halothane enhances the growth of a <i>Saccharomyces cerevisiae</i> strain expressing TOK1 in liquid media	65
4.23 Yeast transformation-associated recombination enables TOK1-VenusYFP fusion protein to be expressed in <i>Saccharomyces cerevisiae</i>	70
<b>Chapter V: Discussion</b>	<b>71</b>
5.1 <i>Saccharomyces cerevisiae</i> may lack proteins to translocate TASK3, TREK1, and 5HT <sub>3A</sub> to the plasma membrane	72
5.2 hTASK3 may be functional in K <sup>+</sup> -efflux but not K <sup>+</sup> -influx deficient <i>Saccharomyces cerevisiae</i> strains	75
5.3 Optimising mammalian codons for a <i>Saccharomyces cerevisiae</i> bias may not contribute to increased gene expression efficiency in yeast	76
5.4 TOK1 gene expression regulation is important to produce functional channels in <i>Saccharomyces cerevisiae</i>	76
5.5 Arachidonic acid is a known agonist of yeast TOK1 and related mammalian TREK1 channels	77
5.6 A novel halothane incubation chamber was set up to provide controlled and consistent gas exposure to yeast cultures	77
5.7 Growth responses to halothane 5 % between yeast strains, protein expression, and potassium concentration	78
5.8 Yeast-transformation associated recombination allows for the transformation, integration, and expression of TOK1-VenusYFP in a single step	79
5.9 Further work	80
5.91 How many random mutations should be introduced by error-prone PCR?	81
5.92 What size would be the mutagenetic library be?	81
5.93 Parallel designer drug selection on mutant TOK1	82
5.94 How could mutated sequences of interest be analysed?	82
5.95 Homology-based mutagenesis	83
5.96 Computer modelling and 3D crystal structure techniques	85
5.97 Establishing workflow and throughput	86
6. Future perspectives	87
6.1 Biophysical characterisation of halothane-hypersensitive TOK1 and TOK1-DREADD	87
6.2 Expression of TOK1-DREADD <i>in vivo</i>	87
6.3 Ablation of TOK1 binding site and exposure in yeast	88
<b>Summary and Conclusions</b>	<b>88</b>
<b>Appendix</b>	<b>90</b>
6.1 Channelrhodopsin-based actuators were developed using rational design	90
6.12 ChIEF	90
6.13 Step-function opsins	90
6.14 CatCh	90
6.15 Red-light activating opsins	91
6.16 Anion <sup>-</sup> -conducting rhodopsins	91
6.17 Naturally-evolved anion-conducting rhodopsins	91
Appendix 6.15 R script for ANOVA of difference in growth of R5421 in 5 K media between halothane and air after 24h	105

# Contents of Figures

	Page number
Figure 1. The anatomical location of the virus containing the DREADD injected into the median preoptic area (linked to sleep recovery) and lateral preoptic area of mice	14
Figure 2. K <sup>+</sup> influx-deficient yeast strains are able to survive in high but not low potassium media	17
Figure 3. The structure of halothane	17
Figure 4. The structure of two-pore domain potassium channels	17
Figure 5. The structure of TOK1	18
Figure 6. Schematic of directed molecular evolution using error-prone PCR and growth screening	19
Figure 7. Schematic of directed molecular evolution steps	22
Figure 8. The main structure of Yeast Tool Kit generated cassette plasmids	35
Figure 9. Cassette entry vector with part 234 dropout.	38
Figure 10. N-terminus VenusYFP and mammalian channel fusions transformed into PLY246 did not translocate to the membrane	47
Figure 11. Venus-YFP and potassium channel fusions with plasma membrane targeting parts form inclusion bodies in PLY246 rather than embed in the plasma membrane	48
Figure 12. PLY246 N-terminus fusion transformations streaked on agar plates with different concentrations of K <sup>+</sup>	49
Figure 13. Decreasing the expression level of VenusYFP:TASK3 under regulation of promoter pPSP2 does not induce the translocation of the protein fusion to the plasma membrane	50
Figure 14. The expression of Venus-YFP:5HT3A under the regulation of promoter pTEF1 and terminator tADH1 initially showed expression at the plasma membrane and growth on low potassium media	50
Figure 15. Western blot of yeast transformed with different plasmid constructs shows little protein expression	51
Figure 16. C-terminus potassium channel and Venus-YFP and fusions form inclusion bodies PLY246	52
Figure 17. Fusing the mating factor alpha signalling sequence to channel:VenusYFP does not induce translocation of the protein fusion to the plasma membrane	52
Figure 18. Mammalian channels fused to Venus-YFP are unable to be translocated to the plasma membrane of <i>S. cerevisiae</i>	53

Figure 19. Growth assays of transformed yeast conducted parallel to expression observation experiments	53
Figure 20. hTASK3:VenusYFP is not translocated to the plasma membrane in SGY1528 or PLY246 under regulation of pMET promoter in plasmid pYES2	54
Figure 21. Expression of TOK1:VenusYFP under different promoters in <i>S. cerevisiae</i>	56
Figure 22. Growth assays of yeast transformed with TOK1 under the regulation of different promoters.	57
Figure 23a-c. Yeast strains with compromised K <sup>+</sup> influx systems were spotted on agar with or without arachidonic acid	59
Figure 24. An airtight, temperature controlled system to incubate yeast samples in the presence of halothane	63
Figure 25. Yeast strains with compromised K <sup>+</sup> influx systems were spotted on agar and grown in halothane 5 % or air	65
Figure 26. Genomic expression of TOK1-VenusYFP in <i>Saccharomyces cerevisiae</i> strains with compromised K <sup>+</sup> -influx systems	70
Figure 27. The process of autophagy in yeast	72
Figure 28. A phylogenetic tree illustrating the relatedness of tandem two-pore domain potassium channels.	73
Figure 29. Proteins involved in the translocation of TASK3 or TREK1 to the plasma membrane in mammals	74
Figure 30. B31 yeast strain lacking a K <sup>+</sup> efflux system survives in high and low external K <sup>+</sup> concentrations	75
Figure 31. Combining BLAST alignments of TOK1, TASK3, and TREK1 peptide sequences shows a stretch of overlapping homology	83
Figure 32a. Residues 257-439 of TASK3 align with residues 80-242 of TOK1	83
Figure 32b. Residues 405-475 of TREK1 align with residues 137-207 of TOK1	84
Figure 32c. Residues 1-292 of TASK3 align with residues 53-349 of TREK1	84
Appendix 6.2. Venus-YFP and potassium channel fusions with plasma membrane targeting parts are not targeted to the plasma membrane in PLY246	92
Appendix 6.3. C-terminus potassium channel and Venus-YFP and fusions form inclusion bodies PLY246	93
Appendix 6.4. Fusing the mating factor alpha signalling sequence to channel:VenusYFP fusions does not induce translocation of the protein fusion to the plasma membrane	93
Appendix 6.5. Mammalian channels fused to Venus-YFP are unable to be translocated to the plasma membrane of <i>S. cerevisiae</i>	94

# Contents of Graphs

Page  
number

Graph 1. Expression strength of promoters and selected terminators used	35
Graph 2a. Growth graphs of PLY246 (-TOK1, -TRK1, -TRK2) at different starting ODs	44
Graph 2b. Growth graphs of SGY1528 (-TRK1, -TRK2) at different starting ODs	45
Graph 2c. Growth graphs of R5421 (-TRK1, -TRK2) at different starting ODs	45
Graph 2d. Natural log of OD600 readings of PLY246 (-TOK1, -TRK1, -TRK2), SGY1528 (-TRK1, -TRK2), and R5421 (-TRK1, -TRK2) lag	46
Graph 3. The frequency of yeast colonies with enhanced growth on 0.5 mM K <sup>+</sup> with arachidonic acid	62
Graph 4. Velocity of air flow though the halothane vapouriser and flow meter are equivalent indicating an airtight system	64
Graph 5. Calibration of the percentage release of halothane gas by the vapouriser using an anaesthetics monitor	64
Graph 6a. Higher growth was observed in R5421 (-TRK1, -TRK2) transformed with an empty vector than TOK1 or TRK1, at 5 mM K <sup>+</sup> , in halothane 5 % compared to air after 24 h	67
Graph 6b. Higher growth was observed in SGY1528 (-TRK1, -TRK2) transformed with TOK1 than an empty vector or TRK1, at 1- and 2-mM K <sup>+</sup> , in halothane 5 % compared to air after 24 h	67
Graph 6c. PLY246 (-TOK1, -TRK1, -TRK2) does not display distinctive growth trends in halothane 5 % compared to air after 24 h	68
Graph 7a. R5421 (-TRK1, -TRK2) does not display distinctive growth trends in halothane 5 % compared to air after 48 h	68
Graph 7b. SGY1528 (-TRK1, -TRK2) does not display distinctive growth trends in halothane 5 % compared to air after 48 h	69
Graph 7c. PLY246 (TOK1, -TRK1, -TRK2) does not display distinctive growth trends in halothane 5 % compared to air after 48 h	69
Appendix 6.11. Average fold-increase in yeast growth in air and halothane after 24 h.	101
Appendix 6.12. Average difference in fold-increase of yeast growth in air and halothane after 24 h	102
Appendix 6.13. Average fold-increase in yeast growth in air and halothane after 48 h	103
Appendix 6.14. Average difference in fold-increase of yeast growth in air and halothane after 48 h	104

# Contents of Tables

	Page number
Table 1. Channel ORF parts generated for Golden Gate cloning using the Yeast Tool Kit	36
Table 2. Cassette plasmids constructed using Yeast Tool Kit parts using the Golden Gate cloning	38
Table 3. <i>Saccharomyces cerevisiae</i> yeast strains used	41
Table 4. Cassette plasmids of N-terminus Venus-YFP and mammalian channel fusions.	47
Table 5. Cassette plasmids of Venus-YFP and mammalian channel fusions with membrane targeting parts	48
Table 6. Venus-YFP:TASK3 fusion cassette plasmids regulated by lower strength expression promoters	49
Table 7. Expression phenotypes of <i>S. cerevisiae</i> strains transformed with TOK1:VenusYFP under two promoters.	55
Table 8. Raw count of yeast colonies displaying enhanced growth on 0.5 and 100 mM K <sup>+</sup> agar in the presence of halothane 5 % compared to air	66
Table 9. Summary of the phenotypes resulting from expression of TOK1 under regulation of different promoters and in different yeast strains	76
Table 10. Parameters as conducted by Armbruster <i>et al.</i> (2007) on the human muscarinic acetylcholine channel 3 (HM3) and Piatkevich <i>et al.</i> (2018) to produce Archon1	81
Table 11. Challenges to the project and how they could be mitigated.	81
Appendix 6.6. Raw count of yeast colonies displaying enhanced growth on 0.5 mM K <sup>+</sup> agar in the presence of 100-300 $\mu$ M arachidonic acid (compared to ethanol vehicle)	96
Appendix 6.7 Raw count of yeast colonies displaying enhanced growth on 100 mM K <sup>+</sup> agar in the presence of 300 $\mu$ M arachidonic acid compared to ethanol vehicle	96
Appendix 6.8 Chi-squared calculations of yeast colonies displaying enhanced growth on 0.5 mM K <sup>+</sup> agar in the presence of 100-300 $\mu$ M arachidonic acid compared to ethanol vehicle.	96
Appendix 6.9. Yeast growth OD600, air 100 %.	97
Appendix 6.10. Yeast growth OD600, halothane 5 %.	99

# Abbreviations

ARC: arcuate nucleus  
ATP: Adenosine triphosphate  
CaM: calmodulin-M13  
ChR: channelrhodopsin  
CiVSD: *Ciona intestinalis* voltage sensing domain  
CNO: clozapine-N-oxide  
cpGFP: circularly permuted green fluorescent protein  
cpRFP: circularly permuted red fluorescent protein  
cpYFP: circularly permuted yellow fluorescent protein  
DREADDs: designer receptors exclusively activated by designer drugs  
eCFP: Enhanced cyan fluorescent protein  
eGFP: enhanced green fluorescent protein  
eYFP: enhanced yellow fluorescent protein  
5-FOA: 5-Fluoroorotic Acid  
GABA: gamma-Aminobutyric acid  
GECI: genetically-encoded calcium indicator  
GEVI: genetically-encoded voltage indicator  
HEK293T: human embryonic 293 cells expressing SV40 large T antigen  
IP: intraperitoneal  
KORD: kappa-opioid receptor DREADD  
FP: fluorescent proteins  
FRET: fluorescent energy transfer  
GFP: green fluorescent protein  
GPCRs: G-protein coupled receptors  
GR: *Gloeobacter violaceus* rhodopsin  
hM3Dq: human muscarinic 3 designer receptor q  
K<sub>2</sub>Ps: tandem two-pore domain potassium channels  
LPO: lateral preoptic area  
M3: muscarinic 3 receptor  
MnPO: median preoptic area  
PVH: paraventricular hypothalamus  
PZ: parafacial zone  
NREM: non-rapid eye movement  
REM: rapid eye movement  
SALB: Salvinorin B  
*S. cerevisiae*: *Saccharomyces cerevisiae*  
SN: substantia nigra  
SWS: slow wave sleep  
TAR: transformation-associated recombination  
TnC: troponin C  
VP: ventral pallidum  
VTA: ventral tegmental area  
WT: wildtype  
YPD: yeast peptone dextrose (media)

# Chapter I: Introduction

The brain is currently the most sophisticated system in the universe. It is the vocation for neuroscientists to collectively contribute to the understanding of the brain's activity, including its control of physiological phenomena. Some of these are conscious, such as feeding and eating, reward-seeking, and movement. Others may be more homeostatic and include temperature regulation, water regulation, and sleep. Specific neurons fire in unique rhythms to regulate such phenomena (Box 1.1). Scientists are aiming to identify links between neuronal sub-populations within brain regions and circuits, and the temporal nature of their electrical activity, with observed physiological and behavioural changes. This thesis proposes the use of directed evolution of potassium channels to make a humble contribution towards the greater endeavour of understanding mechanisms of the brain, particularly for sleep and anaesthesia.

## 1.11 Electrophysiology reveals electrical activity of neurons

Electrophysiology has been traditionally used to understand electrical activity of neurons. To uncover how ions influx and efflux neurons such analysis can be done on brain slice preparations or on cultured neurons (Dingledine *et al.*, 1980). Though allowing high experimental control over the variables affecting the cells and synapses under study (Accardi *et al.*, 2016), *ex vivo* or *in vitro* techniques are unable to provide real-time information linking cause and phenotypic effect. *In vivo* live recordings can be made but intracellular electrodes can be difficult to set up and invasive on the animal model (The Journal of Neuroscience, 2018). Less invasive electrodes are used with techniques such as electroencephalography and electromyography which are often used to monitor loss of consciousness, but do not provide resolution on a cellular scale within the protocol. Correlating recorded neuronal activity with observed behaviour is also unable to provide causal information about brain activity and physiological phenomena.

## 1.12 Genetic approaches link neuronal activity to physiological phenomena

Recent genetic approaches have been enabled scientists to conduct more causal investigations, linking activity of specific neuronal sub-populations and physiological phenomena, by directly modulating neuronal circuitry. Genetically-encoded receptors engineered to be exclusively activated by light or drugs can be expressed in target neuronal sub-populations. Regulating the activation of these receptors modulates the electrochemical potential of neurons and leads to behavioural change. Optogenetics is a technique which includes using genetically-encoded proteins which fluoresce upon detection of an action potential, or channels which can induce neuronal activation / inhibition by shining the appropriate wavelength of light (Fenno *et al.*, 2011). However, optogenetics requires sophisticated equipment and can be invasive. In the field of chemogenetics, designer receptors exclusively activated by designer drugs (DREADDs) do not require such invasive equipment, as these genetically-encoded receptors are activated by drugs with no other physiological targets. However, the most widely used DREADDs are based on G-protein coupled receptors (GPCRs) which, aside from triggering neuronal activation or inhibition, lead to secondary signalling cascades (Armbruster *et al.*, 2007) with longer term unmitigable, immeasurable effects. An ideal DREADD would be ionotropic to increase the certainty that ion transport through the DREADD inducing neuronal activity causes observed phenotypes, and the phenomenon would not be influenced by long-term secondary effects.

This thesis reviews some methods used to develop genetically-encoded tools for elucidating neuronal circuitry, focussing on the technique of directed evolution (Chapter 2). Directed evolution is useful when little is known about the protein being engineered. Lessons learned from the review provide context for future experimental direction in this field. A case study investigating techniques to develop an ionotropic DREADD is used to illustrate this empirically (Chapters 3-5). Preliminary experiments are also performed on an ionotropic channel activated by halothane anaesthetic to understand its binding mechanism. Using the single technique of directed evolution on a set of two parallel experimental studies, the development of a DREADD and elucidation of halothane binding on target channels, could contribute to the understanding of neuronal mechanisms of sleep and anaesthesia.

## Box 1.1 Understanding brain activity

On a molecular level, neuronal depolarisation (intracellular positive charge, primed to conduct an action potential; Hodgkin & Huxley, 1952) or hyperpolarisation (intracellular negative charge, unable to conduct an action potential) are regulated by the opening or closing of ion channels. At resting potential three  $\text{Na}^+$  ions are pumped out the cell for every two  $\text{K}^+$  transported in to maintain a resting membrane potential of about -70 mV (Hodgkin & Huxley 1945). Hyperpolarisation can also be caused by potassium channels opening, allowing  $\text{K}^+$  to flow down its electrochemical gradient out of the cell and lowering the intracellular potential (Mochida, 1990). As a result, to better understand physiological phenomena controlled by the brain, it would be ideal to map patterns of hyperpolarisation and depolarisation on a sub-neuronal level across the brain and over time.

### Neurotransmitters affect neuronal activity

Depolarisation and hyperpolarisation are can be induced following releases of neurotransmitters into synapses between neurons. Activating ionotropic receptors induces immediate effects on target neurons as they open and ions traverse the plasma membrane, changing the electrochemical properties of the cell. Longer term changes lasting over hours to weeks follow the activation of metabotropic receptors coupled to G-proteins. Glutamate is the major excitatory neurotransmitter and binds primarily to cation ionotropic receptors AMPA (Honoré *et al.*, 1982; Hollmann & Heineman, 1994; Reiner and Levitz, 2018). Following AMPA-mediated depolarisation, NMDA receptors change conformation and allow further cation influx to reach the threshold for action potential conduction. Glutamate can also activate target GPCRs. GABA is the main inhibitory neurotransmitter (leading to hyperpolarisation; Curtis *et al.*, 1970). GABA also binds to ionotropic  $\text{Cl}^-$ -permeable ( $\text{GABA}_A$ ; Zhu *et al.*, 2018) and metabotropic receptors ( $\text{GABA}_B$ , leading to  $\text{K}^+$  influx; Frangaj & Fan, 2018). Acetylcholine activates different types of muscarinic metabotropic receptors which conduct cations and anions (Dale, 1914). Acetylcholine also binds to nicotinic ionotropic receptors which allow cation transduction (Colquhoun *et al.*, 1979).

## 1.2 Understanding neuronal plasma membrane protein channel activity is key to understanding neuronal activity

To understand mechanisms of neuronal channel and receptor function, they can be mutated and applied to ways. Ideally, understanding the contribution of amino acids to molecular mechanisms of activation, opening and closing, form a good baseline for modification. Crystal structures may allow for structure-guided mutagenesis or scanning against a database of related proteins to identify conserved motifs. If such structures are not available for target molecules, a more randomised protocol may allow for the generation of receptors or channels with desired characteristics.

### 1.21 Directed evolution is a useful tool when little is known about the target protein

Directed evolution is a process which won Frances Arnold the Nobel Prize for Chemistry in 2018 (Chen & Arnold, 1993). Its ingenuity lies in the ability to emulate molecular evolution on a significantly shorter timescale and towards a desirable phenotype. To do this a protein's DNA sequence is randomly mutated to a defined level of diversification to generate a large library of variants. Following expression, such as in a simple living platform (phage, bacterial, yeast, cell culture), a specified selection pressure is applied, and mass screening is conducted to identify incremental changes related to the desired function. This is repeated several times until the desired function is evolved from these incremental residue changes developed at each generation of library diversification and screening (Arnold, 2018). Directed evolution requires little prior knowledge of structure or molecular mechanism of a protein and can be conducted on several types including enzymes as well as receptors and channels (Cobb *et al.*, 2013). The industrial application of directed evolution has allowed for the production and widespread application of significant molecules.

In neuroscience, lineages of receptors which have been continually mutated by directed evolution or rational design; build and continuously improve on inherited characteristics such as the wavelength of activating light, specificity of ligand binding, opening and closing speed, and length of inactivation state (Lin, 2010). Although directed evolution prescribes a mutagenesis and selection method, these molecular phylogenies demonstrate the process of evolution stemming from a wildtype (WT) ancestor molecule and have also sometimes validated the research theme as a “fast-forward” of natural evolution, where laboratory-evolved characteristics were later found in other species in nature from *de novo* sequencing (Berndt *et al.*, 2014).

This thesis covers a short literature review of the most widely used and cited neuronal receptors found in these laboratory-evolved receptor phylogenies and an empirical case study using directed evolution to develop molecules to better understand neuronal mechanisms of sleep and anaesthesia.

## 1.3 Introduction to the literature review of methods used to develop optogenetic and chemogenetic molecules

Chapter Two reviews methods used to engineer optogenetic and chemogenetic molecules which could be used to analyse neuronal activity. Optogenetic actuators were initially based on Channelrhodopsin-1 and -2 (ChR-1 and-2) from the green alga *Chlamydomonas reinhardtii* where absorbed photons change receptor conformation to pump ions across the membrane (Sineshchekov *et al.*, 2002; Nagel *et al.*, 2003; Suzuki *et al.*, 2003).

### Box 1.3 Genetic approaches reveal sleep-wake circuits with potential therapeutic targets

The use of optogenetic and chemogenetic tools have become widespread in neuroscience labs across the world. Currently in mid-2019, searching for *optogenetics* and *sleep* in *Google Scholar* provides over 7000 search results. For context, probably the first use of ChR2 on a sleep-related circuit was for the activation of hypocretin (orexin)-producing neurons *in vivo* which increased probability of waking (Adamantidis *et al.*, 2007). Loss of hypocretin is linked to narcolepsy, and therefore the finding had clinical significance. Venner *et al.* (2019) have reviewed sleep-wake circuits revealed using optogenetics or chemogenetics, which may be potential therapeutic targets.

#### Drugs could target parafacial zone GABAergic neurons to promote slow wave sleep

For slow wave sleep (SWS; the deepest stage of non-rapid eye movement; NREM sleep), neural circuits in many brain regions have been shown to play a part, with the parafacial zone (PZ) GABAergic neurons in the brainstem contributing to SWS induction and maintenance. The activator DREADD was hM3Dq expressed and activated by clozapine-N-oxide (CNO) in these neurons, causing mice to fall asleep and display SWS which increased in length due to this activation compared to non-hM3Dq expressing mice (Anacleit *et al.*, 2017). Activating genetic tools not only modulates activity of their host neurons, but also leads to downstream impact on projected areas. PZ GABAergic neurons project to the parabrachial accumbens and are likely to suppress them to induce sleep, revealing information about neural circuitry. This could be a target region for sleep-promoting drugs, as current GABAergic drugs target the global GABA system (Venner *et al.*, 2019).

#### Dopaminergic VTA neurons may contribute to sleep-wake and psychiatric disorders

The traditional sleep-wake paradigm placed the dopaminergic neurons of the ventral tegmental area (VTA) as not being involved in sleep but a study expressing the genetically-encoded calcium indicator GCaMP6f into the dopaminergic VTA neurons with an implanted fibre optic cable (for light excitation and fluorescence detection) revealed that the fluorescence signal and calcium transients were lower during NREM sleep than wake or REM (rapid eye movement) sleep. Expressing and activating ChR2 in the same neurons induced wakefulness, even following sleep deprivation. Stimulating dopaminergic VTA neurons which project into the nucleus accumbens, but not other types of neuronal projections, led to maintained wakefulness. This suggests that these neurons do change their activity across sleep-wake states, which was previously not within the paradigm. (Eban-Rothschild *et al.*, 2016). Altered VTA neuronal activity and sleep-wake disturbance in psychiatric disorders (Nestler & Carlezon, 2006) may point to it being key in developing therapies.

#### Neuronal activity underlying loss of consciousness differs between recovery sleep and dexmedetomidine anaesthesia

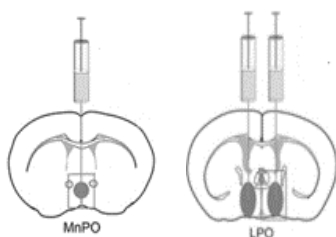


Figure 1. The anatomical location of the virus containing the DREADD injected into the median preoptic area (linked to sleep recovery) and lateral preoptic area of mice (linked to sleep recovery and dexmedetomidine anaesthesia; adapted from Zhang *et al.*, 2015).

In the Franks and Wisden lab, optogenetics and DREADDs are used to understand neuronal circuitry underlying loss of consciousness during sleep and anaesthesia. Neural mechanisms of many clinically-administered anaesthetics are still not completely understood. Zhang *et al.* (2015) showed that expressing and activating hM3Dq in the median preoptic area (MnPO) in the brain is linked to recovery sleep following sleep deprivation, whereas activity in a nearby region, the lateral preoptic area (LPO), is linked to the same phenomenon in addition to loss of consciousness under dexmedetomidine anaesthesia (Figure 1). This was done by controlling expression of the DREADD under the promoter of the immediate early gene *c-fos*, which is expressed when neurons depolarise. In anaesthetised mice, LPO neurons depolarised which led to them being tagged with DREADDs. In sleep-deprived animals, the same occurred in LPO and MnPO neurons. Following this, activating the DREADD by its CNO induced action potentials in the same neurons that had previously depolarised, recapitulating loss of consciousness phenotypes in each experimental group.

### 1.31 Introduction to the development of optogenetic molecules

Optogenetic molecules for reporting neuronal activity were based on endogenous proteins uniting flanking fluorescent protein domains upon  $\text{Ca}^{2+}$  binding, to relay increases in intracellular calcium (Miyawaki *et al.*, 1997). Modifications were also engineered by design to remove dysregulated interactions with original target proteins (Yang *et al.*, 2018). Capturing membrane voltage through a fluorescent output was developed to improve on using intracellular  $\text{Ca}^{2+}$  as a proxy. However the influx of other cations also contributes to depolarisation and increasing intracellular  $\text{Ca}^{2+}$  does not necessarily lead to action potentials. Improving the fluorescent signals of indicators contributed to increasing signal-to-noise ratio during observation and recording of neuronal activity (Hochbaum *et al.*, 2014). Initial problems included fidelity of fluorescence with membrane voltage changes, and decreasing fluorescence output with  $\text{Ca}^{2+}$  or voltage increases (Nagai *et al.*, 2001).

Decreasing desensitisation to light whilst increasing sensitivity to lower light levels reduced the bleaching of fluorescent indicators (Platisa *et al.*, 2017). Some experiments were able to simultaneously express actuators and indicators in different neuronal populations to control neuronal activity and record it. However, activating light spectra can overlap between indicators and actuators which directed evolution cannot always resolve, and makes it quite difficult to use them *in vivo* (Abdelfattah *et al.*, 2016).

Some parameters improved whilst minimising worsening of others alongside deleterious effects on cellular health; for example, sometimes exogenous expression of mutated proteins led to intracellular aggregation. For several constructs certain regions were repeatedly found to be important to function and sometimes transferring mutation of the same residue to other sequences conferred the same change in function (Engqvist *et al.*, 2015). High throughput and multi-parameter selection were demonstrated using robotic methods and may point to a possible future direction for the method (Piatkevich *et al.*, 2018).

### 1.32 Introduction to the development of chemogenetic molecules (DREADDs)

The most widely used DREADDs are engineered from GPCRs (with roles in regulating neuronal activity) to become inert to physiological agonists (Armbruster *et al.*, 2007). DREADD-activating drugs are designed to have no endogenous targets. Like optogenetic tools, DREADDs can be used to modulate spatiotemporal neuronal activity to be correlated with observed phenotypes. Studies investigating the use of DREADD and optogenetic tools on the same neuronal populations identified equivalent effects on physiological readouts with a longer duration from DREADDs (Roth, 2016). Indeed, optogenetic tools enable millisecond precision of channel activation lasting up to seconds, whilst drug activation depends on time taken for metabolism and receptor desensitisation or internalisation and downregulation effects. DREADDs are also less invasive and require less equipment as designer drugs can be delivered orally with food or via intraperitoneal (IP) injection.

High throughput protein modification is becoming increasingly efficient and targeted. Protein engineering methods usually express target proteins in an easy-to-use system. As optogenetic molecules were mainly derived from lower phylogenetic species (such as algae, *Chlamydomonas sp.*, *Volvox carteri*.) they were suitable for expression in *E. coli* platforms (Berndt *et al.*, 2011; Yizhar *et al.*, 2011) DREADDs based on eukaryotic constructs were more appropriately expressed and selected for in *Saccharomyces cerevisiae* yeast that perform some post-translational modifications (Armbruster *et al.*, 2007).

In contrast to lineages of optogenetic molecules, a handful of DREADDs have been sufficient for widespread use *in vivo*. DREADDs use the same receptor signalling pathways as the original metabotropic receptors which they were engineered from. Therefore, it was unnecessary to make multiparameter modifications to channel opening/closing or ion conductance. However, there was a need to direct evolution towards specific ligand binding without modifying other characteristics or induce intracellular protein aggregation (Armbruster *et al.*, 2007).

Metabotropic DREADD activation leads to secondary signalling cascades with longer term unmitigable and immeasurable effects. An ideal DREADD would be ionotropic to increase the certainty that ion transport through the DREADD inducing neuronal activity causes observed phenotypes, and the phenomenon would not be influenced by long-term secondary effects.

## 1.4 An empirical case study using directed evolution to understand neuronal mechanisms of sleep and anaesthesia

As it is impossible to distinguish individual consequences downstream of secondary intracellular signalling cascades, physiological effects result from integrated receptor activity. Optogenetic techniques require the insertion of LEDs into animals, which make them invasive and require more sophisticated equipment to for *in vivo* experiments. As the ionotropic DREADDs engineered so far are formed of heteromeric subunits (Magnus *et al.*, 2011), the certitude of homomeric receptor dimerisation and the ion species conducted is excluded.

**1.41 Initial experiments to evolve an ionotropic DREADD were based on 5-HT<sub>3A</sub>**  
To overcome such limitations, we aimed to subject the homopentameric 5-HT<sub>3A</sub> receptor to directed evolution in order to be exclusively activated by clozapine-N-oxide (CNO). 5-HT<sub>3A</sub> was initially chosen as it was the ionotropic receptor with the highest affinity to the related drug clozapine, although this affinity was insignificant (Roth & Driscoll, 2014). CNO has been revealed since preliminary experiments to convert to clozapine and cross the blood-brain barrier to affect target proteins, and so could be changed to Compound 21 (Jendryka, 2019) which can activate the same binding sites. However, we were unable to direct 5-HT<sub>3A</sub> to the plasma membrane of our chosen model organism, *S. cerevisiae* and therefore considered using the endogenous yeast channel TOK1 as an alternative.

### 1.42 The use of directed evolution to understand the action of halothane anaesthetic on potassium channels

In addition to understanding the spatiotemporal activity of neuronal circuitry underlying loss of consciousness during anaesthesia regulated by DREADD gating, we designed parallel experiments using the same random mutagenesis methods but using halothane as a selection pressure in order to elucidate the mechanism of volatile anaesthetic action on receptors.

To do this we exploited *Saccharomyces cerevisiae* strains with genes contributing to the K<sup>+</sup> influx system which are deleted. The yeast survive only in high potassium media. By expressing channels of interest, we attempted to verify whether recombinant channels could complement deletions so that yeast can survive in low potassium media (Figure 2). Rescuing this phenotype would allow for the mutation of channel sequences and ensuing selection for channels that only open upon the application of specific agonists in low potassium media, whilst cells expressing non-activated mutant channels would be killed in such conditions.

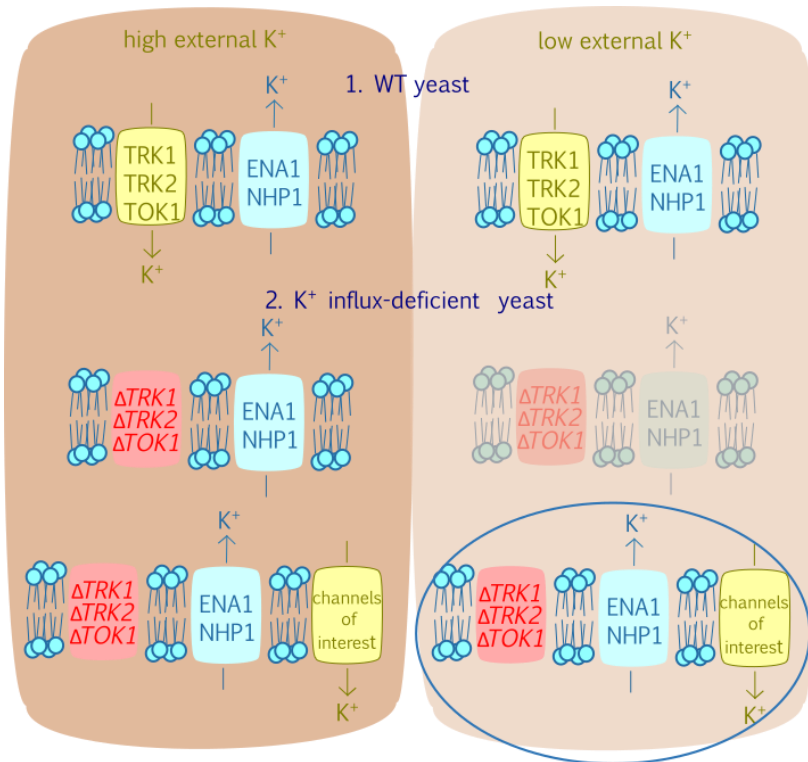


Figure 2. K<sup>+</sup> influx-deficient yeast strains are able to survive in high but not low potassium media. We attempt to overcome this by expressing potassium channels to identify whether they can allow such strains to survive in low potassium media (circled in blue; faded schematics represent cells' inability to survive).

### 1.43 Potassium channel activation contributes to loss of consciousness under halothane anaesthesia

Halothane is a volatile anaesthetic which is inhaled to induce loss of consciousness (Figure 3). It was introduced in 1951 and dominated anaesthetic practice for two decades. Its use has mostly been discontinued in developed countries due to deleterious effects on the heart and liver via local K<sup>+</sup> channels (O'Donnell, 2012). Despite this, the drug remains on the World Health Organisation Model List of Essential Medicines and is widely used in lower income countries (WHO, 2015). Consequently, understanding halothane mode of action on K<sub>2</sub>P<sub>s</sub> remains as important as ever.

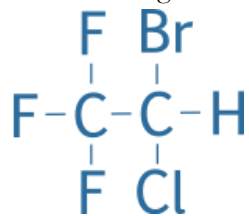


Figure 3. The structure of halothane

The significant role of K<sub>2</sub>P activation in halothane anaesthesia during loss of consciousness has been demonstrated using potassium channel knockout mice. Behavioural manifestations of WT mice under halogenated anaesthetics include decreased locomotion, loss of righting reflex (correction of the orientation of the body onto four limbs when rodents are placed on their back), and loss of limb withdrawal under the induction of pain. In contrast, K<sub>2</sub>P knockout mice display a reduction in these measured anaesthetic endpoints (Steinberg *et al.*, 2015).

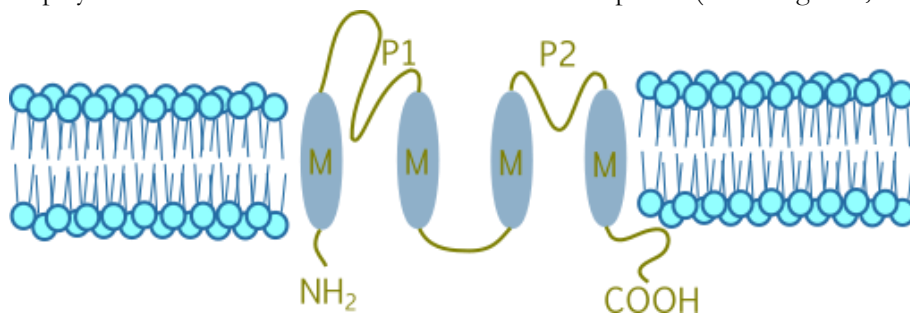


Figure 4. The structure of two-pore domain potassium channels

Mammalian tandem two-pore domain potassium channels are named as such because each subunit is comprised of two P (K<sup>+</sup> sensitive) domains each sandwiched between two M (transmembrane) domains producing a structure of MP<sub>1</sub>M–MP<sub>2</sub>M (Figure 4). Two of these are arranged in tandem to form a functional channel (Kollewe *et al.*, 2009). They contribute to the background membrane conductance of neurons.

Our efforts to understand the mechanism of halothane activation on K<sub>2</sub>Ps were initially focused on two human channels, and progressed onto studying a homologous yeast channel.

#### 1.44 TASK3 is a target of halothane

In mammals, TASK3 is expressed across the brain rather than in solely one or a few regions (Karschin *et al.*, 2001). Like other K<sub>2</sub>P knockout mice, TASK3 knockout animals show decreased loss of consciousness endpoints following exposure to volatile anaesthetics. Little is known about the molecular mechanism underlying this, but amino acid 159 located on the intracellular side of the transmembrane domain 3 (Andres-Enguix *et al.*, 2007; Conway & Cotten, 2012) and a six-amino-acid region between transmembrane domain 4 and the C-terminus (Talley & Bayliss, 2002; Andres-Enguix *et al.*, 2007; Veale *et al.*, 2007) are required for TASK channel activation by halogenated anaesthetics.

#### 1.45 TREK1 is a target of halothane

TREK1 is opened by several stimuli including stretch, heat, intracellular acidosis, depolarisation, lipids and volatile general anaesthetics, and is closed by protein kinase A and protein kinase C phosphorylation pathways. It is also tonically inhibited by the actin cytoskeleton (Honoré, 2007). As with other K<sub>2</sub>P genes, TREK1 knockout mice show decreased loss of righting reflex. Similar to TASK3, only certain parts of the TREK1 channel are known to be indispensable for volatile anaesthetic effects. These include amino acid 306 (Gruss *et al.*, 2004) and a stretch of the C-terminal domain (Patel *et al.*, 1999). These sections of TASK3 and TREK1 halothane activation could be a starting point to specify the exact binding and activation sites of the anaesthetic.

#### 1.46 Yeast TOK1 is related to tandem two-pore potassium channels

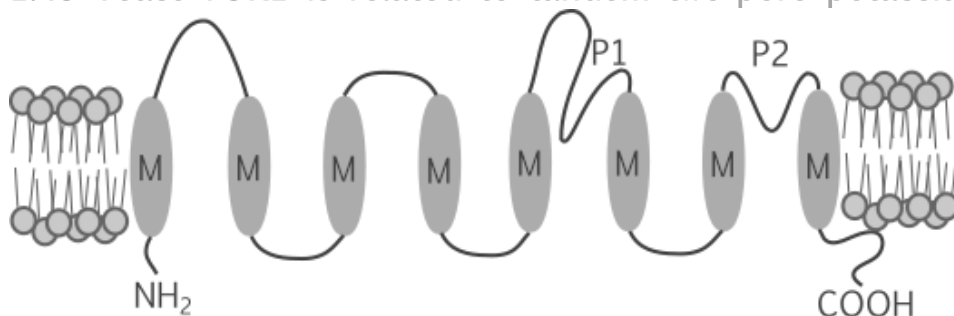
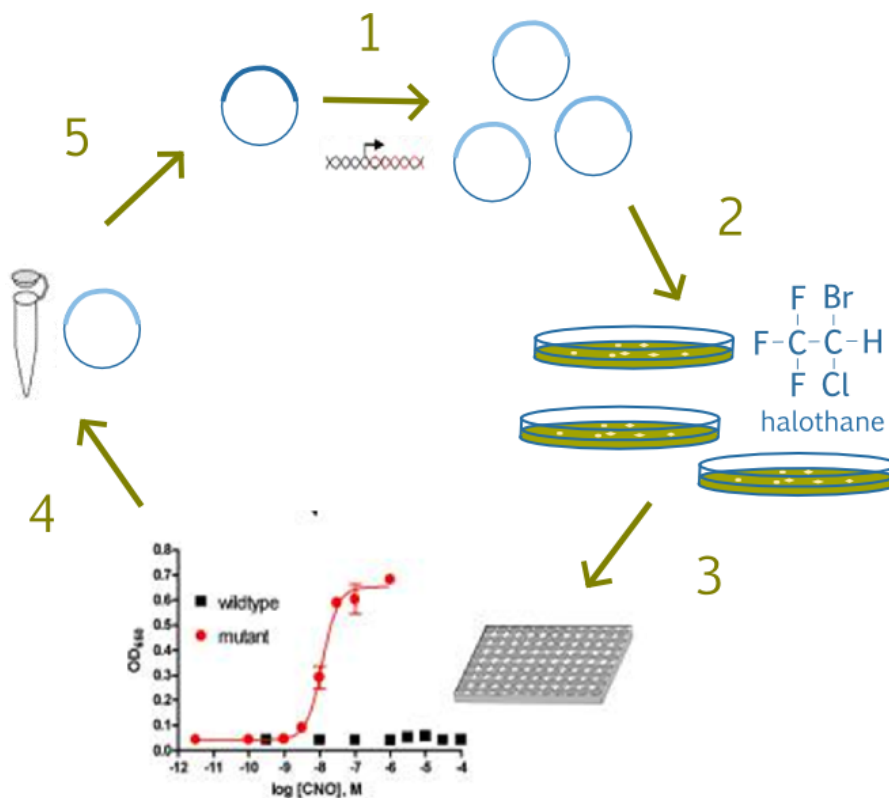


Figure 5. The structure of TOK1

TOK1 is a yeast tandem two-pore potassium channel, but unlike mammalian channels each subunit is comprised of eight transmembrane segments (MMMM–MP<sub>1</sub>M–MP<sub>2</sub>M, Figure 5; Saldaña *et al.*, 2001). As an evolutionary predecessor to mammalian K<sub>2</sub>Ps, it is possible that the four upstream transmembrane segments were lost to leave the mammalian homologues. Indeed, the K<sup>+</sup>-selective region of the P domains remain conserved through evolution (Jiang *et al.*, 2002). Past research has shown that, like other K<sub>2</sub>Ps, TOK1 is also activated by halothane. *Xenopus* oocytes recombinantly expressing the channel demonstrated an influx of K<sup>+</sup> upon exposure to the anaesthetic (Gray *et al.*, 1998). Due to this, we decided to use TOK1 as a model for halothane activation of K<sub>2</sub>Ps as it is endogenously expressed in *Saccharomyces cerevisiae*, rendering the processes of transcription/translation and plasma membrane translocation more straightforward than modifying mammalian K<sub>2</sub>Ps or the cellular environment to achieve recombinant functional mammalian channel function.

In efforts to generate a DREADD in parallel to halothane experiments, and cloning many constructs to express and direct 5-HT<sub>3A</sub> to the plasma membrane of our chosen model organism *S. cerevisiae*, we considered also using the ionotropic TOK1 as an alternative to generate a hyperpolarising DREADD (Figure 6).

Future experiments would involve validating the effect of halothane on WT TOK1 when overexpressed in yeast with modified K<sup>+</sup> influx systems. We also explore ways for establishing a workflow to achieve a high throughput iterative directed evolution method and future perspectives upon the development of a TOK1-DREADD or identification of halothane binding on TOK1 and related K<sub>2</sub>Ps.



**Figure 6.** Schematic of directed molecular evolution using error-prone PCR and growth screening (adapted from Armbruster *et al.*, 2007).

1. Reading frames randomly mutated using low-fidelity PCR
2. Mutation libraries transformed into yeast and exposed to agonists / control conditions in low potassium conditions
3. Growth rate measured to ascertain whether potassium channels are activated to allow cells to survive
4. Yeast with high growth rates only in the presence of the agonist have plasmid obtained and sequenced, and are re-mutated
5. Reading frame re-undergoes random mutagenesis and process repeats

# Chapter II Literature Review:

## The use of directed evolution to develop biological molecules contributing to the understanding of neuronal activity

This chapter is a literature review covering the directed evolution techniques used to develop biological molecules for the understanding of neuronal circuitry. Analysis of tried-and-tested methods will provide useful context for design of future experiments to improve on desirable characteristics of existing proteins for modified function; such as on TOK1 for DREADD function.

Directed evolution emulates molecular evolution on a significantly shorter timescale and towards a desirable phenotype. To do this a protein's DNA sequence is randomly mutated to a defined level of diversification to generate a large library of variants. Following expression, such as in a simple living platform (phage, bacterial, yeast, cell culture), a specified selection pressure is applied, and mass screening is conducted to identify incremental changes related to the desired function. This is repeated several times until the desired function results from these incremental residue changes developed at each generation of library diversification and screening (Figure 7; Arnold, 2018).

Evolved proteins which have contributed to the understanding of brain function began with endeavours to visualise and record neuronal depolarisation. Neuronal genetically-encoded calcium indicators (GECIs) fluoresce upon measuring a detectable influx of intracellular calcium ions. Genetically-encoded voltage indicators (GEVIs) do the same upon the detection of changes in neuronal membrane potential. To directly influence neuronal activity, actuators were developed by rational design based on rhodopsin channels which open via light proton activation for the transverse of ions across the neuronal plasma membrane (Appendix 6.1). These groups of molecules have led to a field termed optogenetics due to their use of light. Using directed evolution, actuators activated by uniquely designed drugs were developed and termed designer receptors exclusively activated by designer drugs (DREADDs).

Coupling optogenetics and DREADD activation with readouts, in the form of *in vivo* behavioural or phenotype changes, and *ex vivo* electrophysiological recordings has led to the elucidation of previously unknown brain mechanisms. These experiments reveal causal links between the activity of neuronal sub-populations, activity of circuits (small neuronal groups projecting from one part of the brain to influence activity of another region), and specific behaviours or physiological phenotypes. Genetic approaches allow for a higher resolution understanding of activity on a temporal and spatial scale. Many neuroscientists aim to understand how the brain works by breaking down integrated codes of neuron populations firing in specific frequencies and amplitudes using particular channels, pumps, and ions leading each biological output. Such codes, sometimes termed engrams, are thought to underlie phenomena including sleep and anaesthetically-induced loss of consciousness (Box 1.1).

## 2.1 Types of optogenetic molecules

Modifications of eukaryotic calmodulin- or troponin-plus partner proteins have led to their use as calcium indicators; fluorescing when  $\text{Ca}^{2+}$  enters the cell and a calcium ion binds to the protein pairs (Miyawaki *et al.*, 1997; Thestrup *et al.*, 2014). Following on from this, voltage indicators were produced by fusing a voltage-sensitive domain to a fluorescing domain used in calcium indicators (Abdelfattah *et al.*, 2016). Calcium and voltage indicators are expressed in mammalian neuronal plasma membranes, hence them being termed genetically-encoded.

Shining certain wavelengths of light on microbial rhodopsins cause a flux of ions across the cell membrane and depolarisation or hyperpolarisation of the cell. Modifying rhodopsins for transexpression and light-activation in mammalian neurons can induce membrane potential changes and demonstrate causal links with behaviour. These modified rhodopsins are actuators (Appendix 6.1).

### Box 2.1 Lessons learned from reviewing methods used to generate optogenetic molecules

This chapter reviews the methods used to generate optogenetic molecules, focussing principally on directed evolution but also including molecules derived from other mutagenesis methods and subsequent screening. We can draw out some key lessons overarching several methods which the reader may like to bear in mind whilst reading the detail of the review. They may be useful during the consideration of future experiments aiming to further improve on optogenetic molecule characteristics.

#### Common techniques used to generate optogenetic molecules

**Receptor regions repeatedly found to be important to function were common targets of mutagenesis.** Modifying charges near the Schiff base which links proteins to *cis*-retinal or the retinal-binding pocket sometimes shifted light activation wavelength or deactivation time. Mutagenesis on the third transmembrane domain induced changes in channel cation conductance of Channelrhodopsin, and the third  $\text{Ca}^{2+}$  binding loop of calmodulin (Miyawaki *et al.*, 1997).

**Residue changes were transferred between channels to recapture changes in function.** This can also be seen during the development of receptors controlled by designer drugs instead of light (Armbruster *et al.*, 2007; Engqvist *et al.*, 2015).

**Calcium indicators exploit endogenous protein domains** that bring flanking fluorescent protein domains together upon ion binding (Miyawaki *et al.*, 1997). Further modifications were made to address concerns that **proteins with an original endogenous function may interfere with cellular processes.** Adding localisation and target affinity motifs could be a transferrable way to remove dysregulated functions of endogenous domains (Yang *et al.*, 2018).

**Resultant lineages of evolved proteins** demonstrate the value of building on inherited properties continually optimised to reach desired functions. **De novo sequencing** by scanning and enhancing variants from novel species was used after exhausting substitution sites using laboratory methods (Berndt *et al.*, 2014).

**High throughput and multi-parameter selection** to simultaneously ameliorate functional characteristics was difficult, as sometimes one parameter would improve at the detriment of another, or *in vitro* but not *in vivo* (Barnett *et al.*, 2012). **Directed evolution has not yet been applied to molecules to generate actuators** for *in vivo* use and could be a way of doing this. Robotic and automated methods may point to a further sophisticated possibility to address these challenges (Piatkevich *et al.*, 2018).

#### Common challenges during the development of optogenetic molecules

**There have been efforts to shift activation maxima to different colours including red and further-red** to reduce chance of overlapping activation and physiological side-effects of blue light (Hochbaum *et al.*, 2014). **Activating light spectra can overlap between indicators and actuators** which directed evolution cannot always resolve (Abdelfattah *et al.*, 2016).

**Actuators had challenges being used *in vivo*** due to sometimes driving subthreshold depolarisation or hyperpolarisation events (Hochbaum *et al.*, 2014). **Voltage indicators also had challenges being used *in vivo*** due to not always showing fidelity to changes in membrane potential events. **Indicators initially did not show fluorescence increases with neuronal  $\text{Ca}^{2+}$  or voltage changes** but further modification was able to change this (Nagai *et al.*, 2001).

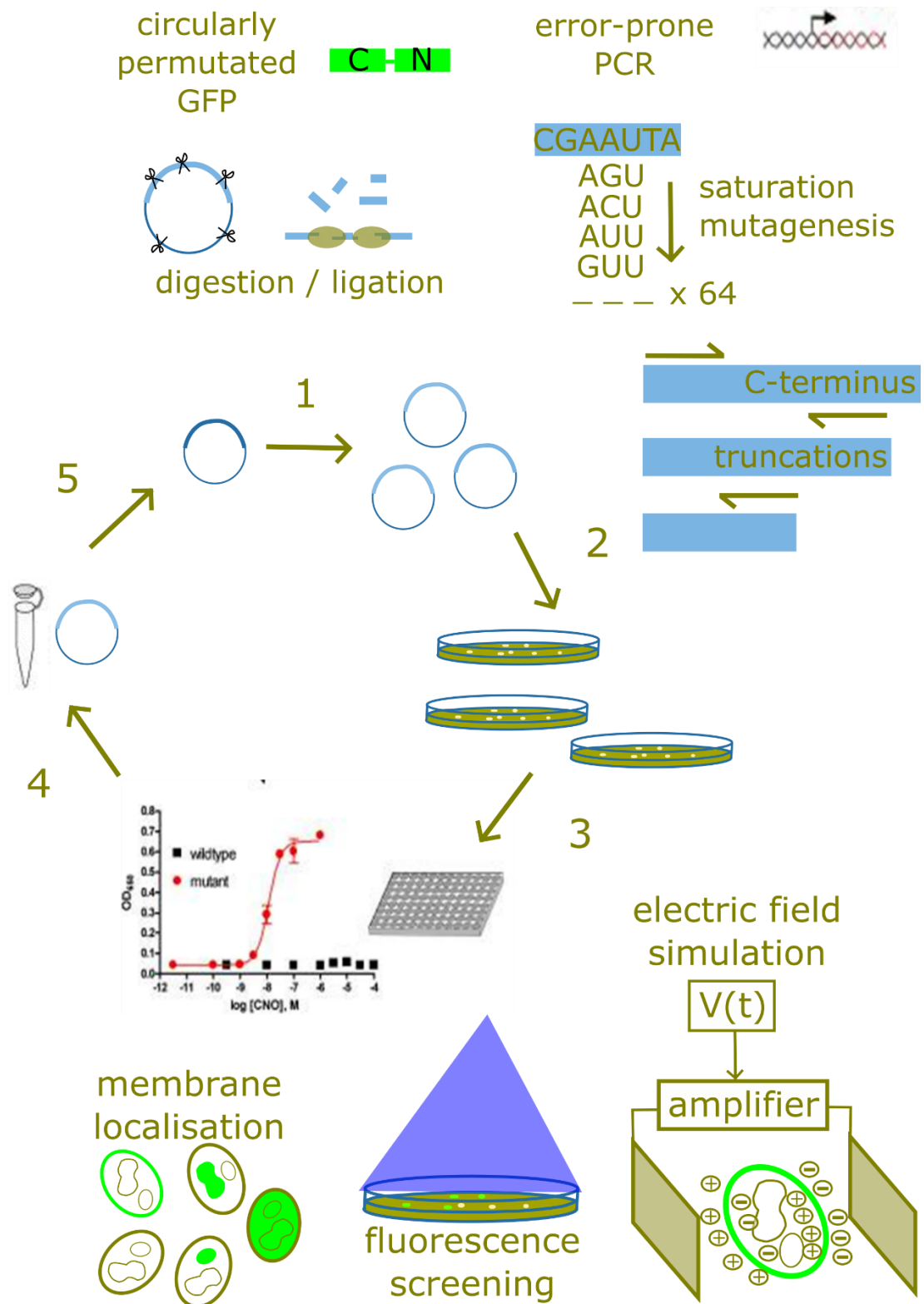


**Figure 7. Schematic of directed molecular evolution steps** (adapted from Armbruster *et al.*, 2007).

1. Reading frames randomly mutated. Examples of techniques include: circular permutation, error-prone PCR, random digestion and ligation, (targeted) saturation mutagenesis, and C-terminus truncations
2. Mutation libraries transformed into *E. coli* or yeast and exposed to selection pressure, such as agonists / control conditions
3. Cells screened or selected by parameters such as: growth rate (to ascertain whether channels are activated to allow survival), fluorescence screening, membrane localisation, and voltage sensitivity
4. Selected clones have plasmid obtained and sequenced, and are re-mutated
5. Reading frame re-undergoes random mutagenesis and process repeats

## 2.2 Methods used to develop genetically-encoded calcium indicators

The evolution of fluorescent proteins into GECIs pioneered the understanding of synaptic activity and neuronal circuits *in vivo* by providing a proxy for action potential spikes. They have proven more practical than chemical-based calcium fluorescent indicators as the latter could not be targeted to subcellular regions, were single-use, and depended on a niche understanding of chemistry (Pologruto *et al.*, 2004). Biologically produced indicators can be continually modified using directed evolution methods. GECIs are based on the interaction between calmodulin and M13-peptide from the calmodulin-binding domain of the myosin light chain kinase domain (Miyawaki *et al.*, 1997). Calcium modulates the environment of linked fluorescent proteins or induces fluorescence resonance energy transfer which leads to a shift in fluorescent emission.

### 2.21 Chameleon was the basis of the first GECI

The first GECI, Chameleon, fused four domains: 1) a blue or cyan fluorescent protein, 2) calmodulin, 3) M13-peptide from the calmodulin-binding domain of the myosin light chain kinase domain, and 4) enhanced green or yellow fluorescent protein. Ca<sup>2+</sup> induced binding of calmodulin and M13 causing fluorescent energy transfer (FRET) between the flanking fluorescent proteins. Conducting mutations on the boundary between calmodulin-M13 and fluorescent proteins improved some functions of this synthetically evolved chimera.

Several residue substitutions demonstrated significant effects on the function of Chameleon. Ameliorated sensitivity to a lower Ca<sup>2+</sup> concentration was enabled by Glu104Gln substitution on the third Ca<sup>2+</sup>-binding loop. Phe64Leu improved green fluorescent protein (GFP) folding in mammalian cells (37 °C) rather than in the *E. coli* platform (28 °C). A couple of mutations in enhanced GFP (eGFP) changed the colour of the fluorescent protein (FP): Tyr66Trp for cyan (eCFP) and Trp203Tyr for yellow (eYFP). The different emitting colours were excited at different light maxima: eCFP at 433 nm and eBlueFP at 381 nm, with increased brightness, signal-to-noise ratio, and extended the length of recording.

To observe the significance of the technique of fusing existing independent proteins into one construct, eCFP-calmodulin and M13-eYFP were mixed in a test tube. The unfused constructs were further apart and it took a higher Ca<sup>2+</sup> concentration to saturate the spectral response. As the team predicted, modifications building on Chameleon paved the way for increasingly effective GECI tools (Miyawaki *et al.*, 1997).

### 2.22 Circularly permutating fluorescent proteins led to Camgaroo

Initially, the integrity of FP structure was thought to be paramount. It was believed that chromophore conformation was maintained by the interaction between the 3D protein structure and posttranslational modifications. Whole FPs were linked via the N- or C-terminus to other domains.

Random mutagenesis of the GFP sequence led to the identification of Tyr145 as the only site that maintained fluorescence when modified. Permutation experiments produced functional circularly permuted GFP (cpGFP) by swapping the two ends of the fluorescent protein with a short spacer between. Inserting calmodulin-M13 in cpGFP produced brighter fluorescence in a non-FRET based Ca<sup>2+</sup> regulatory manner. This molecule was called Camgaroo.

CpGFP was probably one of the first optogenetic molecules onto which random mutagenesis was applied. CpGFP was digested and a ligase was added for gap and sticky end repair. The library was ligated into a triple-stop vector to simultaneously produce three possible reading frames on one construct. Expression and fluorescence-based screening were conducted in *E. coli* where 144 fluorescent clones were selected out of 25,000 to ensure saturation mutagenesis of the 717 bp gene. Sequences differing in length to WT GFP were sequenced and 15 novel circular permutations were found with mutations identified as sites separating autonomous conformational regions but such proteins did not fold well at 37 °C, rendering them unable to be used in experimental application (Baird *et al.*, 1999).

## 2.23 Pericam was developed by rational design

Soon after, Nagai *et al.* (2001) played around with fusing independent proteins and circularly permutating domains.

The resultant Pericam consisted of:

M13-cpEYFP(Val68Leu/Gln69Lys)-calmodulin (instead of calmodulin-M13 between cpGFP as is Camgaroo), with a Glu104Gln mutation in the third Ca<sup>2+</sup> binding loop. Following bacterial expression and purification of Pericam it was found that clefts in the  $\beta$ -can allow the chromophore to be exposed to protons for conversion of domain interactions into electrostatic potential change and induce fluorescence. When bound to Ca<sup>2+</sup>, Pericam peak excitation was at 485 nm and, emitted maximally at 520 nm three times more brightly than cpYFP.

Site-directed mutagenesis in cpEYFP(Val68Leu/Gln69Lys) at residues 148 and 203 and in linker sequences were used to develop Pericams with varied properties. Flash-pericam (His148Asp/Tyr203His) had additional Val163Ala and Ser175Gly mutations to improve folding at 37 °C (but remained inefficient compared to other constructs); and singular wavelength emission, brightening eight-fold upon Ca<sup>2+</sup> binding at 490 nm absorption. Here, M13 interaction with Ca<sup>2+</sup>-CaM led to chromophore ionisation. Due to this, the interaction was also pH-dependent.

Ratiometric-pericam (His148Dsp/Tyr203Phe/Phe46Leu with modified linkers) displayed dual excitation where intensity of green fluorescence increased 10-fold between 494/415 nm when saturated with Ca<sup>2+</sup>. The advantage of bimodal excitation allowed the quantification of Ca<sup>2+</sup> binding and cancelled out artifacts such as the expression level, cell thickness, or movement.

Compared to its predecessors, Ratiometric-pericam was more sensitive than Chameleon to Ca<sup>2+</sup>, and Flash-pericam detected histamine-induced Ca<sup>2+</sup> spikes whereas Camgaroo could not. This shows the usefulness of fusing proteins existing independently in nature to produce new functions.

## 2.24 GCaMP requires the modification of motifs deregulating endogenous protein function

The most widely used GECIs, GCaMP, are based on Pericam. When calcium interacts, the two domains stabilise the GFP chromophore and increased fluorescence more than FRET-based sensors could.

The first GCaMP was developed by testing cpEGFP variants with N-termini starting at original sequence residues 145-155 and C-termini starting at original sequence residues 142-148 expressed in HeLa cells. Testing substitutions of residue 148 within the linker between calmodulin-M13 (CaM) and cpEGFP149–144 (N- and C-termini starting residues respectively) revealed that a hydroxyl side chain is required to project to the interior of the  $\beta$ -barrel and interact with Tyr66 of the fluorophore for photisomerisation to occur. Basic side chains removed Ca<sup>2+</sup> activation.

A relatively bright variant with cpEGFP149–144 (GCaMP) was chosen for further engineering as it also showed a relatively greater and faster response to agonists (ATP, carbachol). Like other fluorescent-protein based channels, activation was pH-dependent. Peak excitation and emission were 489 nm and 509 nm respectively, increasing 4.5-fold in the presence of Ca<sup>2+</sup>. Association kinetics at Ca<sup>2+</sup> concentrations > 500 nM were fast enough for cellular application, with maximal intracellular Ca<sup>2+</sup> concentration attained within 200 ms (Nikai *et al.*, 2001).

## GCaMP6

The most widely-used version of GCaMP (sixth) was developed by semi-random mutagenesis methods. 16 residues on the interface between cpGFP and the CaM domain were mutated, with some to near-saturation, in addition to 18 residues elsewhere. Mutants were expressed in dissociated hippocampal neurons with induced action potentials and were measured for Ca<sup>2+</sup> concentration sensitivity, dynamic range, kinetics, and brightness. Screening 348 point mutants showed that 43 variants improved sensitivity to action potentials compared to antecedent GCaMP3. In a second round of mutagenesis, beneficial mutations for response amplitudes and kinetics were combined to produce 98 variants. Screening in neuronal cultures led to the testing of three GCaMP6 variants *in vivo* producing detailed tracing of synaptic and dendritic activity in the mouse brain. Measurements demonstrated improved sensitivity to action potentials with no detriment to fluorescence and the ability to monitor activity over months (Chen *et al.*, 2013).

## GCaMP may interfere with endogenous Calmodulin cellular processes

GCaMPs and other CaM-based Ca<sup>2+</sup> sensors, in cultured neurons, were found to compete with endogenous CaM for the distal carboxyl tail of L-type Ca<sup>2+</sup> Cav1 channels or endogenous apocalmodulin bound to channels.

In previous experiments, separating Flash-pericam at the binding site linking M13(Val68Leu/Gln69Lys; original sequence residues 145-238) and eYFP(Val68Leu/Gln69Lys; original sequence residues 1–144)-CaM demonstrated interference from CaM and CaM-binding proteins in cells, but no interference from the complete construct (Nagai *et al.*, 2001).

A comprehensive understanding of GCaMP issues has yet been achieved and scientists use CaM-based GECIs with awareness of potential side-effects. Experiments show that mutations of the CaM domain in GCaMP3 led to abnormal signal transduction, meaning that GCaMP did not translocate to the nucleus under the same conditions as CaM. Nuclear GCaMP lowered CaM-dependent kinase II phosphorylation of transcription factor CREB and, perhaps through effects on gene expression, reduced neurite length. Cytosolic GCaMP increased neurite length during Cav1-dependent excitation–transcription coupling. Nuclear filling of GCaMP also caused apoptosis of > 60 % of cultured neurons and deregulated Ca<sup>2+</sup> dynamics, including gain-of-function firing in hippocampal neurons; altering whole-brain activity *in vivo* manifesting as epileptiform phenotypes in GCaMP6-expressing mouse lines. As the basal fluorescence of GCaMP is lower than GFP, neurons deemed to have low expression may still upregulate Cav1 activity (Yang *et al.*, 2018).

## GCaMP-X

Further engineering produced versions of GCaMP-X with abolished Cav1 gating interference. ‘X’-denoted constructs had an additional high apoCaM-affinity motif with low Ca<sup>2+</sup>/CaM-affinity, without affecting M13 binding Ca<sup>2+</sup>; simultaneously abolishing GCaMP nuclear accumulation and apoptosis. GCaMP3-XM (with membrane-tethering sequence) corrected perturbed Cav1 channel gating and Ca<sup>2+</sup> influx. GCaMP3-X and GCaMP3-XC (with cytosolic target-sequence) abolished nuclear accumulation, pCREB signalling dysregulation, or neurite outgrowth in cultured cortical neurons. Therefore adding localisation and target affinity motifs could be a transferrable way to remove dysregulated functions of endogenous domains (Yang *et al.*, 2018).

## 2.3 Genetically-encoded calcium indicators based on FRET

In addition to the array of calmodulin-M13 based GECIs, FRET-based tools were developed with the intention of overcoming shortcomings in early versions of GCaMP and have since spawned a lineage of their own. Species variants of calcium agonist troponin C (TnC) and sometimes with domains of its binding partner troponin I, found in skeletal and cardiac muscle, were used to develop ratiometric GECIs. Like calmodulin, TnC interacts with  $\text{Ca}^{2+}$  and is dumbbell-shaped with a central linker between two globular domains. WT fragments or combinations initially showed low affinity to  $\text{Ca}^{2+}$ . Residues in linkers close to GFPs were mutated to produce over 70 constructs between an upstream CFP donor and downstream citrine acceptor fluorophore, purified, and tested for calcium affinity.

### 2.31 Targeting sequence diversification was efficient for evolving Twitches

#### *Sequence diversification and screening of TnC sensors*

Sampling the C-terminal sequence of troponin C from previously unused toadfish *Opsanus tau* (tsTnC) produced the most recent TnC FRET-based sensor. tsTnC has optimised FRET responses by having fewer calcium binding sites. Some principles of directed evolution were used to develop the sensor. Firstly, variants of C-terminus truncation were expressed in *E. coli* and 1000 colonies were pre-screened *in vitro* by chemically opening cell membranes and measuring difference in fluorescence between baseline and following 100 mM  $\text{CaCl}_2$  application. The C-terminal truncation Ser93 to Gln161 was identified as the minimal length for  $\text{Ca}^{2+}$  binding.

Following this, a library of random diversified residues within interacting hinge regions and nonchelating residues in binding loops of sequences linking fluorophores was expressed in 100,000 *E. coli* colonies. 1000 of these were purified. The brightest and most photostable variants underwent additional NMR structure-guided semi-random mutagenesis in the truncated tsTnC and expressed in 70,000 *E. coli* colonies with 1000 purified. Asn15Asp/Asp17Asn of EF hand 3 and Asn51Asp/Asp53Asn of EF hand 4 had decreased affinity to  $\text{Mg}^{+2}$ , and ratio changes in fluorescence between zero  $\text{Ca}^{2+}$  to saturation were observed as high as 1000 %. Following bacterial screening, 120 variants with maximal ratio change were screened in primary hippocampal neurons.

#### *Properties of Twitches*

Twitch-1 was formed from the minimal domain, double-flanked by Proline and Met65Val mutation with a maximal ratio change of ~400%. Low affinity sensors with faster kinetics were used as a foundation for a variant library with residues inserted in EF hand 3 or 4. Variants Twitch-3 and 4 displayed higher sensitivity to cytosolic calcium and maximal response. By using FPs cpVenus and mCerulean with extended linkers in Twitch-2, variant Twitch-2B retained high FRET and was two-fold brighter in the donor emission channel. In adult-born juxtaglomerular neurons of the mouse olfactory bulb, Twitch-2B displayed stronger signals than Twitch-3 and was able to repeat an *in vivo* signal response to the same odour at two different time points. Only 0.03 % of analysed neurons had filled nuclei and 12 % of the odour-responsive population had decreased responses. Arguments for the use of FRET-based instead of GCaMP sensors were proposed to be based on accuracy due to lower influence of changes in: optical path length, intensity of exciting light, expression level, and developmental growth; and brighter baseline fluorescence to identify expressing cells. As Twitches were also able to only bind two calcium ions, instead of up to four, they were more sensitive and ratiometric. Future sensors may ideally have faster kinetics, which seems to be difficult to achieve with sensitivity (Thestrup *et al.*, 2014).

## 2.4 The use of directed evolution to develop genetically-encoded voltage indicators

Despite successive innovations of GECIs and their contribution to the understanding of neuronal circuitry *in vivo* they remain a proxy readout for action potential firing. They also require suprathreshold spiking and have relatively slow kinetics in response to spiking frequency. Genetically encoded voltage indicators (GEVIs) are ideal to overcome these shortcomings but their development has been slower in comparison. GEVIs are the most recently developed group of optogenetic molecules, for which directed evolution methods were more frequently used.

### 2.4.1 A library of Archaelhodopsin 3 variants were screened to develop QuasArs

Archaelhodopsin 3 is a WT voltage indicator with a further shifted red emission spectrum compared to preceding indicators. The largest mutant library of an optogenetic molecule at that point;  $10^4$  Arch mutants were screened in *E. coli* for brightness for five rounds to ameliorate the dimness of the WT receptor (3-8 fold higher signal-to-noise ratio). Additional libraries of a randomised subset of substitutions at Asp95 which maintained fluorescence in *E. coli* were expressed in HeLa cells leading to mutation Asn95His improving trafficking, speed, and voltage sensitivity under field stimulation and induced transmembrane voltages. Subsequent Asn106 randomisation, limited to amino acids with polar or charged side chains, led to Asn106His and variant QuasAr1.

Patch clamp in HEK cells demonstrated -70 to +30 mV detection (variant QuasAr2 being superior) and 30-1000 fold higher temporal resolution (QuasAr1 being superior). The response time of QuasAr1 had a response time of 50  $\mu$ s which was more than 10-fold faster than previous GEVIs. To improve trafficking, sequences for endoplasmic reticulum export and trafficking were added. This resulted in variants QuasAr1 with five mutations P60S, T80S, D95H, D106H, F161V and QuasAr2 which consisted of QuasAr1(H95Q). Maximal fluorescence excitation was at 590 nm and emission at 715 nm.

CheRiff is a red light activated actuator discovered in a novel species

A Channelrhodopsin screen for WT channels expressed at HEK 293 plasma cell membranes and activated at 474 nm highlighted one originating in *Scherffelia dubia* as an interesting candidate. A plasma membrane trafficking signal sequence and Glu154Ala mutation were added to accelerate kinetics compared to previous actuators and lessen spurious spiking by red light. This was dubbed CheRiff and activation occurred at 460 nm with subthreshold depolarisation of cultured mouse hippocampal neurons at 640 nm.

The Optopatch system uses QuasAr GEVI and CheRiff actuator in the same neuronal population

Optopatch2, a bicistronic vector for ChRiff-eGFP and QuasAr2-mOrange2 co-expression in cultured rat hippocampal neurons demonstrated voltage changes induced by the actuator and simultaneous membrane voltage recordings by the indicator. Membrane translocation had no statistically significant effect on membrane resistance, membrane capacitance, resting potential, threshold current, or threshold potential. 10 ms pulses of blue light stimulated CheRiff and constant red-light illumination excited QuasAr2, imaged at a 1 kHz frame rate with simultaneous membrane voltage recordings.

*Optopatch was able to induce excitatory post-synaptic potentials*

Optical induction of single action potentials in single presynaptic cell soma produced post-synaptic transient fluorescence representing an excitatory post-synaptic potential with < 2ms delay indicative of a monosynaptic connection; validated by patch clamp and synaptic blockers. Action potential propagation could be seen to travel 30-50  $\mu$ m from the soma down axons of single cells. High-throughput quantification was achieved using a bespoke low-magnification, high-speed microscope to observe action potentials via blue light activation on CheRiff in up to 50 cells in user-selected intracellular regions (Hochbaum *et al.*, 2014).

## 2.42 Targeted saturation mutagenesis was efficient for evolving GRb(lue)3 and GRr(ed)3

Directed evolution experiments performed on a proton-pumping *Gloeobacter violaceus* rhodopsin (GR) were used to inform the modification of Arch in order to improve quantum efficiency and brightness. A homology model used to identify putative binding pocket residues in GR for which 19 of 20 sites (the exception, K257, covalently bonded with retinal through a Schiff base linkage) underwent site-saturation mutagenesis. 88 clones were screened for each site-saturation library by expression in *E. coli* followed by protein extraction and purification, where absorption spectra were measured using a plate reader, leading to some variants being brighter than WT.

Mutagenesis at 15 of the targeted binding pocket residues produced 52 blue/red-shifted variants. Maximal blue shift was -42 nm with mutations along the retinal chromophore, and a 22 nm red shift was due mutations clustered near Lys257. Directed evolution allowed the identification of 38 tuning mutations not found in nature. Of the 52 shifted variants, 32 maintained proton pumping activity albeit less than WT level. Fractionated plasmid amplification recombined mutations with significant blue spectral shifts without proton pumping impairments to produce a second library. A filter consisting of including sites with more than one mutation if absorption maxima was less than 528 nm reduced 9000 variants to 600, screened in 1760 clones for 95 % coverage. A red library of 216 variants had 880 clones screened (98 % coverage). These procedures shifted molecules further blue or red. Site-saturation mutagenesis at sites in the retinal-binding pocket not already mutated produced additional shifts. In total, 7216 clones were screened (three libraries) resulting in GRb(lue)3 and GRr(ed)3, differing by only seven mutations, with absorption maxima 161 nm apart (Engqvist *et al.*, 2015).

### Mutations discovered from directed evolution to produce GRr-b and -c were transferred to Archers

Resulting GR mutations were applied to Archaeorhodopsin (Arch) in an endeavour to produce improved GEVIs for *in vivo* application in *Caenorhabditis elegans*. Two variants responded to 655 nm light with sensitivity to -100 to + 50 mV. Variant Archer1 (Arch with enhanced radiance; Asp95Glu and Thr99Cys) displayed up to 3 times higher baseline and 40 % increased fluorescence than Arch WT; under lower intensity light than other Arch-based sensors.

In addition to voltage sensing, under green light Archer1 was able to act as an inhibitory actuator. Archer2 (Asp95Glu, Thr99Cys, and Ala225Met), had five times higher baseline fluorescence and 99% less photocurrent induction than Arch WT. Sensitivity was 85%  $\Delta F/F$  and 60%  $\Delta F/F$  per 100 mV for Archer1 and Archer2 respectively with fast kinetics and sensitivity over minutes.

In single rat hippocampal neurons, Archer1 tracked action potentials in the cell body and processes, mimicking spatiotemporal current injection changes with 25–40%  $\Delta F/F$  at 40 Hz action potential firing. Archer1 expression in a two-neuron network showed fluorescence increase in one neuron in response to an induced voltage step and spontaneous spiking simultaneous to the step in the second neuron. A third neuron nearby outside of the network had no fluorescence change. *In vivo* expression of Archer1 in the olfactory neuron AWC-ON of *C. elegans* demonstrated fluorescence within 2 s of turning off isoamyl alcohol odorant stimulus, reflecting previous GCaMP fluorescence where  $Ca^{2+}$  transients peaked within 10 s of turning off the stimulus (Flytzanis *et al.*, 2014).

## 2.43 Targeted saturation mutagenesis, error-prone PCR, and DNA shuffling produced FlicR1

In 2016, Abdelfattah *et al.* reported a GEVI based on a circularly permuted red fluorescent protein (cpmApple) and CiVSD. The Lys80 side chain in cpmApple interacts with the chromophore and fusing it with the C terminus of CiVSD brings the side chain close to CiVSD S4 helix. As a result, voltage-induced conformational changes influence the chromophore directly. Directed evolution principles were applied to CiVSD to improve fluorescence, membrane localisation, and voltage sensitivity over several library generations and ensuing screening.

The C terminus of CiVSD was truncated at residues 236–242 and following fusion to cpmApple produced seven variants. Site-saturation mutagenesis of Pro240 and Val241 in the linker produced 1024 gene variants for each of the seven libraries. Fluorescence screening using a 560/40 nm excitation filter and 630/60 nm emission filter was done on *E. coli* plates where threshold fluorescence brightness was set at the top 0.01 % of fluorescent clones. A secondary step consisted of screening in HeLa cells for plasma membrane localisation and voltage sensitivity by electric field stimulation. Variant with mutation Pro240Arg was identified as FlicR0.1 with a dim fluorescent response. Seven rounds of random mutagenesis (error-prone PCR and DNA shuffling) on one to six variants identified from HeLa screening generated thousands of libraries of variants. 10,000 transformed *E. coli* colonies (10–20 plates) were screened following each round which equated to around three times the size of each library. Val207Ala on the S3 to S4 linker of the CiVSD was identified, and on the eighth round of evolution residue 207 was mutated to all 20 amino acids. Variant Val207Phe was the most sensitive to voltage changes. Despite the size of libraries and rounds of evolution, this variant (FlicR1) had only 12 mutations that differed to FlicR0.1.

During whole-cell voltage patch clamp of HEK cells, it was found that fluorescence reporting under 561 nm wavelength light increased almost linearly with membrane voltage almost an order of magnitude larger than previous cpRFP-based sensors. However, FlicR1 bleached too quickly to be used with two-photon imaging. FlicR1 was able to track voltage oscillations up to 100 Hz in dissociated rat hippocampal neurons in single trial recordings, a speed which was unable to be resolved by previous GEVIs. Use alongside blue-light photoactivating Channelrhodopsin actuators demonstrated overlapping activation of FlicR1.

## 2.44 Targeted saturation mutagenesis was efficient for evolving Marina

A recent innovation in using directed evolution to produce GEVIs involved fusing CiVSD with super ecliptic pHluorin fluorescent protein to produce super ecliptic ArcLight. Fluorescence brightness was increased in response to voltage. Action potential detection kinetics and fluorescence signal-to-background noise ratios also overcame limitations which previously excluded GEVI use *in vivo* (Jin *et al.*, 2012).

Four site-directed substitutions were made on the  $\beta$ -barrel of super ecliptic pHluorin fluorescent protein in ArcLight, turning it into eGFP. Mutagenesis saturation libraries of three of these four key residues (Asp389, Phe444 and Thr446) and six others (Arg338, His390, Tyr442, Thr445, Ser447, and Glu464) were created and expressed in *E. coli*. 96 clones were selected from each mutagenic library, to ensure 20 amino acids at each residue were accounted for, and screened two to four times using whole-cell patch clamp electrophysiology on cultured primary neurons or spontaneously spiking HEK293 cells. As Asp389 mutants displayed a reduction in negative fluorescence with membrane voltage depolarisations, 96 Asp389 mutants were sequenced and constructs for 19 novel amino acids at this residue were tested in whole-cell patch clamp electrophysiology in HEK293 cells. Asp389Ala demonstrated a small fluorescence signal increase with membrane voltage depolarisations due to its hydrophobic side chain.

In a second round, ArcLight(Ala389) template had the same six residues undergo saturation mutagenesis. 19 amino acid substitutions at His390 led to Arclight(Ala389, Ala390) showing biexponential kinetics.

During the third round of mutagenesis, site-directed mutations targeted residue Tyr442 in ArcLight(Ala389, Ala390) leading to Tyr442Val having increased signal magnitude due to its hydrophobicity. This triple mutant was named Marina.

In murine primary neuronal culture, Marina was able to detect membrane transients in cell bodies and processes; captured optically. Further saturation libraries at residues of potential interest were unable to improve properties of Marina and some at the dimerisation interface with GFP disrupted voltage sensitivity, suggesting that intramolecular dimerisation is intrinsic to the functioning of Arclight, Marina, and perhaps other dimolecular GEVIs.

## 2.45 Automated screening allowed for unprecedented high throughput evolution of Archon1

Piatkevich *et al.* (2018) developed an off the shelf robotic cell picking method for multi-parameter screening of namely: plasma membrane localisation, increased fluorescent-voltage spiking sensitivity, high fluorescence signal-to-noise ratio, fluorescence changes proportional to voltage fluctuations, and empirically decreased photobleaching *in vitro*. The throughput of the method was quantified at 300,000 HEK293T cells over four hours, allowing three rounds of directed molecular evolution to be conducted on libraries of  $10^6$  variants. This demonstrates a possible future perspective for automated multi-parameter screening of large randomly mutated libraries in directed evolution.

Random mutagenesis by error-prone PCR was performed on the opsin core of the voltage sensor Quasar2 with excitation maximum at 590 nm producing  $10^6$  variants. Following expression in HEK293T cells, FACS of cell populations 1.5 times the number of library variants allowed the high throughput identification of non-functional mutants (filtering out >99.9 % of the population). Screening was conducted using microscopy-guided robotic picking of cells with membrane localisation as the primary parameter and brightness as a secondary.

Cells were screened for augmented fluorescent-voltage sensitivity by placing a pair of platinum electrodes, either side of a 4 mm gap, into well plates. Voltages were induced across cell culture, and imaged. Four amino acid residues in  $\alpha$ -helices and two in  $\beta$ -strands were identified as significant and targeted alongside mutations near the Schiff base linkage for site-directed mutagenesis in a second round of directed evolution producing nearly  $10^7$  variants. 21 of these constructs were selected based on the same screening parameters and voltage sensitivity was quantified using patch-clamp and simultaneous imaging.

Following expression in mouse brain slices, one variant eventually named Archon1 localised to the membrane and was brighter than QuasAr2 and Archer1. Archon1-eGFP expression *in vitro* Zebrafish neurons reported action potentials with voltage sensitivity and signal-to-noise ratio higher than previous GEVIs. Photobleaching occurred over 300 s (around double that of FlicR) but imaging was stable over minutes. In *C. elegans*, Archon1-eGFP was expressed in AVA interneurons involved in backward locomotion alongside channelrhodopsin-2 in an upstream ASH neuron. 51 out of 60 blue light pulses led to Archon1 fluorescence lasting around 38 s with photobleaching occurring after eight minutes.

## 2.5 The use of DREADDs and comparison to optogenetics

Designer receptors exclusively activated by designer drugs (DREADDs) are engineered G protein-coupled receptors (GPCRs) with no physiological agonists. The drugs activating designer receptors were also designed to have no endogenous targets. In the field of neuroscience, DREADDs – like optogenetic tools – can be expressed and activated *in vivo* to correlate spatiotemporal neuronal activity with changes in behaviour or physiological phenotype. Studies investigating the use of DREADD and optogenetic tools on the same neuronal populations identified equivalent effects on physiological readouts with a longer duration from DREADDs (Roth, 2016). Indeed, optogenetic tools enable millisecond precision of channel activation lasting up to seconds, whilst drug activation will depend on the time taken for metabolism, receptor desensitisation, or internalisation, and downregulation effects. DREADDs are also less invasive and require less equipment as designer drugs can be delivered orally with food or via intraperitoneal injection.

DREADDs utilise the same receptor signalling pathways as WT GPCRs. Agonists stabilise the active state of the receptor to form a signalling complex consisting of the agonist, receptor, and heteromeric G protein. GPCRs can spontaneously isomerise to the active state and interact with G proteins in the absence of a ligand. Lowering the DREADD expression can circumvent issues of basal activity. As G protein signalling pathways have several downstream effects, enhancing or silencing neural activity may not only be the sole results of DREADD activation. GPCRs indirectly link to ion channels and sites of neurotransmitter release and therefore impact membrane potential (depolarisation or hyperpolarisation) via a subset of their signalling cascades (Huang & Thathiah, 2015).

This chapter reviews the most widely used DREADDs developed by directed evolution methods. There are only a handful: five based on muscarinic receptors and one based on kappa-opioid receptor which eventually required rational design to produce. This demonstrates the mixed success of directed evolution which may depend on the protein onto which it is applied and the desired function. However, when successful the technique has proved immensely useful. This is demonstrated by an absence of a lineage of receptors with mutations building on inherited characteristics, as is the case for genetically-encoded calcium and voltage indicators.

### 2.51 Expression and drug screening of library variants in yeast evolved HM3Dq

The first DREADD, of which remains one of the most used, generated by directed evolution was evolved from the human muscarinic acetylcholine 3 receptor (M3) to be solely activated by clozapine-N-oxide (CNO). Previous receptors activated solely by a synthetic ligand (such as Ro1; Gi/o-coupled kappa opioid receptor) were activated by synthetic ligands that had other physiological targets. CNO was chosen as it did not demonstrate activation of endogenous mammalian receptors. Related compound clozapine has a high affinity to M3 receptors and it was predicted that few mutations were required for it to become a target CNO target (Armbruster *et al.*, 2007). However, recent studies have demonstrated that CNO can convert to clozapine *in vivo* and therefore target endogenous as well as modified M3 receptors and therefore experiments correlating DREADD activation with phenotypical outputs require careful controls (Manvich *et al.*, 2018).

Rat M3 receptor with a deletion in the third intracellular loop ( $i3$ ; rM3 $\Delta i3$ ) had been previously successfully expressed in *S. cerevisiae* and able to recapitulate the pheromone signalling pathway to promote cellular growth on selective media. Yeast provides some innate advantages to bacterial expression platforms (used for optogenetic molecule experiments) as yeast are eukaryotic and able to perform some post-translational modifications such as glycosylation (Gerngross & Wildt, 2005).

Three successive generations of random mutagenesis at a rate of 3.5 mutations per kb, and drug screening for relative yeast fitness as a proxy for receptor activation, were conducted on *S. cerevisiae* expressing rM3 $\Delta i3$ . The first round generated  $3 \times 10^4$  independent clones, with  $6 \times 10^4$  colonies screened. Clones activated by 10-100  $\mu\text{M}$  CNO were not

responsive to agonists carbachol or acetylcholine, whereas non-mutated receptors were activated by the agonists but not CNO.

Five CNO-responsive, but not constitutively active, clones were re-subjected to mutation, producing a second-generation library of  $7 \times 10^4$  independent clones, with  $2.5 \times 10^4$  colonies screened, of which some could be selectively activated by 35-5000 nM CNO with 1000-fold reduced acetylcholine potency.

A third-generation library based on five second-generation clones led to  $6 \times 10^5$  independent clones, with  $8 \times 10^4$  colonies screened, and two activated by <10 nM CNO and  $\approx$  0.1 nM clozapine. Tyr149Cys/Ala239Gly, later named hM3Dq, was identified as optimal for CNO activation with simultaneously removed acetylcholine activity.

To verify CNO activation in mammalian cells a subset of mutants were expressed in HEK293T cells, where it was found that Tyr148X was the most consistent mutation in positive clones. Activation of receptors with a mutation at this residue were able to produce inositol monophosphate (a metabolite of inositol triphosphate when phospholipase C  $\beta$  catalyses phosphatidylinositol) and had reduced acetylcholine potency. CNO was inactive on WT receptors in HEK293T cells. Combination Tyr149Cys/Ala239Gly showed increased response to CNO and decreased response to acetylcholine.

hMD3q expression and activation by CNO (but not by acetylcholine) in immortalised human pulmonary artery smooth muscle cells *in vitro* demonstrated an increase in ERK-1/2 phosphorylation, suggesting an association of the MAPK-arrestin complex with the activated receptor; which excludes a simultaneous association with G-proteins. This suggested that various signalling cascades downstream of receptor activation were maintained following random mutagenesis. WT receptor expression and acetylcholine (but not CNO) activation was used as a control (Armbruster *et al.*, 2007).

## 2.52 Transferring mutations discovered by directed evolution of HM3Dq led to a family of DREADDs

Following the directed evolution of hM3Dq, amino acid sequence alignment of the mammalian muscarinic acetylcholine receptor family highlighted conserved residues Tyr149 and Ala239. Substituting Tyr149/Ala239 rendered M1, 2, 4, and 5 into a CNO-activatable DREADD. hM4 receptors coupled to Gi/o induce G protein inward-rectifying K<sup>+</sup> channels to hyperpolarise hippocampal neurons. In hippocampal neurons *in vitro*, WT hM4 expression with carbachol activation and hM4Di DREADD with CNO activation enabled hyperpolarisation without agonist overlap (Armbruster *et al.*, 2007).

## 2.53 Directed evolution was unsuccessful during attempts to develop hKORD

To remove the need for using CNO, a DREADD based on human kappa-opioid receptor (KORD) was developed by the same group that developed the CNO DREADDs (Vardy *et al.*, 2015). Kappa-opioid receptors are coupled to heterotrimer Gi/o proteins and inhibit adenylyl cyclase through the G $\alpha$  subunit to increase potassium channel conductance. Coupling with the G $\beta\gamma$  subunit decreases calcium conductance. Together these signalling cascades lead to neuronal inhibition and hyperpolarisation. Initially KORD was developed using the same directed evolution technique used to develop hM3Dq in *S. cerevisiae* (a strain which enables ligand-induced activation of heterologously expressed mammalian Gi-coupled GPCRs to engage the pheromone signaling pathway, thereby promoting growth on selective media) and screened using the physiologically inert drug Salvinorin B (SALB).

However, positive KORD constructs were constitutively active and therefore a rational mutagenesis approach was undertaken instead utilising crystallographic, modelling, and mutagenesis data (Wu *et al.*, 2012; Vardy *et al.*, 2013). Asp138Asn lowered affinity to the endogenous KOR peptides and increased that of Salvinorins on KORD up to 30-fold. Transfecting HEK293T cells with increasing levels of KORD demonstrated an increased potency of SALB.

*In vivo* expression in the substantia nigra (SN), ventral tegmental area (VTA), paraventricular hypothalamus (PVH), and arcuate nucleus (ARC) of mice followed by patch-clamp of slices showed Salvinorin B (SALB) activating KORD-mediated hyperpolarisation. SALB also reduced the frequency of miniature inhibitory post-synaptic currents in VTA/SN neurons expressing KORD. KORD activation in mice VTA/SN neurons demonstrated SALB dose-dependent increase in locomotion; in PVH neurons augmented feeding was observed; and KORD-mediated inhibition of hunger-promoting orexigenic ARC neurons projecting to a subpopulation of PVH decreased food intake. To validate the multiplex regulation of DREADDs on behaviour, co-expression of KORD (inhibitory)/hM3Dq (activation) expression in VTA/SN of mice was able to increase and diminish locomotor activity with the application of SALB and CNO respectively. When the designer drugs were applied simultaneously, locomotion was depressed but less so due to the effect of SALB on KORD. Double expression in ARC with CNO application increased feeding, with a blunted effect upon the administration of SALB.

*In vivo* CNO responses have been observed 5-10 minutes following IP injection and a persists for several hours. Plasma SALB increases within seconds and begins to rapidly decline, showing a behavioural effect lasting one hour in KORD-expressing mice and providing a DREADD alternative for shorter activation if necessary. It should also be noted that SALB may have some activity on KOR; particularly in neurons with high KOR reserve low levels (<10 mg/kg) of SALB should be administered.

## Box 2.5 Lessons learned since the development of DREADDs

Since the development of CNO DREADDs it has been discovered that CNO does not cross the blood-brain-barrier *in vivo* and rather back converts to clozapine to activate DREADDs (Manvich *et al.*, 2018). To overcome this Compound 21 is able to penetrate the nervous system without metabolising to clozapine first and has a particularly strong effect on hM3Dq and hM4Di (Jendryka *et al.*, 2019). Agonists stabilise the GPCR active state to enable the formation of a signalling complex with a heteromeric G proteins.

To reduce any basal receptor activity, DREADD expression can be decreased by lowering the titer of the viral vehicle, using a weaker promotor, or using post-transcriptional modification. Although, when DREADD expression is high, a lower agonist potency is required for the effect of maximal activation. It should also be noted that following activation, GPCRs can desensitise, be internalised to the cell, and downregulated. Testing DREADD and optogenetic technologies on the same neuronal populations has demonstrated equivalent physiological readouts, with longer-lasting effects of DREADDs (hours compared to milliseconds of optogenetic opsins). However, it is probable that activity additional to neuronal depolarisation and hyperpolarisation occurs with the activation of GPCRs (Roth, 2016) as they regulate multiple signalling cascades and G proteins are heteromeric and are not guaranteed to dimerise in a predictable manner. This may be observed via phenotypical side effects such as hypotension, sedation, and anticholinergic syndrome which are not apparent when low potency of designer drugs are used and such side-effects can be separated when comparing to appropriate control animals (Roth, 2016).

Following the demonstration of designer drugs CNO and SALB *in vivo*, it may be useful to develop analogues with similar properties of: exclusive receptor activation, CNS penetration, low toxicity, and pharmacokinetic parameters to suit the timeframe of experiments. Water-soluble SAL analogues would also be useful as SALB is not water-soluble, and vehicles may have side effects *in vivo*.

Further DREADDs for multiplex control could be developed using yeast to express GPCRs and subjecting variants to directed evolution. However, the inability for a DREADD to be developed from KOR by this method may demonstrate the usefulness of trialling several mutagenic methods (including rational approaches), which were also used in combination to develop optogenetic tools (Roth, 2016).

As the most widely used DREADDs are metabotropic heterodimers, it may also be useful to develop a DREADD based on an ionotropic receptor. This would prevent association of different G-proteins or  $\beta$ -arrestins and secondary signalling effects. This is something explored in the empirical case study of directed evolution on TOK1.

# Chapter III: Materials and Methods

## 3.1 Experimental design

To contribute to the understanding of the electrical brain activity underlying behavioural phenotypes such as sleep and anaesthesia; patterns of neuronal action potentials are measured, unique in time and space. On a molecular level, they translate down to ions passing through neuronal plasma membrane channels, which in turn are regulated by protein channel opening and closing.

As the way in which agonists activate receptor channels and neuronal circuits is not completely understood we sought to better understand the molecular activation of tandem two-pore domain potassium channels (K<sub>2</sub>Ps) by volatile anaesthetics and attempted to develop a designer receptor to be activated by a designer drug (DREADD). The activation of a neuronal K<sup>+</sup> inward rectifying designer channels would hyperpolarise cells and lead to them being unable to fire action potentials.

### 3.11 Aims

The main aim of this project was to identify the activation site of halothane on tandem two-pore potassium channels. A secondary aim was to generate an ionotropic designer receptor to be exclusively activated by clozapine-N-oxide.

### 3.12 Objectives

Specific objectives relating to these aims were to:

- 1 i. Identify the amino acids involved in halothane binding of two-pore domain potassium channels
- 1 ii. Gain a better understanding of the mechanism of two-pore domain potassium channel activation upon halothane binding
- 2 i. Engineer an ionotropic channel to be activated exclusively by CNO / Compound 21 binding
- 2 ii. Enable *Saccharomyces cerevisiae* expressing the ionotropic receptor to only survive in low potassium media if the channel is activated by CNO / Compound 21 binding

### 3.13 Experimental procedure

To study human TASK3, human TREK1, mouse 5HT<sub>3A</sub> and yeast TOK1 channels, they were transformed in *Saccharomyces cerevisiae*. Yeast strains with deleted genes involved in K<sup>+</sup> influx, only surviving in high potassium media, have been used in this project:  $\Delta TRK1 \Delta TRK2 \Delta TOK1$  PLY246,  $\Delta TRK1 \Delta TRK2$  SGY1528, and  $\Delta TRK1 \Delta TRK2$  R5421. Open reading frames (ORFs) encoding a subunit of TASK3, TREK1, 5HT<sub>3A</sub>, and TOK1 fused to Venus-YFP were assembled into yeast expression vectors and transformed into these yeast strains.

We have been able to construct and test over 50 combinations of promoter, open reading frame (ORF), and terminator so far thanks to the Yeast Tool Kit (Lee *et al.*, 2015) and Golden Gate cloning method. This is a method of cloning that consists of distinct parts which fit together in a specific order, due to the prefix and suffix overhang sequences, which allowed us to construct cassette plasmids from scratch (Figure 8).

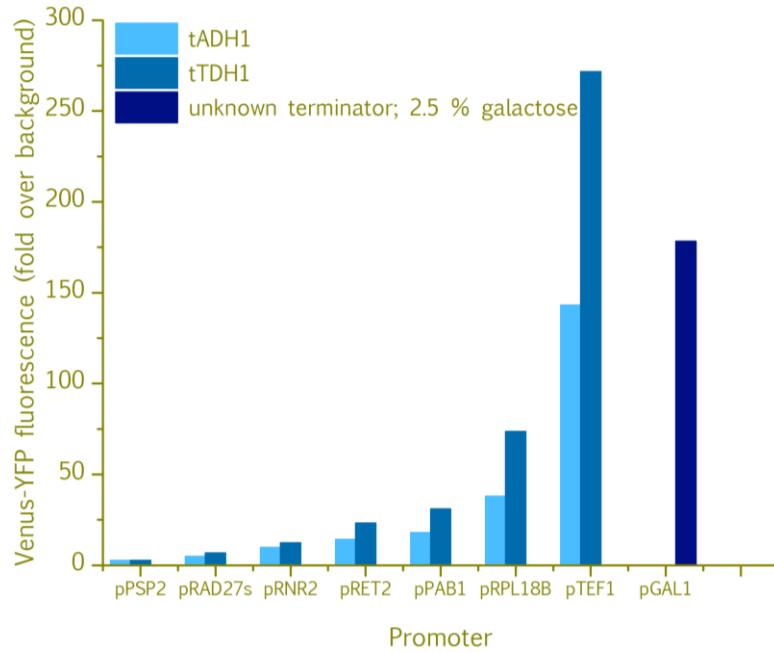
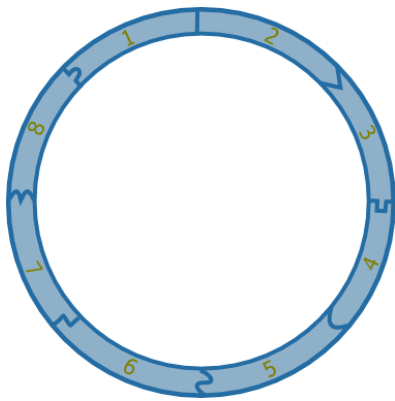


**Figure 8. The main structure of Yeast Tool Kit generated cassette plasmids.**

This consists of the following:

1. Connector
2. Promoter
3. ORF
4. Terminator
5. Connector
6. Yeast auxotrophic marker
7. Yeast origin
8. *E. coli* antibiotic marker and origin

**Graph 1. Expression strength of promoters and selected terminators used.**

Expression level of Venus-YFP is illustrated as fold fluorescence over background by flow cell cytometry. Data produced by the Dueber lab (unpublished).

The cloning also consisted of a “one-pot” reaction (i.e. digestion and ligation occur in one reaction), rendering it more efficient. By creating and using ready-made part plasmids we were able to combine parts quickly and efficiently to test parameters that may affect gene expression (such as promoters, Graph 1) and protein translocation in yeast. Due to this, we decided that due to time constraints and an overwhelming number of parameters that could affect protein processing in yeast, it may be more efficient to study the TOK1 channel as this can be expressed well in yeast; rather than mammalian channels which did not translocate to the plasma membrane under the conditions tried. Efforts focussed on working with the TOK1 channel for which we were able to demonstrate translocation at the plasma membrane.

Prior to exposing K<sup>+</sup> influx-deficient yeast overexpressing TOK1 to halothane, preliminary experiments included investigating the effect of liquid TOK1 agonist arachidonic acid on yeast growth; setting up an airtight, stable, and adjustable halothane exposure system in which yeast agar plates and liquid cultures can be grown, and demonstration of successful gene expression after performing yeast transformation-associated recombination. These procedures are tried and tested techniques which can be used to transform yeast with randomly mutated TOK1 sequences and expose them to selection pressures of halothane and CNO / Compound 21. They provide a foundation for next experimental steps as well as detailed further work to increase efficiency and throughput of methods.

Next steps would involve exposing K<sup>+</sup> influx-deficient yeast overexpressing TOK1 to halothane. This would allow for the identification of whether the drug is able to open the channel to allow a greater uptake of K<sup>+</sup> and yeast survival in low potassium media.

To evolve TOK1, we planned to follow a similar method to Armbruster *et al.* (2007; Figure 6). The ORF of TOK1 would be subjected to error-prone PCR mutagenesis before mutant libraries are transformed and expressed in *S. cerevisiae*. Following this, yeast would be exposed to halothane and growth rate would be measured to identify cells growing at a statistically significantly higher rate than those expressing WT TOK1. Mutated ORFs would then be sequenced to identify amino acid changes which allow halothane to increase TOK1 activation. Site directed mutagenesis of these codons on TOK1 and related K<sub>2</sub>P<sub>s</sub> would then be carried out to verify whether these amino acids are indeed involved in halothane binding.

Upon successful cloning of mutant TOK1 libraries in a suitable yeast vector, the process of random mutagenesis and transformation into yeast would be repeated until mutated TOK1 allow cells to survive in low potassium media in the presence of clozapine. Rounds of random mutagenesis would be carried out, with transformed yeast cultured in decreasing concentrations of CNO / Compound 21. The resultant construct should allow yeast to survive in 5 μM CNO / Compound 21 but not in clozapine, acetylcholine, or media without the ligand. Control yeast strains expressing WT TOK1 and/or Venus-YFP would be grown in the same conditions.

## 3.2 Materials and Methods

### 3.2.1 Golden Gate Part Plasmid Cloning

Part plasmids of the Golden Gate Yeast Tool Kit (Lee *et al.*, 2015) were donated by the Ellis lab. The following part plasmids were cloned to for later use in cassette plasmids (Table 1).

Part Type	Channel	
3b	5HT3A	
3b	TASK3	
3b	TREK1	
3a	5HT3A	
3a	TASK3	
3a	TREK1	
3b	5HT3A	STOP codon removed
3b	TASK3	
3b	TREK1	
3a	TOK1	

Table 1. Channel ORF parts generated for Golden Gate cloning using the Yeast Tool Kit

## PCR for Golden Gate cloning

The inserts were generated by PCR using the following primers:

5HT3A part 3a forward GCATCGTCTCATCGGTCTCATATGAGATTGTGCATACCACAAGTCTTGT;  
5HT3A part 3a reverse ATGCCGTCTCAGGTCTCAAGAACCGGATCCGCTATAATGCCAGATAGAC;  
TASK3 part 3a forward GCATCGTCTCATCGGTCTCATATGAAGAGACAAAACGTCAGAACATTA;  
TASK3 part 3a reverse ATGCCGTCTCAGGTCTCAAGAACCCACAGATTTCCCTCCTCTTCATCAAC;  
TREK1 part 3a forward GCATCGTCTCATCGGTCTCATATGGCAGCTCCAGACTTGTGGATCC;  
TREK1 part 3a reverse ATGCCGTCTCAGGTCTCAAGAACCCCTTGATGTTCTCTATCACAGCAATTTTC;  
5HT3A –STOP part 3b forward GCATCGTCTCATCGGTCTCATTCTAGATTGTGCATACCACAAGTCTTG;  
5HT3A –STOP part 3b reverse ATGCCGTCTCAGGTCCGGATCCGCTATAATGCCAGATAGACC;  
TASK3 –STOP part 3b forward  
GCATCGTCTCATCGGTCTCATTCTAAGAGACAAAACGTCAGAACATTAAG;  
TASK3 –STOP part 3b reverse ATGCCGTCTCAGGTCCGGATCCCACAGATTTCCCTCCTCTTCATCAACC;  
TREK1 –STOP part 3b forward GCATCGTCTCATCGGTCTCATTCTGCAGCTCCAGACTTGTGGATCC;  
TREK1 –STOP part 3b reverse TGCCGTCTCAGGTCCAGGATCCCTTGATGTTCTCTATCACAGC.

The protocol and reagent volumes used were: 95 °C pre-cycle initialisation 1 min, 95 °C denaturation 30 s, 65 °C annealing 30 s, 72 °C elongation 3 m, 35 cycles, 72 °C final elongation 15 m; forward primer (20 µM) 1 µL, reverse primer (20 µM) 1 µL, template DNA 200 ng, *Pfu* Buffer with MgSO<sub>4</sub> (Thermofisher Scientific) 5 µL, *Pfu* DNA Polymerase recombinant (2.5 U.µL<sup>-1</sup>; Thermofisher Scientific) 1 µL, RNase-free water total the reaction to 50 µL.

## Golden Gate cloning

These constructs were assembled into part plasmids using 25 fmoles of each construct and entry vector pYTK001, NEB BsmBI and T7 ligase both 0.5 µL, NEB T7 ligase buffer 5 µL, and RNase-free water for a total reaction of 10 µL. The reactions were subjected to 42 °C 2 m digestion, 16 °C 5 m ligation, 40 cycles, 60 °C 10 m final digestion, 80 °C 10 m enzyme denaturation.

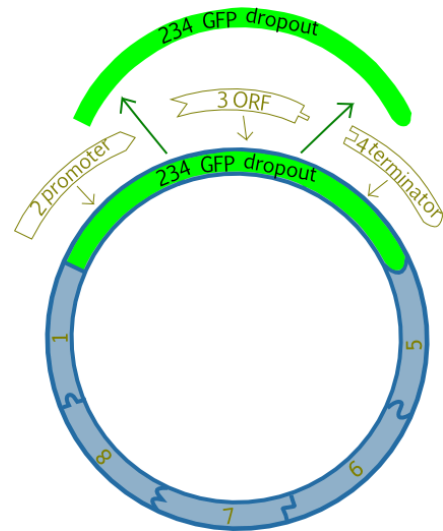
The cassettes were amplified using New England Biolabs® Turbo Competent *E. coli* (High Efficiency; catalogue number C2984) via heat-shock transformation using bacteria 42 µL and KCM (500 mM KCl, 150 mM CaCl<sub>2</sub>, 250 mM MgCl<sub>2</sub>) 8 µL per assembly mix on ice for 10 min, 1 m heat shock at 42 °C, placed on ice for 1 min, addition of SOC broth (tryptone 1 g, yeast extract 250 mg, NaCl 25 mg, MgCl<sub>2</sub> (1 M) 0.5 mL, MgSO<sub>4</sub> (1 M) 0.5 mL, glucose (2 M) 0.5mL) 450 µL and incubated at 37 °C 1 h. The cells were then plated on agar plates containing chloramphenicol for screening. Single colonies not expressing GFP underwent mini-inoculations by growing them in Sigma-Aldrich LB broth with chloramphenicol 5 mL at 37 °C for 16 h, and plasmids were purified using Sigma GenElute Plasmid Miniprep Kit according to manufacturer's instructions. The part plasmids were then digested with NEB BsaI and Cutsmart buffer, electrophoresed on 0.8 % agarose, and then sequenced.

### 3.22 Golden Gate cassette plasmid cloning

The part plasmid assemblies were used to assemble cassette plasmids with Venus using the same Golden Gate protocol as described previously. To increase the likelihood of assembling up to 10 parts, an entry vector previously assembled with a part 234 GFP dropout was used. This meant that only parts 2-4 needed to be cloned into the entry vector by replacing the GFP dropout (Figure 9). The cassette plasmids were then transformed following the same protocol as previously described, purified using Sigma GenElute Plasmid Miniprep Kit according to manufacturer's instructions, digested with NEB BsmBI and Buffer 3.1, electrophoresed on 0.8 % agarose, and partially sequenced (Table 2).

**Figure 9. Cassette entry vector with part 234 dropout.**  
 The GFP dropout is removed by Bsal digestion and replaced by parts 2, 3 (or 3a and 3b), and 4 (or 4a and 4b) during cassette plasmid cloning.

1. Connector
2. Promoter
3. ORF
4. Terminator
5. Connector
6. Yeast auxotrophic marker
7. Yeast origin
8. *E. coli* antibiotic marker and origin



Cassette ID #	Part 2 (promoter)	Part 3a (ORF)	Part 3b (ORF)	Part 4a (ORF)	Part 4b (ORF)
1	pRNR2	Part 3 Venus-YFP		tADH1	
2	pRNR2			tTDH1	
3	pTEF1			tADH1	
4	pTEF1			tTDH1	
5	pRPL18B			tADH1	
6	pRPL18B			tTDH1	
13	pRNR2	Venus-YFP	5HT <sub>3A</sub>	tADH1	
14	pTEF1	Venus-YFP	5HT <sub>3A</sub>	tTDH1	
15	pRPL18B	Venus-YFP	5HT <sub>3A</sub>	tADH1	
19	pRNR2	Venus-YFP	TREK1	tTDH1	
20	pTEF1	Venus-YFP	TREK1	tADH1	
21	pRPL18B	Venus-YFP	TREK1	tTDH1	
25	pRNR2	Venus-YFP	TASK3	tADH1	
26	pTEF1	Venus-YFP	TASK3	tTDH1	
27	pRPL18B	Venus-YFP	TASK3	tADH1	
33	pTEF1	Venus-YFP	5HT <sub>3A</sub>	GSCIICGS (plasma membrane targeting part; PMT)	tADH1
34	pRNR2	Venus-YFP	TREK1		tADH1
35	pRPL18B	Venus-YFP	TASK3		tADH1
36	pRPL18B	GSCIICGS (plasma membrane targeting part; PMT)	5HT <sub>3A</sub>	Venus-YFP	tADH1
37	pTEF1		TREK1	Venus-YFP	tADH1
38	pRNR2		TASK3	Venus-YFP	tADH1
39i	pRPL18B		TASK3	Venus-YFP	tADH1

Cassette ID #	Part 2 (promoter)	Part 3a (ORF)	Part 3b (ORF)	Part 4a (ORF)	Part 4b (ORF)
39ii	pPAB1	Venus-YFP	TASK3	Part 4 tADH1	
40	pPAB1	Venus-YFP	TASK3	Part 4 tTDH1	
41	pRET2	Venus-YFP	TASK3	Part 4 tADH1	
42	pRET2	Venus-YFP	TASK3	Part 4 tTDH1	
43	pRAD27s	Venus-YFP	TASK3	Part 4 tADH1	
44	pRAD27s	Venus-YFP	TASK3	Part 4 tTDH1	
45	pPSP2	Venus-YFP	TASK3	Part 4 tADH1	
46	pPSP2	Venus-YFP	TASK3	Part 4 tTDH1	
45a	pRNR2	Mating factor alpha signal sequence	5HT <sub>3A</sub>	Venus-YFP	tADH1
46a	pRPL18B	Mating factor alpha signal sequence	5HT <sub>3A</sub>	Venus-YFP	tADH1
47	pTEF1	Mating factor alpha signal sequence	5HT <sub>3A</sub>	Venus-YFP	tADH1
48	pRNR2	Mating factor alpha signal sequence	TASK3	Venus-YFP	tADH1
49	pRPL18B	Mating factor alpha signal sequence	TASK3	Venus-YFP	tADH1
50	pTEF1	Mating factor alpha signal sequence	TASK3	Venus-YFP	tADH1
51	pRNR2	Mating factor alpha signal sequence	TREK1	Venus-YFP	tADH1
52	pRPL18B	Mating factor alpha signal sequence	TREK1	Venus-YFP	tADH1
53	pTEF1	Mating factor alpha signal sequence	TREK1	Venus-YFP	tADH1
54	pRNR2	5HT <sub>3A</sub>	Venus-YFP	Part 4 tADH1	
55	pRPL18B	5HT <sub>3A</sub>	Venus-YFP	Part 4 tADH1	
56	pTEF1	5HT <sub>3A</sub>	Venus-YFP	Part 4 tADH1	
57	pRNR2	TREK1	Venus-YFP	Part 4 tADH1	
58	pRPL18B	TREK1	Venus-YFP	Part 4 tADH1	
59	pTEF1	TREK1	Venus-YFP	Part 4 tADH1	
60	pRNR2	TASK3	Venus-YFP	Part 4 tADH1	
61	pRPL18B	TASK3	Venus-YFP	Part 4 tADH1	

Cassette ID #	Part 2 (promoter)	Part 3a (ORF)	Part 3b (ORF)	Part 4a (ORF)	Part 4b (ORF)
62	pTEF1	TASK3	Venus-YFP	Part 4 tADH1	
63	pTEF1	TOK1	Venus-YFP	Part 4 tADH1	
64	pRNR2	TOK1	Venus-YFP	Part 4 tADH1	
65	pRPL18B	TOK1	Venus-YFP	Part 4 tADH1	
Empty vector	pTEF1	Part 3 Empty spacer		Part 4 tADH1	

Table 2. Cassette plasmids constructed using Yeast Tool Kit parts using the Golden Gate cloning

### 3.23 Digestion/ligation cloning

The transformation of hTASK3 (h indicating lack of codon optimisation for *S. cerevisiae*) under the regulation of the MET promoter in the plasmid pYES2 was unable to complement the deletion of genes required for the influx of K<sup>+</sup> in *S. cerevisiae*. As Bernstein *et al.* (2013) had demonstrated that the same plasmid construct was functional in efflux-deficient yeast strain B31 (*MATa ena1-4\_::HIS3 nba1\_::LEU2*), which is isogenic to influx-deficient yeast strain SGY1528 as they were both derived from WT W303 (see below for genotypes), we constructed N and C terminus fusions with Venus-YFP to observe spatial location of the protein.

#### PCR for digestion / ligation cloning

To generate a Venus-YFP sequence to be cloned upstream of hTASK3 a PCR reaction was carried out using forward primer CGAAATGGATCCATGTCTAAAGGTGAAGAATTATTCACTGGTGTGTCC and reverse primer GCTTTAGAATTCACAAATAATACATTTGTACAATTCATACCTGG.

To clone the C-terminus hTASK3:Venus-YFP fusion, two PCR products for each sequence were generated using primers:

hTASK3 for C-terminus fusion forward CGAAATGGATCCATGAAGAGGCAGAACGTGCGGACTCTGT;

hTASK3 for C-terminus fusion reverse GCTTTACCCGGGAACGGACTTCCGGCGTTTCATCAG; Venus-YFP and Venus-YFP for C-terminus fusion reverse

GCACGCGAATTCCTATTTGTACAATTCATCCATACCATGGGTAATACCAGC.

#### Digestion and ligation

For N terminus fusion cloning, Venus-YFP PCR product and 6 µg of plasmid construct pYES2-hTASK3 were digested using NEB BamHI-HF and EcoRI-HF in 1 x Cutsmart buffer at 37 °C for 3.5 h. Following digestion, linearised pYES2-hTASK3 was gel purified using Qiagen Gel Extraction Kit according to manufacturer's instructions. For C-terminus fusion cloning, hTASK3 PCR product and pYES2-hTASK3 were digested using NEB enzymes BamHI-HF and SmaI at 30 °C for 3.5 h. Vector pYES2 was then separated from hTASK3 using Qiagen Gel Extraction Kit according to manufacturer's instructions. The purified vector backbone was then ligated to the PCR amplified constructs using 50 ng plasmid to 1:1, 1:3, 1:5, 1:7 molar ratio of plasmid to insert using NEB T4 DNA Ligase according to manufacturer's specifications in the presence of its buffer. This resulting pYES2-hTASK3 plasmid and Venus-YFP PCR product were then digested using enzymes SmaI and EcoRI, before linearised pYES2-hTASK3 was gel purified using Qiagen Gel Extraction Kit. The ligation of pYES2-hTASK3 and Venus-YFP was then carried out using molar ratios of vector and insert as above.

Plasmid constructs were amplified and purified using the methods described previously. 3  $\mu$ L of each eluted plasmid was then digested using the same restriction enzymes used in the cloning protocol for 2.5 h before verifying the digested insert size by 0.8 % agarose gel electrophoresis.

### 3.24 Colony PCR for yeast transformation-associated recombination

PCR was conducted using transformed yeast samples that had been imaged and primers that had been used to generate linear TOK1-VenusYFP sequences. The touchdown PCR protocol and reagent volumes used were: 95 °C pre-cycle initialisation 1 min, 95 °C denaturation 30 s, 65 °C annealing 30 s, 72 °C elongation 3 m, 10 cycles decreasing annealing temperature by 1°C each time; 95 °C denaturation 30 s, 55 °C annealing 30 s, 72 °C elongation 3 m, 24 cycles , 72 °C final elongation 5 m; forward primer (5  $\mu$ M) 0.25  $\mu$ L, reverse primer (5  $\mu$ M) 0.25  $\mu$ L, transformed yeast or positive control template , *Pfu* Buffer with MgSO<sub>4</sub> (Thermofisher Scientific) 5  $\mu$ L, *Pfu* DNA Polymerase recombinant (2.5 U. $\mu$ L<sup>-1</sup>; Thermofisher Scientific) 1  $\mu$ L, RNase-free water total the reaction to 50  $\mu$ L.

### 3.25 Yeast growth

The haploid *Saccharomyces cerevisiae* yeast strains used are listed on the Table 3, below.

Strain	Genotype	Source
WT PLY232	<i>MATa his3D200 leu2-3,112 trp1D901 ura3-52 suc2D9</i>	Bertl <i>et al.</i> , 2003 Donated from Prof. Per O. Ljungdahl
$\Delta$ <i>TRK1</i> $\Delta$ <i>TRK2</i> $\Delta$ <i>TOK1</i> PLY246	<i>MATa his3D200 leu2-3,112 trp1D901 ura3-52 suc2D9 trk1D51 trk2D50::lox-kanMX-lox tok1D1::HIS3</i>	Bertl <i>et al.</i> , 2003 Donated from Prof. Stephen Tucker
$\Delta$ <i>TRK1</i> $\Delta$ <i>TRK2</i> SGY1528	<i>MATa ade2-1 can1-100 his3-11,15; leu2-3,112 trp1-1 ura3-1 trk1::HIS3 trk2::TRP1</i>	Donated from Prof. Stephen Tucker
$\Delta$ <i>TRK1</i> $\Delta$ <i>TRK2</i> R5421	<i>ura3-52 his3D200 leu2<math>\Delta</math>1 trp1<math>\Delta</math>1 ade2 trk1::HIS3 trk2::HIS3</i>	Donated from Prof. Stephen Tucker
WT BY4741	<i>MATa his3<math>\Delta</math>1 leu2<math>\Delta</math>0 met15<math>\Delta</math>0 ura3<math>\Delta</math>0</i>	Donated from Dr. Tom Ellis
WT W303	<i>MATa/MAT<math>\alpha</math> {leu2-3,112 trp1-1 can1-100 ura3-1 ade2-1 his3-11,15 [ph<sup>+</sup>]}</i>	Used under supervision of Prof. Susan Ferro-Novick

Table 3. *Saccharomyces cerevisiae* yeast strains used

The growth of PLY246, SGY1528, and R5421 were measured by inoculating colonies previously streaked on Fluka Yeast Extract Agar (Sigma-Aldrich) in 5mL YPD media (glucose 20 g, peptone 20 g, yeast extract 10 g dissolved in water 1 L), and measuring OD<sub>600</sub> at various time intervals. 1 OD unit at 600 nm wavelength light is equivalent to 1 x 10<sup>7</sup> cells. Growth analysis was carried out on OriginPro 2016 (Academic) using a sigmoidal curve and Boltzmann Fit or linear fit with iterations.

### 3.26 Yeast transformations

Strain PLY246, was transformed with the cassette plasmids listed in the table above. PLY232 was transformed with the empty vector to be used as a positive control in growth assays. BY4741, SGY1528 and R5421 were transformed with cassettes 13 to 53. Plasmids 63 and 65 were also transformed into SGY1528 and R5421. Plasmid pBG1805 containing TOK1 under the regulation of pGAL1 promoter (GE Dharmacon, catalogue number YSC3867-202327698) was also transformed into PLY246, SGY1528, and R5421.

Yeast were stored in 30 % glycerol at -80 °C and streaked on Fluka Yeast Extract Agar (Sigma-Aldrich) before 24 h incubation at 30 °C. Per three transformations, one yeast colony was used to inoculate 5 mL YPD media at 30 °C whilst shaking at 225 rpm overnight until OD 600 reached 0.5-1.3 (around 16 h; measured using Amersham Ultraspec10 with an accuracy of  $\leq \pm 0.05$ ). The culture was centrifuged for 5 minutes at 2000 G before supernatant was discarded and cells were washed with sterile water and a second time with lithium acetate 100 mM. Polyethylene

glycol 3350 (50 %) 240  $\mu$ L, lithium acetate (1M) 36  $\mu$ L, and salmon sperm DNA (2  $\mu$ g.mL<sup>-1</sup>) 25  $\mu$ L which had been boiled at 100 °C for 10 minutes were added to the cell pellet. The pellet was resuspended and 1  $\mu$ g of each plasmid or TOK1-VenusYFP linear DNA was added to 117  $\mu$ L of the transformation mixture and heat shocked at 42 °C for 1 h. Following this, the mixture was centrifuged at 6000 G for 1 m and the supernatant was discarded. Each pellet was resuspended in 1 mL YPD and incubated at 30 °C whilst shaking at 225 rpm for 1h. The mixture was centrifuged as previously described, and washed twice with water before being resuspended in 100  $\mu$ L water and plated on -URA plasmid selective agar (bacto agar 20 g, -URA dropout powder 1.15g, yeast nitrogen base (without amino acids) 6.7 g, glucose 20 g, KCl 7.46 g dissolved in water 1L; Bagriantsev & Minor Jr., 2013) and cultured at 30 °C for 72-120 h. For experiments involving transformation-associated recombination of linear DNA, the pellet was resuspended in 100  $\mu$ L water and pipetted at 2  $\mu$ L at a time to generate 50 artificial colonies on Fluka Yeast Extract Agar (Sigma-Aldrich) plates. Plates were incubated at 30 °C for 3-5 days.

### 3.27 Fluorescence microscopy

Transformed colonies were purified by streaking single colonies on -URA plates. Single colonies were then grown in -URA selective media (as described but without agar) overnight at 30 °C and 225 rpm until they reached an OD<sub>600</sub> of 0.8-1.3 and were imaged on a light microscope at 100 x magnification. At the University of San Diego, this was done using the Axio Imager Z1 fluorescence microscope (Carl Zeiss) using a 100 $\times$  1.3 NA oil-immersion objective. Images were captured with an AxioCam MRm digital camera under DIC or fluorescence and analysed using AxioVision software (Carl Zeiss). In the Franks and Wisden lab, this was the Nikon Eclipse 80i fluorescence microscope using a 100 $\times$  1.3 NA oil-immersion objective. Image capture was done using the Qimaging publisher 3.3 camera under brightfield or fluorescence and Q Capture Pro-7 software.

### 3.28 Spotting assays

Single purified colonies were inoculated in -URA selective media at 30 °C and 225 rpm for 16-24h. For cells to be spotted on plates alongside yeast transformed with pBG1805-TOK1, growth of cultures was stopped after 16h. 40  $\mu$ L of the culture was then added to 5 mL of -URA selective media with 2 % raffinose (instead of glucose). Cultures were grown for 40 h before YPD with 6% galactose (instead of 2 % glucose) was added and grown for a further 6 h. This was carried out in order to activate the pGAL1 promoter on the plasmid to express TOK1.

OD<sub>600</sub> measurements were taken of cultures and they were washed twice by pelleting at 6000 G and using sterile water. They were then diluted to match the lowest OD reading of the samples that were to be spotted on the same plate. 10-fold serial dilutions were then carried out. 2  $\mu$ L of each sample was then pipetted onto -URA K<sup>+</sup>-selective agar plates (arginine (free base) 2.1 g, dropout powder -URA 1.15 g, dextrose or galactose 10 g, 1,000 $\times$  trace minerals stock solution (boric acid 50 mg, CuSO<sub>4</sub> 4 mg, KI 10 mg, FeCl<sub>3</sub> 50 mg, MnSO<sub>4</sub> 40 mg, molybdic acid 90 mg, ZnSO<sub>4</sub>, 100 mL water, HCl 1 mL) 1 mL, 1,000 $\times$  vitamin stock solution (biotin 2 mg, D-pantothenic acid 400 ng, pyridoxine 400 mg, thiamin 400 mg, inositol 2 g, 100 mL water) 1 mL, 1 M MgSO<sub>4</sub> 1 mL, 1 M CaCl<sub>2</sub> 100  $\mu$ L; Bagriantsev & Minor Jr., 2013).

In arachidonic acid experiments, 3, 6, or 9  $\mu$ L arachidonic acid (Cayman Chemical, catalogue CAY90010) was added to agar plates prior to setting to obtain 100, 200, and 300  $\mu$ M concentrations respectively. Control plates had 3, 6, or 9  $\mu$ L ethanol added. For halothane experiments, one plate from each replicate pair was incubated in air and halothane 5 % at 30 °C for 3 days. Three to five replicates were carried out per yeast strain, vector, potassium concentration, and arachidonic acid / equivalent ethanol or air / halothane 5 % condition. Plates were incubated at 30 °C for 5-7 days.

### 3.29 Halothane exposure chamber

A valve on a regulator of an air cylinder was connected to a halothane vapouriser (Medical Supplies and Services Intl. Ltd) via polytetrafluoroethylene tubing of 1 cm diameter. The vapouriser was connected to flow meter RS1 (GPE Scientific Ltd.). A tube was connected to a second valve on the gas regulator. Tubing from the flow meter and the second gas regulator valve was threaded through an access port of a temperature-controlled incubator (Genlab INC/150/DIG) to connect to two airtight plastic boxes. An outlet tube was connected from the halothane box out of a thermometer port to a veterinary fluorosorber (Harvard Apparatus). Two holes were drilled at opposite ends of plastic boxes (Lock & Lock Rectangular Storage Container, 2.6 L) to fit tubing connectors (Bel-Art, 6-9 mm) using air leak-proof epoxy resin (Araldite® Standard). Boxes were tested for airtightness by submerging them in water after being pumped full of air and observing lack of bubbles.

The airflow system was tested for airtightness by submerging tubes coming from the vapouriser outlet in water, flowing air through at 1 atm and measuring water displacement in an inverted measuring cylinder over 10, 15, and 25 s and verifying that volume displacement of air through the flow meter outlet at 15 RS units was the same. A minimum of ten readings were taken at each time point.

To verify the percentage of halothane released by the vapouriser, it was connected to Anaesthetic Agent Monitor 7860 (Kontron Instruments) and the vapouriser was set to 1, 2, 3, 4, and 5 % with air pumped through at 1 atm. Readings were taken after 20 minutes at each percentage level.

### 3.210 Yeast growth with agonists

Yeast strains  $\Delta TRK1\Delta TRK2\Delta TOK1$  PLY246,  $\Delta TRK1\Delta TRK2$  SGY1528,  $\Delta TRK1\Delta TRK2$  R5421 transformed with vectors Empty Vector, #63 pTEF1-TOK1, #65 pRPL18B-TOK1, or pYES-TRK1 were grown as described.

#### *Liquid growth assays*

Single purified colonies were inoculated in 96  $\mu$ L of 0.5 mM K<sup>+</sup> -URA selective media (arginine (free base) 2.1 g, dropout powder -URA 1.15 g, dextrose 10 g, 1,000 $\times$  trace minerals stock solution (boric acid 50 mg, CuSO<sub>4</sub> 4 mg, KI 10 mg, FeCl<sub>3</sub> 50 mg, MnSO<sub>4</sub> 40 mg, molybdic acid 90 mg, ZnSO<sub>4</sub>, 100 mL water, HCl 1 mL) 1 mL, 1,000 $\times$  vitamin stock solution (biotin 2 mg, D-pantothenic acid 400 ng, pyridoxine 400 mg, thiamin 400 mg, inositol 2 g, 100 mL water) 1 mL, 1 M MgSO<sub>4</sub> 1 mL, 1 M CaCl<sub>2</sub> 100  $\mu$ L; distilled water 1 L; Bagriantsev & Minor Jr., 2013) in at 30 °C and from which 7  $\mu$ L was added to 6 wells on the same 96 well micro-titer plate and 7 wells on another 96 well plate. Sets of -URA media were made up produce 0.5, 1, 2, 3, 5, 20, and 100 mM K<sup>+</sup> total, and 143  $\mu$ L of -URA media at each K<sup>+</sup> concentration was added to each colony on the two sets of plates.

OD<sub>600</sub> readings were taken using the Tecan *Sunrise*<sup>TM</sup> microplate reader using Megallan<sup>TM</sup> software. Plates were then separated into airtight boxes and halothane 5 % or air was pumped through the boxes at a flow rate of 2.12 cm<sup>3</sup>.sec<sup>-1</sup> and incubated at 30 °C and 225 rpm for 24 or 48 h following which OD<sub>600</sub> were taken again. Three to five replicates were carried out per yeast strain, vector, and potassium concentration condition.

### 3.211 Statistical Analysis

#### Chi-squared test

Chi-squared test was carried out using Excel Office 2013 to identify the effect of arachidonic acid on yeast growth.

#### Post-hoc Fisher's exact test

Following Chi-squared, a Fisher's exact was carried out using R version 3.5 to identify the statistical significance of differences between expected and observed growth of yeast in the presence or absence of arachidonic acid.

#### Analysis of Variance

ANOVA was carried out using R version 3.5 to identify effects of receptor expression and presence or absence of agonists halothane 5 % on yeast growth.

#### Post-hoc t-test

Following ANOVA, a t-test was carried out using R version 3.5 to identify the statistical significance of growth difference due to effects of receptor expression (empty vector, TOK1, and TRK1) in yeast strain R5421 between halothane 5 % and air 100 %.

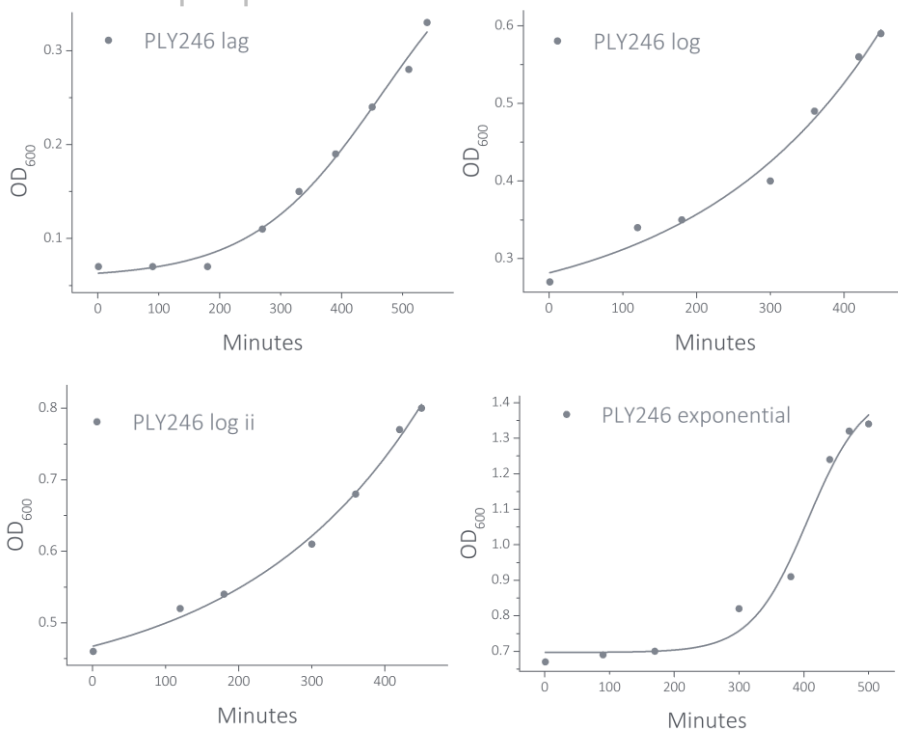
# Chapter IV: Results

Experiments were performed on *Saccharomyces cerevisiae* yeast for convenience of protein expression in a eukaryotic organism. Yeast strains had modified K<sup>+</sup>-influx systems and only survived in high potassium media. Overexpressing a functioning potassium channel at the plasma membrane could complement this disrupted system and allow cells to grow in low potassium media. We decided to use yeast TOK1 as a model channel, as it is evolutionarily related to mammalian channels providing a close approximation of activation of mammalian two-pore domain channels (K<sub>2</sub>P<sub>s</sub>). In early experiments we aimed to use mammalian counterparts. However, we made an important discovery that fusing a fluorescent marker to either the N or C terminus interrupts membrane localisation and thus cannot be used in the yeast model.

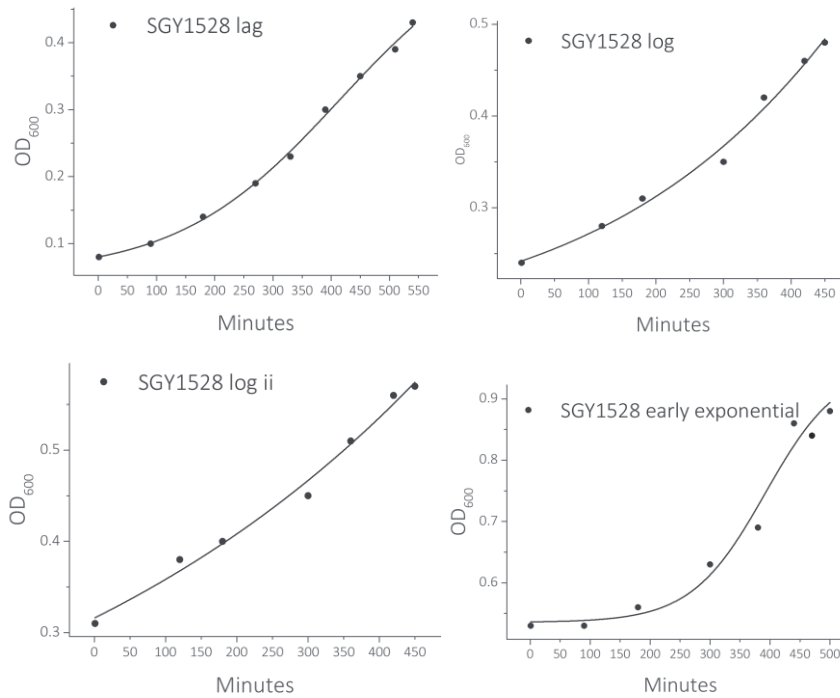
Following observation of yeast growth rates for the basis of inoculation experiments, we endeavoured to clone mammalian channels TASK3 and TREK1 (halothane targets) and 5HT<sub>3A</sub> (for designer drug activation) in *S. cerevisiae*. By using a synthetic biology Yeast Tool Kit designed for Golden Gate based modular assembly of promoter, open reading frame (ORF), tagging, and terminator parts; we were able to generate over 50 expression plasmids encoding the mammalian channels. Despite changing combinations of these modular parts, the channels were not able to be directed to the plasma membrane.

We moved onto demonstrating the expression of TOK1-VenusYFP localisation at the plasma membrane and expressed them in yeast with modified K<sup>+</sup>-influx systems. These yeast expression systems were grown in low potassium media (alongside controls), exposed to the K<sub>2</sub>P agonist arachidonic acids, and exposed to halothane anaesthetic with growth rates measured.

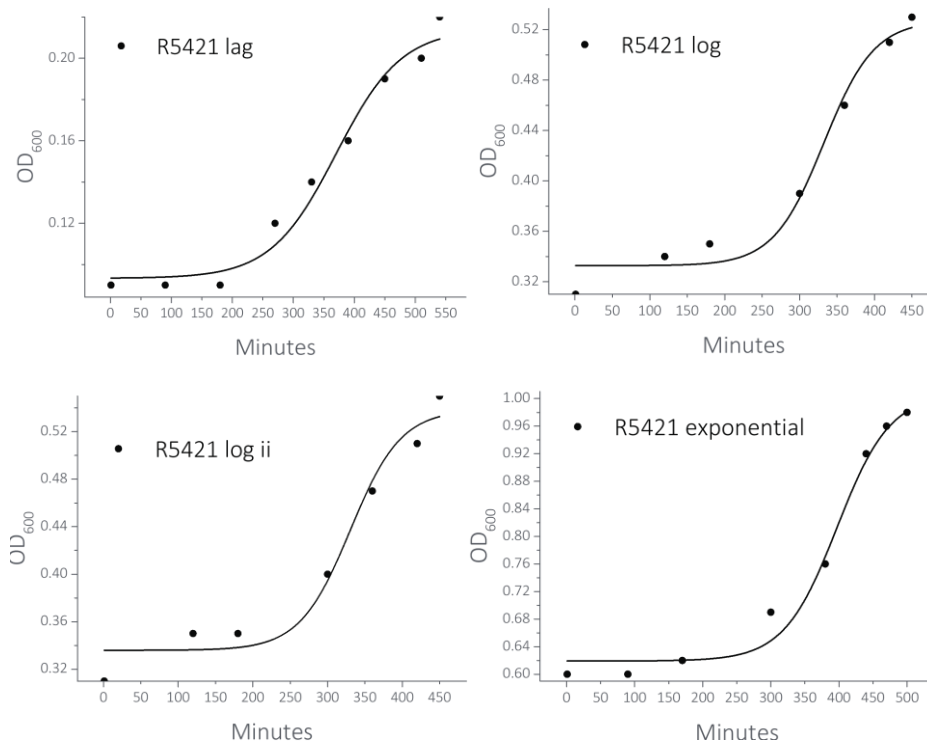
## 4.11 Understanding yeast growth rates contributes to more efficient preparation of transformations



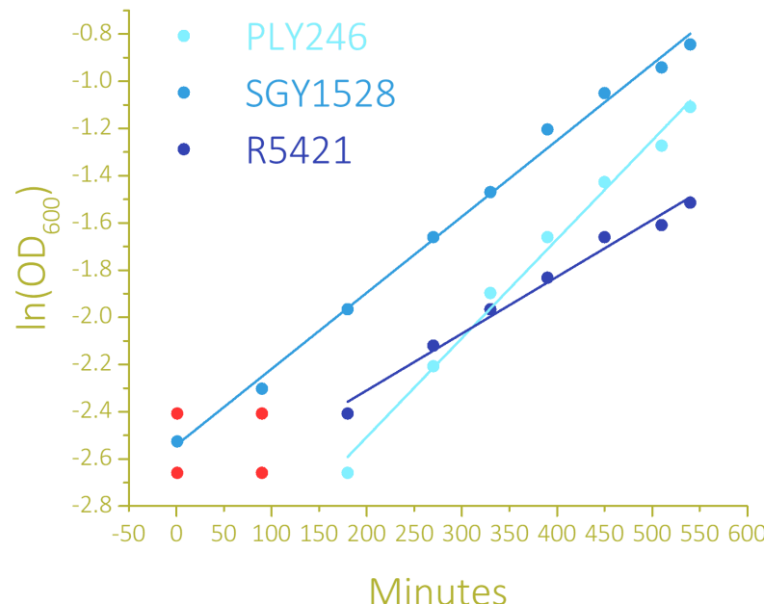
**Graph 2a. Growth graphs of PLY246 (-TOK1, -TRK1, -TRK2) at different starting ODs.** Y-axes show OD<sub>600</sub> units in increments of 0.1, but note that the maximum and minimum differ on each graph. On the graph labelled as *lag*, the starting OD<sub>600</sub> was 0.07 units. There is a clear slow lag phase before the cells reach log phase where they demonstrate a growth rate that could be illustrated as linear. On the *log* graphs, the starting OD<sub>600</sub> was 0.27 and 0.46. On the graph labelled as *exponential*, the starting OD<sub>600</sub> of 0.67 showed a clear lag phase, entered a faster growth phase, and growth slowed towards the end of the measurements which could be interpreted as the beginning of a stationary phase.



**Graph 2b. Growth graphs of SGY1528 (-TRK1, -TRK2) at different starting ODs.** Y-axes show OD<sub>600</sub> units in increments of 0.1, but note that the maximum and minimum differ on each graph. On the graph labelled as *lag*, the starting OD<sub>600</sub> was 0.08 units. On the *log* graphs, the starting OD<sub>600</sub> was 0.24 and 0.31. On these graphs, there is no clear lag phase and exponential phase and growth can be illustrated as linear, but this could be because growth had not exited lag phase before the final measurement was taken. On the graph labelled as *exponential*, the starting OD<sub>600</sub> of 0.53 did show a clear lag phase, but also reached a faster growing phase. Red indicates an anomalous measurement.



**Graph 2c. Growth graphs of R5421 (-TRK1, -TRK2) at different starting ODs.** Y-axes show OD<sub>600</sub> units in increments of 0.04, but note that the maximum and minimum differ on each graph. On the graph labelled as *lag*, the starting OD<sub>600</sub> was 0.09 units. On the *log* graphs, the starting OD<sub>600</sub> was 0.31 for both. On the graph labelled as *exponential*, the starting OD<sub>600</sub> was 0.6. All demonstrate a clear slow lag phase and following this is a log phase.



**Graph 2d. Natural log of OD<sub>600</sub> readings of PLY246 (-TOK1, -TRK1, -TRK2), SGY1528 (-TRK1, -TRK2), and R5421 (-TRK1, -TRK2) lag.** The measurements with the lowest starting OD<sub>600</sub> were used for each strain as most overnight yeast inoculations are started with an OD of *c.* 0.04. These graphs also had the most data points with a linear growth rate. The slope of each of these graphs are 0.004, 0.003, and 0.002 and R-values are 0.995, 0.997, and 0.992 respectively. Red indicates excluded measurements. Red data points are anomalies.

Yeast strains were grown in YPD media for 8-9 hours with different starting OD<sub>600</sub> (optical density at 600 nm wavelength light) units where 1 unit is equivalent to 1 x 10<sup>7</sup> cells per mL of culture (Graphs 2a-c). Observing strain growth rate is useful for several reasons. Firstly, it is important to get an idea of the growth pattern of healthy cells as this allows for the recognition of contaminated growth or unhealthy yeast cells more easily. Secondly, growth can more effectively be timed so that optical density desired (usually around 1 for most experiments, indicating late exponential phase) can be calculated and estimated during overnight growth ready for experimentation the following morning.

The three yeast strains with modified potassium influx systems  $\Delta TRK1 \Delta TRK2 \Delta TOK1$  PLY246,  $\Delta TRK1 \Delta TRK2$  SGY1528, and  $\Delta TRK1 \Delta TRK2$  R5421 were expected to have slightly different growth rates as they were derived from different parent strains affected by different background genetics. By comparing the slope of growth measurements starting with OD<sub>600</sub> inoculations in the order of magnitude 10<sup>-3</sup> units (10<sup>4</sup> cells) per mL of culture (Graph 2d) we can work out the doubling time of 173 minutes for PLY246, 231 minutes for SGY1528, and 347 minutes for R5421. This was done using the equations

$$y = mx + c \text{ and } y = \ln(2c).$$

To work out the starting OD unit for inoculations we can use the equation:

$$\text{starting OD} = \text{target OD units} / (2^{(16\text{h} / \text{doubling time})}).$$

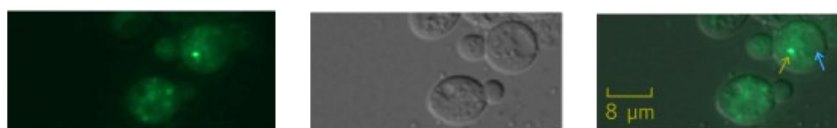
For a target OD of 1 unit, the starting inoculation used was 0.02 OD units for PLY246, 0.06 OD units for SGY1528, and 0.15 OD units for R5421 per mL of culture. We accounted for the fact that growth is not constant empirically, and therefore the concentration after 16 hours was sometimes more or less than OD 1.

4.12 Mammalian potassium channels fused to Venus-YFP at the N terminus are not translocated to the plasma membrane in  $\Delta TRK1 \Delta TRK2 \Delta TOK1$  PLY246

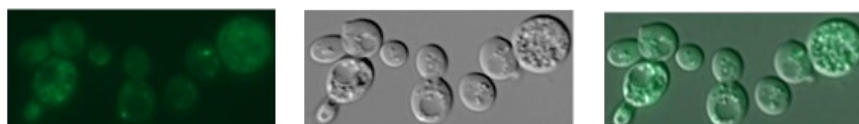
Cassette ID	Part 1 connector	Part 2 promoter	Part 3a ORF	Part 3b ORF	Part 4 terminator	Part 5 connector	Part 6 Yeast selection ORF	Part 7	Part 8 Bacterial selection ORF
13	ConS	pRNR2	Venus-YFP	5HT <sub>3A</sub>	tADH1	ConRE	URA3	CEN6/ARS4	AmpR-CoIE1
14		pTEF1			tTDH1				
15		pRPL18B			tADH1				
19		pRNR2		TREK1	tTDH1				
20		pTEF1		tADH1					
21		pRPL18B		tTDH1					
25		pRNR2		TASK3	tADH1				
26		pTEF1			tTDH1				
27		pRPL18B			tADH1				

Table 4. Cassette plasmids of N-terminus Venus-YFP and mammalian channel fusions.

a) 20 pTEF1-VenusYFP:TREK1-tADH1



26 pTEF1-VenusYFP:TASK3-tTDH1



b)

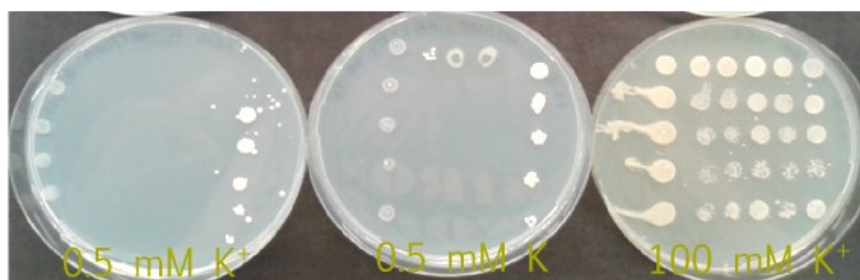


Figure 10. N-terminus VenusYFP and mammalian channel fusions transformed into PLY246 did not translocate to the membrane; a) Examples of inclusion bodies (example shown by olive arrow) formed upon expression of proteins. Blue arrow denotes a vacuole. Fluorescence, DIC, and merged images shown; b) growth assays of PLY246 transformed left to right in descending rows of ten-fold dilutions on first plate: 3 pTEF1-VenusYFP-tADH1, 13 pRNR2-VenusYFP-5HT<sub>3A</sub>-tADH1, 15 pRPL18B-VenusYFP:TREK1, 19 pRNR2-VenusYFP:TREK1-tADH1, 21 pRPL18B-VenusYFP:TREK1-tTDH1, pYES2-TRK1, middle and right plate: 3 pTEF1-VenusYFP-tADH1, 25 pRNR2-VenusYFP:TASK3-tADH1, 27 pRPL18B-VenusYFP:TASK3-tADH1, pYES2-hTASK3, pYES2-TRK1

Human TASK3 and TREK1 potassium channels, and mouse 5HT<sub>3A</sub> were codon optimised for *Saccharomyces cerevisiae* and cloned with Venus-YFP at the N terminus using the Golden Gate cloning Yeast Tool Kit (Table 4). Promoters which have been shown to induce strong (pTEF1), medium (pRPL18B) and low (pRNR2) levels of Venus-YFP expression in *S. cerevisiae* were trialled to ascertain whether this would affect the cellular location of the proteins. However, fusion proteins were not translocated to the plasma membrane to form functional channels in yeast strain PLY246 (Figure 10). Transformations which did not show Venus-YFP expression or where the fluorochrome bleached before an image could be captured are not shown.

Cassette ID	Part 2 promoter	Part 3a ORF	Part 3b ORF	Part 4a ORF	Part 4b terminator	Entry Vector
33	pTEF1	Venus-YFP	5HT <sub>3A</sub>	pYTK001	tADH1	Part 234 GFP dropout
34	pRNR2		TREK1	GSCIICGS 4a		
35	pRPL18B		TASK3	(plasma membrane targeting part)		
36	pRPL18B	GSCIICGS 3a	5HT <sub>3A</sub>	Venus-YFP 4a		
37	pTEF1	(plasma membrane targeting part)	TREK1			
38	pRNR2	TASK3				

Table 5. Cassette plasmids of Venus-YFP and mammalian channel fusions with membrane targeting parts. 38 pRNR2-PMT-TASK3:VenusYFP

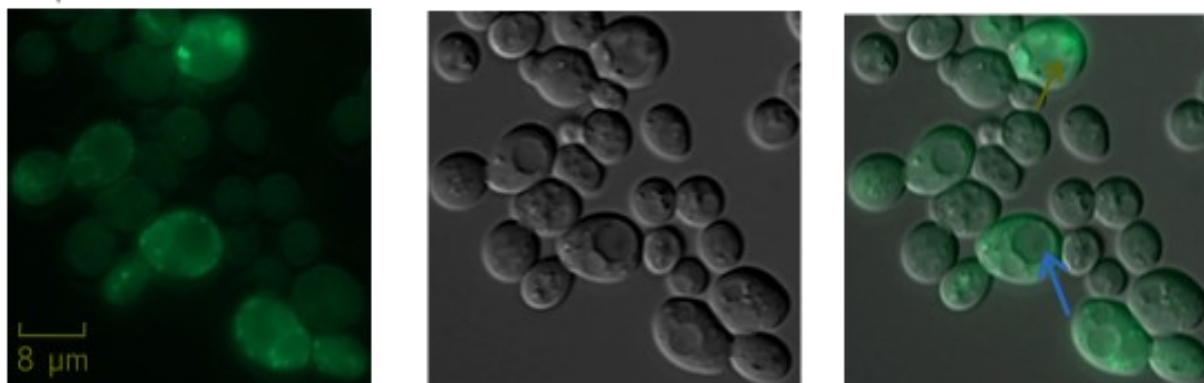
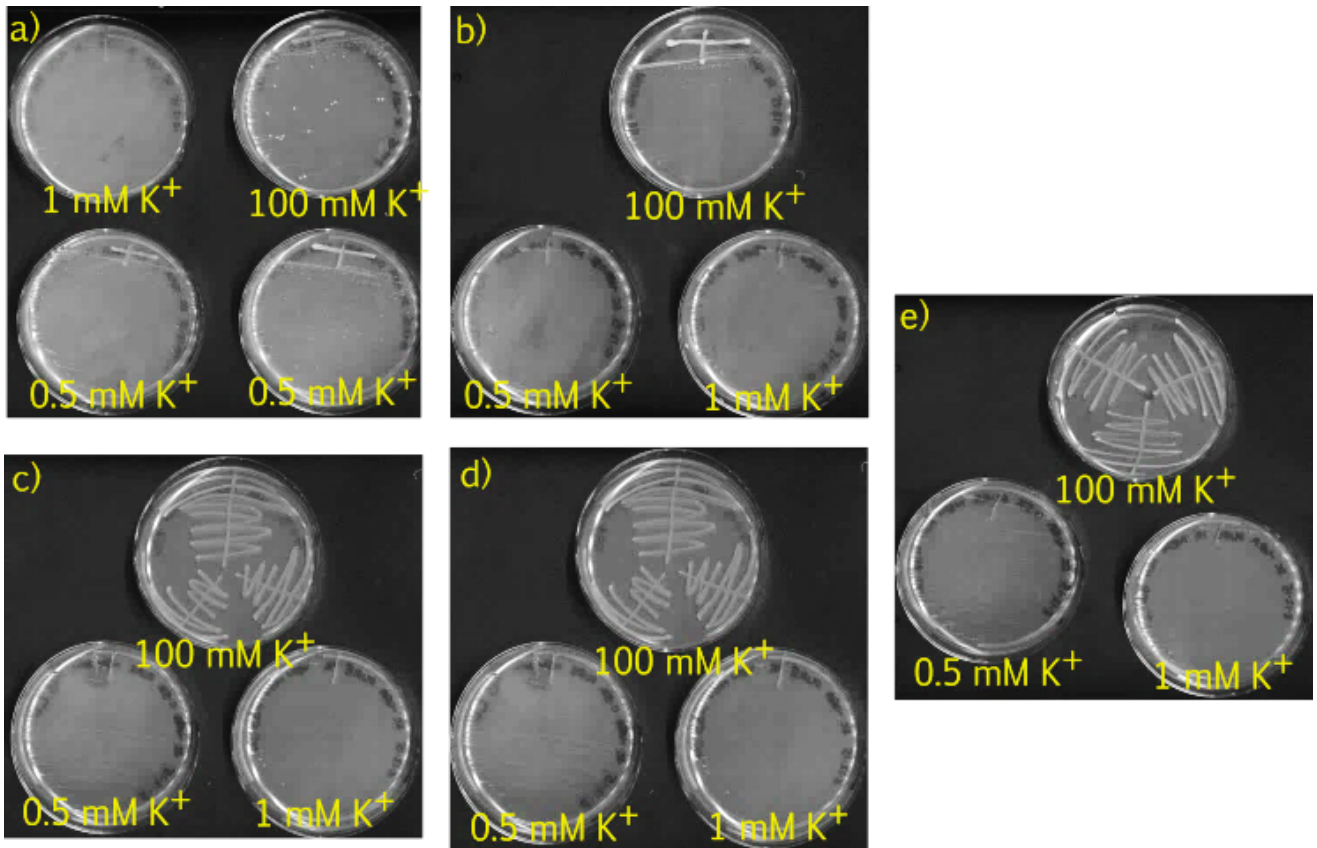


Figure 11. Venus-YFP and potassium channel fusions with plasma membrane targeting parts form inclusion bodies in PLY246 rather than embed in the plasma membrane. Expression in 38 pRNR2-PMT-TASK3:VenusYFP is representative of yeast transformed with plasmids containing plasma membrane targeting sequences (Appendix 6.4, 6.5). Images were taken at the University of California San Diego.

To try and overcome cytoplasmic expression of the exogenous protein, cassettes with N and C terminus fusions were also constructed using a part that had previously demonstrated plasma membrane targeting (donated from the Ellis Group; Table 5). This was done by using an entry vector with the same parts as those used for N-terminus cloning, save parts 2 (promoter), 3 (open reading frame), and 4 (terminator). A GFP dropout part replaced parts 2, 3, and 4 which was exchanged with the required parts during Golden Gate cloning (Figure 9). However, the membrane targeting part used was not successful in translocating the channel to the plasma membrane (Figure 11 & Appendix 6.2).



**Figure 12.** PLY246 N-terminus fusion transformations streaked on agar plates with different concentrations of  $K^+$ . The following plasmid cassettes containing N-terminus mammalian channel:VenusYFP fusions:

- a) 14 pTEF1-VenusYFP:5HT<sub>3A</sub>, b) 20 pTEF1-VenusYFP:TREK1, c) 26 pTEF1-VenusYFP:TASK3, d) 33 pTEF1-VenusYFP:5HT<sub>3A</sub>-PMT, and e) 38 pRNR2-PMT:VenusYFP:TASK3

As a final verification of lack of channel translocation, and therefore function at the plasma membrane, yeast transformed with N-terminus and plasma membrane targeting site fusions were streaked on plates with low (0.5 mM and 1mM) and high (100 mM, used as a positive control)  $K^+$  to verify that they were unable to allow PLY246 to grow in low potassium media by compensating for the deleted yeast potassium transporters and channel (Figure 12). As pTEF1-VenusYFP:5HT<sub>3A</sub> grew on media containing 0.5 mM  $K^+$  (Figure 12a), it was spotted to better observe its growth phenotype (Figure 14b).

Cassette ID	Part 2 promoter	Part 3a ORF	Part 3b ORF	Part 4 terminator	Entry Vector
39	pPAB	Venus-YFP	TASK3	tADH1	GFP part 234 dropout
40	pPAB			tTDH1	
41	pRET2			tADH1	
42	pRET2			tTDH1	
43	pRAD27			tADH1	
44	pRAD27			tTDH1	
45	pSP2			tADH1	
46	pSP2			tTDH1	

**Table 6.** Venus-YFP:TASK3 fusion cassette plasmids regulated by lower strength expression promoters

45 pPSP2-VenusYFP:TASK3-tADH1 46 pPSP2-VenusYFP:TASK3-tTDH1

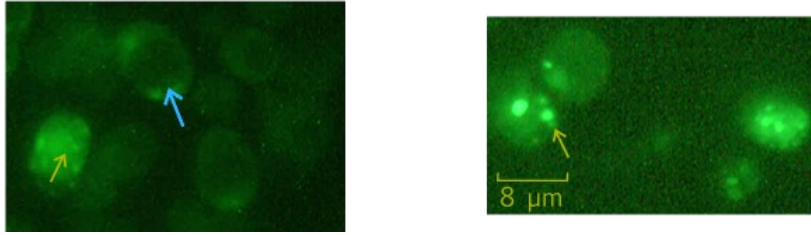


Figure 13. Decreasing the expression level of VenusYFP:TASK3 under regulation of promoter pPSP2 does not induce the translocation of the protein fusion to the plasma membrane. Blue arrow shows a vacuole and olive arrows point to inclusion bodies

As overexpression of proteins can lead to aggregation, TASK3 cassettes were constructed with lower strength promoters (Table 6 & Figure 13), but this did not relieve the problem and therefore it is unlikely that protein overexpression was the cause of aggregation. Transformations which did not show Venus-YFP expression or where the fluorochrome bleached before an image could be captured are not shown.

#### 4.13 An expression of 5HT<sub>3A</sub> at the plasma membrane of yeast strain $\Delta TRK1 \Delta TRK2 \Delta TOK1$ PLY246 was a false positive result

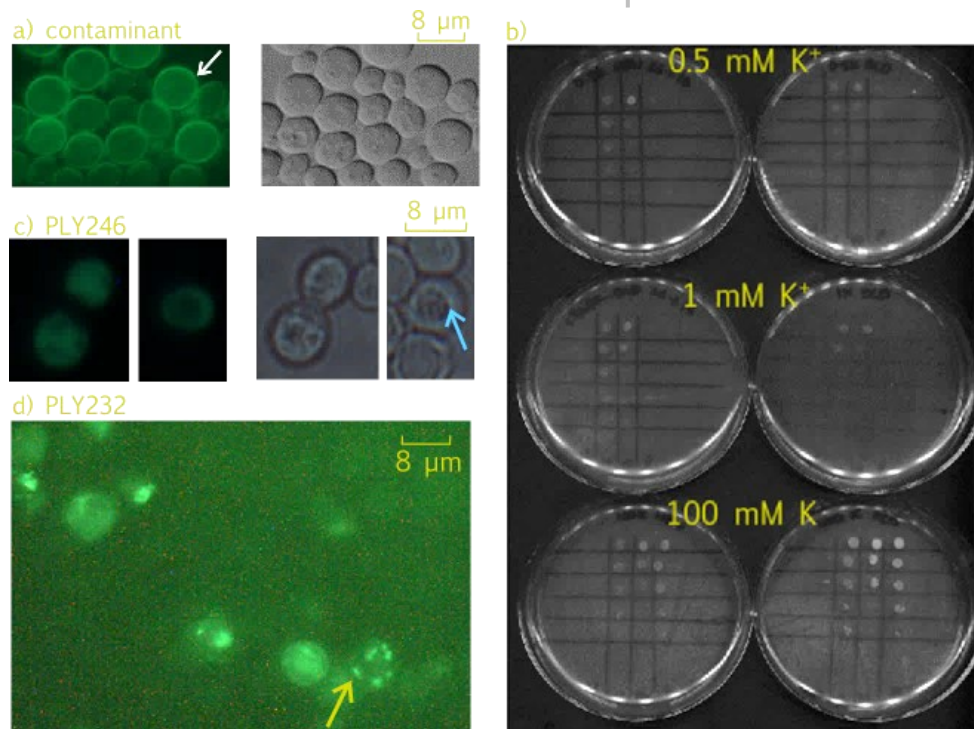


Figure 14. The expression of Venus-YFP:5HT<sub>3A</sub> under the regulation of promoter pTEF1 and terminator tADH1 initially showed expression at the plasma membrane and growth on low potassium media; a) VenusYFP:5HT<sub>3A</sub> expression at the plasma membrane of contaminated yeast (white arrow; images taken at the University of California San Diego) b) from left to right on each plate W303 WT yeast strain, PLY246 with 14 pTEF1- VenusYFP:5HT<sub>3A</sub> -tADH1, PLY246 with 3 pTEF1-VenusYFP-tADH1 spotted on 0.5 mM, 1 mM, and 100 mM K<sup>+</sup> plates in descending rows of ten-fold dilutions, c) protein fusions were cytoplasmic when transformation of 14 pTEF1-5HT<sub>3A</sub> was repeated in PLY246 (blue arrow shows a vacuole), d) protein fusions formed inclusion bodies (olive arrow) when 14 pTEF1-5HT<sub>3A</sub> was transformed in the WT strain *TRK1 TRK2 TOK1* PLY232 .

Construct pTEF1-VenusYFP:5HT<sub>3A</sub> was transformed in PLY246 and showed Venus-YFP expression at the plasma membrane. Spotting on low potassium media with a wildtype positive control strain and negative control PLY246 expressing only Venus-YFP showed that the channel was able to compensate for the deleted yeast channel and transporters. However, repeating the transformation led to cytoplasmic expression in yeast cells and no growth on low potassium media (Figure 14).

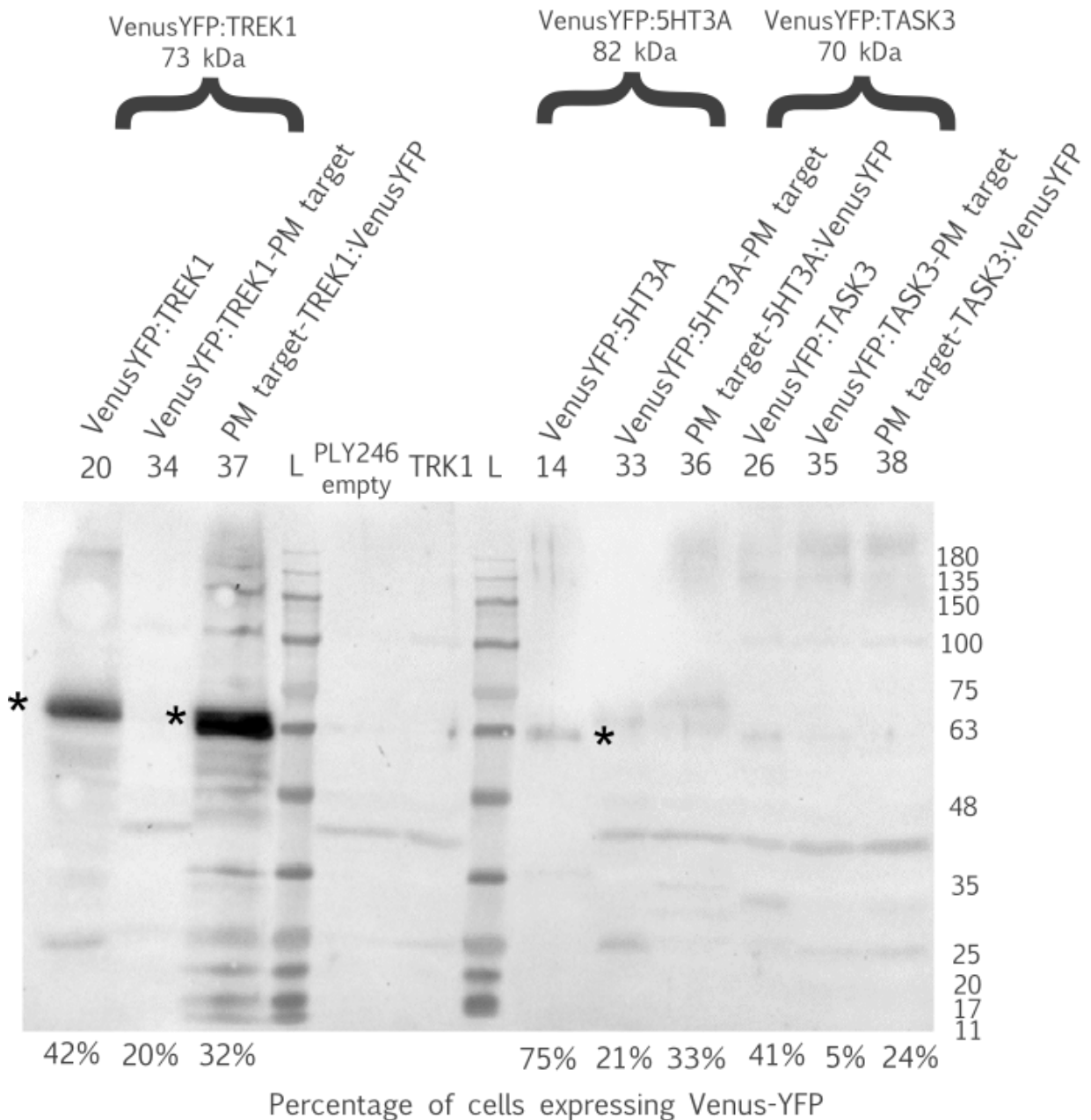


Figure 15. Western blot of yeast transformed with different plasmid constructs shows little protein expression. The contaminate yeast strain transformed with pTEF1-VenusYFP:5HT<sub>3A</sub> showing plasma membrane translocation was used for this blot. Bands do not appear to be at the correct size. Venus-YFP is 27 kDa.

A Western blot was carried out as a secondary way to validate protein expression (Figure 15). However, expression levels were low and were not able to be detected at the expected size on the blot. This was also the case for Venus-YFP:5HT<sub>3A</sub>.

Due to these results, PLY246 transformed with pTEF1-VenusYFP:5HT<sub>3A</sub> was grown in media lacking leucine. As PLY246 has a deleted *LEU* gene, it should not have survived in this media as it did. The transformed strain was also grown in 5-Fluoroorotic Acid (5-FOA). 5-FOA is converted to 5-flurouracil in cells with a *URA3* gene coding for the uracil synthesis enzyme orotidine-5-monophosphate decarboxylase, which becomes toxic. As no cells were able to grow in the presence of 5-FOA, it indicated that the strain did have an intact chromosomal *URA3* gene and therefore was not PLY246, but an unidentified contaminant.

## 4.14 Mammalian potassium channels fused to Venus-YFP at the C-terminus are not translocated to the plasma membrane in $\Delta TRK1 \Delta TRK2 \Delta TOK1$ PLY246

56 pTEF1-5HT<sub>3A</sub>:VenusYFP

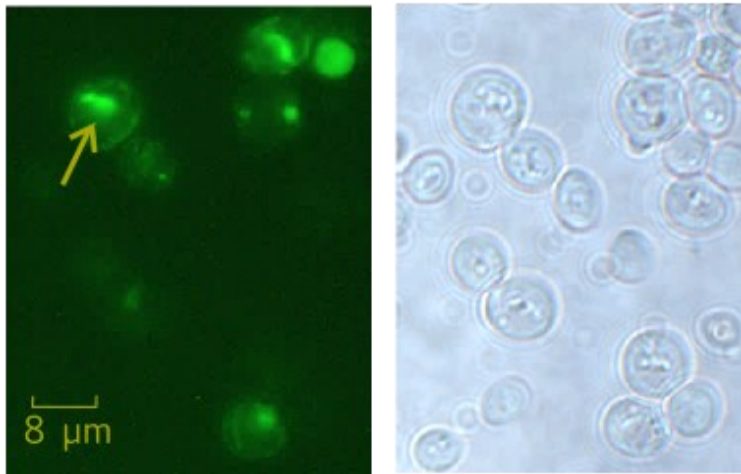


Figure 16. C-terminus potassium channel and Venus-YFP and fusions form inclusion bodies PLY246. Phenotype of cells transformed with cassette plasmid 56 pTEF1-5HT<sub>3A</sub>:VenusYFP is representative of the inclusion bodies (arrow) formed by expression of other C-terminus fusions (Appendix 6.2, 6.3, 6.5).

As Western blotting showed low level of fusion protein expression at unexpected sizes, C-terminus fusion constructs were cloned in order to be confident that cellular Venus-YFP signals would indicate fully expressed fusions, and not a truncation. However, these proteins also aggregated in cells (Figure 16 & Appendix 6.2, 6.3).

51 pRNR2-MFaSS-TREK1:VenusYFP

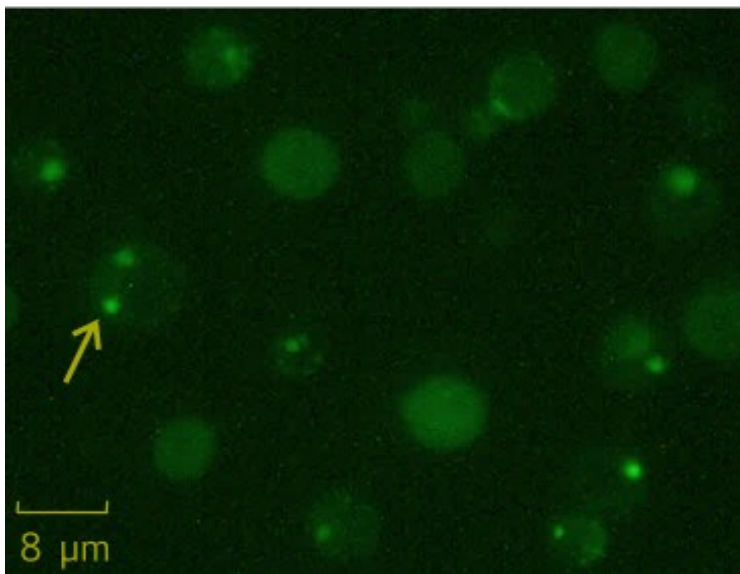


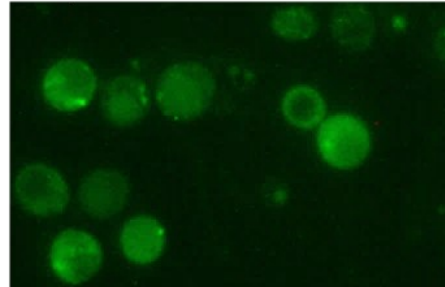
Figure 17. Fusing the mating factor alpha signalling sequence to channel:VenusYFP does not induce translocation of the protein fusion to the plasma membrane. Cells formed inclusion bodies (arrow) as represented in transformation 51 pRNR2-MFaSS-TREK1:VenusYFP or proteins were cytoplasmic (Appendix 6.5).

Following this constructs were fused to the mating factor alpha signal sequence as it is sometimes used to target proteins to membranes (Routledge *et al.*, 2016), but this was unsuccessful in directing the mammalian potassium channels to the plasma membrane (Figure 17 & Appendix 3).

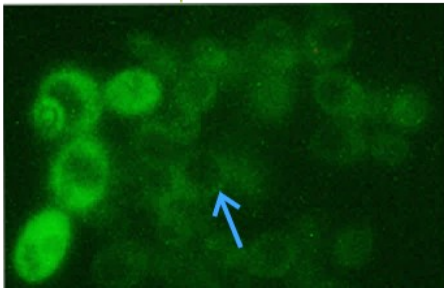
## 4.15 Several yeast strains are unable to translocate TASK3, TREK1, and 5HT<sub>3A</sub> to the plasma membrane

As previous experiments have demonstrated the expression of functional potassium channels in *S. cerevisiae* (Tang *et al.*, 1995; Bichet *et al.*, 2004; Haass *et al.*, 2007; Schwarzer *et al.*, 2008), plasmid constructs were transformed into other yeast strains to verify that genetic background differences were not responsible for the inability of PLY246 to translocate channel:Venus-YFP fusions to the plasma membrane.

a) SGY1528 + 37 pTEF1-PMT:TREK1:VenusYFP + 42 pRET2-VenusYFP:TASK3



b) R5421 + 40 pPAB-VenusYFP:TASK3



c) BLY4741 + 13 pRNR2-VenusYFP:5HT3A

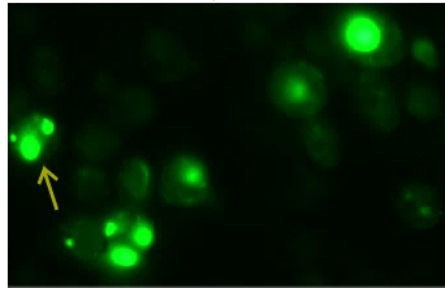


**Figure 18. Mammalian channels fused to Venus-YFP are unable to be translocated to the plasma membrane of *S. cerevisiae*.** a) channels are cytoplasmic or form inclusion bodies in SGY1528 b) mammalian channel and Venus-YFP expression is cytoplasmic in R5421, and c) form inclusion bodies in BY4741 (blue arrow shows a vacuole and olive arrow shows an inclusion body). Selected images are representative of gene expression in these strains. See Appendix 6.2-6.5 for more images.

SGY1528 is widely used as a potassium influx-deficient strain. R5421 is similar but was derived from a different parental strain. We also used WT BY4741 which is a commonly used laboratory WT strain. None of them were able to translocate the protein fusions expressed from the plasmid cassettes originally transformed in PLY246 to form functional channels (Figure 18 & 19; transformations which did not show Venus-YFP expression or where the fluorochrome bleached before an image could be captured are not shown). Therefore, the yeast strain was not the factor limiting the translocation of potassium channels to the membrane.

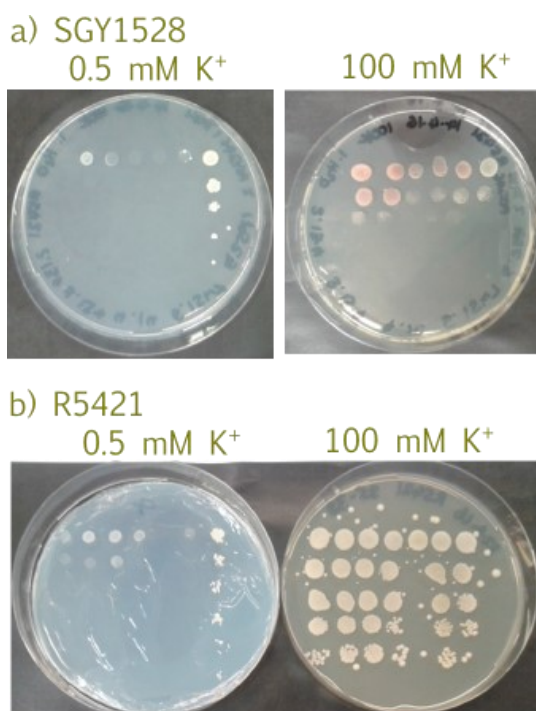


**Figure 19. Growth assays of transformed yeast conducted parallel to expression observation experiments.** Left to right on each plate in descending rows of ten-fold dilutions

a) SGY1528 with  
13 pRNR2-VenusYFP:5HT3A x 2,  
14 pTEF1-VenusYFP:5HT3A,  
15 pRPL18B-VenusYFP:5HT3A,  
25 pRNR2-VenusYFP:TASK3, pYES2-TRK1;

b) R5421 transformed with  
35 pRPL18B-VenusYFP:TASK3:PMT,  
36 pRPL18B-PMT:5HT3A:VenusYFP  
37 pTEF1-PMT:TREK1:VenusYFP,  
38 pRNR2-VenusYFP:TASK3:PMT,  
empty vector,  
pYES-TRK1.

#### 4.16 Previous experiments expressing human TASK3 in *Saccharomyces cerevisiae* were unable to be replicated

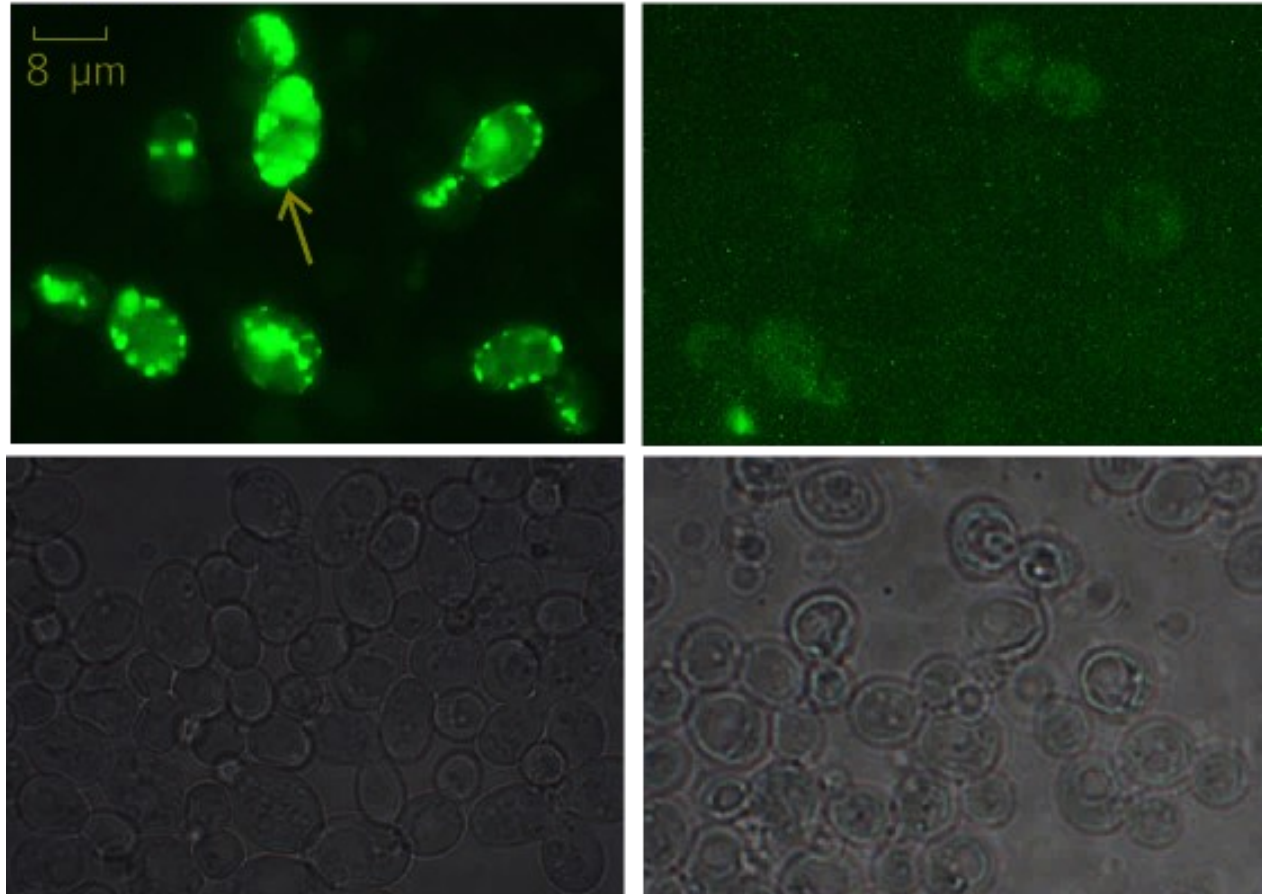


**Figure 20.** hTASK3:VenusYFP is not translocated to the plasma membrane in SGY1528 or PLY246 under regulation of pMET promoter in plasmid pYES2. Arrow shows an example of an inclusion body formed.

Bernstein *et al.* (2013) had previously demonstrated expression of the human TASK3 (hTASK3) potassium channel (without codon optimisation for *S. cerevisiae*) in strain B31 which was derived from the same parental strain as SGY1528 (W303-a). However, we were unable to replicate functional expression of hTASK3 in the same vector (pYES2) and SGY1528 (or other strains); as these transformed yeast were unable to grow on low potassium media. To try and understand the intracellular causes of this, we decided to clone N and C terminus fusions of hTASK3 to Venus-YFP to verify transcription, translation, and observe the location of the channel. We found that the proteins were translated but formed inclusion bodies in the cell (Figure 20). Venus-YFP could have affected translation and folding, but potassium titration experiments demonstrated that non-fused proteins were also unable to complement the deletion of yeast potassium transporters and channel as there was no growth in spotting assays (data not shown). Therefore it is unlikely that Venus-YFP was the factor preventing hTASK3 from translocating and correctly folding at the plasma membrane. Although external experiments showed that the expression of hTASK3 in B31 (a strain that is unable to efflux potassium) killed cells by overwhelming them with excess potassium. This phenotype is an indirect measurement of expression and translocation and the group did not demonstrate plasma membrane translocation (e.g. by GFP fusions and microscopy) and therefore we cannot conclude that hTASK3 can be successfully expressed at the membrane of *S. cerevisiae*.

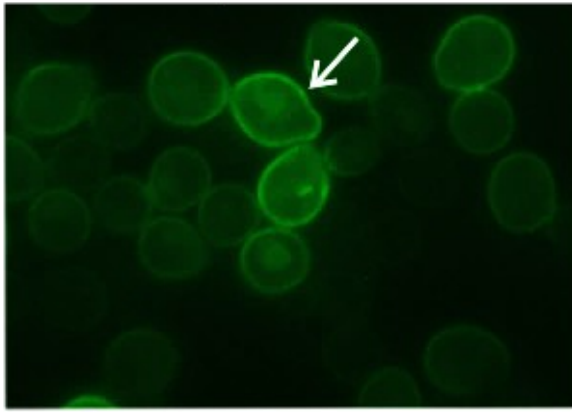
## 4.17 TOK1:Venus-YFP is successfully translocated to the plasma membrane of *Saccharomyces cerevisiae*

As we were unable to successfully express functional mammalian potassium channels in *S. cerevisiae* by varying the promoter, terminator, protein fusion structure, and yeast strain, we decided to try using TOK1 to better understand the activation of halothane on two-pore domain potassium channels as it is evolutionarily related to the mammalian channels.

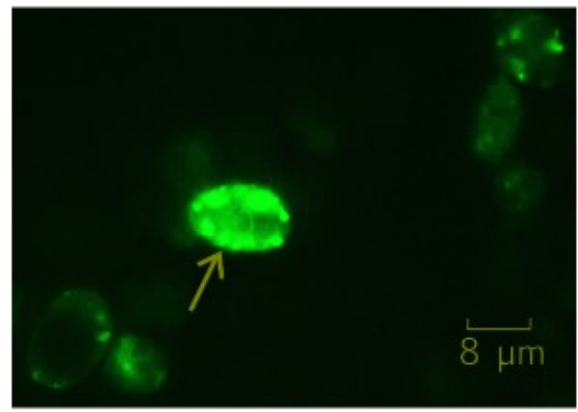
Yeast strain	Plasmid cassette	Phenotype	Frequency of Venus-YFP expression at the plasma membrane (# cells at membrane / #cells total)
PLY246	63 pTEF1-TOK1:VenusYFP-tADH1	Intracellular aggregation	-
	65 pRPL18B-TOK1:VenusYFP-tADH1	Translocation to plasma membrane	877/1985 = 0.442
SGY1528	63 pTEF1-TOK1:VenusYFP-tADH1	Translocation to plasma membrane	1276/2390 = 0.534
	65 pRPL18B-TOK1:VenusYFP-tADH1	Translocation to plasma membrane and aggregation	601/1953 = 0.308 at plasma membrane 183/1953 = 0.032 with inclusion bodies
R5421	63 pTEF1-TOK1:VenusYFP-tADH1	Translocation to plasma membrane	517/825 = 0.627
	65 pRPL18B-TOK1:VenusYFP-tADH1	Intracellular aggregation	-

Table 7. Expression phenotypes of *S. cerevisiae* strains transformed with TOK1:VenusYFP under two promoters.

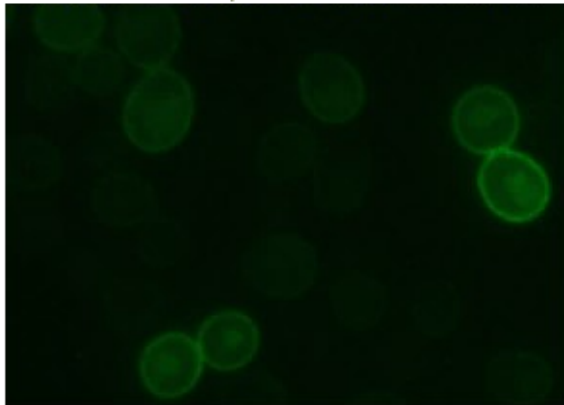
a) PLY246 + 65 pTEF1-TOK1:VenusYFP



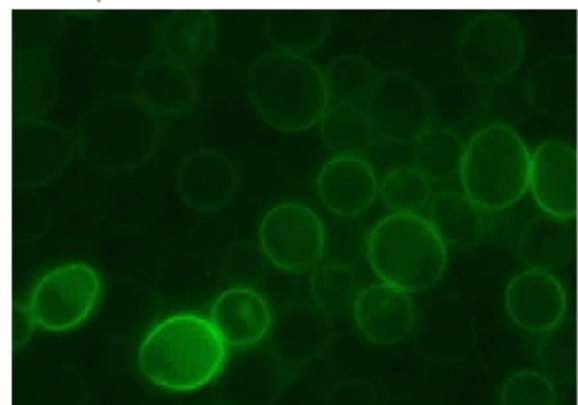
+ 63 pRPL18B-TOK1:VenusYFP



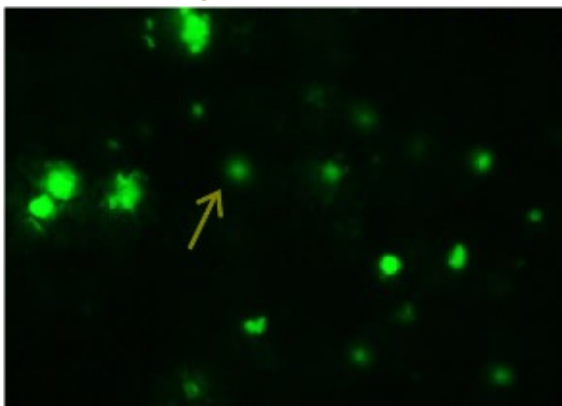
b) SGY1528 + 65 pTEF1-TOK1:VenusYFP



+ 63 pRPL18B-TOK1:VenusYFP



c) R5421 + 65 pTEF1-TOK1:VenusYFP



+ 63 pRPL18B-TOK1:VenusYFP

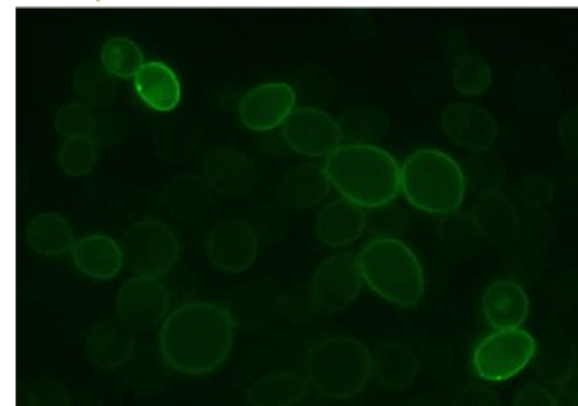


**Figure 21.** Expression of TOK1:VenusYFP under different promoters in *S. cerevisiae*. Proteins are translocated to the plasma membrane a) in PLY246 under the regulation of promoter pTEF1, b) under pTEF1 and pRPL18B in SGY1528, and c) under pRPL18B in R5421. Olive arrows show inclusion bodies and white arrow points to an example of plasma membrane Venus-YFP expression.

TOK1 was fused at the C-terminus to Venus-YFP and expressed under the regulation of promoters pTEF1 and pRPL18B and terminator tADH1 (Table 7). Under these parameters, fusion proteins were trafficked to the membrane and rings of GFP could be seen around cells (Figure 21).

## 4.18 The transexpression of TOK1 may be able to compensate for yeast potassium transporters and channel deletions

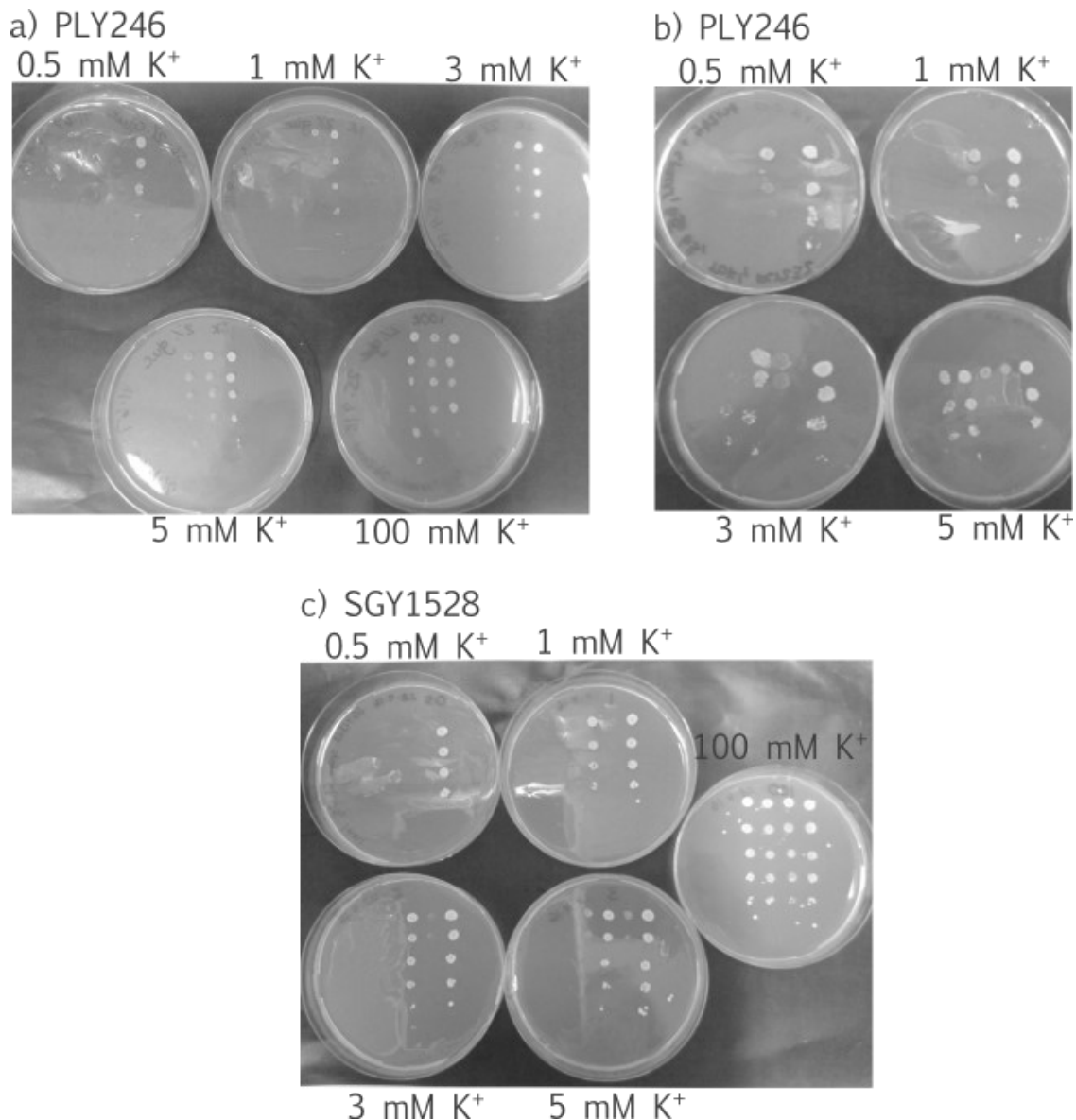


**Figure 22. Growth assays of yeast transformed with TOK1 under the regulation of different promoters.**

Left to right on each plate in descending rows of ten-fold dilutions

a) PLY246 transformed with empty vector, 63 pRPL18B-TOK1:VenusYFP, and PLY232 transformed with an empty vector;

b) PLY246 transformed with empty vector, 65 pTEF1-TOK1:VenusYFP, 63 pRPL18B-TOK1:VenusYFP, pGAL1-TOK1, and PLY232 transformed with empty vector;

c) SGY1528 transformed with empty vector, 65 pTEF1-TOK1:VenusYFP, 63 pRPL18B-TOK1:VenusYFP, and pYES2-TRK1

*TOK1* regulated under promoters pTEF1, pRPL18B, and pGAL1 was expressed in PLY246, SGY1528, and R5421 and spotted on agar plates containing different levels of potassium with a negative control (yeast with an empty vector) and positive control (yeast expressing TRK1, or additionally with TRK2 and TOK1; Figure 22). All yeast grew between 5-100 mM K<sup>+</sup> but transformed yeast were unable to grow at 0.5 mM K<sup>+</sup> (considered a low concentration), whilst positive controls were able to grow in low potassium. However, at 1 mM K<sup>+</sup> pTEF1 regulation of *TOK1* allowed strain SGY1528 to survive and pRPL18B regulation allowed PLY246 to survive whereas yeast without *TOK1* transexpression did not survive. More repetitions need to be carried out to verify if this result is consistent.

## 4.19 Arachidonic acid is able to enhance the growth of *Saccharomyces cerevisiae*

Electrophysiology experiments (Manville *et al.*, 2016) have demonstrated that 100  $\mu\text{M}$  arachidonic acid is able to activate TOK1 and is a known physiological agonist of the human K<sub>2</sub>P channel TREK1 (also a biological target of halothane). Based on this, three strains of *Saccharomyces cerevisiae* with a compromised potassium influx system were grown in the presence of arachidonic acid to assess whether the activation of K<sup>+</sup> channel TOK1 by an agonist would allow potassium to enter the cell and manifest as increased growth in low potassium (0.5 mM K<sup>+</sup>). SGY1528 and R5421 (both -TRK1, -TRK2 but expressing genomic TOK1) grew visibly more in the presence of 300  $\mu\text{M}$  of arachidonic acid than in the equivalent volume of the vehicular solvent on agar (Figure 23a). The growth pattern of PLY246 (-TRK1, -TRK2, -TOK1) was also similar when transformed with TOK1 in an expression vector (Figure 23c). However, this latter strain also had improved growth in arachidonic acid without a transgenic TOK1 receptor and all strains grew better in arachidonic acid when expressing TRK1 (Figure 23a-c); therefore there is the possibility that arachidonic acid enhanced yeast growth via another mechanism rather than opening the TOK1 channel.

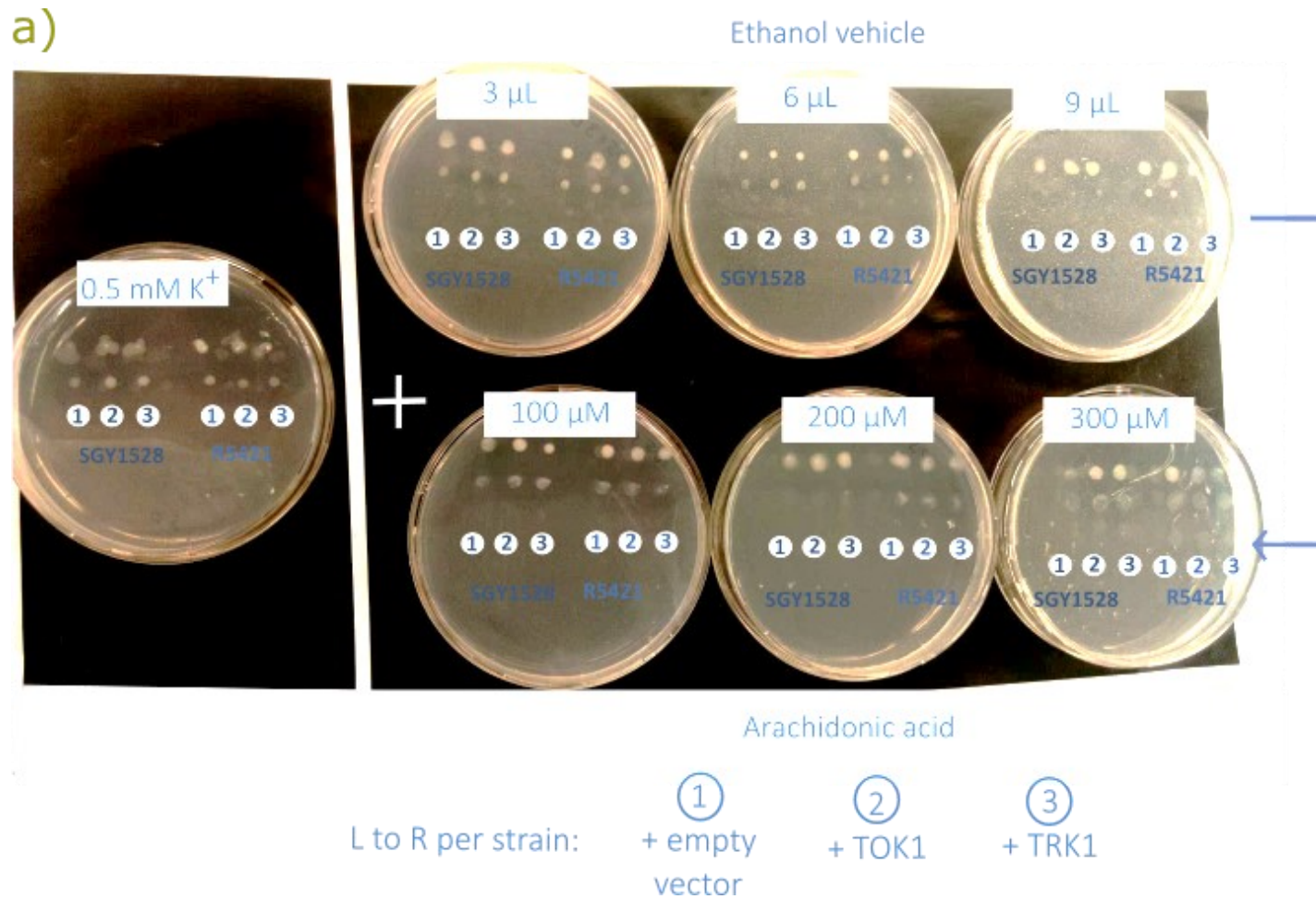
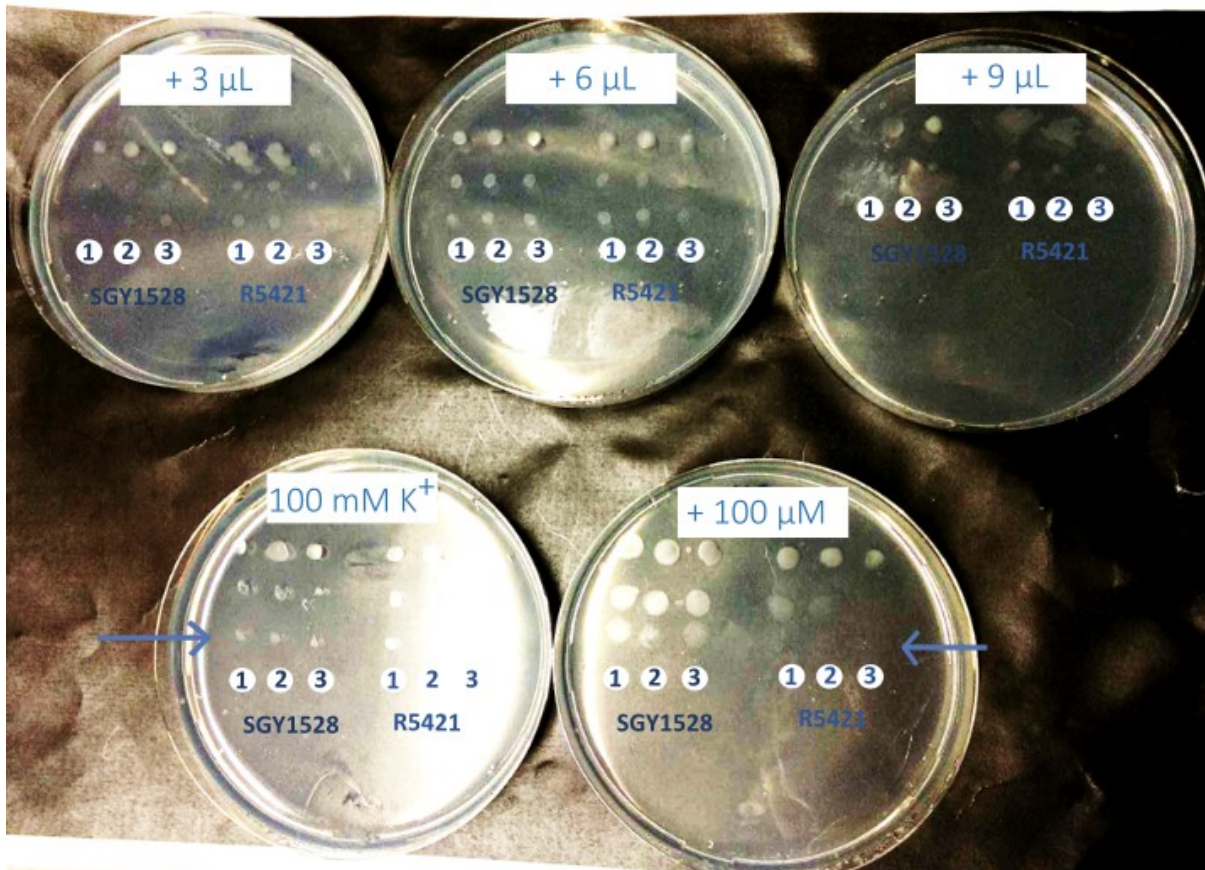


Figure 23a. Yeast strains with compromised  $\text{K}^+$  influx systems were spotted on agar with or without arachidonic acid. Yeast were spotted on 0.5 mM  $\text{K}^+$  or 100 mM  $\text{K}^+$  and ethanol vehicle or 100-300  $\mu\text{M}$  arachidonic acid. Colonies were diluted ten-fold with each descending row with a total of four rows spotted. a) SGY1528 and R5421 (-TRK1, -TRK2) transformed with ① an empty vector, ② a TOK1 expression vector, or ③ a TRK1 expression vector on 0.5 mM  $\text{K}^+$  with 3, 6, or 9  $\mu\text{L}$  ethanol vehicle or the equivalent with dissolved 100, 200, or 300  $\mu\text{M}$  arachidonic acid respectively. The blue arrow points to yeast which have grown better when spotted on 300  $\mu\text{M}$  arachidonic acid than 9  $\mu\text{L}$  ethanol vehicle.

b)

Ethanol vehicle



Arachidonic acid

L to R per strain:      ①                      ②                      ③  
                                 + empty                      + TOK1                      + TRK1  
                                 vector

**Figure 23b.** SGY1528 and R5421 (-TRK1, -TRK2) transformed with ① an empty vector, ② a TOK1 expression vector, or ③ a TRK1 expression vector on 100 mM K<sup>+</sup> with 3, 6, or 9 μL ethanol vehicle or the equivalent with dissolved 100, 200, or 300 μM arachidonic acid respectively. The blue arrow points to yeast which have grown better when spotted on 100 μM arachidonic acid than without

c)

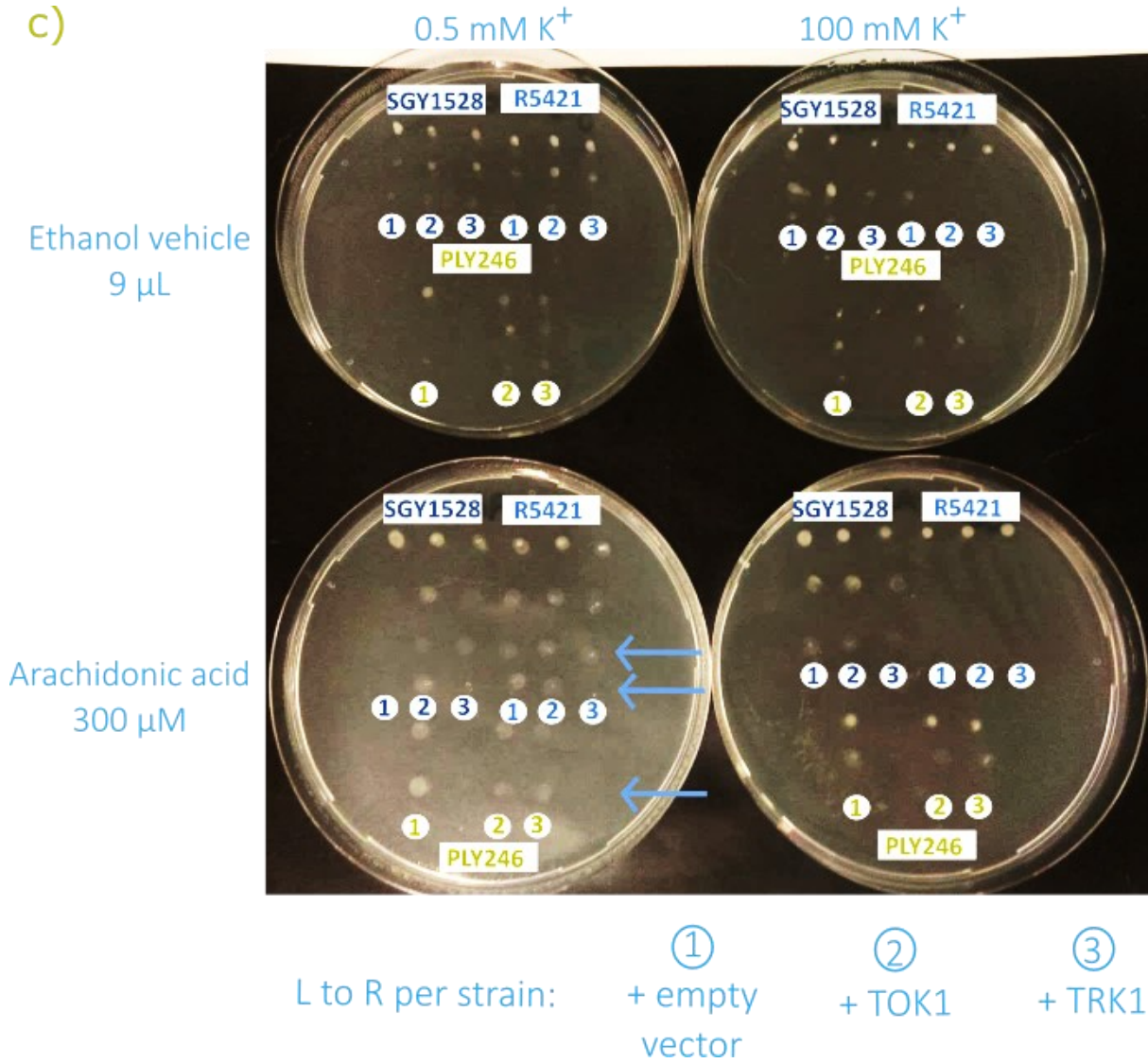
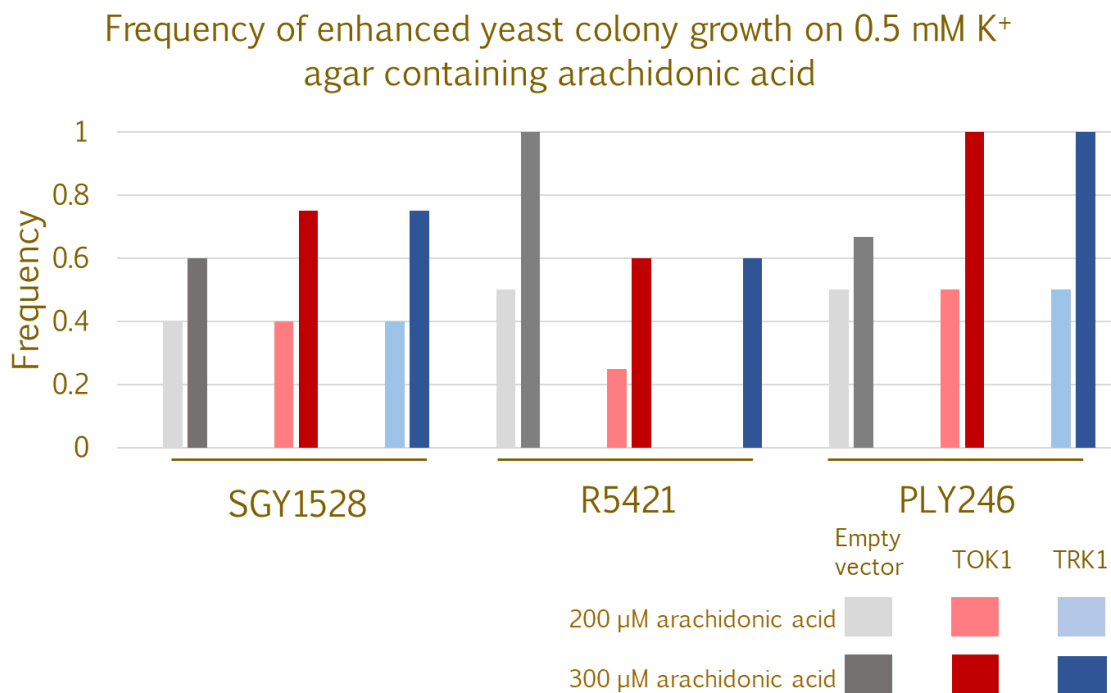


**Figure 23c.** PLY246 (-TRK1, -TRK2, -TOK1) transformed with ① an empty vector, ② a TOK1 expression vector, or ③ a TRK1 expression vector on 0.5 or 100 mM K<sup>+</sup> with 9 μL ethanol vehicle or the equivalent with dissolved 300 μM arachidonic acid. The blue arrow points to yeast which have grown better when spotted on 300 μM arachidonic acid than 9 μL ethanol vehicle.

## 4.2 *Saccharomyces cerevisiae* colonies show growth variation in the presence of arachidonic acid



**Graph 3. The frequency of yeast colonies with enhanced growth on 0.5 mM K<sup>+</sup> with arachidonic acid.** Colony frequencies were counted from agar plates containing 200 or 300 μM arachidonic acid compared with equivalent 6 or 9 μL ethanol vehicles. No growth enhancement was shown on plates containing 100 μM arachidonic acid compared with equivalent 3 μL ethanol vehicle. Chi-squared test showed no significant difference between the observed enhanced growth and expected mean frequency of enhanced growth between arachidonic acid and ethanol plates. P-values for arachidonic acid concentrations were: 100 μM p = 0.06 (lack of enhanced growth was not due to chance), 200 μM p = 0.95 (enhanced growth was due to chance), 300 μM p = 0.54 (enhanced growth may have been due to chance). Enhanced growth was judged by eye. Raw counts are displayed on Appendix 6.6-6.8

To quantify whether yeast with compromised K<sup>+</sup> influx systems displayed enhanced growth in the presence of arachidonic acid than equivalent vehicular ethanol solvent, spotting experiments were repeated for yeast strains SGY1528 (-TRK1, -TRK2), R5421 (-TRK1, -TRK2), and PLY246 (-TRK1, -TRK2, -TOK1). Yeast showed the same level of growth in 100 μM arachidonic acid compared with equivalent 3 μL ethanol vehicle. Strains showed improved growth in 200 μM arachidonic acid, but growth of colonies was more frequently enhanced in 300 μM arachidonic acid compared to growth in equivalent ethanol vehicles. However, there was no significance in the frequency of enhanced colony growth in arachidonic acid compared to ethanol equivalent, but this could be dependent on the sample size of total number of colonies (between three to five per strain and vector). Colony growth did not seem to vary with the absence or presence of TOK1 or TRK1 (Graph 3; Appendix 6.6-6.8), suggesting that arachidonic acid may affect yeast growth via another mechanism rather than opening the TOK1 channel. Despite this, as the method was able to demonstrate some variation in growth levels of *Saccharomyces cerevisiae* in the presence of a known agonist, we decided to move onto the drug of interest, haloethane.

## 4.21 A halothane incubation chamber was set up to verify the effect of halothane gas on the growth of *Saccharomyces cerevisiae*

Following experiments with the TOK1 agonist arachidonic acid, an incubation chamber was set up to grow yeast in the presence of halothane gas or air (Figure 24). The system was verified as airtight by quantifying the velocity of gas flow through the halothane vapouriser and additionally through a flow meter. The velocity at 0.5 atm and 15 RS units was calculated to be  $2.7 \text{ cm}^3 \cdot \text{s}^{-1}$  (Graph 4). Airtight boxes were drilled in order to attach inlet and outlet tubes for continuous gas flow over samples and were verified for leakage by flowing air through whilst boxes were underwater. No bubbles emerged. The boxes were made easily using commercial airtight food boxes. The outlet tube of the halothane box led to an anaesthetics absorber to which could be changed as necessary to ensure the gas did not leak into the atmosphere.

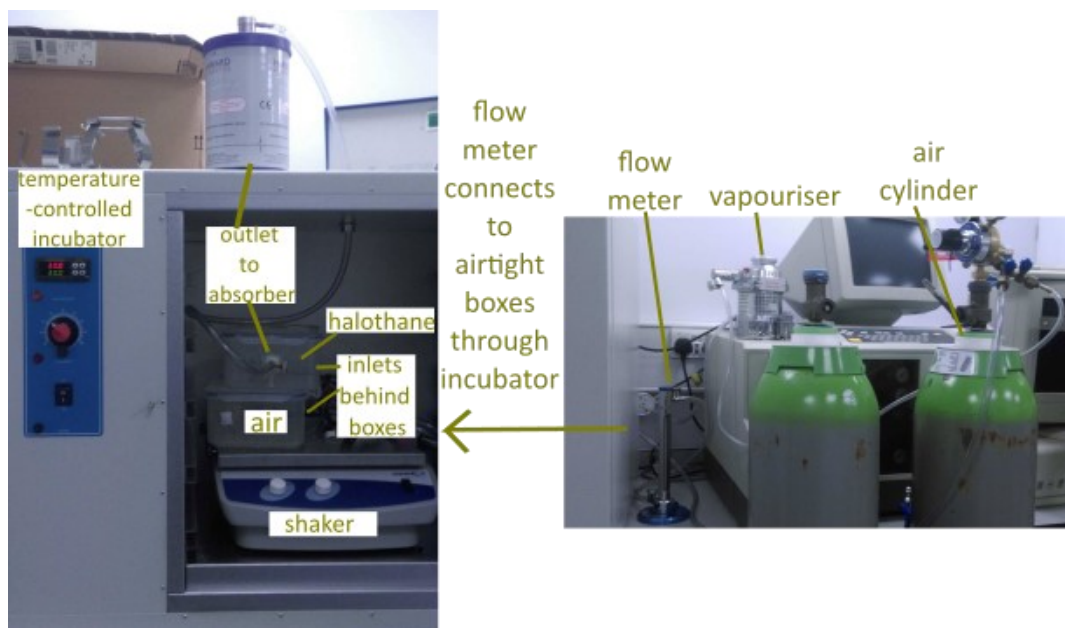


**Figure 24.** An airtight, temperature controlled system to incubate yeast samples in the presence of halothane. An air cylinder with controlled pressure release system was connected to a halothane vapouriser with an adjustable vaporisation of anaesthetic between 1-5 %. The vapouriser was then connected to a flow meter to adjust flow rate. A tube connected the flow meter to an airtight plastic box. The air cylinder was joined directly to a second box to allow 100 % air flow. The two boxes were placed on a shaker in a temperature-controlled incubator, and the halothane box was connected to an anaesthetics absorber to prevent the gas entering the atmosphere. The system was tested to ensure airtightness. Samples are exposed to a continuous flow of gas.

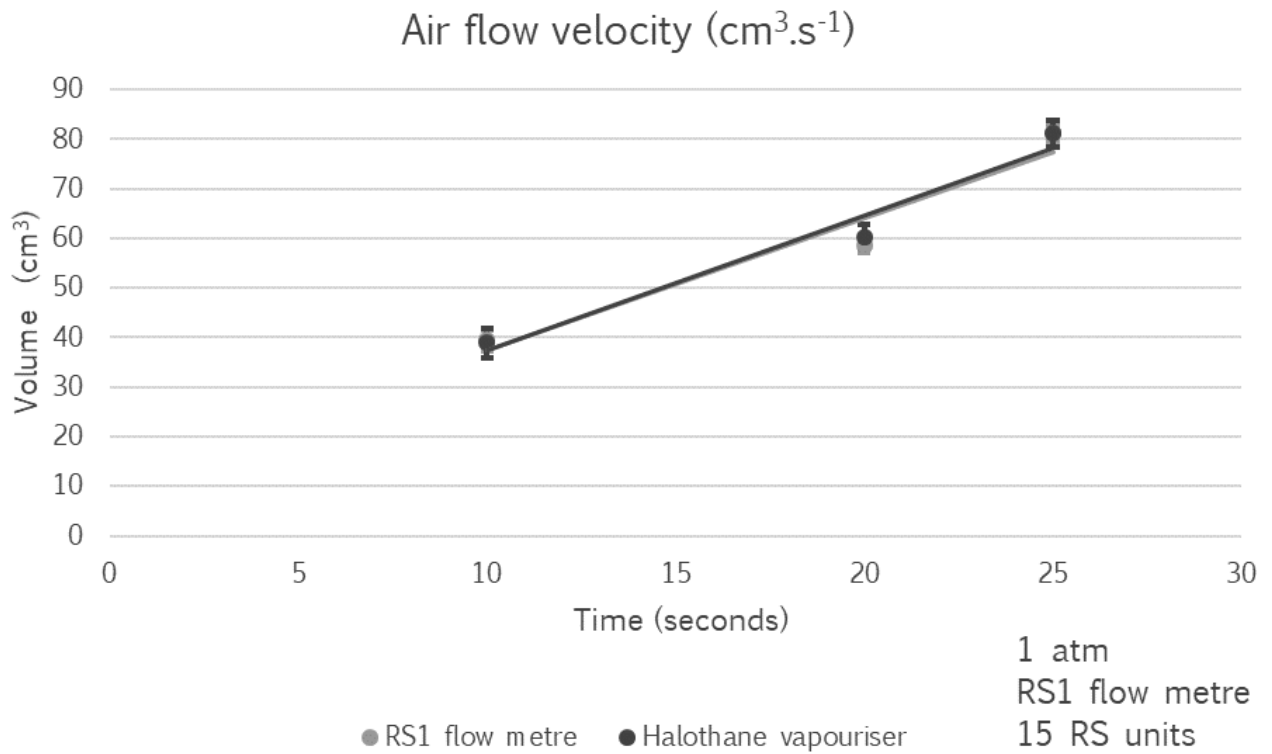
The vapouriser was calibrated using an anaesthetics monitor which showed that a 5 % of halothane in air was actually equivalent to 4.3 % (Graph 5). Therefore, all references to halothane 5 % may signify this latter figure. As the percentage of halothane was proportional to a readout of the anaesthetic monitor at a constant of 0.85 we decided to go ahead with yeast exposure experiments to the gas.

The gas flow rate was calculated using the equation

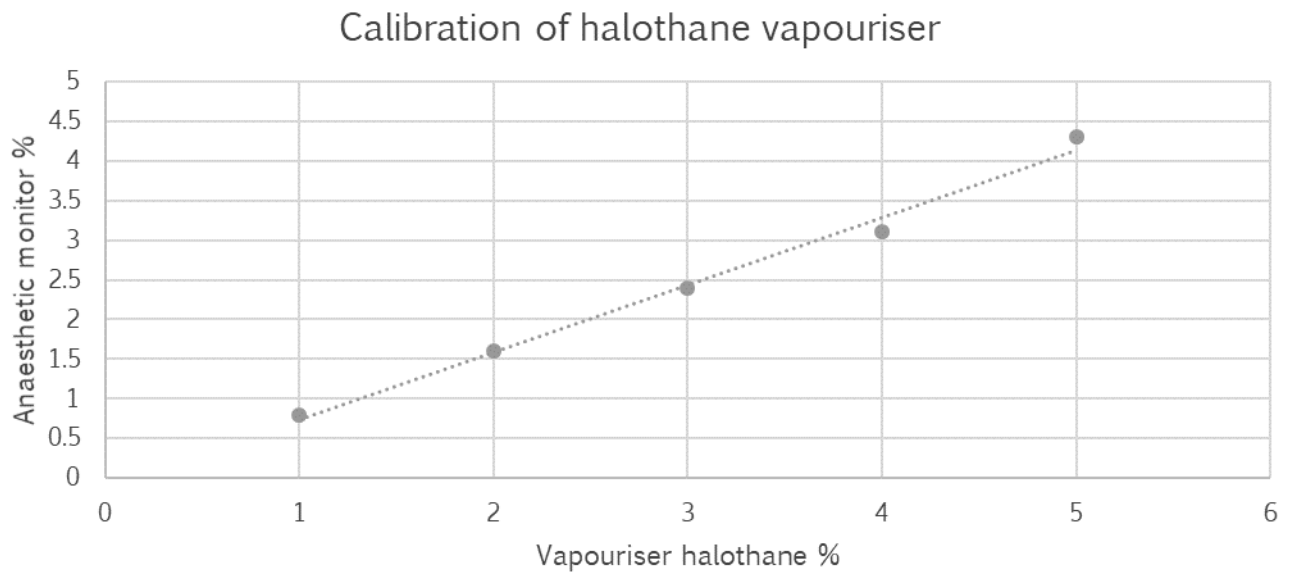
$$0.25 \times \pi \times (\text{pipe diameter})^2 \times \text{velocity}$$

and comes to

$$0.25 \times \pi \times 1^2 \times 2.7 = 2.12 \text{ cm}^3 \cdot \text{sec}^{-1} \text{ or } 127 \text{ cm}^3 \cdot \text{min}^{-1}.$$



Graph 4. Velocity of air flow through the halothane vapouriser and flow meter are equivalent indicating an airtight system. Air was released at 1 atm firstly through the halothane vapouriser and then with an RS1 flow meter attached. As velocity is the same in both cases ( $2.7 \text{ cm}^3 \cdot \text{s}^{-1}$ ) this confirms an airtight flow from the air cylinder to the incubation boxes;  $n = 12$  and standard deviations are shown.



Graph 5. Calibration of the percentage release of halothane gas by the vapouriser using an anaesthetics monitor. The vapouriser in the airtight system was connected to an anaesthetics monitor and readout of actual gas percentage was recorded. The gas flow rate through the airtight boxes was too low to be measured by the monitor therefore real-time recordings were unable to be made during experiments

## 4.22 Halothane enhances the growth of a *Saccharomyces cerevisiae* strain expressing TOK1 in liquid media

Using a similar method to preliminary arachidonic acid experiments, the same three strains of yeast with compromised  $K^+$  influx systems were first spotted on low (0.5 mM  $K^+$ ) or high (100 mM  $K^+$ ) potassium agar and exposed to halothane 5 % in air or pure air. However, it was difficult to clarify the effect of halothane 5 % on growth by spotting colonies on plates (Figure 25) and after several repeats (Table 8), yeast were grown in liquid media to quantify growth during exposure to gases. Agar plates and micro-titre well plates containing liquid media cultures were set up using inoculations from an original single colony per replicate pair, which were then separated into the air or halothane 5 % chamber. This ensured that there was no colony variation between replicate pairs per experiment, but changing parent colony for each experiment aimed to mitigate variation between colonies. Different concentrations of  $K^+$  media were set up to identify whether there was a specific threshold where lack of TOK1 would not allow yeast to grow, but TOK1 (and/or TRK1) expression would allow enough  $K^+$  to enter cells and manifest as statistically significantly more growth.

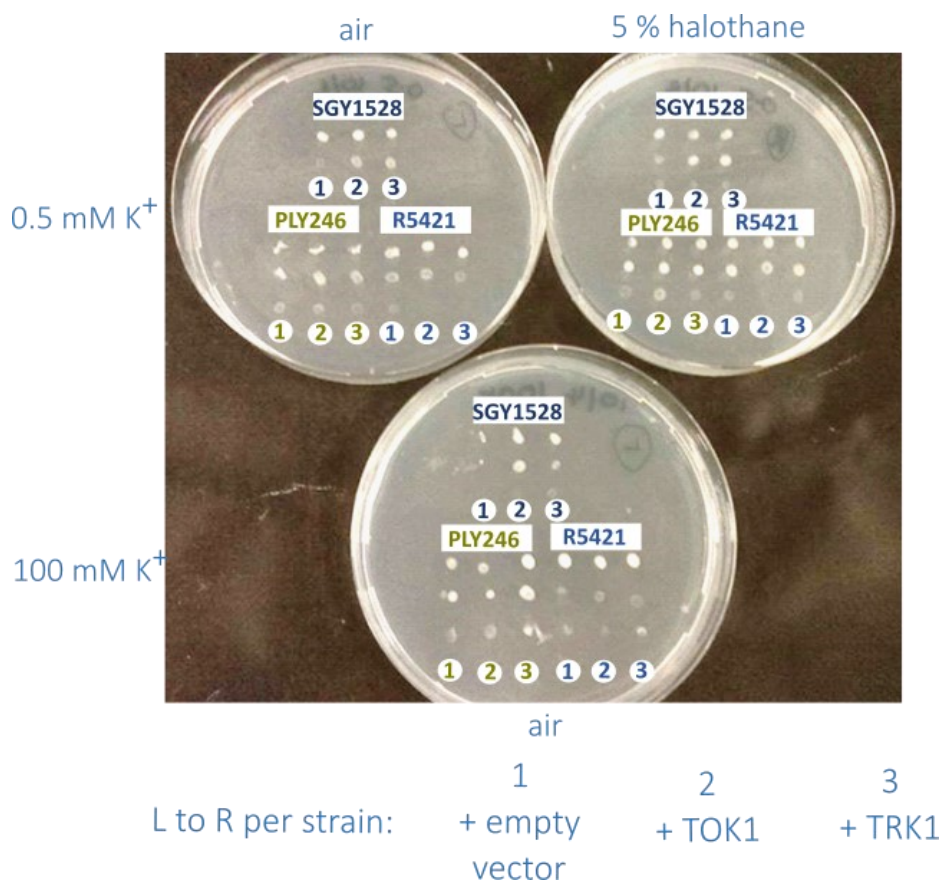


**Figure 25.** Yeast strains with compromised  $K^+$  influx systems were spotted on agar and grown in halothane 5 % or air. Colonies were diluted ten-fold with each descending row with a total of four rows spotted. SGY1528 and R5421 (-TRK1, -TRK2) and PLY246 (-TRK1, TRK2, -TOK1) transformed with ① an empty vector, ② a TOK1 expression vector, or ③ a TRK1 expression vector on 0.5 mM  $K^+$  or 100 mM  $K^+$  and grown in halothane 5 % or air. There was no clear difference in growth between plates.

Yeast strain + vector	0.5 K enhanced growth	100 K enhanced growth
SGY1528 + empty vector	2/3	1/2
SGY1528 +TOK1	2/3	1/2
SGY1528 + TRK1	2/3	1/2
R5421 + empty vector	2/3	1/2
R5421 + TOK1	1/3	1/2
R5421 + TRK1	2/3	1/2
PLY246 + empty vector	2/3	1/2
PLY246 +TOK1	2/3	1/2
PLY246 +TRK1	2/3	1/2

**Table 8. Raw count of yeast colonies displaying enhanced growth on 0.5 and 100 mM K<sup>+</sup> agar in the presence of halothane 5 % compared to air.**

0.5 mM K<sup>+</sup> is considered to be a low concentration of potassium where yeast with compromised K<sup>+</sup> influx systems cannot grow. 100 mM K<sup>+</sup> is the known concentration of potassium at which they can grow. Colony frequencies were counted from agar plates paired replicates in halothane 5 % or air. Enhanced growth was judged by eye.

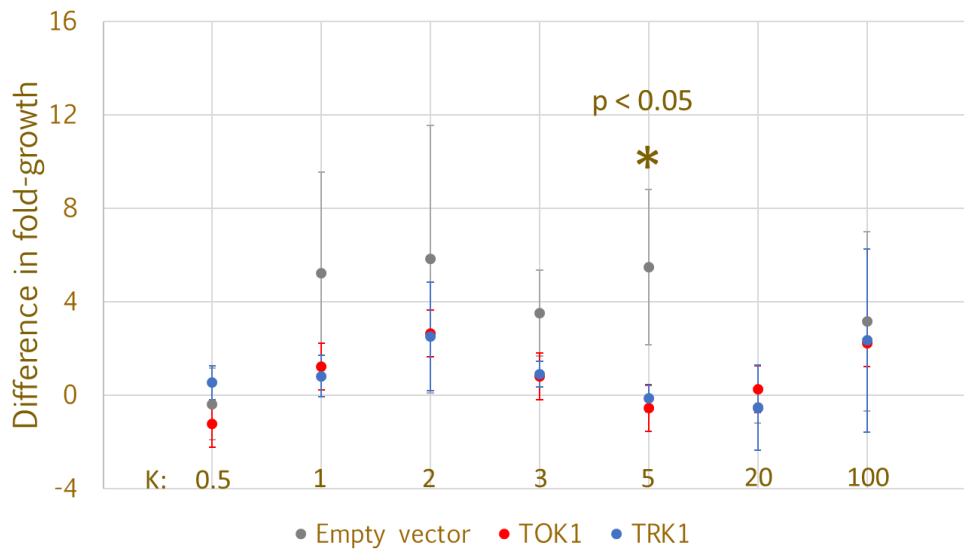
Yeast populations were measured prior to exposure to gas and after 24 hours (Graphs 6a-c; Appendix 6.11 & 6.12). Comparisons were made between constructs expressed (empty vector, TOK1, or TRK1) in air or halothane, at each K<sup>+</sup> concentration. Comparisons were not made between strains or between K<sup>+</sup> concentration levels.

Statistical analysis yielded significantly increased growth of R5421 (-TRK1, -TRK2) in halothane 5 % at 5 mM K<sup>+</sup> compared to when transformed with a TOK1 or TRK2 expression vector, but no other statistically-significant difference in growth underlay by transgene expression, presence or absence of halothane, or K<sup>+</sup> concentration (Graph 6a & Appendix 6.12). Growth after 48 h was measured. However, this also proved to lack statistically-significant difference between growth of strains expressing different transgenes in different conditions (Graphs 7a-c; Appendix 6.13 & 6.14).

ANOVA showed that variation in growth was too high to be able to link growth patterns to controlled variables. As the sample number was relatively low (three to five repeats per strain and expression vector), an increase in sample size may allow us to draw clearer conclusions on the effect of halothane on yeast growth.

### Average difference in fold-growth of R5421 between halothane 5 % and air, 24h

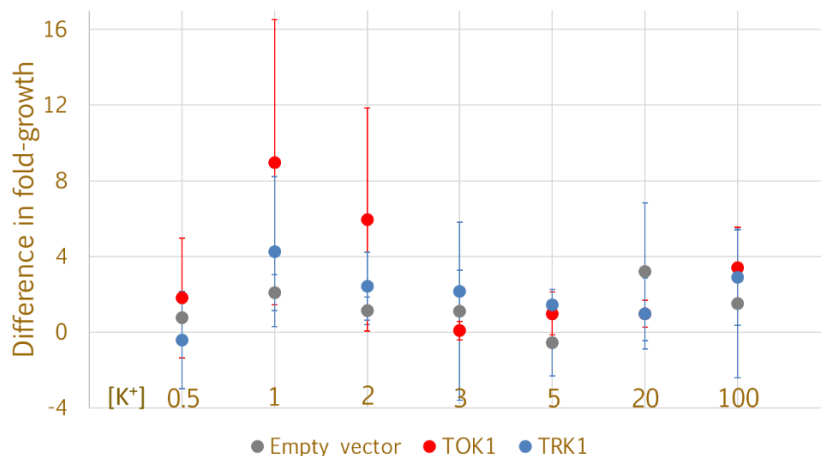
Average of  $n = 3-5$ ; standard error



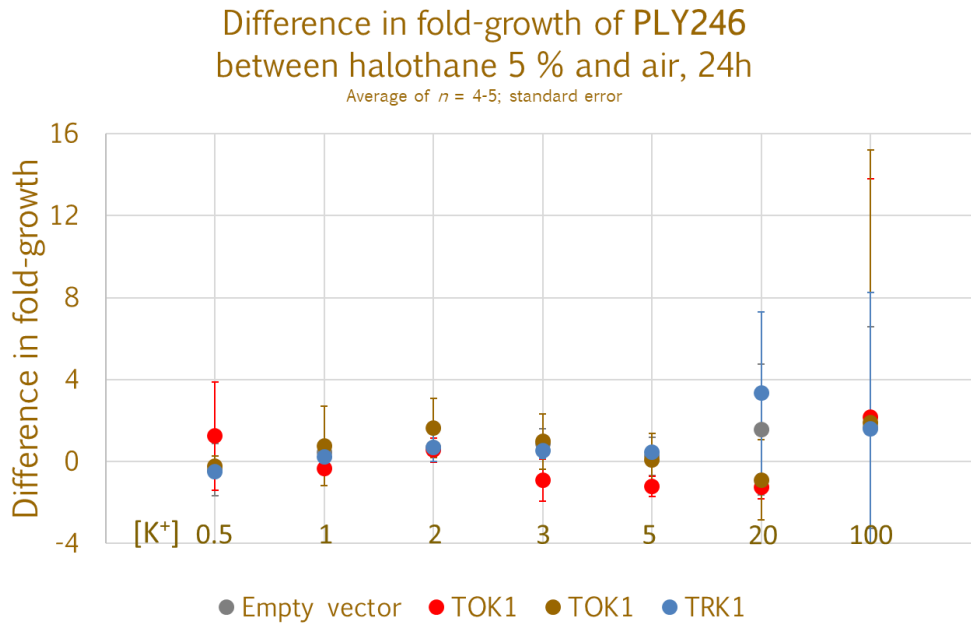
**Graph 6a.** Higher growth was observed in R5421 (-TRK1, -TRK2) transformed with an empty vector than TOK1 or TRK1, at 5 mM K<sup>+</sup>, in halothane 5 % compared to air after 24 h. Growth of transformed yeast was conducted at different concentrations of potassium to investigate whether clearer trends could be seen at different concentrations, for which paired replicates were exposed to air 100 % and halothane 5 % per sample. Average difference in fold-growth between halothane 5 % and air was calculated by doing the following. Growth after 24 h measured in optical density (OD) was divided by baseline OD, termed “fold-growth”. Average fold-growth of samples ( $n = 3-5$ ) for each treatment condition (K<sup>+</sup> concentration, and air or halothane exposure) was calculated. Average fold-growth in halothane 5 % minus average fold-growth in air produced the values plotted on the graph. A post-hoc t-test was conducted following ANOVA to obtain the p-value. One standard error above and below the mean is displayed on each bar

### Difference in fold-growth of SGY1528 between halothane 5 % and air, 24h

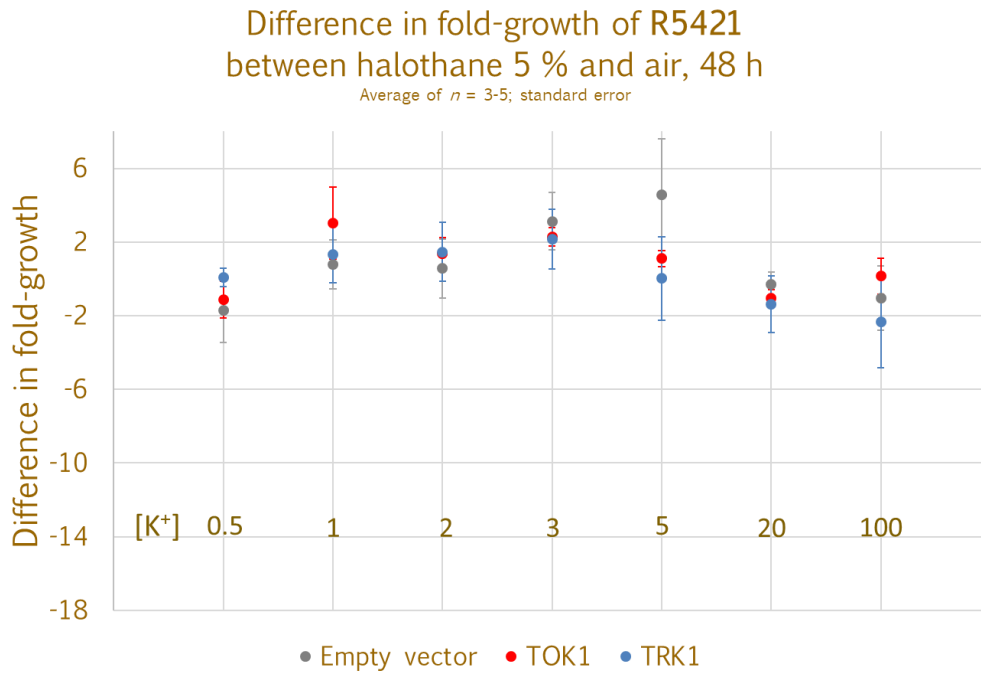
Average of  $n = 3-5$ ; standard error



**Graph 6b.** Higher growth was observed in SGY1528 (-TRK1, -TRK2) transformed with TOK1 than an empty vector or TRK1, at 1- and 2-mM K<sup>+</sup>, in halothane 5 % compared to air after 24 h. However, this observation is not statistically significant. See Graph 10a for information about how average difference in fold-growth between halothane 5 % and air was calculated. One standard error above or below the mean is displayed on each bar;  $n = 3-5$ .



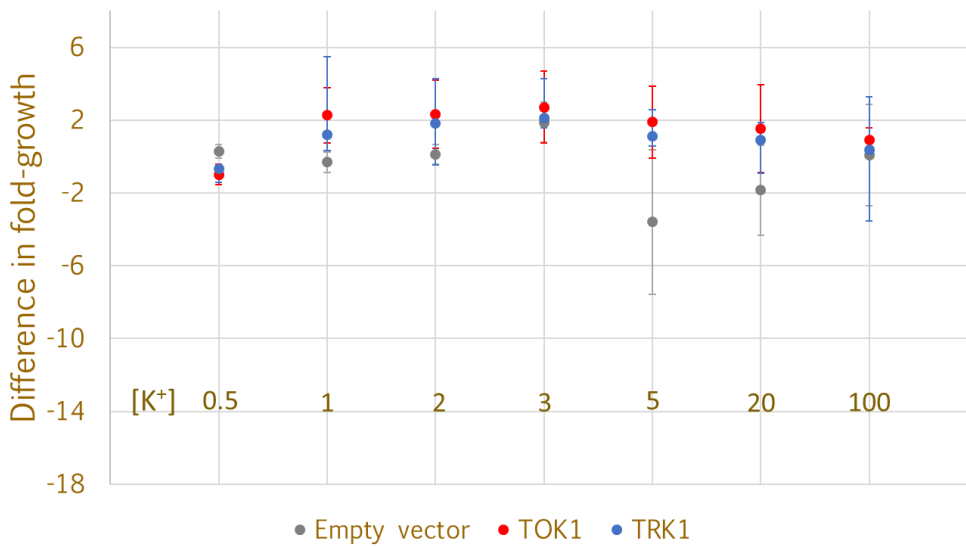
**Graph 6c.** PLY246 (-TOK1, -TRK1, -TRK2) does not display distinctive growth trends in halothane 5 % compared to air after 24 h. See Graph 10a for information about how average difference in fold-growth between halothane 5 % and air was calculated. One standard error above or below the mean is displayed on each bar and demonstrate high variation in growth response for several conditions, particularly at 20- and 100-mM K<sup>+</sup>;  $n = 3-5$ .



**Graph 7a.** R5421 (-TRK1, -TRK2) does not display distinctive growth trends in halothane 5 % compared to air after 48 h. See Graph 10a for information about how average difference in fold-growth between halothane 5 % and air was calculated. One standard error above or below the mean is displayed on each bar and demonstrate high variation in growth response for several conditions;  $n = 3-5$ .

### Difference in fold-growth of SGY1528 between halothane 5 % and air, 48 h

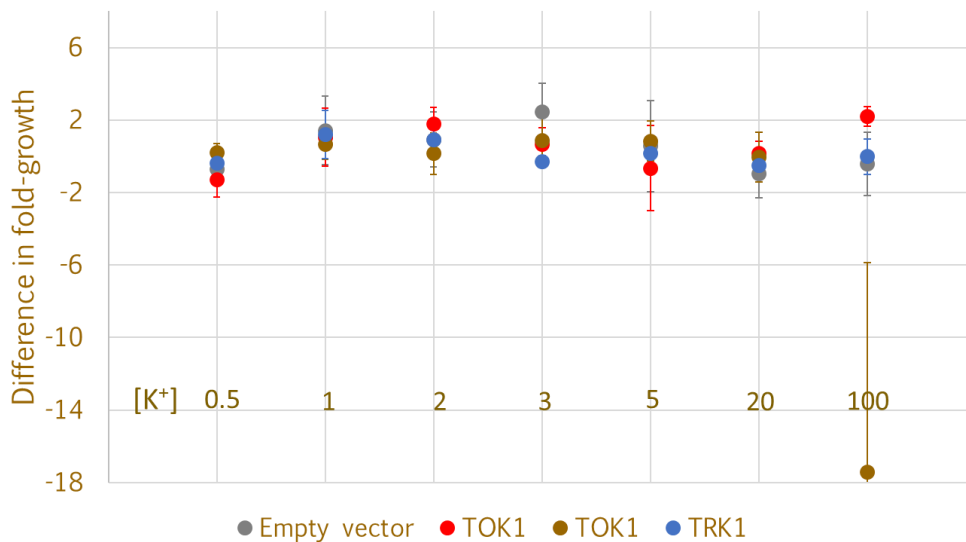
Average of  $n = 3-5$ ; standard error



Graph 7b. SGY1528 (-TRK1, -TRK2) does not display distinctive growth trends in halothane 5 % compared to air after 48 h. See Graph 10a for information about how average difference in fold-growth between halothane 5 % and air was calculated. One standard error above or below the mean is displayed on each bar and demonstrate high variation in growth response for several conditions;  $n = 3-5$ .

### Difference in fold-growth of PLY246 between halothane 5 % and air, 48 h

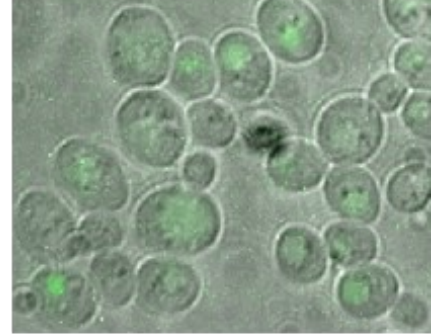
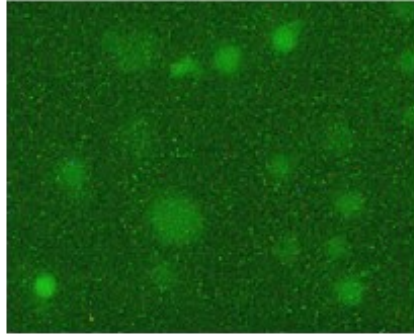
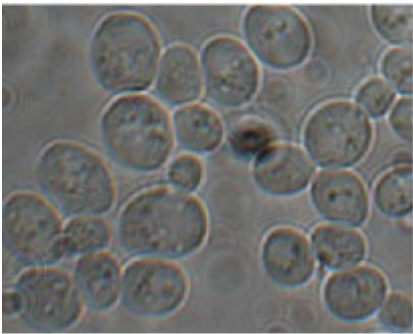
Average of  $n = 4-5$ ; standard error



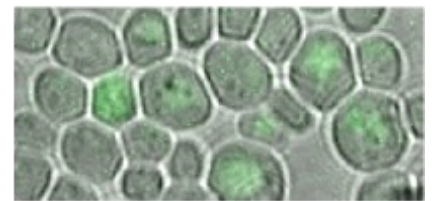
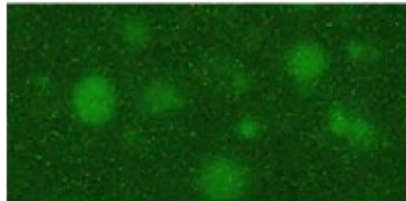
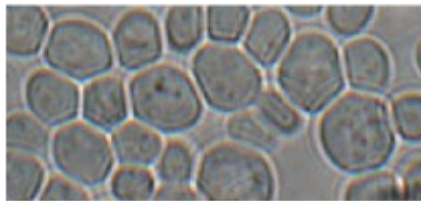
Graph 7c. PLY246 (TOK1, -TRK1, -TRK2) does not display distinctive growth trends in halothane 5 % compared to air after 48 h. See Graph 10a for information about how average difference in fold-growth between halothane 5 % and air was calculated. One standard error above or below the mean is displayed on each bar and demonstrate high variation in growth response for several conditions;  $n = 3-5$ .

## 4.23 Yeast transformation-associated recombination enables TOK1-VenusYFP fusion protein to be expressed in *Saccharomyces cerevisiae*

a) R5421 + TOK1-Venus linear DNA



b) SGY1528 + TOK1-Venus linear DNA



10  $\mu$  m

**Figure 26. Genomic expression of TOK1-VenusYFP in *Saccharomyces cerevisiae* strains with compromised  $K^+$ -influx systems.** Yeast transformation-associated recombination of TOK1-VenusYFP linear DNA targeted at the TOK1 locus resulted in a) R5421 and b) SGY1528 cells displaying Venus-YFP signal in the vacuole or cytoplasm. Signal in strain PLY246 was too faint to capture. L to R: brightfield, Venus-YFP, merge.

As yeast transformation-associated recombination has been shown to increase the transformation and expression efficiency of transgenes in yeast, a TOK1-VenusYFP fusion protein was generated by PCR with 5' and 3' ends homologous to sequences flanking the TOK1 locus in the genome. This experiment was conducted to investigate whether the linear DNA would recombine with the target locus which could then be repeated with mutant TOK1 libraries generated by low fidelity PCR.

As the TOK1-Venus fusion protein was targeted at the original genomic TOK1 locus, rather than a gene involved in auxotrophic selection, as is the classical selection method in yeast molecular biology, there was no way to solely grow successfully transformed colonies. Therefore, artificial colonies were created by spotting the transformation mixture onto agar plates and screening colonies for Venus-YFP expression by microscopy.

Venus-YFP was expressed in some yeast cells. However, YFP signal was mainly seen in the vacuole or cytoplasm rather than on the plasma cell membrane (Figure 26), where TOK1 is expected to be located and where it has been demonstrated to be trafficked to in past experiments expressing TOK1-VenusYFP from exogenous expression vectors (Figure 21).

# Chapter V: Discussion

To contribute to the understanding of neuronal mechanisms underlying sleep and anaesthesia, we endeavoured to use directed evolution on yeast potassium channel TOK1 to do two things. TOK1 is evolutionarily related to mammalian potassium channels (K<sub>2</sub>Ps), which are targets of halothane anaesthesia. By randomly mutating TOK1 residues and using halothane as a selection pressure; halothane binding site on K<sub>2</sub>Ps could potentially be identified. Parallel random mutagenesis of TOK1 and application of designer drug CNO / Compound 21 could generate a receptor exclusively activated by these drugs. This TOK1-DREADD could be expressed and activated in specific neurons *in vivo* to correlate with induced behaviours. We expressed yeast TOK1 in our model organism *Saccharomyces cerevisiae* and performed preliminary experiments to design further empirical methods for directed evolution on TOK1.

Directed evolution methods were reviewed for, and can be drawn from, the field of optogenetics. The thesis reviewed the techniques used to develop genetically-encoded voltage indicators (GEVIs) which fluoresce upon a detectable change of neuronal membrane potential. From collating the lessons about directed evolution in optogenetics, we learned that the technique has led to lineages of evolved molecules, where scientists have incrementally and continually modified inherited characteristics to improve parameters such as sensitivity, light activation spectra, the colour of emitted fluorescence, fidelity to voltage changes, speed, bleaching time, and emission brightness proportional to voltage change. We also looked at how directed evolution principles were partly applied to genetically-encoded calcium receptors. Random mutagenesis of GFP identified the site around which circularised permutation could be conducted.

We reviewed how directed evolution generated the most widely used designer receptors exclusively activated by designer dugs (DREADDs) based on the cholinergic muscarinic receptors M1 to M5. The development of these receptors was successful enough to not require further modification for use, and therefore there are no evolved muscarinic lineages as there are for evolved GEVIs. Nevertheless muscarinic-DREADDs are metabotropic and activate the same signalling cascades associated with G proteins; therefore unintended side effects such as modified gene expression could result from their activation.

In order to better understand the neurological processes of anaesthetic action, we attempted to generate expression vectors containing potassium channels to be expressed and studied in *S. cerevisiae* using the process of directed evolution. Initially we tried and tested combinations of promoters and terminators to regulate the expression of human tandem two-pore domain potassium channels TASK3 and TREK1, both targets of halothane anaesthetic, and the mouse cation channel 5HT<sub>3A</sub>, shown to have the highest affinity to clozapine drug of all ionotropic receptors (though still insignificant; Roth & Driscoll, 2014). However, we were unable to translocate these channels to the membrane, even when they were codon optimised for *S. cerevisiae*. Following from this we decided to work with the yeast two-pore potassium channel, TOK1. TOK1 is an ancestral homologue of mammalian K<sub>2</sub>Ps TASK3 and TREK1 and therefore could shed light on halothane activation mechanisms of these mammalian counterparts. We were able to direct TOK1:Venus-YFP protein fusions to the plasma membrane of three yeast strains ( $\Delta TRK1\Delta TRK2\Delta TOK1$  PLY246,  $\Delta TRK1\Delta TRK2$  SGY1528, and  $\Delta TRK1\Delta TRK2$  R5421) with modified K<sup>+</sup> influx systems under the regulation of promoters specific to each strain.

Next we exposed WT TOK1 to known agonists arachidonic acid and halothane to identify whether activation of the anaesthetic on the channel is able to increase the fitness of cells grown in low potassium media by increasing the efficiency of  $K^+$  uptake.

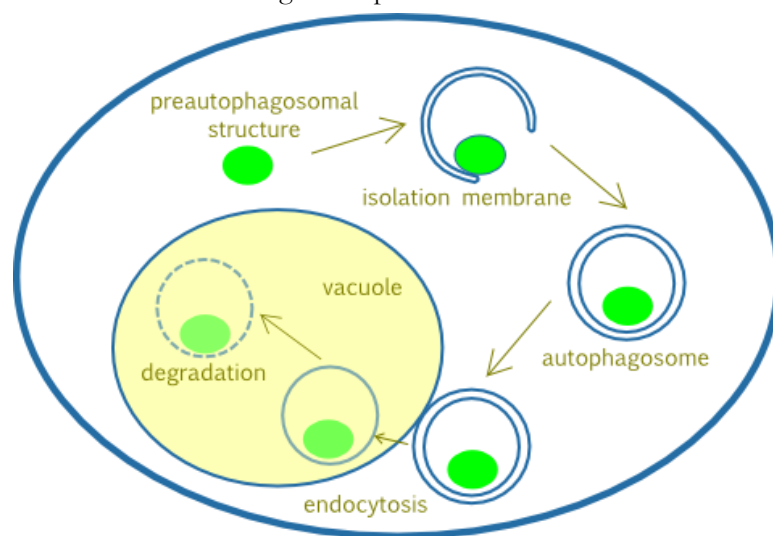
By establishing parameters for this assay, a randomly mutated TOK1 library generated by error-prone PCR could be cloned using transformation-associated recombination in yeast with modified  $K^+$  influx systems and exposed to halothane to identify mutations that render the channel more efficiently activated. Halothane activation on TOK1 would increase uptake of  $K^+$  and resultant yeast fitness. Parallel experiments involving exposure to clozapine could also evolve TOK1, rather than 5HT<sub>3A</sub> unable to be directed to yeast plasma membrane, to be a target of clozapine drug. Expressing a library of randomly mutated clozapine-activating TOK1 in yeast with modified  $K^+$  influx systems, and applying CNO / Compound 21, could also eventually lead to a TOK1-DREADD.

## 5.1 *Saccharomyces cerevisiae* may lack proteins to translocate TASK3, TREK1, and 5HT<sub>3A</sub> to the plasma membrane

In order to identify the activation site of halothane on two-pore domain potassium channels and to engineer a designer receptor to be exclusively activated by a designer drug, we first aimed to express the human potassium channels TASK3 and TREK1 and the mouse cation channel 5HT<sub>3A</sub> in yeast with deleted genes coding for the potassium transporters TRK1 and TRK2, and the channel TOK1. The channels were expressed with Venus-YFP fusions at the N and C terminus, under different promoters and terminators in different yeast strains. However, none of these combinations resulted in the trafficking of the channels to the plasma membrane and therefore they were unable to form functional channels to take up potassium ions in yeast.

We chose 5HT<sub>3A</sub> to be engineered into a DREADD because it is a homomeric protein and therefore requires only the expression of a single subunit, which usually self-assembles into a pentamer *in vivo*. It is also the ionotropic channel which has the highest affinity to clozapine (Roth & Driscoll, 2014). However, the subunit formed inclusion bodies. Initially, we tried to counteract this by regulating expression using weaker strength promoters or terminators that also affect expression strength but they were unable to redirect trafficking to the plasma membrane.

**Figure 27. The process of autophagy in yeast.** Inclusion bodies of non-functional proteins can form pre-autophagosomal structures that are enveloped in isolation membranes. These form autophagosomes that fuse with the vacuole. In the vacuole the proteins are degraded and contents are recycled (adapted from Suzuki & Oshumi, 2010)



5HT<sub>3A</sub> requires N-glycosylation at four asparagine residues for plasma membrane translocation and serotonin binding (Barnes *et al.*, 2009). Yeast do not N-glycosylate in the same manner as mammals, the main difference being that the yeast process adds more mannose to the oligosaccharide than the mammalian. This is because yeast is unable to do

anything more than add mannose and mannosylphosphate sugars at the Golgi apparatus (i.e. they lack enzymes to add key components of higher mammalian oligosaccharides N-acetylglucosamine, galactose, fucose and N-acetylneuraminic acid; Gerngross & Wildt, 2005). As sugars are important for targeting and recognition, this could prevent the cell from sending 5HT<sub>3A</sub> from the Golgi apparatus to the plasma membrane. The cell may instead form inclusion bodies – potentially pre-autophagosomal structures - to targeted to the vacuole for autophagy (Figure 27).

Unlike the two-pore domain potassium channels, 5HT<sub>3A</sub> does not have any obvious orthologous channels in *S. cerevisiae*, yet plenty of other non-yeast channels have been successfully expressed and folded to form the correct structure in *S. cerevisiae* (Tang *et al.*, 1995; Bichet *et al.*, 2004; Haass *et al.*, 2007; Schwarzer *et al.*, 2008; Bagriantsev & Minor Jr., 2013). However, sometimes this has required extensive modification of the channels by trial and error, for which the refinements are not consistent across different channel types (Routledge *et al.*, 2015). There is potential to overcome the lack of correct expression and translocation by “humanising” yeast (Laurent *et al.*, 2016). In the case of N-linked glycosylation, this would be to introduce genes to de-hypermannosylate and add other sugars necessary for WT 5HT<sub>3A</sub> glycosylation. It would also require rendering the cellular environment receptive to recognising the mammalian oligosaccharide in order to direct it to the correct location. However, the genetic manipulation required to create this intracellular environment had not yet been achieved and experimentation for this was beyond the scope of this current project.

Two-pore domain potassium channels, including TASK3 and TREK1 are evolutionarily related to the yeast potassium channel TOK1 (Figure 28). Structurally, it appears that TOK1 lost four of its eight transmembrane sections during the evolutionary process. However, their basic function of opening depending on membrane potential remains the same. It was hoped that replacing the potassium uptake system with TASK3 and TREK1 would allow for the complementation of this function. However, “humanising” *S. cerevisiae* in this way was not sufficient to do this.

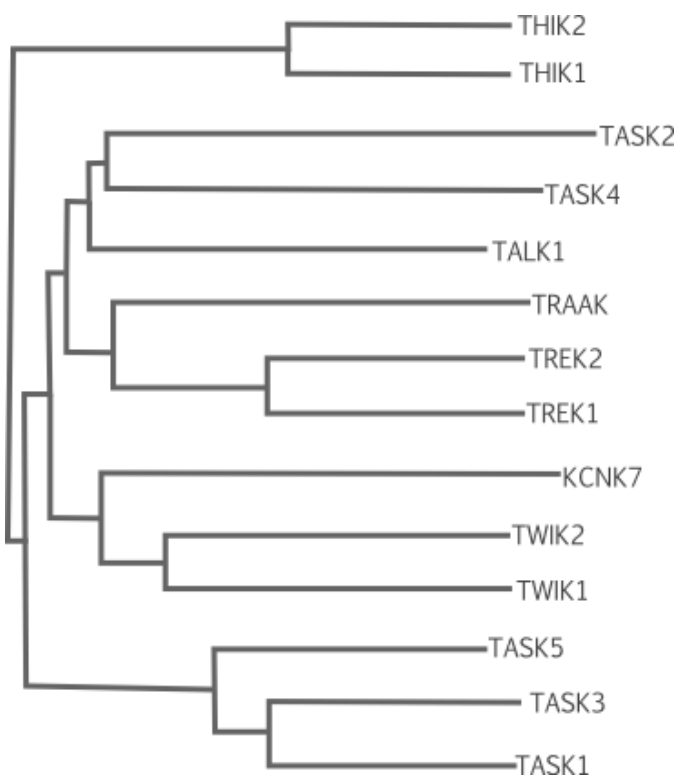
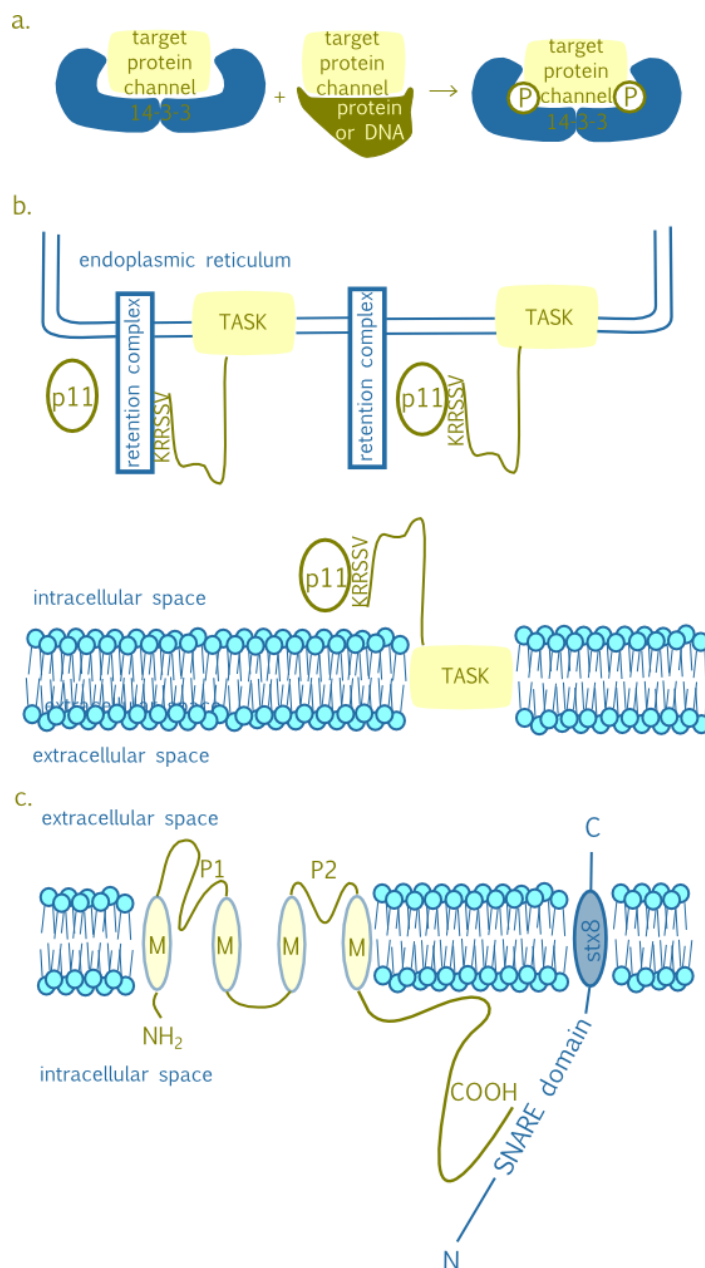


Figure 28. A phylogenetic tree illustrating the relatedness of tandem two-pore domain potassium channels. TOK1 is an ancestral homologue of mammalian channels (adapted from O'Donnell, 2012)

Although there have been few studies on the post-translational modification of K<sub>2</sub>P<sub>s</sub>, it is also the case (as it is for 5HT<sub>3A</sub>) that the yeast cell lacks protein partners that may be required to correctly process and fold the channels and target them to the plasma membrane. Although 14-3-3 proteins are ubiquitous in eukaryotes and are necessary for binding to signalling proteins, the number of paralogous genes in mammals outnumber those in yeast (Rajan *et al.*, 2002; van Heusden & Steensma, 2006; Figure 29a), and so it is possible that yeast 14-3-3 proteins are not sufficient to direct TASK3 and TREK1 to the plasma membrane. Furthermore, the p11 protein, also present in mammals, is necessary for the regulation of TREK1 and TASK3 translocation to the plasma membrane, shown to bind to a retention signal on the channel at the ER before it is released (Renigunta *et al.*, 2006; Kilisch *et al.*, 2015; Figure 29b). However, *S. cerevisiae* does not seem to have a homologous counterpart. Despite this, much of the translational and protein-processing machinery in eukaryotes is shared, and a syntaxin 8-like SNARE (necessary to dock TREK1 but not TASK3 endosomes to the plasma membrane) has been discovered in yeast and has been shown to fulfil many of the same endocytic roles as syntaxin-8 (Lewis & Pelham, 2002; Figure 29c). Therefore, although it is not impossible for yeast to express mammalian channels, it seems that the machinery in *S. cerevisiae* is unable to produce channels that assemble in a functional formation at the plasma membrane under the parameters tried so far.



**Figure 29. Proteins involved in the translocation of TASK3 or TREK1 to the plasma membrane in mammals;** a) 14-3-3 binds many signalling proteins in eukaryotes (adapted from Ginsburg, 2016); b) p11 interacts with TASK3 and TREK1. On TASK channels it binds to amino acid sequence KRRSSV to relieve it from an ER retention complex. This allows the channel to leave the ER (adapted from Tinel *et al.*, 2002); c) Syntaxin 8-like SNARE docks TREK1 endosomes to the plasma membrane (adapted from Renigunta *et al.*, 2014).

## 5.2 hTASK3 may be functional in K<sup>+</sup>-efflux but not K<sup>+</sup>-influx deficient *Saccharomyces cerevisiae* strains

As several mammalian channels have been previously expressed in *S. cerevisiae*, we hoped to replicate this with our channels of interest. In the past, Bernstein *et al.* (2013) successfully expressed hTASK3 (h signifying that codons were not optimised for *S. cerevisiae*) in B31, a strain derived from the same parental strain as SGY1528. The only difference between these two strains was that the genes for the potassium efflux system was deleted in the former and some genes for the influx system were deleted in the latter. They demonstrated that hTASK3 allowed an influx of K<sup>+</sup> and at excessive high external K<sup>+</sup> concentrations this phenotype killed cells. We also transformed hTASK3 under the regulation of the same promoter (pMET) into SGY1528 and grew them in low potassium, but were unable to demonstrate channel function as hTASK3 was not able to complement K<sup>+</sup> uptake gene deletions to allow yeast to grow. We also fused hTASK3 to Venus-YFP at the N terminus and C terminus to observe expression and saw that the fusion proteins formed inclusion bodies and were not trafficked to the plasma membrane (Figure 20). As a result, we were unable to conclude that hTASK3 is directed to the membrane.

There is a chance that the fusion of VenusYFP affected the channel's folding and processing in cells. Yet when hTASK3 was expressed without Venus-YFP fusion, cells did not survive in low external K<sup>+</sup> concentrations. This could be because channel expression may not have been sufficient to complement the modified uptake system. Indeed, even without a potassium uptake system, *S. cerevisiae* grows in high potassium media (Figure 10b, 12, 14b, 19, 22), demonstrating that this system becomes redundant at a certain concentration of potassium and therefore any additional pathway for K<sup>+</sup> uptake may become deadly (Figure 30).

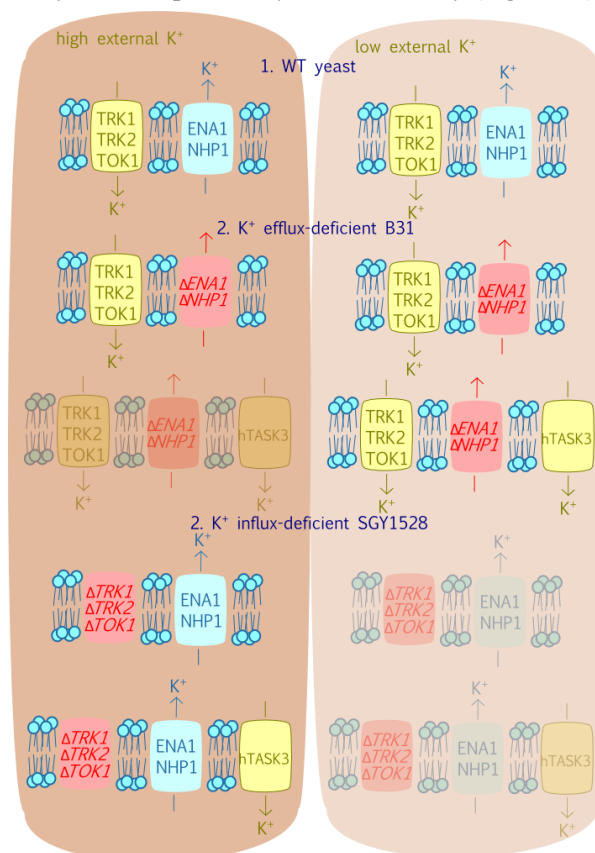


**Figure 30. B31 yeast strain lacking a K<sup>+</sup> efflux system survives in high and low external K<sup>+</sup> concentrations.** Upon expression of hTASK3, excessive internal K<sup>+</sup> causes cell death (represented by faded schematics). SGY1528 lacks a K<sup>+</sup> influx system and is able to survive only in high potassium media. The introduction of hTASK3 is unable to compensate for the endogenous yeast system.

Nevertheless, as Bernstein *et al.* (2013) did not show direct translocation to the plasma membrane, the death of B31 cells expressing hTASK3 remains an indirect way of demonstrating the successful assembly of hTASK3 at the plasma membrane.

### 5.3 Optimising mammalian codons for a *Saccharomyces cerevisiae* bias may not contribute to increased gene expression efficiency in yeast

Instead of humanising the yeast cell to render an environment more capable of processing mammalian ion channels in the correct way, we initially tried optimising the codons for *S. cerevisiae*. This changed the genetic code so that the most representative codons for each amino acid in *S. cerevisiae* replaced the human-biased codons and is frequently used for recombinant protein expression to prevent the rate-limiting effect of codon recognition by tRNAs (Ikemura, 1982). However, this could negatively affect expression because a biased code may have evolved in a way that contributes to translational processing. For example, less-representative codons may decelerate translation as it may take more time for the ribosome to recognise the codon and attach the correct amino acid. This slow-down may be necessary for proteins to fold correctly (Buchan & Stansfield, 2007). Incorrectly folded proteins form inclusion bodies which are degraded by the vacuole (Figures 10a, 14d, 18c). As a result, optimising the codons for *S. cerevisiae* may not have increased efficiency of translation and folding as intended. Instead the sequence could be harmonised, so that codons are replaced with those that are present at an equivalent frequency in yeast (Angov *et al.*, 2011).

### 5.4 TOK1 gene expression regulation is important to produce functional channels in *Saccharomyces cerevisiae*

Yeast strain	Promoter	Protein	Phenotype
$\Delta TRK1$ $\Delta TRK2$ $\Delta TOK1$  PLY246	pGAL1	TOK1	<ul style="list-style-type: none"> <li>Growth on media containing 5 mM K<sup>+</sup> or more.</li> <li>No difference in growth compared to cells without TOK1 transexpression.</li> </ul>
	pTEF1	TOK1:VenusYFP	<ul style="list-style-type: none"> <li>Intracellular protein inclusions.</li> <li>No translocation of protein to the plasma membrane.</li> </ul>
	pRPL18B	TOK1:VenusYFP	<ul style="list-style-type: none"> <li>Protein translocated to plasma membrane.</li> <li>Growth on media containing 1 mM K<sup>+</sup> or more.</li> <li>Fitness is greater than cells without TOK1 transexpression up to 5 mM.</li> </ul>
$\Delta TRK1$ $\Delta TRK2$  SGY1528	pGAL1	TOK1	<ul style="list-style-type: none"> <li>Growth on media containing 5 mM K<sup>+</sup> or more.</li> <li>No difference in growth compared to cells without TOK1 transexpression.</li> </ul>
	pTEF1	TOK1:VenusYFP	<ul style="list-style-type: none"> <li>Protein translocated to plasma membrane.</li> </ul>
	pRPL18B	TOK1:VenusYFP	<ul style="list-style-type: none"> <li>Protein translocated to plasma membrane.</li> </ul>
$\Delta TRK1$ $\Delta TRK2$  R5421	pGAL1	TOK1	<ul style="list-style-type: none"> <li>Growth on media containing 5 mM K<sup>+</sup> or more.</li> <li>No difference in growth compared to cells without TOK1 transexpression.</li> </ul>
	pTEF1	TOK1:VenusYFP	<ul style="list-style-type: none"> <li>Protein translocated to plasma membrane.</li> <li>No difference in growth compared to cells without TOK1 transexpression.</li> </ul>
	pRPL18B	TOK1:VenusYFP	<ul style="list-style-type: none"> <li>Intracellular protein inclusions.</li> <li>No translocation of protein to the plasma membrane.</li> </ul>

**Table 9. Summary of the phenotypes resulting from expression of TOK1 under regulation of different promoters and in different yeast strains**

As TOK1 is an evolutionarily ancestral homologue of mammalian tandem two-pore potassium channels, we decided to try to identify the activation site of halothane on this channel as we were not able to traffic mammalian channels to the plasma membrane. To verify that non-chromosomal TOK1 would be expressed, folded, and translocated correctly to the plasma membrane, the transgene was expressed in a range of vectors in several yeast strains. We found that the combination of promoter and strain was important to produce channels that are trafficked to the plasma membrane and that are functional (Table 9). This baseline step was necessary to ensure that a mutated channel would not be non-functional due to expression or plasma membrane translocation being inhibited by default.

## 5.5 Arachidonic acid is a known agonist of yeast TOK1 and related mammalian TREK1 channels

As arachidonic acid has been shown to activate TOK1 from pathogenic yeast when expressed in *Xenopus laevis* oocytes (Manville *et al.*, 2016), we decided to investigate whether it would be able to activate the channel in *S. cerevisiae* with compromised potassium influx systems to allow them to survive in low potassium media. We found that yeast strains SGY1528 and R5421 expressing genomic TOK1 (but with deleted TRK1 and TRK2 potassium transporters) and PLY246 lacking all three proteins grew better in the presence of increased arachidonic acid when transgenically expressing TOK1, TRK1, or neither (Graph 3 & Figures 23a-c). This was expected with TOK1 expression but was not consistent with the concept of TOK1 activation allowing potassium to enter the cell conducting survival in low potassium media. Although observations included that 100  $\mu$ M arachidonic acid was too low a concentration to improve colony growth, and growth enhancement at 200 and 300  $\mu$ M arachidonic acid was blunted in R5421 expressing TRK1 in comparison to TOK1 (Graph 3); little is known about potential targets of arachidonic acid in non-pathogenic yeast.

Arachidonic acid is a known precursor to important metabolites in yeast and contribute to membrane integrity and pathogenesis. Prostaglandins produced from exogenous arachidonic acid in yeast aids in the production of biofilms during infection (Ells *et al.*, 2012). Arachidonic acid from host cells affects the fluidity of yeast cell membranes by contributing to phospholipid structure and one group found that pre-treating biofilms with the fatty acid increased their susceptibility to antifungals (Ells *et al.*, 2009), whilst other experiments show that inhibiting cyclooxygenases which produce arachidonic acid decreased infection (Grózer *et al.*, 2015). Therefore, it could be that exogenous arachidonic acid was taken up by *S. cerevisiae* via a TOK1-independent pathway and improved growth efficacy in a similar mechanism which influences pathogenic yeast biofilm viability.

After conducting three to five repeats per yeast strain and treatment, as well as positive control growth on 100 mM K<sup>+</sup> agar plates, we tried quantifying growth using liquid media. However, arachidonic acid formed lipid globules due to its hydrophobic nature. We decided to move on and focus on our agonist of interest, halothane.

## 5.6 A novel halothane incubation chamber was set up to provide controlled and consistent gas exposure to yeast cultures

Gray *et al.* (1998) previously showed, using electrophysiology experiments in *Xenopus* oocytes, the activation of TOK1 and K<sup>+</sup> current flow upon exposure to fluorinated anaesthetics halothane, isoflurane and desflurane. Based on this, we set up an airtight system to expose *S. cerevisiae* to halothane or air with adjustable pressure, flow rate, percentage of halothane gas (1-5 %; empirically demonstrated to reach a maximum of 4.3 %), temperature, and shaking speed (Figure 24). As the system was constructed internally it would be straightforward enough to modify any of these parameters, and even the size of incubation boxes to augment the number of simultaneously exposed cultures and subsequently to increase the throughput of the method. Boxes hold agar plates as well as 96-well micro-titer plates which are traditionally used for high throughput growth screening methods.

## 5.7 Growth responses to halothane 5 % between yeast strains, protein expression, and potassium concentration

Although spotting experiments on agar were sufficient to observe growth patterns of yeast colonies in the presence versus the absence of arachidonic acid, yeast colony exposure to halothane did not seem as efficient in differentiating impact on growth. This could be due to the fact that setting the fatty acid in warm agar allowed it to disperse through the agar jelly but its hydrophobic nature prevented emulsification in liquid media. Oppositely, halothane may not have been able to effectively penetrate the agar to affect yeast growth, whilst it would have dissolved more easily in liquid media

Gray *et al.* (1998) used 0.016 atm (814  $\mu$ M) for 50 % potentiation (EC50) of recombinant TOK1 expressed in *Xenopus* oocytes. This is lower than the minimum inhibitory concentration of 0.06 atm, which is the concentration that was shown to inhibit growth of *S. cerevisiae* strain RLK88-3C (*Mata his4-260 leu2-3, 112ura3-52 ade2-1 trp1-HIII lys2 $\Delta$ BX can1R*) on solid media after three days (Keil *et al.*, 1996). Due to our setup of flowing halothane with air parallel to control condition of 100 % air, we did not use the same units to measure the level of halothane exposure of yeast with compromised potassium influx systems expressing genomic TOK1, transgenic TOK1, transgenic TRK1, or not expressing TOK1. Yeast were exposed to air and halothane 5 % at different concentrations of K<sup>+</sup> (0.5-100 mM), for 24 h or 48 h.

Analyses were conducted between single strains expressing different proteins, and between paired replicates in air and halothane 5 %. (Comparisons were not made *between* strains, levels of potassium, or growth time.) As variation in growth response was high per replicate averages, no statistical significance was found relating treatment condition to growth rate.

A single significant result by ANOVA suggests that after 24 h, R5421 (-TRK1, -TRK2, genomic TOK1) has a higher growth rate in 5 mM K<sup>+</sup> media when exposed to halothane 5 % compared to expressing an additional TOK1 or TRK2 transgene (Graph 6a; Appendix 6.12). It is difficult to interpret this result on its own, especially because literature published on the function of TOK1 as a K<sup>+</sup> channel is not consistent. It could be that halothane is indeed opening the endogenous TOK1 channel in and allowing K<sup>+</sup> to influx and improve the survival of this strain. Additional TOK1 transexpression may be a burden on cells, decreasing viability. Indeed, it is not uncommon for the health of yeast to decrease when overexpressing transgenes, especially if the protein is functional in the cell (as is the case for TOK1). Previous TOK1 electrophysiological experiments demonstrated outward K<sup>+</sup> current flow and research suggests that direction of flow depends on the polarised state (electrochemical potential) of the yeast cell (Loukin & Saimi, 1999), and in this case halothane activation of additional TOK1 channels may initially cause high K<sup>+</sup> influx followed by a reversal in flow direction where excess in either direction could be detrimental to cell viability. Despite past publications demonstrating TOK1 transexpression able to complement the deletion of yeast K<sup>+</sup> influx channel genes, Johansson and Blatt (2005) came to the conclusion that TOK1 was unable to open at concentrations above 3 mM K<sup>+</sup>. This directly contradicts the findings of other groups. Indeed, survival in low potassium media is an indirect way of verifying that TOK1 is functional as a K<sup>+</sup> influx channel, but Johansson and Blatt (2005) also concluded that TOK1 is an efflux-only channel, which has also been contested with.

5 mM K<sup>+</sup> could be a threshold concentration where endogenous TOK1 activation increases viability but the opening of TRK1, a more efficient K<sup>+</sup> transporter, may uptake surplus K<sup>+</sup> and in turn decrease cell viability. This pattern of yeast growth is similar after 48 h - though without statistical significance - and expression of exogenous TOK1 or TRK1 seems to be detrimental to growth rate in the presence of halothane (Graph 7a; Appendix 6.14).

It is interesting to look at results using a different strain, SGY1528, with the same modified K<sup>+</sup> system (-TRK1, -TRK1, genomic TOK1) with growth patterns differing to R5421, suggesting that genetic background affects transgenic protein expression and growth rate. Variation in growth rate as a response to halothane is too high to infer statistical significance, but an interesting pattern can be observed in 1 and 2 mM K<sup>+</sup> media after 24 or 48 h, and additionally in 3 mM K<sup>+</sup> media after 48 h, where growth rate is highest with the additional transexpression of TOK1 compared to an empty vector or TRK1 expression in halothane 5 % versus air (Graphs 6b and 7b; Appendix 6.12 and 6.14). In this case, if halothane is activating TOK1, additional transgene expression may allow the influx of K<sup>+</sup> to increase cell viability in concentrations (1-3 mM K<sup>+</sup>) which may otherwise be too low for high growth rate.

There does not seem to be any clear or interesting inferences that can be drawn from growth experiments involving strain PLY246 (-TRK1, -TRK2, -TOK1). However, there are differences in growth response to treatment conditions even between clones transformed with the same TOK1 vector. In some conditions halothane is detrimental to the growth of one clone but not the other (e.g. 0.5, 1, 5, and 100 mM media after 48 h; Graph 7c; Appendix 6.14) which may suggest that the health of cells and protein function can differ between clones.

Regarding the overall health of cells with transgenes, from observation it is noticeable that colonies transformed with TOK1-VenusYFP transgenes look smaller and grow more slowly than cells without transgenes; whereas cells transformed with TRK1 transgenes form very robust colonies (results not shown). Therefore, higher growth rates in the presence of halothane of clones transexpressing TOK1 compared to those which do not may be worth bearing in mind, because in non-stressful growth conditions this is not the observed norm.

Sample sizes would have to increase to infer statistical significance between differences in growth rate, if it is the case that halothane has a direct effect on *S. cerevisiae* growth (via TOK1) as variation in growth rate per treatment conditions should decrease. Although it is already interesting to observe that growth rate of yeast strains is higher in halothane after 24 h compared to with air, as difference in fold-increase in growth (fold-increase in growth of cells in air subtracted from halothane) is positive on all graphs (Graphs 6a-c; Appendix 6.11 & 6.12). After 48 h, there is more variation in data (Graphs 7a-c; Appendix 6.13 & 6.14).

## 5.8 Yeast-transformation associated recombination allows for the transformation, integration, and expression of TOK1-VenusYFP in a single step

Following the exposure of yeast strains with compromised K<sup>+</sup> influx systems to halothane 5 %, cells were transformed with linear TOK1-VenusYFP sequences flanked by sequences homologous to the 3' and 5' sites of the genomic TOK1 locus. This technique allows for DNA to be transformed, integrated into the genome, and then expressed using the endogenous TOK1 promoter in a single step. A previous group quantified yeast transformation-associated recombination (TAR) to have produced 32% positive clones versus only 0.03 % from a bacterial artificial chromosome DNA library (Kouprina & Larionov, 2016).

Following transformation, cells were spotted to form artificial colonies on agar and screened using Venus-YFP signal in microscopy (Figure 26). For SGY1528 and R5421, expression was observed in the vacuole and cytoplasm and signalling was too faint in PLY246 to be captured. These locations were unexpected, as previous observations showed the fusion protein targeted to the plasma membrane (Figure 21). Successful expression had previously depended on the promoter strength and yeast strain combination (again, highlighting the importance of unique yeast strain genetics). It was assumed that expression driven by the endogenous TOK1 promoter would be optimal, but vacuolar translocation usually signifies the recycling of non-functional proteins during autophagy.

To verify that integration was successful, colony PCR was conducted on the screened samples but the PCR conditions proved suboptimal (as the positive control template being the original plasmid which the linear DNA was copied from did not yield a positive signal). Optimising this verification step would be the next immediate part of the project.

Artificial colonies were inoculated in media and grown to late log phase to observe Venus-YFP signal to rule out the possibility that fusion protein location was in the vacuole after the functional life-cycle of the protein during the cell's stationary phase. However, no Venus-YFP signal could be observed from cells grown in liquid media after a couple of attempts. It is likely that the inoculation colony could have contained successfully and non-successfully transformed cells, and those without a transgene to express would be healthier and outgrow those expressing the fusion protein.

Although classical screening methods based on auxotrophy were unable to be employed in this experiment, for halothane-exposure experiments mutant TOK1 sequences with a higher affinity for TOK1 activation would increase the fitness of their host cells and outgrow those without TOK1. R5421 could have its genomic TOK1 sequence replaced by Venus-YFP as a negative control. The screening selection would be based on cells which express mutant TOK1 sequences that have a higher growth rate in halothane than air compared to this R5421 Venus-YFP negative control. Therefore, the next step would be to generate a Venus-YFP sequence with upstream and downstream homologous ends to those flanking the TOK1 genomic locus and perform TAR on R5421. These cells could also be used to conduct yeast TAR targeting the site immediately upstream to Venus-YFP with mutant TOK1 sequences encoding a 3' linker, so that cellular location of mutant TOK1-VenusYFP fusion proteins can be observed.

Based on halothane exposure experiments, transformation of Venus-YFP and mutant TOK1 sequences could be conducted in the strain R5421 and grown in 5 mM K<sup>+</sup> for 24 h in halothane 5 % and air. Electroporation methods could also increase transformation uptake of linear DNA.

## 5.9 Further work

Upon the validation of the baseline parameters for the experimental assay, including the amount of halothane to expose yeast to, the length of time, external K<sup>+</sup> concentration, and yeast strains with deleted K<sup>+</sup>-influx genes for TOK1 overexpression; the TOK1 sequence can be subjected to random mutagenesis, transformation-associated recombination, and screened by exposing yeast to halothane or CNO / Compound 21. Mutant TOK1 sequences which improve cell viability would be re-subjected to several rounds of directed evolution. To develop a better understanding of halothane binding sites on tandem two-pore domain K<sup>+</sup> channels, sequences which improve cell viability can be aligned to identify similarities which may elucidate where this could be. Experiments involving designer drugs may allow for the development of an inhibitory DREADD without the secondary signalling cascades of GPCR-based DREADDs.

### 5.91 How many random mutations should be introduced by error-prone PCR?

Using the directed evolution methods for development of hM3Dq (Armbruster *et al.*, 2007) and GEVI Archon1 (Piatkevich *et al.*, 2018), random mutagenesis could be conducted using the Stratagene GeneMorph II Random Mutagenesis Kit following parameters in established methods. A key question is the number of mutations to introduce to the TOK1 sequence. Armbruster *et al.* (2007) introduced a conservative average of 3.5 mutations/kb (1770 bp sequence length), whilst Piatkevich *et al.* (2018) introduced 10-15/kb (759 bp sequence length). As initial selection following random mutagenesis by Piatkevich *et al.* (2018) was based on fluorescence level and protein location, this may have afforded them to introduce a high number of mutations whereas the selection for Armbruster *et al.* (2007) was based on cell viability in the presence of a drug. Therefore, if too many mutations were introduced into hM3, there may have been fewer cells with functional receptors able to respond to the selection pressure.

TOK1 (2077 bp in length) could be subjected to 3.5-15 mutations/kb, iterating the protocol to identify the optimal frequency to produce variation in affinity to halothane but not so many that it becomes non-functional (Table 10).

Channel	PCR cycles	Mass	Molecular concentration	DNA copy number	Mutations/kb
HM3 1770 bp	30	250 ng	228 amol	$1.3 \times 10^{11}$	-
mHM3 1770 bp	-	375 ng - 2.5 $\mu$ g	343 amol - 228 fmol	$2 \times 10^{11}$ - $1.3 \times 10^{12}$	3.5
Archon1 759 bp	Not mentioned	Not mentioned	-	-	10-15
TOK1 2073	30	250 ng	195 amol	$1.1 \times 10^{11}$	-
mTOK1 2073	-	375 ng - 2.5 $\mu$ g	293 fmol - 1.95 pmol	$1.8 \times 10^{11}$ - $1.1 \times 10^{12}$	3.5-15

Table 10. Parameters as conducted by Armbruster *et al.* (2007) on the human muscarinic acetylcholine channel 3 (HM3) and Piatkevich *et al.* (2018) to produce Archon1 calculated using NEBioCalculator™ v.1.1 (NewEngland Biolabs Inc., 2019).

### 5.92 What size would be the mutagenetic library be?

To gauge an idea of the library size required to produce responsive clones we can look at past directed evolution experiments. Random mutagenesis of complete protein sequences does not aim to change every base pair to every possible nucleotide in every combination, as this would be impossible to carry out empirically. Instead, scientists aim to change every codon to every other possible codon (64) at least once. This usually generates library sizes of around four orders of magnitude ( $1-7 \times 10^4$  variants; Table 11). Piatkevich *et al.* (2018) screened libraries of size  $1.2-4.6 \times 10^6$  clones, but used automated screening methods including a robot to initially sort 300,000 cells in four hours which allowed them to generate such a large library size.

Molecular tool and basis protein	Length of peptide	Mutagenesis library size
hM3Dq based on M3	590 amino acids	$3 \times 10^4$ clones, $6 \times 10^4$ colonies screened $7 \times 10^4$ clones, $2.5 \times 10^4$ colonies screened Based on five 2 <sup>nd</sup> generation clones: $6 \times 10^5$ clones, $8 \times 10^4$ colonies screened
Camagaroo based on cpGFP	239	$2.5 \times 10^4$ clones screened
QuasArs based on Archaelhodopsin	260	Five rounds of mutagenesis $10^4$ clones per round
Archon1 based on QuasAr2	253	Three rounds of $10^6$ variants
TOK1	691	Estimated $4.4 \times 10^4$ clones per library

Table 11. Library sizes of past directed evolution studies for optogenetic and chemogenetic molecules. A TOK1 library size by accounting for a change of every codon to every other possible codon once.

We can also use established engineering methods to predict potential library sizes. Design of experiments is a systematic method to determine cause and effect relationships. It allows the user to identify the likelihood of a factor being able to produce a certain response by using the fewest number of experimental runs, thus saving on resources such as time and money (Antony, 2014). It is an iterative process where the higher the number of runs ( $n$ ), the higher the statistical significance of the cause and effect relationship, but calculates the minimal  $n$  number to reach a significant p-value. This means that it calculates the minimum library size needed in order to identify a region of the TOK1 sequence activated by a drug with statistical significance, where increasing library size increases the specificity of activation location on the sequence. This iterative design method accounts for the gaps in size between the number calculated for the fractional factorial design, actual library size, and full factorial design. The calculations necessary to work out the minimum library size design of experiments requires training to understand and use specialist software which is outside of the scope of this Discussion.

### 5.93 Parallel designer drug selection on mutant TOK1

Initially, parallel experiments were suggested to identify transformed cells which would respond to the selection pressure of CNO or Compound 21 in order to generate an ionotropic designer receptor to be exclusively activated by a designer drug. Following the methods of Armbruster *et al.* (2007), cells can be spotted on agar. Upon growth, the plate would be stamped and replicated onto two new plates containing a low concentration of  $K^+$ , one of which would contain 1  $\mu$ M CNO/ Compound 21 (for the 1<sup>st</sup> generation library) or 5 nM CNO / Compound 21 (for the 2<sup>nd</sup> generation library), and a control without drugs. After 5-7 days of growth, cells in low potassium with enhanced growth in the presence of CNO / Compound 21 but not in the absence would then be inoculated into liquid media, of which replicate pairs would contain CNO / Compound 21 and a control without drugs. Once growth differences are quantified, clones of interest would then be identified.

### 5.94 How could mutated sequences of interest be analysed?

Selected yeast cells could be grown on a larger scale in the presence of halothane or CNO after which PCR would be conducted on cells to obtain copies of the mutated TOK1 sequence. PacBio single molecule real time sequencing could be used as it has faster run times than second generation methods. It is extremely high throughput and one read can sequence  $1.5 \times 10^5$  reads up to 20 kb. Shorter sequences produce more accurate results (Rhoads & Au, 2015) and TOK1 is only 2077 bases long.

Adapters with unique barcodes would be ligated to the amplicons to tag unique mutated TOK1 sequences of interest and link them with yeast clones. To increase the throughput of this stage we can use programs to analyse DNA sequences to identify those with frequent mutations in single locations, potentially pointing to activation sites of TOK1 by agonists.

The sequence could then be re-cloned into entry vectors using established Golden Gate cloning methods and the Yeast Tool Kit, before being resubmitted to random mutagenesis and repeating the transformation, plating, drug exposure, and screening.

## 5.95 Homology-based mutagenesis

BLAST alignment of *S. cerevisiae* TOK1 with mouse TREK1 and mouse TASK3 peptide sequences show areas of high homology: residues 80 to 242 of TOK1 align with residues 257 to 439 of TASK3 (Figure 32a), and residues 137 to 207 of TOK1 align with residues 405 to 475 of TREK1 (Figure 32b). Aligning TASK3 and TREK1 highlights the first 292 residues of TASK3 as having high homology to residues 53 to 349 of TREK1 (Figure 32c). Therefore it might be worth focussing initial directed evolution techniques on residues 80 to 115 of TOK1 (Figure 31) to reduce the number of variants for screening to  $(35 \times 64 = 2240)$ . Mutated variants could be electroporated into yeast cells using for transformation-associated recombination following the establishment of the strain and growth parameters to be used.

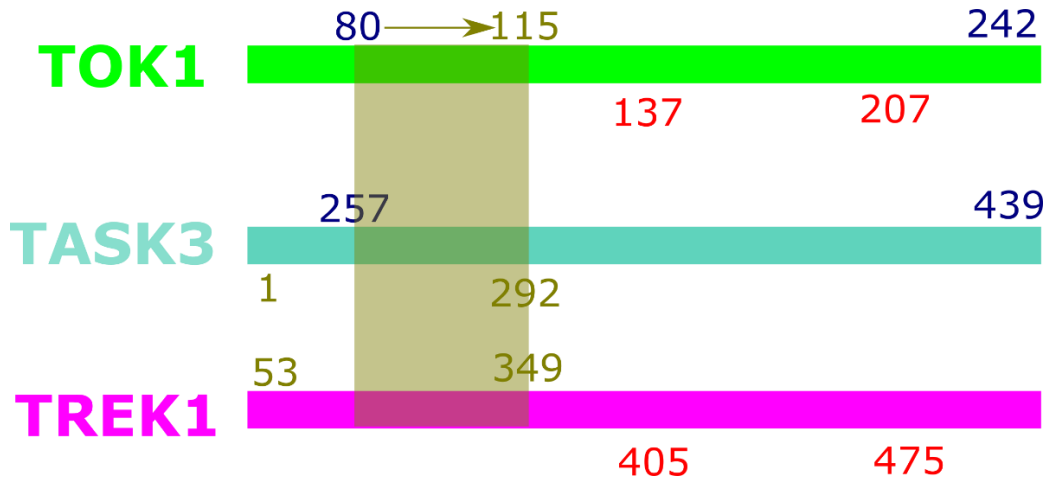


Figure 31. Combining BLAST alignments of TOK1, TASK3, and TREK1 peptide sequences shows a stretch of overlapping homology. Level of alignment specificity not taken into account. Illustration not to scale.

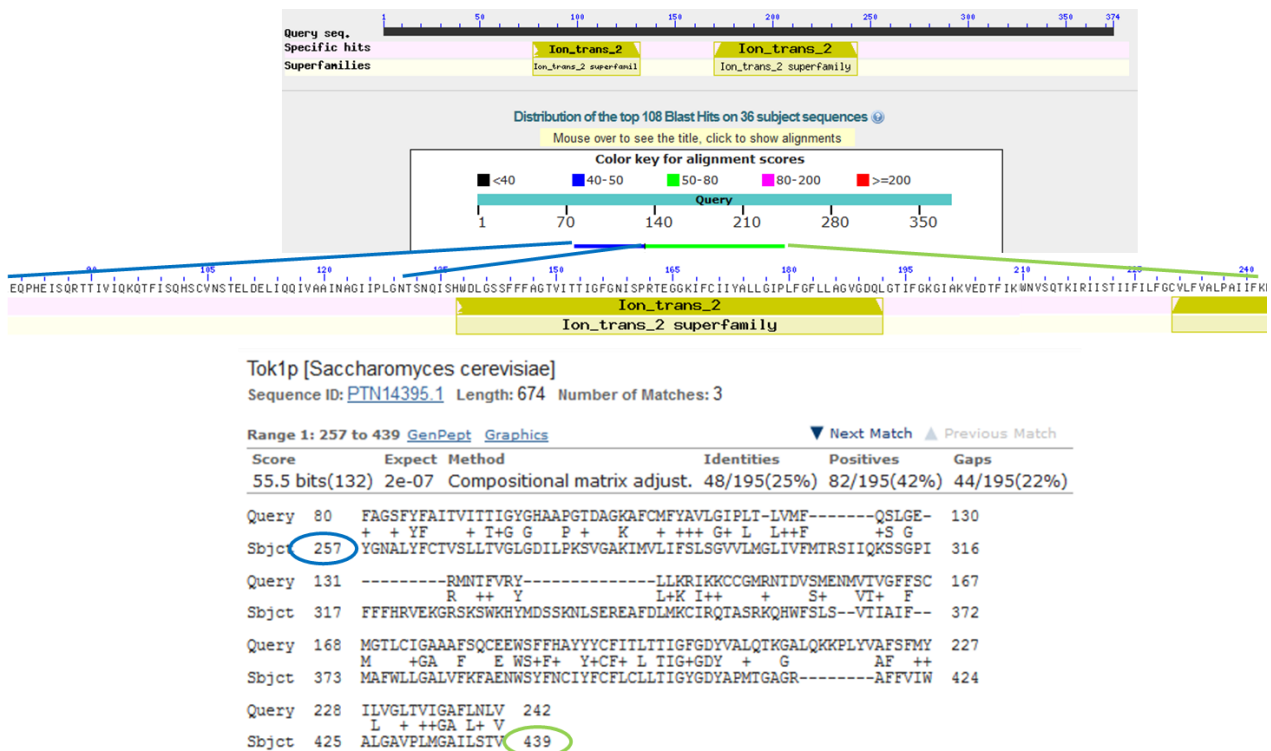
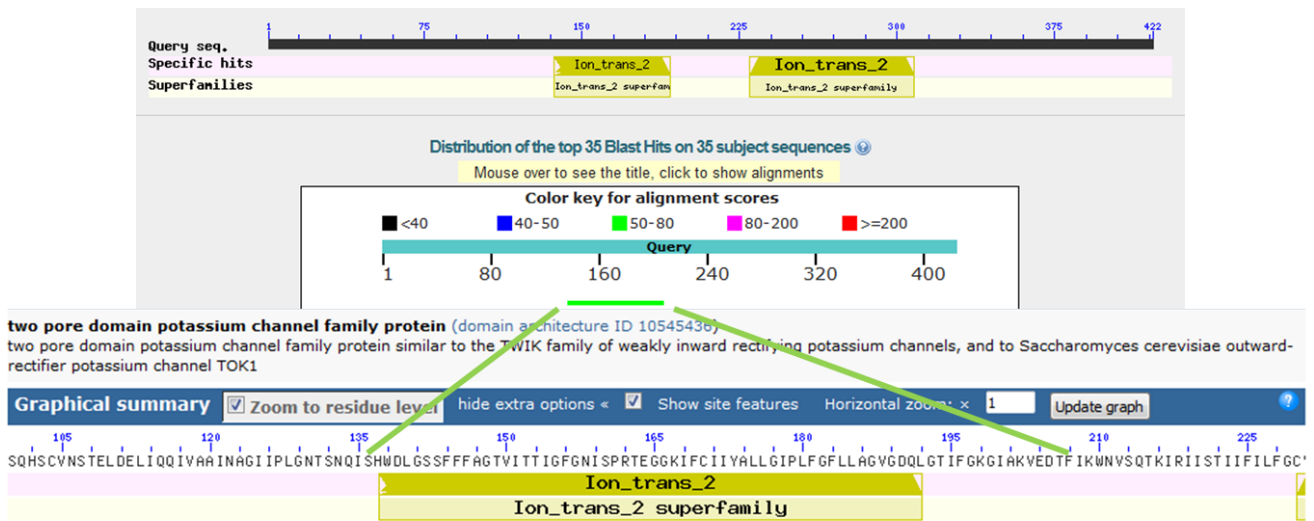


Figure 32a. Residues 257-439 of TASK3 align with residues 80-242 of TOK1. Blastp alignment of TASK3 and TOK1 (query) amino acid sequence (U.S. National Library of Medicine, 2018).



Tok1p [Saccharomyces cerevisiae YJM248]

Sequence ID: [AJR60749.1](#) Length: 691 Number of Matches: 1

Range 1: 405 to 475 [GenPept](#) [Graphics](#) [Next Match](#) [Previous Mat](#)

Score	Expect	Method	Identities	Positives	Gaps
52.0 bits(123)	3e-06	Compositional matrix adjust.	25/71(35%)	42/71(59%)	0/71(0%)

```

Query 137 HWDLGSSFFAGTVITTIIGFNGISPRTEGGKIFCIIYALLGIPFLGFLLAGVGDQLGTIF 196
           +W + +F ++IIG+G+ +PRI G+ F +I+AL +PL G +L+ VGD L I
Sbjct 405 NWSYFNCIYFCFLCLSTIIGYGDYAPRTGAGRAFFVIWALGAVPLMSAILSTVGDLLDIS 464

Query 197 GKGIKVEDIF 207
           K+ ++F
Sbjct 465 TSLDIKIGEST 475
  
```

Figure 32b. Residues 405-475 of TREK1 align with residues 137-207 of TOK1. Blastp alignment of TREK1 and TOK1 (query) amino acid sequence (U.S. National Library of Medicine, 2018).

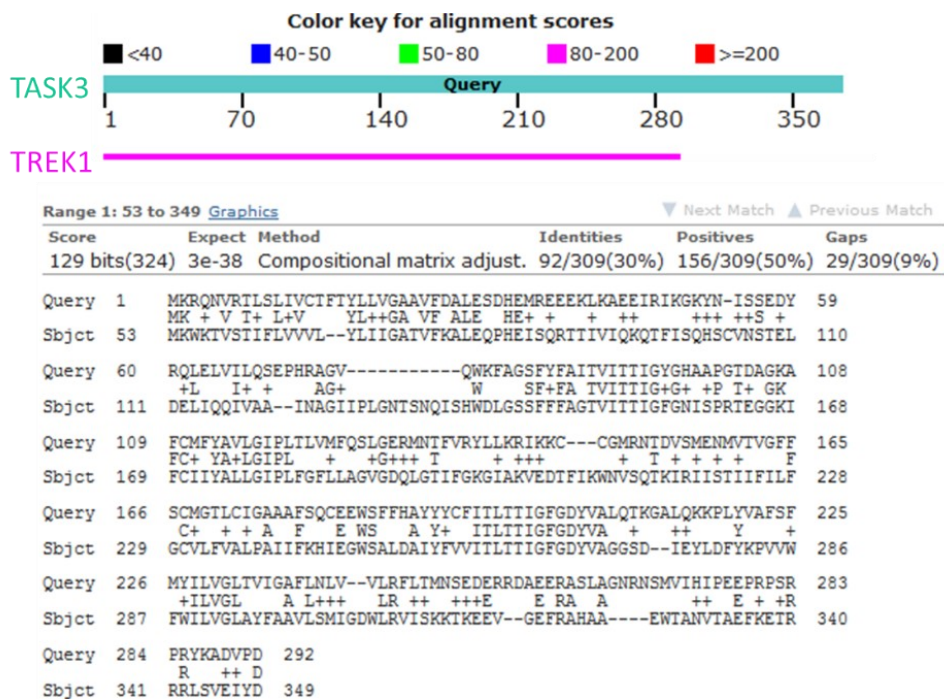


Figure 32c. Residues 1-292 of TASK3 align with residues 53-349 of TREK1. Blastp alignment of the TASK3 (query) and TREK1 amino acid sequence (U.S. National Library of Medicine, 2018).

## 5.96 Computer modelling and 3D crystal structure techniques

Building on methods to increase the efficiency of directed evolution, the putative halothane binding site could be estimated algorithms comparing selected binding sites or whole protein surface structures with databases of other proteins structures. There are several commercially available tools able to conduct such database scanning. For example, structures can be scanned against known binding motifs, or focus on surface patches perhaps in putative binding pockets. Breaking down the structure into patches can aid in the recognition of similar sectional binding structures modified by exogenous protein dynamics (Konc & Janežič, 2014). Similarities may not necessarily indicate sites of ligand binding, as non-binding residues can also be highly conserved.

As two-pore domain K<sup>+</sup> channels are evolutionary related and are all activated by halothane, with enough time there could be scope to undertake such a study to identify putative binding sites prior to empirical investigation.

However, sometimes protein structural models can be of low resolution. This could be resolved by directed evolution conducted on the area of putative halothane binding. This would simultaneously remove the need substitute amino acids to all combinations within the peptide. Relying on computational methods would not be sufficient as little experimental data is available on the Protein Data Bank for protein-ligand complexes. Studies have shown that prediction methods can overlook 30 % of known binding sites (Chen *et al.*, 2011).

If query proteins cannot be aligned with other proteins with similar activity, conserved binding sites can be investigated, as binding sites are sometimes common across proteins if occupied by similar ligands. Related ligand-binding may have led to conserved functional groups but with site variation for ligand specificity. For investigations of drug binding, some tools agglomerate weakly related structures and model drug docking. In such instances, parameters including size, shape, hydrophobicity and pocket similarities are taken into account. Studies have shown that global and binding site structural similarity can play a larger role in underlying drug interactions across several proteins than ligand properties such as flexibility, hydrophobicity, or molecular weight (Konc and Janežič, 2014).

Molecular dynamics model ways in which ligands of interest can bind to the protein query, although exhaustively modelling all combinations of ligand-protein interactions is not possible. High resolution interaction models can simulate various temperature, pressure, solvation and pH conditions. Thermodynamics calculations can approximate protein-ligand affinity and stability, but can be computationally costly (Broomhead & Soliman, 2017).

TOK1 does not yet have an available crystal structure, but mapping homologous regions to extant gated K<sup>+</sup> channel crystal structures can help identify common conserved sites. Johansson and Blatt (2005) mapped TOK1 pore domains to bacterial KcsA, MthK (*Methanobacterium thermoautotrophicum* K<sup>+</sup> channel), KvAP and Kv1.2 K<sup>+</sup> channels, to identify residues contributing to K<sup>+</sup> gating. Voltage-gated K<sup>+</sup> channels span across seven phylogenetic evolutionary families (Doyle *et al.*, 1998; Jiang *et al.*, 2002; Long *et al.*, 2005; Chen *et al.*, 2003; Kuang *et al.*, 2015). Extracellular domains were demarcated using this method, which may also be similarly useful in identifying agonist binding sites. This may also suggest that mutations rendering TOK1 able to be activated by halothane could be transferred to related potassium channels (similar to the transfer of mutations across muscarinic-DREADDs), which may provide a useful range of tools to be expressed in and inhibit neurons.

Some optogenetic molecules have been developed using similar methods. Structure-guided mutagenesis of the Chr2 retinal-binding pocket produced just over 50 variants that were screened in *Xenopus* oocytes. Rationally introducing

E123T led to ChR ET/TC led to augmented photocurrents ten times larger than WT ChR-2 and faster repolarisation (Berndt *et al.*, 2011). Computer modelled molecular dynamics highlighted targeting of glutamate residues lining the pore on ChR transmembrane helix 2. Molecular dynamics demonstrated that water distributed with discontinuity around E90 which interacts with the retinal Schiff base, and undergoes a protonation change during the photocycle regulating ion gating (Wietek *et al.*, 2014).

To ameliorate an engineered ChR1-ChR2 hybrid, iC1C2, the mutated residues in the ion-conduction pathway were reviewed using a second round of structure-guided mutagenesis. Screening 11 variants highlighted five interesting point mutations. Combining mutations improved iC1C2 to iC++. When compared with WT rhodopsin GtACR2, electrostatics of the engineered pore was found to be very similar, demonstrating that structure-guided mutagenesis as a process of directed evolution produced a solution consistent with natural evolution in a faster time. However, *in vivo* expression and activation of iC++ did not mediate an engram underlying Pavlovian conditioning better than iC1C2 (Berndt *et al.*, 2016).

Following the identification of mutated TOK1 residues which render the channel more sensitive to halothane activation and transform them into DREADDs, residues could also be mapped to related mammalian potassium channels. Mapping could give some indication as to whether the activation regions are evolutionarily conserved. If residues are transferrable, it would be ideal to generate a 3D structure (with and without halothane or Compound 21 docking) to scan it against a database of related channels. Related ligand-binding may have led to conserved functional groups but with site variation for ligand specificity (Konc and Janežič, 2014).

### 5.97 Establishing workflow and throughput

Empirical limitations can be identified by analysing each stage of the method and depend on efficiency, time required, and available manpower (Table 12). A clearer idea of throughput efficiency and limitation can be established upon the refinement of protocols and continuity of throughput methods.

Challenge	Mitigation
Low fidelity PCR products	Run maximum number of PCR reactions simultaneously (once mutation frequency per kb is empirically established)
Number of plates that fit in incubator	Make bigger airtight boxes For plates and cultures that do not require continuous gas flow, they can be grown at RT instead of in the incubator at 30 °C
Number of PCR, transformation, and growth experiments that can be conducted each day	Can be established empirically
Number of days required to grow colonies: 24 h for halothane and air exposure Overnight for non-agonist liquid media inoculations 5-7 days for agar plate growth in air at RT 3-5 days for agar plate growth at 30 °C 3-5 days for Compound 21 liquid media growth at RT	Experiments can be conducted in a staggered order
Number of replicates required for experimental validation	3
Screening of mutated sequences of interest	Use (and potentially modify) an automated computer program for sequence analysis
Library size	Estimated $4.4 \times 10^4$
Entry vector cloning of sequence of interest	Optimise existing protocol using Golden Gate cloning method and Yeast Tool Kit

Table 12. Challenges to the project and how they could be mitigated.

## 6. Future perspectives

### 6.1 Biophysical characterisation of halothane-hypersensitive TOK1 and TOK1-DREADD

Halothane-hypersensitive TOK1 and TOK1 DREADDs could be characterised using electrophysiological techniques, as were done on optogenetic molecules. If transferring residue changes to related mammalian potassium channels confers the same properties, these channels could also be investigated in the same way. Channel constructs can be codon harmonised to human genome bias, tagged with fluorescent proteins, and transfected in HEK293. 48-72h post transfection whole-cell voltage clamp can be used to record photocurrents of fluorescent cells in response to different concentrations of drugs. Currents and peak current amplitude could be measured at biophysical voltages (e.g. -60 mV to +60 mV as depolarisation occurs around +55 mV, and action potentials are fired around +40mV; Jin *et al.*, 2012; Hochbaum *et al.*, 2014; Abdelfattah *et al.*, 2016; Piatkevich *et al.*, 2018).

Electroporation can also be used to transfect mouse-harmonised TOK1 DREADDs in hippocampal neurons dissected from postnatal pups (0-1 day old) in order to conduct patch-clamp recordings (Lin *et al.*, 2010). Cells expressing fluorescently tagged constructs can be exposed to drugs to identify channel maximum response and subsequent sustained plateau as a percentage of this maximum. The difference between the two would demonstrate the percentage of initial current inactivated. Rate of channel closure (membrane potential returning to baseline) and time closure constants would be useful to understand the action of activated channels. Measuring relative fluorescence of transfected cells would allow for some control over considering the contribution of protein expression to observed current measurements. However, variation in membrane localisation, effects of fused fluorescent proteins, contaminated intracellular fluorescence, and non-functional errors are difficult to be accounted for.

To identify the ions which can be permeated by genetically modified channels, shifts in reversal potentials can be measured at varied extracellular concentrations of cations at physiological pH 7.35. The actual cellular pH could also have an effect on channels - acidosis is known to open TOK1-related TREK1 and has been demonstrated to shift reversal potentials. Measuring transfected HEK293 cells with opsin-based actuator ChEF has shown higher intracellular pH levels (~pH 7.6) compared to the extracellular solution used (pH 7.35), causing a positive equilibrium potential at ~19 mV and greater electromotive force for proton entry which can lower the intracellular pH of small cells such as HEK293 (Lin *et al.*, 2010).

### 6.2 Expression of TOK1-DREADD *in vivo*

TOK1-based or mammalian K<sub>2</sub>P DREADDs could also be expressed in mice *in vivo*. This would allow investigation of channels on neuronal activity and behavioural outputs established during previously-validated behavioural assays. Chang *et al.* (2015) expressed hM4Di in ventral pallidum (VP) neurons and activated them using systemic injections of CNO. Mice were trained to press levers in order to receive food (a conditioned stimulus in sign-tracking) but those with modified VP activation via hM4Di had a disrupted connotation of the incentive linked to the lever cue. This is an example of an assay which could be repeated with a TOK1-based or mammalian K<sub>2</sub>P DREADDs to observe their usage *in vivo*.

### 6.3 Ablation of TOK1 binding site and exposure in yeast

Upon the identification residues for halothane-binding, the residues on TOK1 can be mutated to ablate functionality and tested using electrophysiology methods and expressed in yeast with modified K<sup>+</sup> channel systems. TOK1 with ablated halothane binding site would be compared alongside controls of VenusYFP and halothane-sensitive channels. Residue ablation could also be transferred to related mammalian potassium channels and investigated in the same manner. This would contribute to the verification the residues across two-pore potassium channels contributing to halothane activation.

Recent proteins which have been investigated this way include viral H proteins, involved in receptor binding, oncolysis, and infection. Site-directed mutagenesis produced nine constructs ablating binding specificity of receptors (SLAM, nectin4, CD46) in cell culture (Liu *et al.*, 2014).

Recombinant mouse translocator protein (TSPO) is a conserved membrane protein (Fan *et al.*, 2012) in eukaryotic cell mitochondria used for neuropharmacological diagnostics and therapeutics. Its atomic structure has been resolved using NMR revealing a ligand binding pocket and conserved residues (Jaremko *et al.*, 2014; Guo *et al.*, 2015; Li *et al.*, 2015). Mutagenesis studies on binding pocket residues and deletion mutants of cytosolic facing domains specified domains affecting binding to radioactively-labelled PK 11195. Mouse TSPO was expressed in *E. coli*, solubilised, and incorporated into proteoliposomes. Mutations were made to disrupt residues contributing to conformational change upon binding and observed by NMR: some in the binding pocket, a residue between loops able to change orientation, and a section of the C-terminus shown to stabilise whole-protein structure. The first part of the N-terminus was also deleted, showing reduced affinity. By fitting data to obtain the affinity constant and stoichiometry, investigators concluded that three cytosolic-facing regions contribute to PK 11195 to TOSP pocket binding (Iatmanen-Harbi *et al.*, 2019).

## Summary and Conclusions

Directed evolution has been immensely useful in generating proteins with novel functions for mass application. The invention does not need much justification in this regard as it was awarded the accolade of Nobel Prize for Chemistry in 2018. In the field of neuroscience, directed evolution has contributed to the development of optogenetic genetically encoded calcium and voltage indicators (GECIs, GEVIs) as well as designer receptors exclusively activated by designer drugs (DREADDs). During neuronal expression, the GECIs and GEVIs detect changes in cellular calcium or voltage and DREADDs can be selectively activated to enable neuronal activation or inhibition. These evolved molecules have enabled a causal understanding between neuronal activity on spatial and temporal levels contributing to a clearer understanding of the brain as a whole.

To contribute to these methods in understanding the brain, we started a research project using directed evolution with two aims. Firstly, we wanted to better understand the activation mechanism of the anaesthetic halothane on tandem two-pore domain potassium channels (K<sub>2</sub>Ps) TASK3 and TREK1. In parallel we wanted to develop an ionotropic DREADD based on 5HT<sub>3A</sub>. As we were unable to express these channels in our platform organism *Saccharomyces cerevisiae*, we turned our efforts to working on an ancestral homologue of K<sub>2</sub>Ps, yeast TOK1. We expressed TOK1 in yeast with a modified K<sup>+</sup> uptake system and demonstrated localisation to the plasma membrane when fused to VenusYFP and increased survival in low potassium media.

Although TOK1-expressing yeast demonstrated increased fitness in high concentrations of the K<sub>2</sub>P agonist arachidonic acid, we could not decipher whether this was TOK1-mediated. The next step involved setting up a chamber to grow liquid cultures of the TOK1 exogenously-expressing yeast and controls in halothane or air. Yeast strain R5421 (with deleted potassium pumps TRK1 and TRK2 but endogenous TOK1) showed some increased growth when exposed to 5 % halothane compared to air 100 %, but more replicates are required to confirm this. Conducting yeast transformation-associated recombination of TOK1-VenusYFP to recombine at the chromosomal TOK1 codon may also remove some variability by ensuring that only one copy of (randomly mutated) TOK1 is expressed per cell. This would also increase efficiency of the yeast transformation step.

Future experiments could include establishing the workflow for directed evolution of TOK1. This would begin with random mutagenesis of the DNA sequence by error-prone PCR and establishing a baseline mutation rate to modify ligand binding affinity for channel conductance without affecting structural integrity. The variant library size would also have to be iteratively worked out, though from previous successful directed evolution of brain receptor tools it has tended to be within the order of magnitude 10<sup>4</sup> variants. The throughput of the workflow, which would be repetitive processes of random mutagenesis, transformation, screening by exposure to halothane or CNO / Compound 21, and sequence analysis; would depend on the day-to-day capacity to conduct experiments and the extent to which automation can be applied which would be most realistic in terms of sequencing and sequence alignment analysis.

In efforts to increase the efficiency of identifying putative binding regions to halothane, random mutagenesis could be restricted to TOK1 residues 80 to 115 which corresponds to a stretch of amino acids with highest alignment across TASK3, TREK1, and TOK1 sequences. With additional time, sequencing mapping of TOK1 to potassium channels with available crystallised structures of related K<sub>2</sub>Ps, could be scanned against a database of extant related channels. This may identify conserved domains and regions involved in ligand binding and potentially reveal target domains to evolve CNO / Compound 21 affinity.

Upon the identification of the binding region of halothane on TOK1, the residues could be ablated and used in an assay to validate the significance of the identified residues to anaesthetic binding and activation. The residues of interest should also be mapped to related mammalian potassium to investigate whether the activation regions are evolutionarily conserved.

The residue changes rendering TOK1 hypersensitive to halothane or transforming TOK1 into a DREADD could be transferred to related potassium channels. It would be ideal to generate a 3D structure (with and without halothane or Compound 21 docking) to scan activated channels against a database of related channels. This would also provide a better understanding of how these drugs of interest activates target K<sub>2</sub>Ps.

Transferring residues enabling TOK1 to be activated by Compound 21 / CNO could develop a range of inhibitory DREADD tools, as other channels may have certain preferred biophysical characteristics. Biophysical parameters should be measured by expressing TOK1-DREADD (tagged with a fluorescent protein) in cell cultures and conducting basic electrophysiology techniques such as patch clamp to record photocurrents of fluorescent cells in response to different concentrations of drugs. To identify ions conducted by the channel, shifts in reversal potentials can be measured at varied extracellular concentrations of cations at physiological pH 7.35 and further experiments can measure effects of pH change on channel function. The final step to validating the evolution of TOK1 to a DREADD would be to express it *in vivo* and use an assay to demonstrate the disruption of selected neuronal activity on a behaviour.

# Appendix

## 6.1 Channelrhodopsin-based actuators were developed using rational design

Light photons are able to change the conformation of rhodopsin receptors, pumping ions such as protons, chloride ions, or nonspecific cations through the channel pore. Expressing and activating rhodopsins across plasma membranes can lead to intracellular signalling cascades. The first rhodopsins identified for modification were Channelrhodopsin-1 and -2 (ChR-1 and ChR-2) from the green alga *Chlamydomonas reinhardtii* (Sineshchekov *et al.*, 2002; Nagel *et al.*, 2003; Suzuki *et al.*, 2003). They are ionotropic channels with a seven transmembrane alpha-helical fold (G protein-coupled receptor fold): on the seventh alpha-helix exists a polyene chromophore retinal covalently attached to a covalently linked to a group of conserved epsilon-lysine residues. Light changes the conformation of all-*trans* retinal to 13-*cis* and a photocycle transports ions across the plasma membrane.

Expression of WT Channelrhodopsin in mammalian neurons elicit action potentials controlled by light (Tsai *et al.*, 2009). WT rhodopsins have been refined for use *in vivo* for several reasons. They can be activated using a broad spectrum of blue light 420-570 nm which initially meant simultaneous control of spatially overlapping neuronal population was not possible. Efforts have been made to improve receptor plasma membrane expression without inducing cell toxicity, increase channel conductance, regulate opening and closing kinetics, and decrease desensitisation whilst increasing light sensitivity. Attempts made demonstrated the difficulty in improving one parameter without worsening another and improvements have been incremental by using various approaches by rational design rather than directed evolution. Modifying excitation spectra has also become an endeavour for the application of channel variants without excitation crosstalk.

### 6.12 ChIEF

The first significant modification of ChR tested three chimeras of ChR1 and ChR2 transmembrane domains crossing over at various sites. An identified variant with crossing-over at loop E-F, and additional site-directed Ile170Val substitution led to ChIEF. ChIEF had a destabilised positive charge at the protonated retinal Schiff base reducing deactivation time and improving light-exposure fidelity. Firing was able to go up to 200 Hz (Lin *et al.*, 2010) However, it proved less sensitive than ChR-2, had low conduction, and required exposure to 570 nm light to be deactivated.

### 6.13 Step-function opsins

Paradoxically, slowing deactivation to maintain the open pore state by mutations at Cys128-Asp156 of the Helix 3-4 interaction also prolonged neuronal activation to > 30 mins. There was also an added advantage of lower intensity and frequency of light exposure and decreased phototoxicity; coining the name step-function opsins (Berndt *et al.*, 2009; Yizhar *et al.*, 2011). Thr59Ser and Thr246Asn have also been found to induce a bi-stable effect (Berndt *et al.*, 2014).

### 6.14 CatCh

To increase photocurrents, CatCh was developed by generating variants the third transmembrane domain of ChR-2 by individually substituting Arg115 to Thr139 with a small and hydrophilic cysteine. This was followed by screening for desired biophysical parameters in HEK 293 cells. Leu123Cys was proposed to increase the flexibility of the targeted hydrophobic helical segment to allow more Ca<sup>2+</sup> through the pore. Modifying cation permeability had a side effect of increasing light sensitivity 70 times more than WT ChR-2. Though spiking frequency was relatively less than previously engineered channels (50 Hz), the open state slightly lengthened and repolarisation was accelerated (Kleinlogel *et al.*, 2011). Augmented Ca<sup>2+</sup> signalling was shown not to induce toxicity in cell culture, and indeed the channel has been used *in vivo* experiments. However, it may be preferable to avoid increasing this secondary messenger in cells if other options are available.

## 6.15 Red-light activating opsins

Green fluorescent ChRs are not ideal for the control of neurons deeper into the brain as the activation spectrum is absorbed by water, lipids, and endogenous chromophores such as haemoglobin, flavins and melanin (Svoboda & Block, 1994). Blue light can damage cellular structures and scatter in tissue. It also excludes the use of co-expression of green fluorescent genetically encoded calcium indicators (Nagel *et al.*, 2003).

### C1V1

The first discovered red-shifted Channelrhodopsin, VChR1, was identified in *Volvox carteri* and was able to be activated by > 560 nm light (Zhang *et al.*, 2008). Nevertheless, this was in addition to blue light activation with low expression of proteins that induced small currents. This was overcome by systematically replacing VChR1 helices with ChR1 homologues, leading to a chimera variant of ChR1 helix 1 and 2 followed by the VChR1 sequence to produce C1V1 activated at 570 nm. Expressing it alongside ChR2 (405 nm activation) allowed the control of two separate cortico-thalamic and thalamocortical neurons onto thalamic reticular nucleus neurons (Yizhar *et al.*, 2011).

### Chrimson

Rather than trying to activate ChR-2 variants into the further red spectrum; Klapoetke *et al.* (2014) conducted *de-novo* sequencing on 167 algal transcriptomes and identified 61 channels to be screened. This seemed like a logical next step for nature to have evolved several light-activated channels, and hence there was a chance that more than two could prove useful. Indeed, biophysical characterisation in HEK293 cells led to the discovery of Chrimson from *Chlamydomonas noctigama* which could be activated by 590-625 nm light with a 30-times higher photocurrent than C1V1. As well as decreased photon scattering and absorption, an advantage of using further-red light wavelengths decreases the chance that innate photoreceptors will be activated, especially in *Drosophila melanogaster* where ideally exploitation of the clear cuticle would render optogenetics relatively straightforward without the need for physiologically invasive light probes.

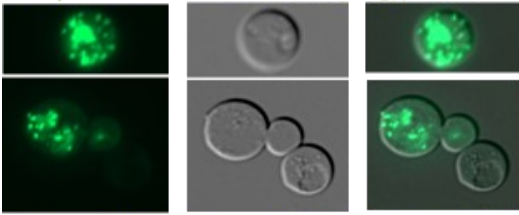
## 6.16 Anion-conducting rhodopsins

As well as activating neurons, rhodopsins have been engineered to inhibit them by eliciting an influx of Cl<sup>-</sup> ions to hyperpolarise cells. Wildtype pumps such as Halorhodopsin (NpHR) from *Natronomonas pharaonis* and Archaerhodopsin (aR) from *Halorubrum sp.* were deemed not to be maximally efficient at transporting ions *in vivo* in mammals and were unable to be subjected to increased light sensitivity or photocurrent stability as it requires a transmembrane pore (Berndt *et al.*, 2009; Bamann *et al.*, 2010; Yizhar *et al.*, 2011). They do not sufficiently decrease input resistance (ions/net charge movement) in order to inhibit action potentials. Being pumps rather than channels there was a possibility that abnormal electrochemical gradients could be established and therefore not emulate natural neuronal activity (Mattis *et al.*, 2012)

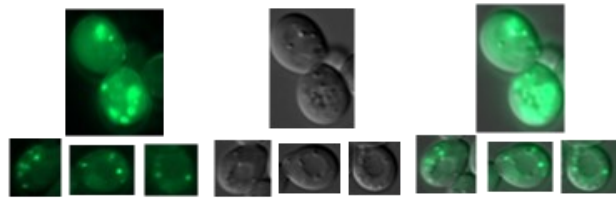
## 6.17 Naturally-evolved anion-conducting rhodopsins

Following the engineering of first-generation anion-conducting rhodopsins, two WT multi-anion conducting channels were discovered in the cryptophyte alga *Guillardia theta*, GtACR1 activated at 515 nm and GtACR2 activated at 470 nm (*Guillardia theta* anion rhodopsins; Govorunova *et al.*, 2015). Like ChRs, these also consisted of seven transmembrane domains and were able to be used in *Drosophila* and mouse experiments *in vivo* (Mauss *et al.* 2017; Mohammad *et al.*, 2017; Mardinly *et al.*, 2018) which engineered ACRs were unable to be used for. Homologous green (520 nm) light-activating receptors were discovered in the cryptophyte alga *Proteomonas sulcata* PsACR1 and ZipACR which has faster closing kinetics than GtACR1 green-light activating homologue (Govorunova *et al.*, 2016 & 2017). RapACR from *Rhodomonas salina* was found from searching 2000 algal transcriptomes and screening 13 constructs in HEK 293 cells where it was found to have remarkably high and fast photocurrents, able to suppress firing frequencies of up to 100 Hz. T111C mutation on transmembrane helix 3 accelerated photocurrent decay kinetics (Govorunova *et al.*, 2018).

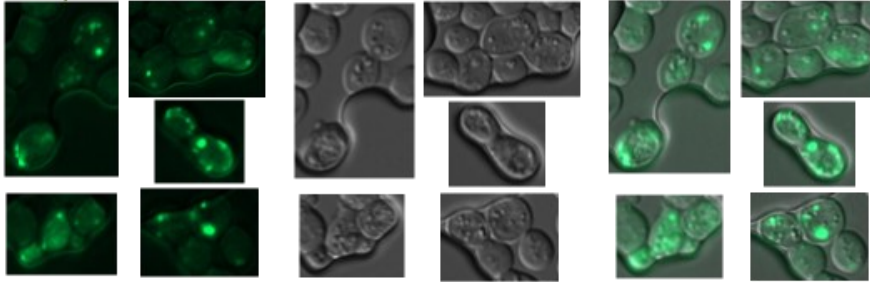
33 pTEF1-VenusYFP:5HT<sub>3A</sub>-PMT



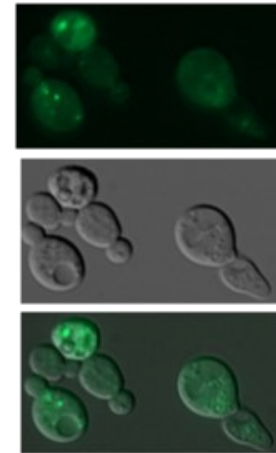
35 pRPL18B-VenusYFP:TASK3-PMT



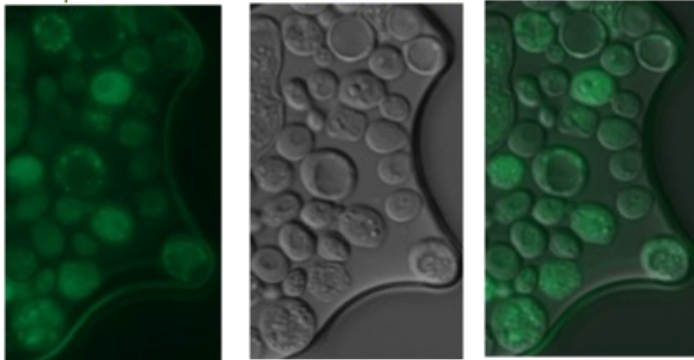
34 pRNR2-VenusYFP:TREK1-PMT



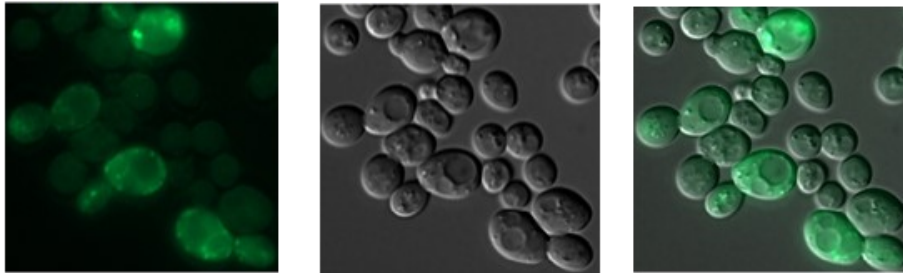
36 pRPL18B-PMT-5HT<sub>3A</sub>:VenusYFP



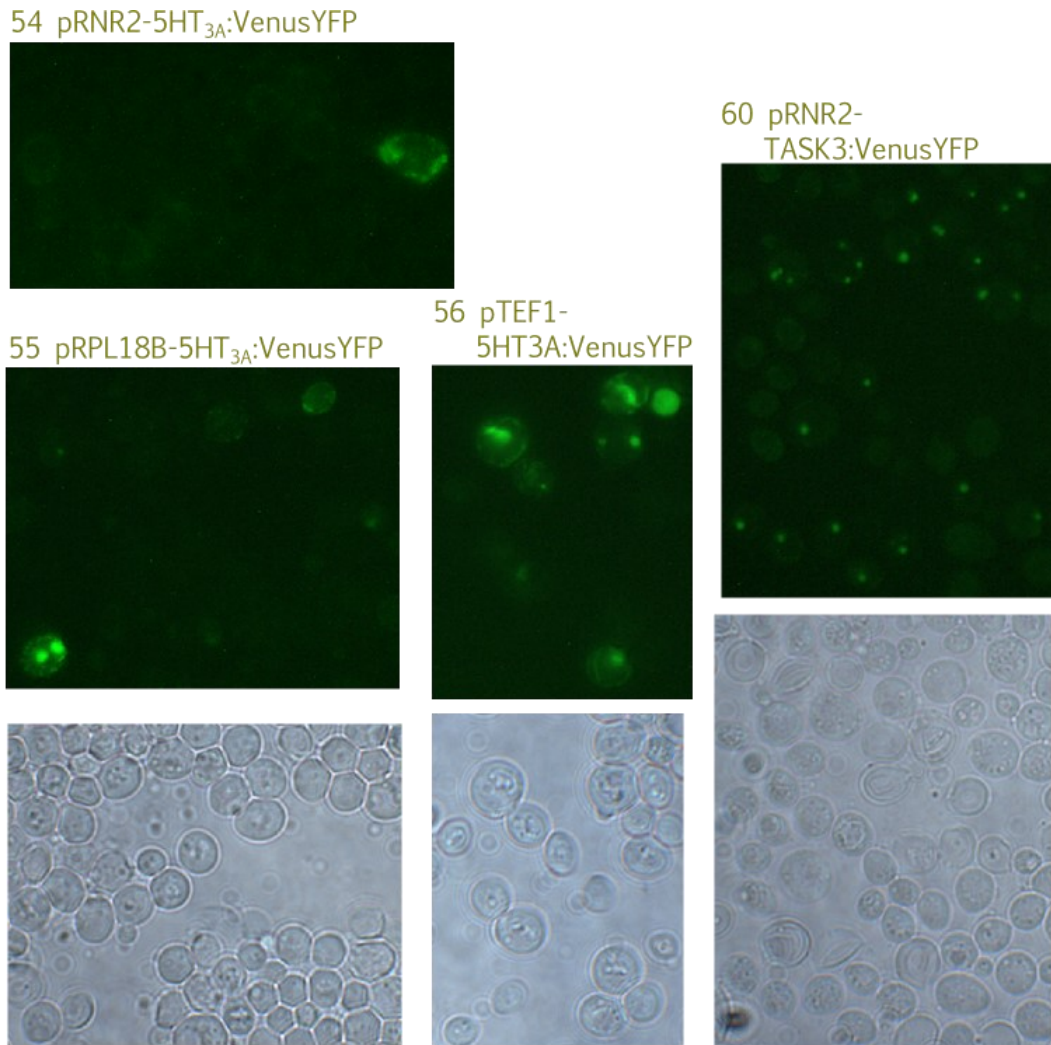
37 pTEF1-PMT-TREK1:VenusYFP



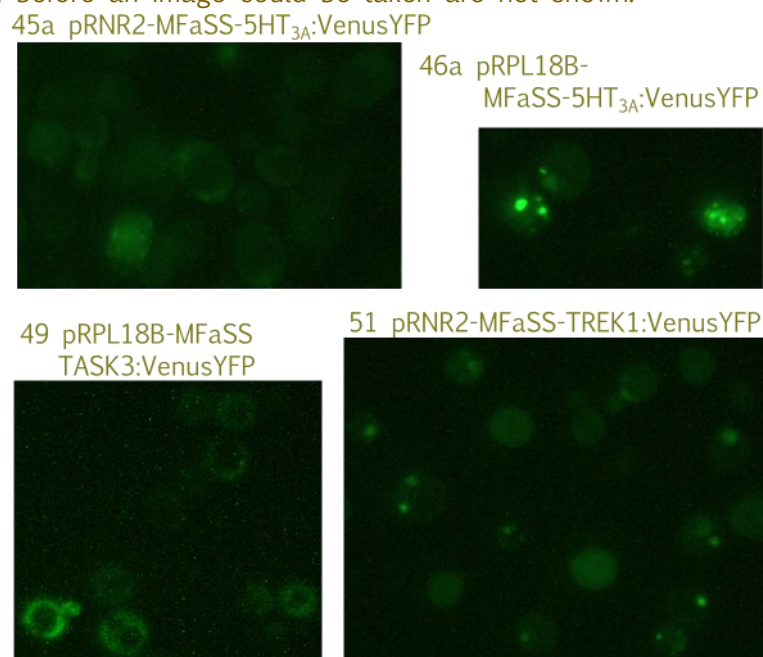
38 pRNR2-PMT-TASK3:Venus-YFP



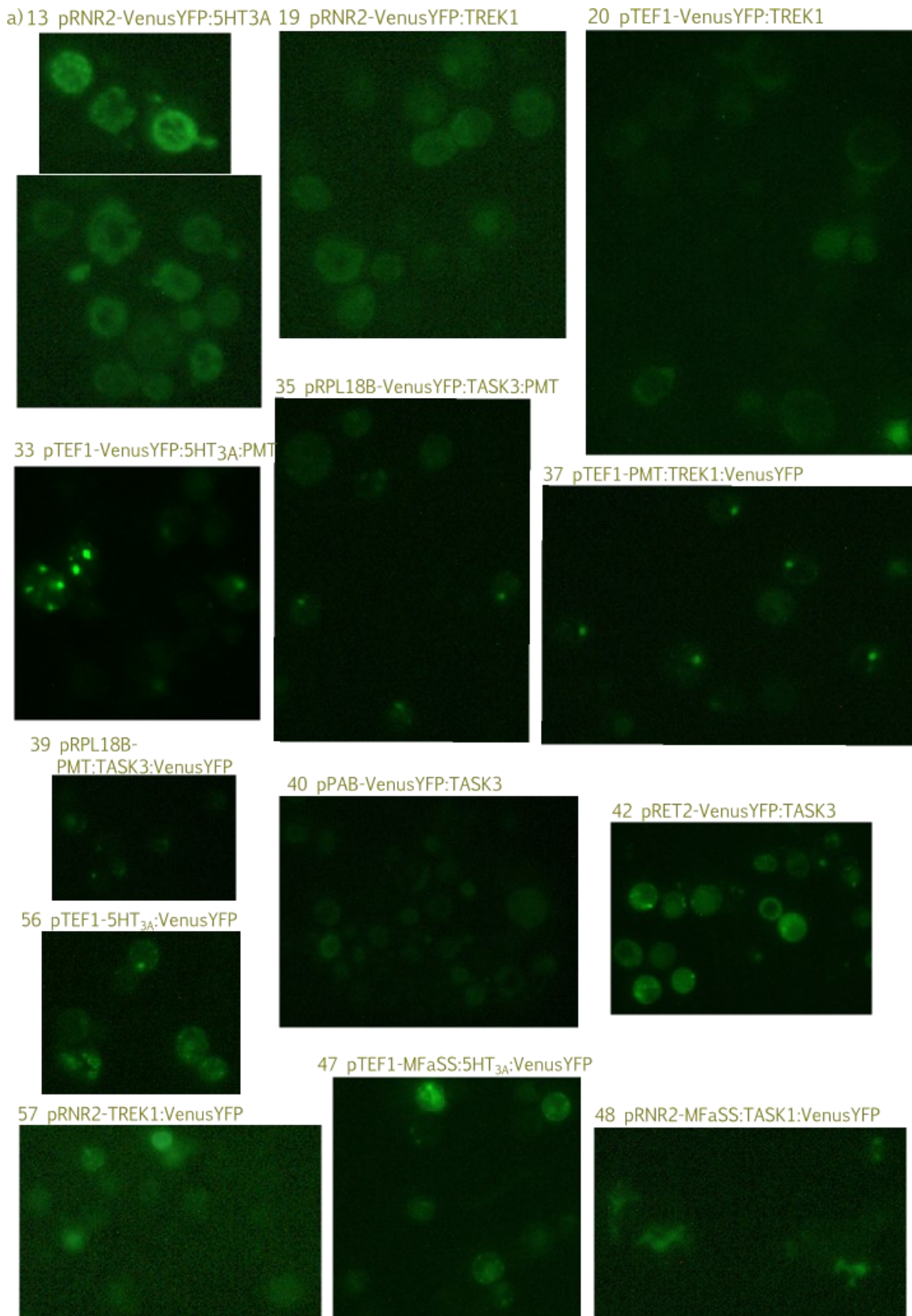
**Appendix 6.2. Venus-YFP and potassium channel fusions with plasma membrane targeting parts are not targeted to the plasma membrane in PLY246.** Images are cropped to include only those with inclusion bodies. Cells without fluorescence or whose fluorochrome bleached before an image could be taken are not shown. Fluorescence, DIC, and superimposed images were taken and analysed at the University of California San Diego.



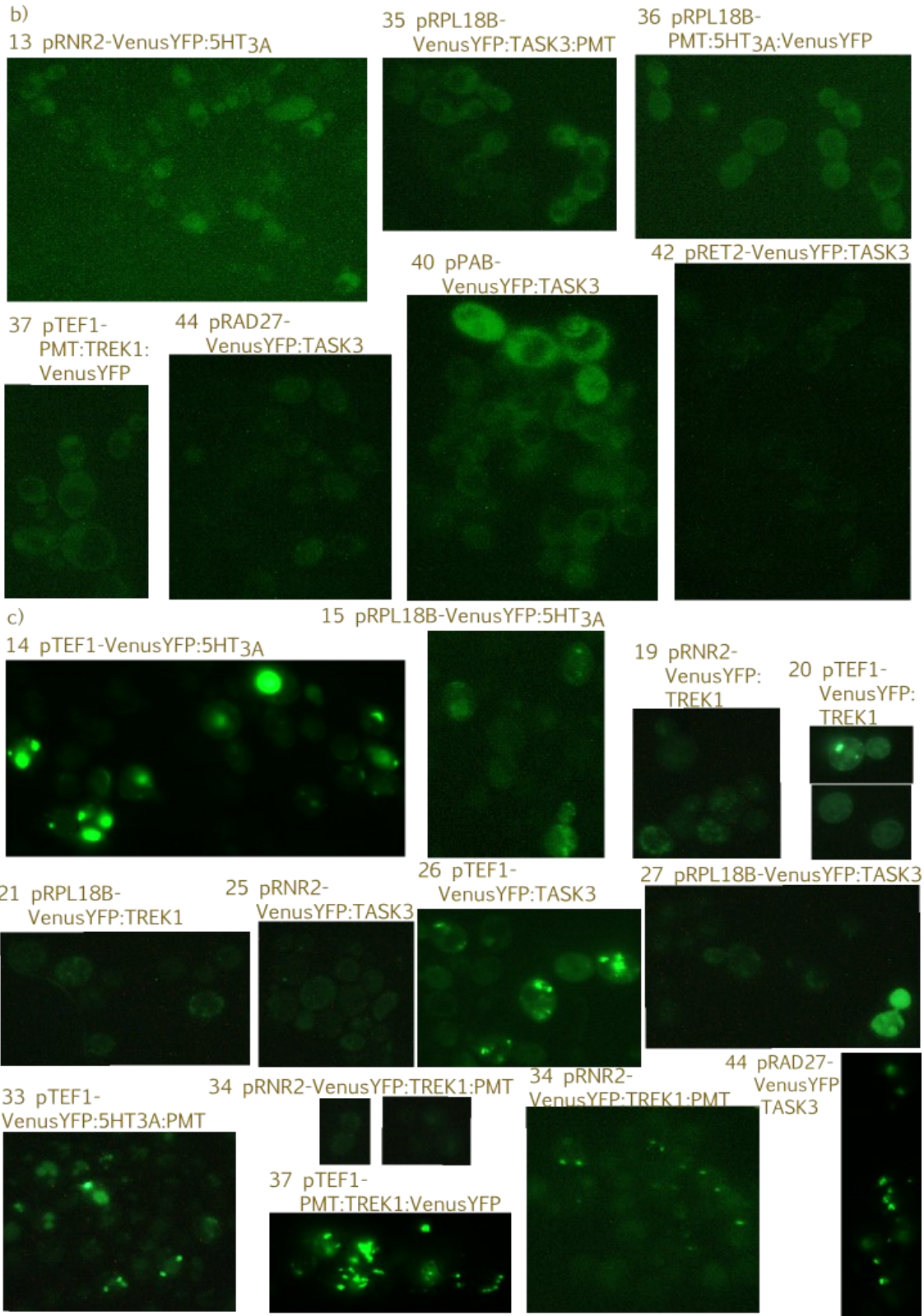
**Appendix 6.3. C-terminus potassium channel and Venus-YFP and fusions form inclusion bodies PLY246.** Images are cropped to include only those with cytoplasmic Venus-YFP. Cells without fluorescence or whose fluorochrome bleached before an image could be taken are not shown.



**Appendix 6.4. Fusing the mating factor alpha signalling sequence to channel:VenusYFP fusions does not induce translocation of the protein fusion to the plasma membrane.** Cells formed inclusion bodies or proteins were cytoplasmic. Images are cropped to include only those with cytoplasmic Venus-YFP. Cells without fluorescence or whose fluorochrome bleached before an image could be taken are not shown.



**Appendix 6.5. Mammalian channels fused to Venus-YFP are unable to be translocated to the plasma membrane of *S. cerevisiae*.** Images are cropped to include only those with cytoplasmic Venus-YFP. Cells without fluorescence or whose fluorochrome bleached before an image could be taken are not shown. a) channels are cytoplasmic or form inclusion bodies in SGY1528



b) mammalian channel and Venus-YFP expression is cytoplasmic in R5421, and c) form inclusion bodies in BY4741

Yeast strain + vector	100 $\mu$ M	200 $\mu$ M	300 $\mu$ M
SGY1528 + empty vector	0/4	2/5	3/5
SGY1528 +TOK1	0/4	2/5	3/4
SGY1528 + TRK1	0/4	2/5	3/4
R5421 + empty vector	0/3	2/4	5/5
R5421 + TOK1	0/3	1/4	3/5
R5421 + TRK1	0/3	0/4	3/5
PLY246 + empty vector	0/3	2/4	2/3
PLY246 +TOK1	0/3	2/4	3/3
PLY246 +TRK1	0/3	2/4	3/3

Appendix 6.6. Raw count of yeast colonies displaying enhanced growth on 0.5 mM K<sup>+</sup> agar in the presence of 100-300  $\mu$ M arachidonic acid (compared to ethanol vehicle). Colonies with enhanced growth were counted from agar plates containing 100, 200 or 300  $\mu$ M arachidonic acid compared with equivalent 3, 6 or 9  $\mu$ L ethanol vehicle. Enhanced growth was judged by eye.

Yeast strain + vector	300 $\mu$ M arachidonic acid
SGY1528 + empty vector	1/3
SGY1528 +TOK1	1/3
SGY1528 + TRK1	1/3
R5421 + empty vector	2/4
R5421 + TOK1	2/4
R5421 + TRK1	2/4
PLY246 + empty vector	1/2
PLY246 +TOK1	1/2
PLY246 +TRK1	1/2

(Left) Appendix 6.7 Raw count of yeast colonies displaying enhanced growth on 100 mM K<sup>+</sup> agar in the presence of 300  $\mu$ M arachidonic acid compared to ethanol vehicle. 100 mM K<sup>+</sup> is the known concentration of potassium at which yeast with compromised K<sup>+</sup> influx systems have been shown to be able to grow. Colony frequencies were counted from agar plates containing 300  $\mu$ M arachidonic acid compared with equivalent 9  $\mu$ L ethanol vehicle. Enhanced growth was judged by eye.

(Below) Appendix 6.8 Chi-squared calculations of yeast colonies displaying enhanced growth on 0.5 mM K<sup>+</sup> agar in the presence of 100-300  $\mu$ M arachidonic acid compared to ethanol vehicle. Significance calculated using Fisher's exact test on R version 3.0.

H <sub>0</sub> : growth enhancement is not different to mean of growth	100 $\mu$ M observed	100 $\mu$ M expected	200 $\mu$ M observed	200 $\mu$ M expected	300 $\mu$ M observed	300 $\mu$ M expected
SGY1528 + empty vector	0	2	2	2.5	3	2.5
SGY1528 +TOK1	0	2	2	2.5	3	2
SGY1528 + TRK1	0	2	2	2.5	3	2
R5421 + empty vector	0	1.5	2	2	3	2.5
R5421 + TOK1	0	1.5	1	2	5	2.5
R5421 + TRK1	0	1.5	0	2	3	2.5
PLY246 + empty vector	0	1.5	2	2	2	1.5
PLY246 +TOK1	0	1.5	2	2	3	1.5
PLY246 +TRK1	0	1.5	2	2	3	1.5
<b>p(observation is different to expected mean)</b>	0.059		0.946		0.540	
<b>Result</b>	zero growth enhancement not due to chance		observed not growth due to chance		likely due to chance	
<b>Conclusion</b>	AA does not increase growth		Growth is increased due to an external variable		Growth may be increased due to an external variable	

Appendix 6.9. Yeast growth OD<sub>600</sub>, air 100 %. Some values are negative as 0.08 was subtracted to account for the measurement of an empty well. Paired replicates grown in parallel halothane 5 % are listed below.

Air 100 %		SGY1528 + empty vector	SGY1528 + TOK1	SGY1528 + TRK1	R5421 + empty vector	R5421 + TOK1	R5421 + TRK1	PLY246 + empty vector	PLY246 +TOK1	PLY246 +TOK1	PLY246 +ve
<i>n1</i> baseline	0.5 K	0.43	0.28	0.49	0.20	0.01	0.26	0.15	0.47	-0.01	0.06
	0.5 K	-0.07	0.01	0.01	0.01	0.01	0.01	0.01	0.01	0.01	0.01
	1 K	0.02	0.03	0.23	0.06	0.03	0.05	0.07	0.08	0.15	0.03
	2 K	0.05	0.11	0.26	0.07	0.05	0.07	0.04	0.08	0.08	0.03
	3 K	0.02	0.04	0.06	0.06	0.04	0.06	0.05	0.07	0.03	0.04
	5 K	0.04	0.05	0.08	0.07	0.05	0.06	0.13	0.08	0.04	0.05
	20 K	0.01	0.03	0.04	0.04	0.03	0.03	0.03	0.06	0.04	0.03
	100 K	0.01	0.04	0.04	0.04	0.03	0.03	0.03	0.03	0.03	0.03
<i>n1</i> 24 h growth	0.5 K	0.539	0.459	0.641	0.397	0.21	0.343	0.249	0.61	0.118	0.081
	0.5 K	0.029	0.053	0.056	0.061	0.05	0.039	0.044	0.044	0.025	0.026
	1 K	0.049	0.055	0.24	0.096	0.067	0.084	0.105	0.121	0.214	0.05
	2 K	0.07	0.153	0.259	0.131	0.11	0.167	0.16	0.208	0.156	0.063
	3 K	0.063	0.073	0.165	0.167	0.175	0.202	0.189	0.206	0.148	0.071
	5 K	0.083	0.085	0.19	0.195	0.193	0.201	0.278	0.203	0.177	0.08
	20 K	0.08	0.06	0.133	0.152	0.166	0.17	0.153	0.17	0.136	0.069
	100K	0.041	0.076	0.077	0.069	0.062	0.065	0.067	0.073	0.083	0.085
<i>n1</i> 48 h growth	0.5 K	0.613	0.424	0.515	0.352	0.165	0.278	0.243	0.614	0.063	0.084
	0.5 K	0.011	0.02	0.011	0.02	0.02	0.014	0.021	0.013	0.005	0.018
	1 K	0.024	0.026	0.172	0.053	0.031	0.041	0.052	0.077	0.142	0.022
	2 K	0.039	0.109	0.312	0.199	0.182	0.182	0.141	0.138	0.078	0.024
	3 K	0.026	0.034	0.184	0.167	0.15	0.14	0.157	0.17	0.026	0.032
	5 K	0.037	0.034	0.18	0.165	0.187	0.17	0.231	0.176	0.122	0.042
	20 K	0.019	0.019	0.124	0.165	0.167	0.193	0.153	0.143	0.105	0.03
	100K	0.021	0.033	0.032	0.026	0.025	0.028	0.029	0.031	0.029	0.028
<i>n2</i> baseline	0.5 K	0.17	0.499	0.165	0.28	0.155	0.202	0.272	0.139	0.09	0.281
	1 K	0.138	0.137	0.195	0.231	0.131	0.17	0.138	0.103	0.066	0.242
	2 K	0.156	0.174	0.214	0.164	0.139	0.169	0.242	0.107	0.065	0.116
	3 K	0.262	0.102	0.196	0.154	0.147	0.168	0.147	0.113	0.105	0.171
	5 K	0.129	0.136	0.194	0.144	0.129	0.126	0.116	0.099	0.084	0.165
	20 K	0.155	0.102	0.197	0.12	0.127	0.149	0.112	0.129	0.103	0.131
	100K	0.171	0.165	0.223	0.142	0.16	0.37	0.412	0.168	0.071	0.138
	<i>n2</i> 24 h growth	0.5 K	0.184	0.184	0.184	0.184	0.184	0.184	0.184	0.184	0.234
1 K		0.204	0.205	0.301	0.23	0.277	0.384	0.377	0.312	0.288	0.37
2 K		0.232	0.276	0.346	0.363	0.291	0.366	0.522	0.295	0.24	0.21
3 K		0.194	0.023	0.319	0.319	0.27	0.333	0.398	0.304	0.285	0.262
5 K		0.195	0.229	0.287	0.286	0.234	0.274	0.325	0.279	0.254	0.263
20 K		0.192	0.188	0.282	0.175	0.135	0.198	0.181	0.182	0.154	0.256
100 K		0.188	0.224	0.245	0.167	0.189	0.483	0.556	0.218	0.118	0.276
<i>n3</i> baseline		0.5 K	0.017	0.038	0.058	0.021	0.029	0.099	0.091	0.016	0.08
	1 K	0.136	0.224	0.761	0.09	0.137	0.746	0.582	0.045	0.078	0.684
	2 K	0.147	0.13	0.431	0.138	0.232	0.576	0.474	0.1	0.102	0.411
	3 K	0.12	0.086	0.506	0.117	0.117	0.514	0.375	0.028	0.167	0.71
	5 K	0.089	0.166	0.621	0.146	0.117	0.672	0.468	0.039	0.165	0.634
	20 K	0.046	0.087	0.186	0.056	0.044	0.123	0.085	0.016	0.007	0.055
	100 K	0.144	0.215	0.475	0.323	0.348	0.479	0.326	0.193	0.313	0.214

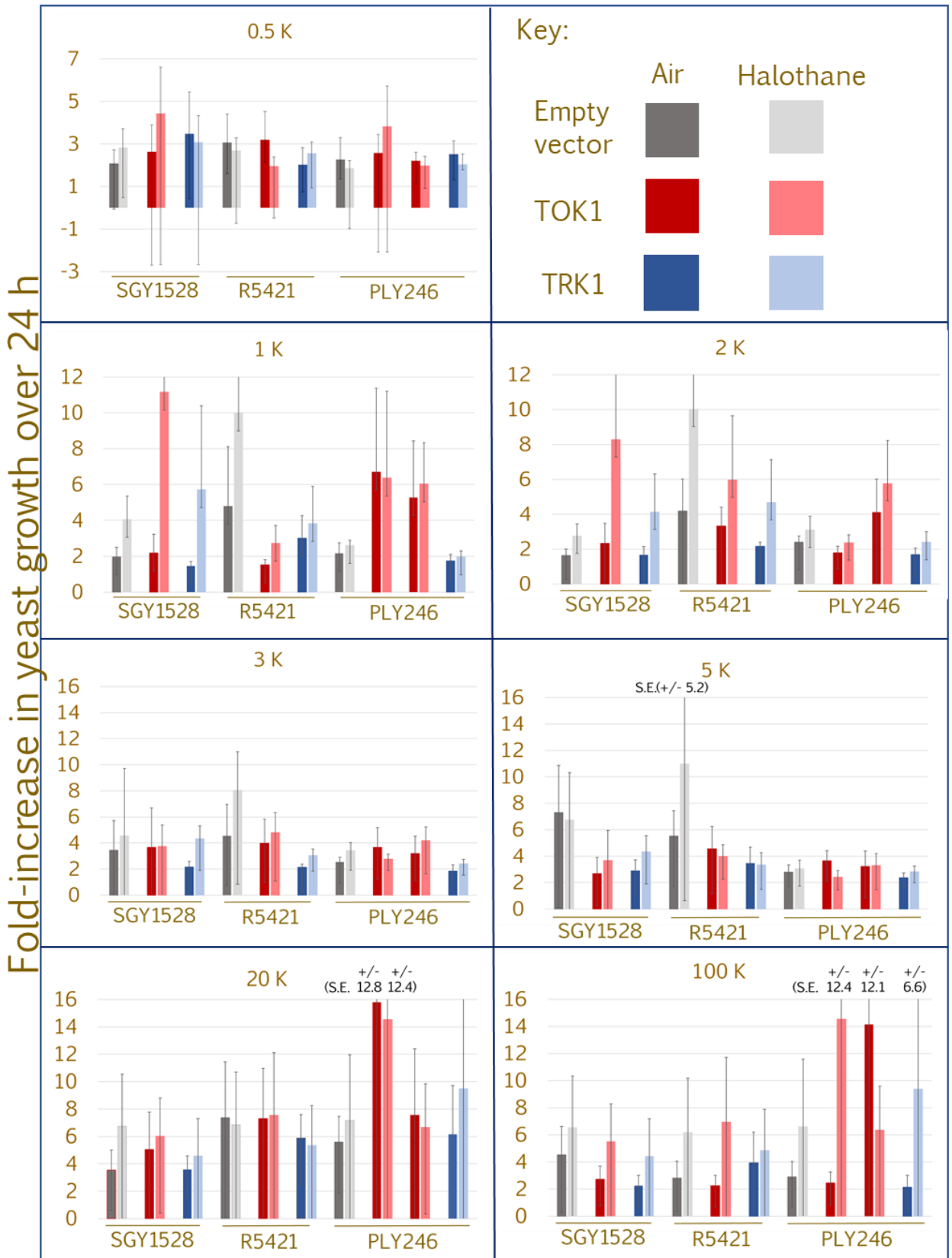
Air 100 %		SGY1528 + empty vector	SGY1528 + TOK1	SGY1528 + TRK1	R5421 + empty vector	R5421 + TOK1	R5421 + TRK1	PLY246 + empty vector	PLY246 +TOK1	PLY246 +TOK1	PLY246 +ve
n3 24h growth	0.5 K	0.08	1.048	0.879	0.981	0.696	1.062	0.845	0.691	0.749	0.666
	1 K	0.218	1.193	1.36	1.322	0.911	1.401	1.071	0.931	1.126	1.245
	2 K	0.227	0.748	1.305	1.329	1.418	1.44	1.044	0.158	0.97	1.098
	3 K	1.228	1.091	1.383	1.376	1.097	1.393	1.035	0.227	1.165	1.249
	5 K	1.353	1.029	1.476	1.408	1.11	1.546	1.093	0.22	1.076	1.249
	20 K	0.182	1.11	1.162	1.088	0.791	1.175	0.903	0.86	0.151	0.925
	100 K	0.763	0.868	1.351	1.078	1.094	1.382	1.147	0.884	1.089	1.022
n4 baseline growth	0.5 K	0.382	0.342	0.114	0.123	0.086	0.319	0.098	0.028		0.025
	1 K	0.242	0.163	0.183	0.116	0.078	0.173	0.243	0.102		0.11
	2 K	0.246	0.246	0.164	0.161	0.236	0.102	0.145	0.076		0.084
	3 K	0.026	0.088	0.077	0.055	0.068	0.136	0.102	0.086		0.106
	5 K	0.066	0.11	0.079	0.12	0.061	0.146	0.097	0.093		0.143
	20 K	0.049	0.07	0.07	0.093	0.067	0.06	0.062	0.06		0.051
	100 K	0.134	0.043	0.101	0.044	0.054	0.08	0.051	0.053		0.024
n4 24h growth	0.5 K	0.322	0.428	0.161	0.119	0.038	0.168	0.079	0.06		0.051
	1 K	0.116	0.101	0.032	0.091	0.067	0.109	0.075	0.024		0.034
	2 K	0.233	0.224	0.249	0.24	0.367	0.211	0.297	0.102		0.056
	3 K	0.032	0.055	0.182	0.166	0.17	0.222	0.226	0.111		0.077
	5 K	0.097	0.061	0.157	0.195	0.151	0.217	0.214	0.094		0.142
	20 K	0.094	0.027	0.055	0.073	0.069	0.053	0.048	0.038		0.054
	100 K	0.058	0.034	0.065	0.038	0.068	0.081	0.042	0.025		0.051
n4 48 h growth	0.5 K	0.319	0.317	0.111	0.093	0.026	0.11	0.08	0.054		0.019
	1 K	0.066	0.084	0.039	0.075	0.045	0.071	0.052	0.027		0.024
	2 K	0.178	0.157	0.22	0.221	0.329	0.198	0.244	0.036		0.035
	3 K	0.04	0.046	0.199	0.174	0.155	0.239	0.234	0.051		0.051
	5 K	0.091	0.05	0.183	0.176	0.179	0.195	0.219	0.046		0.085
	20 K	0.081	0.032	0.044	0.049	0.06	0.065	0.036	0.029		0.032
	100 K	0.039	0.024	0.048	0.035	0.046	0.054	0.035	0.025		0.038
n5 baseline	0.5 K	0.123	0.078	0.069	0.05	0.068	0.097	0.13	0.042	0.201	0.285
	1 K	0.074	0.26	0.09	0.074	0.205	0.066	0.048	0.082	0.175	0.101
	2 K	0.043	0.27	0.222	0.099	0.244	0.112	0.11	0.228	0.085	0.144
	3 K	0.061	0.231	0.127	0.113	0.166	0.077	0.124	0.138	0.095	0.057
	5 K	0.008	0.091	0.028	0.02	0.052	0.015	0.032	0.045	0.14	0.095
	20 K	0.015	0.031	0.038	0.027	0.023	0.018	0.025	0.027	0.035	0.043
	100 K	0.011	0.055	0.036	0.019	0.049	0.01	0.022	0.073	0.002	0.247
n5 24h growth	0.5 K	0.372	0.353	0.198	0.326	0.206	0.259	0.305	0.153	0.534	0.463
	1 K	0.265	0.263	0.158	0.189	0.239	0.156	0.161	0.171	0.259	0.268
	2 K	0.115	0.271	0.197	0.184	0.284	0.175	0.201	0.234	0.207	0.196
	3 K	0.098	0.206	0.153	0.165	0.207	0.121	0.186	0.192	0.213	0.181
	5 K	0.092	0.198	0.149	0.158	0.134	0.106	0.138	0.179	0.339	0.298
	20 K	0.113	0.153	0.121	0.121	0.109	0.123	0.126	0.151	0.22	0.148
	100 K	0.112	0.26	0.15	0.116	0.194	0.106	0.128	0.208	0.101	0.265
n5 24h growth	0.5 K	0.23	0.334	0.213	0.453	0.268	0.296	0.306	0.222	0.434	0.431
	1 K	0.341	0.28	0.177	0.213	0.327	0.155	0.174	0.277	0.346	0.25
	2 K	0.135	0.291	0.273	0.334	0.379	0.264	0.315	0.362	0.278	0.17
	3 K	0.152	0.23	0.217	0.204	0.242	0.18	0.24	0.278	0.275	0.181
	5 K	0.123	0.277	0.26	0.204	0.252	0.224	0.256	0.303	0.34	0.258
	20 K	0.141	0.212	0.152	0.107	0.108	0.138	0.143	0.174	0.279	0.114
	100 K	0.111	0.306	0.218	0.131	0.203	0.106	0.132	0.215	0.083	0.084

Appendix 6.10. Yeast growth OD<sub>600</sub>, halothane 5 %. Some values are negative as 0.08 was subtracted to account for the measurement of an empty well. Paired replicates grown in parallel air 100 % are listed above.

Halothane 5 %	SGY1528 + empty vector	SGY1528 + TOK1	SGY1528 + TRK1	R5421 + empty vector	R5421 + TOK1	R5421 + TRK1	PLY246 + empty vector	PLY246 +TOK1	PLY246 +TOK1	PLY246 +ve	
<i>n1</i> baseline	0.5 K	0.679	0.438	0.755	0.385	0.173	0.371	0.191	0.701	0.217	0.285
	0.5 K	0.008	0.007	0.007	0.007	0.005	0.009	0.021	0.011	0.005	0.007
	1 K	0.01	0.018	0.035	0.03	0.017	0.024	0.023	0.061	0.059	0.018
	2 K	0.019	0.022	0.031	0.027	0.022	0.03	0.024	0.057	0.044	0.021
	3 K	0.006	0.02	0.031	0.02	0.025	0.029	0.021	0.036	0.034	0.015
	5 K	0.013	0.028	0.033	0.035	0.027	0.041	0.029	0.071	0.057	0.027
	20 K	0.013	0.017	0.029	0.038	0.024	0.03	0.022	0.039	0.028	0.027
	100 K	0.012	0.038	0.026	0.026	0.021	0.019	0.021	0.016	0.014	0.022
<i>n1</i> 24 h growth	0.5 K	0.828	0.587	0.922	0.516	0.24	0.41	0.233	0.799	0.322	0.286
	0.5 K	0.02	0.022	0.034	0.06	0.045	0.056	0.055	0.07	0.065	0.146
	1 K	0.039	0.031	0.136	0.131	0.11	0.131	0.127	0.156	0.061	0.123
	2 K	0.019	0.027	0.145	0.127	0.124	0.139	0.132	0.131	0.097	0.098
	3 K	0.032	0.033	0.129	0.142	0.139	0.138	0.139	0.153	0.155	0.133
	5 K	0.031	0.022	0.03	0.089	0.082	0.072	0.075	0.076	0.057	0.118
	20 K	0.029	0.04	0.029	0.025	0.022	0.021	0.025	0.026	0.026	0.07
	100K	0.013	0.028	0.019	0.024	0.017	0.034	0.024	0.024	0.022	0.021
<i>n1</i> 48 h growth	0.5 K	0.845	0.574	0.845	0.515	0.292	0.317	0.176	0.746	0.308	0.318
	0.5 K	0.01	0.008	0.007	0.007	0.007	0.009	0.011	0.017	0.014	0.009
	1 K	0.016	0.11	0.14	0.127	0.121	0.126	0.132	0.176	0.142	0.02
	2 K	0.023	0.155	0.185	0.176	0.155	0.177	0.177	0.204	0.132	0.029
	3 K	0.011	0.15	0.192	0.18	0.182	0.179	0.175	0.178	0.143	0.006
	5 K	0.019	0.165	0.186	0.205	0.185	0.182	0.191	0.2	0.206	0.073
	20 K	0.018	0.114	0.16	0.171	0.159	0.148	0.135	0.144	0.142	0.05
	100K	0.019	0.069	0.033	0.041	0.036	0.052	0.066	0.065	0.053	0.012
<i>n2</i> baseline	0.5 K	0.198	0.492	0.366	0.175	0.145	0.173	0.268	0.132	0.3	0.378
	1 K	0.15	0.129	0.266	0.14	0.121	0.123	0.105	0.118	0.037	0.181
	2 K	0.175	0.18	0.226	0.164	0.201	0.186	0.182	0.124	0.034	0.227
	3 K	0.17	0.175	0.219	0.138	0.186	0.209	0.147	0.093	0.087	0.149
	5 K	0.155	0.132	0.23	0.134	0.143	0.157	0.114	0.101	0.09	0.177
	20 K	0.159	0.149	0.202	0.118	0.13	0.207	0.15	0.339	0.08	0.163
	100K	0.145	0.472	0.276	0.099	0.098	0.113	0.132	0.229	0.061	0.146
	<i>n2</i> 24 h growth	0.5 K	0.243	0.581	0.372	0.338	0.189	0.297	0.45	0.226	0.429
1 K		0.247	0.24	0.282	0.227	0.151	0.226	0.217	0.202	0.12	0.327
2 K		0.284	0.266	0.228	0.259	0.213	0.267	0.343	0.225	0.097	0.371
3 K		0.253	0.258	0.241	0.214	0.202	0.272	0.297	0.171	0.187	0.272
5 K		0.23	0.214	0.246	0.19	0.159	0.223	0.247	0.197	0.193	0.348
20 K		0.232	0.253	0.231	0.158	0.166	0.281	0.266	0.435	0.199	0.33
100 K		0.294	0.747	0.377	0.174	0.174	0.222	0.283	0.346	0.155	0.287
<i>n3</i> baseline	0.5 K	0.059	0.066	0.122	0.252	0.279	0.295	0.287	0.087	0.258	0.6
	1 K	0.019	0.025	0.048	0.033	0.241	0.105	0.192	0.057	0.102	0.472
	2 K	0.039	0.034	0.11	0.029	0.076	0.081	0.169	0.043	0.097	0.469
	3 K	0.032	0.024	0.137	0.049	0.058	0.401	0.362	0.032	0.088	0.791
	5 K	0.069	0.045	0.21	0.054	0.199	0.466	0.52	0.07	0.193	0.442
	20 K	0.133	0.056	0.26	0.395	0.544	0.804	0.556	0.275	0.316	0.43
	100 K	0.002	0.021	0.029	0.042	0.04	0.035	0.018	0.026	0.01	0.004

Halothane 5 %		SGY1528 + empty vector	SGY1528 + TOK1	SGY1528 + TRK1	R5421 + empty vector	R5421 + TOK1	R5421 + TRK1	PLY246 + empty vector	PLY246 +TOK1	PLY246 +TOK1	PLY246 +ve
n3 24h growth	0.5 K	0.212	0.956	1.075	1.222	0.757	1.131	0.922	1.111	0.872	1.019
	1 K	0.126	1.011	0.948	1.15	1.329	1.052	0.651	1.191	1.166	1.143
	2 K	0.183	0.998	1.127	0.944	1.265	0.948	0.552	0.15	1.23	1.157
	3 K	1.107	0.27	1.139	1.038	0.661	1.45	0.914	0.125	0.587	1.297
	5 K	1.181	0.473	1.22	1.298	1.003	1.51	1.001	0.272	0.918	1.166
	20 K	0.928	0.172	1.049	0.867	1.246	1.534	1.216	0.837	1.049	1.216
	100 K	0.004	0.127	0.122	0.135	0.135	0.13	0.12	0.1	0.094	0.041
n4 baseline growth	0.5 K	0.421	0.224	0.543	0.45	0.271	0.632	0.448	0.238		0.56
	1 K	0.295	0.137	0.094	0.109	0.05	0.249	0.231	0.048		0.045
	2 K	0.118	0.12	0.05	0.071	0.034	0.137	0.108	0.029		0.061
	3 K	0.098	0.045	0.074	0.047	0.026	0.13	0.046	0.102		0.029
	5 K	0.076	0.027	0.054	0.061	0.028	0.103	0.025	0.019		0.027
	20 K	0.044	0.034	0.049	0.074	0.264	0.277	0.139	0.059		0.029
	100 K	0.045	0.018	0.016	0.026	0.022	0.05	0.022	0.016		0.024
n4 24h growth	0.5 K	0.4	0.197	0.602	0.835	0.541	0.932	0.555	0.286		0.242
	1 K	0.157	0.252	0.131	0.116	0.217	0.126	0.189	0.183		0.187
	2 K	0.166	0.2	0.123	0.126	0.135	0.151	0.133	0.136		0.057
	3 K	0.212	0.092	0.191	0.184	0.139	0.123	0.083	0.078		0.031
	5 K	0.125	0.072	0.118	0.101	0.094	0.123	0.074	0.068		0.024
	20 K	0.139	0.04	0.076	0.085	0.082	0.076	0.056	0.044		0.015
	100 K	0.095	0.036	0.043	0.037	0.024	0.03	0.029	0.026		0.017
n4 48 h growth	0.5 K	0.658	0.395	0.55	0.608	0.591	0.95	0.494	0.363		0.273
	1 K	0.291	0.122	0.092	0.069	0.09	0.087	0.246	0.272		0.343
	2 K	0.142	0.097	0.133	0.137	0.139	0.341	0.252	0.188		0.14
	3 K	0.151	0.064	0.191	0.217	0.206	0.253	0.2	0.169		0.102
	5 K	0.125	0.048	0.16	0.193	0.175	0.229	0.156	0.146		0.115
	20 K	0.144	0.092	0.113	0.129	0.174	0.169	0.152	0.128		0.094
	100 K	0.103	0.076	0.103	0.077	0.092	0.034	0.091	0.087		0.075
n5 baseline	0.5 K	0.026	0.213	0.096	0.081	0.209	0.041	0.067	0.107	0.15	0.14
	1 K	0.034	0.236	0.13	0.102	0.181	0.05	0.046	0.078	0.11	0.058
	2 K	0.043	0.242	0.182	0.117	0.153	0.055	0.069	0.091	0.081	0.036
	3 K	0.011	0.193	0.038	0.043	0.065	0.035	0.039	0.076	0.099	0.047
	5 K	0.015	0.122	0.018	0.007	0.022	0.011	0.039	0.068	0.129	0.041
	20 K	0.025	0.02	0.033	0.019	0.025	0.022	0.055	0.03	0.048	0.074
	100 K	0.04	0.072	0.073	0.065	0.235	0.026	0.064	0.033	0.023	0.194
n5 24h growth	0.5 K	0.169	0.251	0.156	0.156	0.203	0.097	0.136	0.143	0.163	0.177
	1 K	0.202	0.265	0.141	0.152	0.166	0.086	0.118	0.134	0.153	0.147
	2 K	0.115	0.216	0.151	0.128	0.123	0.088	0.132	0.128	0.136	0.147
	3 K	0.099	0.179	0.122	0.134	0.115	0.087	0.111	0.132	0.14	0.155
	5 K	0.088	0.17	0.118	0.101	0.097	0.062	0.13	0.117	0.174	0.163
	20 K	0.131	0.16	0.115	0.108	0.107	0.081	0.104	0.099	0.178	0.142
	100 K	0.139	0.422	0.276	0.143	0.663	0.095	0.154	0.165	0.149	0.402
n5 24h growth	0.5 K	0.083	0.4	0.158	0.183	0.226	0.079	0.111	0.128	0.137	0.146
	1 K	0.109	0.333	0.152	0.165	0.191	0.102	0.106	0.115	0.135	0.118
	2 K	0.083	0.297	0.189	0.154	0.189	0.175	0.173	0.17	0.116	0.113
	3 K	0.072	0.216	0.179	0.179	0.179	0.158	0.176	0.162	0.129	0.119
	5 K	0.057	0.176	0.165	0.144	0.149	0.123	0.159	0.102	0.182	0.141
	20 K	0.095	0.127	0.089	0.074	0.089	0.056	0.083	0.101	0.171	0.129
	100 K	0.107	0.332	0.279	0.151	0.649	0.087	0.14	0.181	0.186	0.433

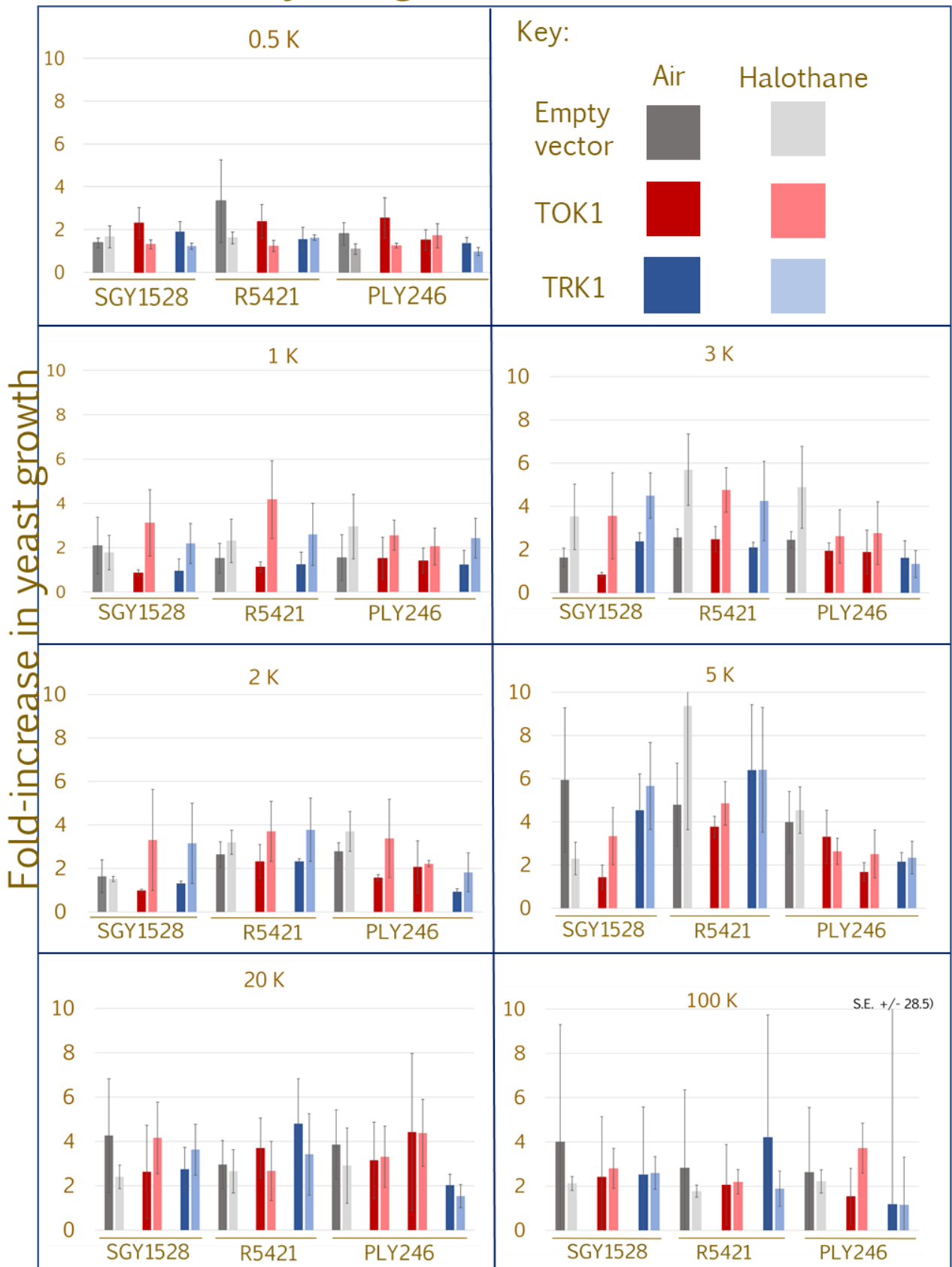
# Fold-increase in yeast growth in air and halothane 24h



**Appendix 6.11. Average fold-increase in yeast growth in air and halothane after 24 h.** SGY1528 and R5421 (-TRK1, -TRK2, genomic TOK1) and PLY246 (-TRK1, -TRK2, -TOK1) were transformed with an empty vector, TOK1, and TRK1. Growth was conducted at different concentrations of potassium to investigate whether clearer trends could be seen at different concentrations. No statistical trends could be inferred between receptor combinations at each concentration of potassium. One standard error above and below the mean is displayed on each bar and demonstrate high variation in growth response for many conditions;  $n = 4$  to  $5$

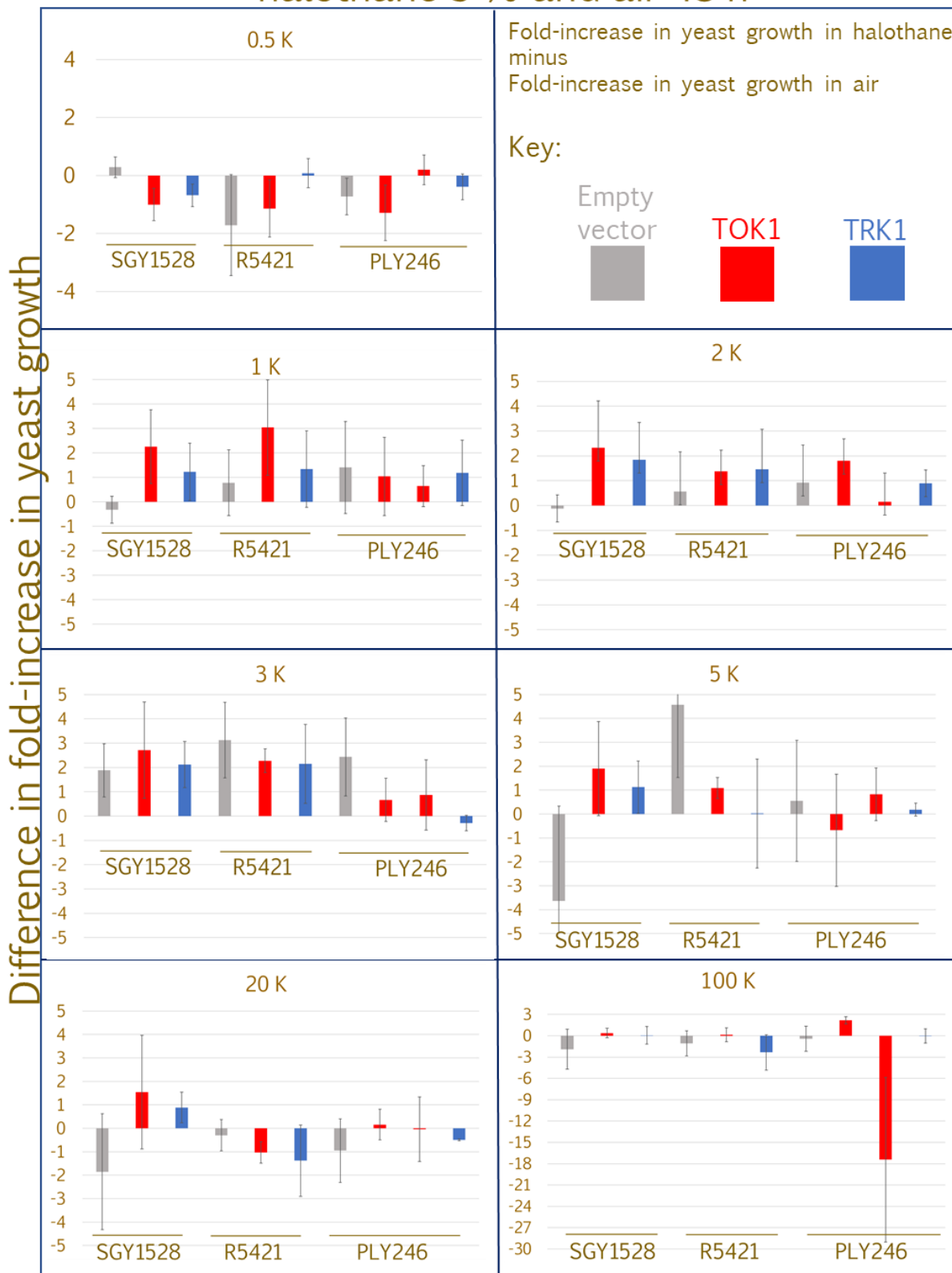


# Fold-increase in yeast growth in air and halothane 48h



**Appendix 6.13. Average fold-increase in yeast growth in air and halothane after 48 h.** SGY1528 and R5421 (-TRK1, -TRK2, genomic TOK1) and PLY246 (-TRK1, -TRK2, -TOK1) were transformed with an empty vector, TOK1, and TRK1. Growth was conducted at different concentrations of potassium to investigate whether clearer trends could be seen at different concentrations. No statistical trends could be inferred between receptor combinations at each concentration of potassium. One standard deviation above and below the mean is displayed on each bar;  $n = 3$  to 4.

## Difference in fold-increase in yeast growth between halothane 5 % and air 48 h



**Appendix 6.14. Average difference in fold-increase of yeast growth in air and halothane after 48 h.** SGY1528 and R5421 (-TRK1, -TRK2, genomic TOK1) and PLY246 (-TRK1, -TRK2, -TOK1) were transformed with an empty vector, TOK1, and TRK1. Growth was conducted at different concentrations of potassium to investigate whether clearer trends could be seen at different concentrations. No statistical trends could be inferred between receptor combinations at each concentration of potassium. One standard error above and below the mean is displayed on each bar or is written above the bar, and demonstrate high variation in growth response for many conditions;  $n = 3$  to 4.

Appendix 6.15 R script for ANOVA of difference in growth of R5421 in 5 K media between halothane and air after 24h

```
air.SGY1528.empty.vector<-c(0.973684211,1.511627907,15.20224719,11.5)
halothane.SGY1528.empty.vector<-c(2.461538462,1.483870968,17.11594203,5.866666667)
air.SGY1528.TOK1<-c(0.693877551,1.683823529,6.198795181,2.175824176)
halothane.SGY1528.TOK1<-c(1.178571429,1.621212121,10.51111111,1.393442623)
air.SGY1528.TRK1<-c(2.337662338,1.479381443,2.376811594,5.321428571)
halothane.SGY1528.TRK1<-c(3.909090909,1.069565217,5.80952381,6.555555556)
air.R5421.empty.vector<-c(3.061538462,2.213414634,9.630434783,1.858585859)
halothane.R5421.empty.vector<-c(4.057142857,1.417910448,24.03703704,14.42857143)
air.R5421.TOK1<-c(3.978723404,2.174603175,9.487179487,2.576923077)
halothane.R5421.TOK1<-c(5.148148148,1.420382166,5.040201005,4.409090909)
air.R5421.TRK1<-c(2.741935484,1.813953488,2.300595238,7.066666667)
halothane.R5421.TRK1<-c(3.365853659,1.11888112,3.240343348,5.636363636)
air.PLY246.empty.vector<-c(1.75,2.801724138,2.335470085,4.3125)
halothane.PLY246.empty.vector<-c(4.793103448,2.166666667,1.925,3.333333333)
air.PLY246.TOK1<-c(2.172839506,2.818181818,5.641025641,3.977777778)
halothane.PLY246.TOK1<-c(2.154929577,1.95049505,3.885714286,1.720588235)
air.PLY246.TOK1ii<-c(0.933333333,3.023809524,6.521212121,2.421428571)
halothane.PLY246.TOK1ii<-c(4.925925926,2.144444444,4.756476684,1.348837209)
air.PLY246.TRK1<-c(2.772727273,1.593939394,1.970031546,3.136842105)
halothane.PLY246.TRK1<-c(2.719298246,1.966101695,2.63800905,3.975609756)

SGY1528.empty.vector<-c(1.48785425,-0.02775694,1.91369484,-5.633333333)
SGY1528.TOK1<-c(0.48469388,-0.06261141,4.31231593,-0.78238155)
SGY1528.TRK1<-c(1.5714286,-0.4098162,3.4327122,1.2341270)
R5421.empty.vector<-c(0.9956044,-0.7955042,14.4066023,12.5699856)
R5421.TOK1<-c(1.169425,-0.754221,-4.446978,1.832168)
R5421.TRK1<-c(0.6239182,-0.7020654,0.9397481,-1.4303030)
PLY246.empty.vector<-c(3.0431034,-0.6350575,-0.4104701,-0.9791667)
PLY246.TOK1<-c(-0.01790993,-0.86768677,-1.75531135,-2.25718954)
PLY246.TOK1ii<-c(3.9925926,-0.8793651,-1.7647354,-1.0725914)
PLY246.TRK1<-c(-0.05342903,0.37216230,0.66797750,0.83876765)

data<-
c(SGY1528.empty.vector,SGY1528.TOK1,SGY1528.TRK1,R5421.empty.vector,R5421.TOK1,R5421.TRK1,
PLY246.empty.vector,PLY246.TOK1,PLY246.TOK1ii,PLY246.TRK1)

receptor<-gl(10,4)
```

```
anova.5k24h<-aov(data~receptor)
```

```
summary(anova.5k24h)
```

```
          Df Sum Sq Mean Sq F value Pr(>F)
receptor    9  184.0   20.44   2.015 0.0727 .
Residuals  30  304.3   10.14
```

---

Signif. codes: 0 '\*\*\*' 0.001 '\*\*' 0.01 '\*' 0.05 '.' 0.1 ' ' 1

Tables of means

Grand mean

0.7537749

receptor

receptor

	1	2	3	4	5	6	7	8	9	10
	-0.565	0.988	1.457	6.794	-0.550	-0.142	0.255	-1.225	0.069	0.456
					*	*				

Standard errors for differences of means

receptor

2.252

replic. 4

```
> qt(0.975,6)*2.252
```

```
[1] 5.510445
```

# References

- Adamantidis, A. R.; Zhang, F.; Aravanis, A. M.; Deisseroth, K.; De lecea, L. Neural substrates of awakening probed with optogenetic control of hypocretin neurons. *Nature*. 2007;450(7168):420-4.
- Armbruster, B. N.; Li, X. Pausch, M. H.; Herlitze, S. & Roth, B. L. (2007) Evolving the Lock to Fit the Key to Create a Family of G Protein-Coupled Receptors Potently Activated by an Inert Ligand. *Proceedings of the National Academy of Sciences of the United States of America*. 104 (12)
- Abdelfattah, A. S., Farhi, S. L., Zhao, Y., Brinks, D., Zou, P., Ruangkittisakul, A., Platasa, J., Pieribone, V. A., Ballanyi, K., Cohen, A. E. & Campbell, R. E. (2016) A Bright and Fast Red Fluorescent Protein Voltage Indicator That Reports Neuronal Activity in Organotypic Brain Slices. *The Journal of Neuroscience: The Official Journal of the Society for Neuroscience*. 36 (8), 2458-2472.
- Accardi, M. V., Pugsley, M. K., Forster, R., Troncy, E., Huang, H. & Authier, S. (2016) The emerging role of in vitro electrophysiological methods in CNS safety pharmacology. *Journal of Pharmacological and Toxicological Methods*. 81 47-59.
- Anacleit, C., Ferrari, L., Arrigoni, E., Bass, C. E., Saper, C. B., Lu, J. & Fuller, P. M. (2014) GABAergic parafacial zone is a medullary slow-wave-sleep promoting center. Available from: <http://nrs.harvard.edu/urn-3:HUL.InstRepos:14351306>.
- Andres-Enguix, I., Caley, A., Yustos, R., Schumacher, M. A., Apanu, P. D., Dickinson, R., Maze, M. & Franks, N. P. 2007. Determinants of the anesthetic sensitivity of two-pore domain acid-sensitive potassium channels: molecular cloning of an anesthetic-activated potassium channel from *Lymnaea st agnalis*. *The Journal of biological chemistry*, 282, 20977-20990.
- Angov, E., Legler, P. M. & Mease, R. M. (2011) Adjustment of Codon Usage Frequencies by Codon Harmonization Improves Protein Expression and Folding. In: Evans, J., Thomas C. & Xu, M. (eds.). *Heterologous Gene Expression in E.coli: Methods and Protocols*. [e-book] Totowa, NJ, Humana Press. pp. 1-13.
- Antony, J. (2014) Design of Experiments for Engineers and Scientists. *Burlington: Elsevier Science*.
- Arnold, F. H. (2018) Directed Evolution: Bringing New Chemistry to Life. *Angewandte Chemie International Edition*. 57 (16), 4143-4148.
- Bagriantsev, S. N. & Minor, J., Daniel L. (2013) Using yeast to study potassium channel function and interactions with small molecules. *Methods in Molecular Biology* (Clifton, N.J.). 995 31.
- Baird, G. S.; Zacharias, D. A. & Tsien, R. Y.(1999) Circular Permutation and Receptor Insertion within Green Fluorescent Proteins. *Proceedings of the National Academy of Sciences of the United States of America*. 96 (20), 11241-11246.
- Bamann, C., Gueta, R., Kleinlogel, S., Nagel, G. & Bamberg, E. (2010) Structural Guidance of the Photocycle of Channelrhodopsin-2 by an Interhelical Hydrogen Bond. *Biochemistry*. 49 (2), 267-278.
- Barnett, L.; Platasa, J.; Popovic, M.; Pieribone, V. A. & Hughes, T. (2012) A Fluorescent, Genetically-Encoded Voltage Probe Capable of Resolving Action Potentials. *PLoS One*. 7 (9), e43454.
- Barnes, N. M., Hales, T. G., Lummis, S. C. & Peters, J. A. 2009. The 5-HT<sub>3</sub> receptor-the relationship between structure and function. *Neuropharmacology*, 56, 273-84.
- Berndt, A., Yizhar, O., Deisseroth, K., Gunaydin, L. A. & Hegemann, P. (2009) Bi-stable neural state switches. *Nature Neuroscience*. 12 (2), 229-234.
- Berndt, A.; Schoenenberger, P.; Mattis, J.; Tye, K. M.; Deisseroth, K.; Hegemann, P.; Oertner, T. G. & Nicoll, R. A. (2011) High-efficiency channelrhodopsins for fast neuronal stimulation at low light levels. *Proceedings of the National Academy of Sciences of the United States of America*. 108 (18), 7595-7600.
- Berndt, A.; Lee, S. Y.; Ramakrishnan, C. & Deisseroth, K. (2014) Structure-Guided Transformation of Channelrhodopsin into a Light-Activated Chloride Channel. *Science*. 344 (6182), 420-424.

- Berndt, A.; Lee, S. Y.; Wietek, J.; Ramakrishnan, C.; Steinberg, E. E.; Rashid, A. J.; Kim, H.; Park, S.; Santoro, A.; Frankland, P. W.; Iyer, S. M.; Pak, S.; Ährlund-Richter, S.; Delp, S. L.; Malenka, R. C.; Josselyn, S. A.; Carlén, M.; Hegemann, P. & Deisseroth, K. (2016) Structural foundations of optogenetics. *Proceedings of the National Academy of Sciences of the United States of America*. 113 (4), 822-829.
- Bernstein, J. D., Okamoto, Y., Kim, M. & Shikano, S. (2013) Potential use of potassium efflux-deficient yeast for studying trafficking signals and potassium channel functions. *FEBS Open Biology* 3 (1), 196-203.
- Bichet, D.; Lin, Y. F.; Ibarra, C. A.; Huang, C. S.; Yi, B. A.; Jan, Y. N. & Jan., L. Y. (2004) Evolving Potassium Channels by Means of Yeast Selection Reveals Structural Elements Important for Selectivity. *Proceedings of the National Academy of Sciences of the United States of America*. 101 (13), 4441-4446.
- Broomhead, N. & Soliman, M. (2017) Can We Rely on Computational Predictions To Correctly Identify Ligand Binding Sites on Novel Protein Drug Targets? Assessment of Binding Site Prediction Methods and a Protocol for Validation of Predicted Binding Sites. *Cell Biochemistry and Biophysics*. 75 (1), 15-23.
- Buchan, J. R. & Stansfield, I. (2007) Halting a cellular production line: responses to ribosomal pausing during translation. *Biology of the Cell*. 99 (9), 475-487.
- Chang, S. E., Todd, T. P., Bucci, D. J., Smith, K. S. & Costa, R. (2015) Chemogenetic manipulation of ventral pallidal neurons impairs acquisition of sign-tracking in rats. *European Journal of Neuroscience*. 42 (12), 3105-3116.
- Chen, K. & Arnold, F. H. (1993) Tuning the Activity of an Enzyme for Unusual Environments: Sequential Random Mutagenesis of Subtilisin E for Catalysis in Dimethylformamide. *Proceedings of the National Academy of Sciences of the United States of America*. 90 (12), 5618-5622.
- Chen, J., MacKinnon, R., Jiang, Y., Lee, A., Cadene, M., Chait, B. T. & Ruta, V. (2003) X-ray structure of a voltage-dependent K<sup>+</sup> channel. *Nature*. 423 (6935), 33-41.
- Chen, K., Mizianty, M., Gao, J. & Kurgan, L. (2011) A Critical Comparative Assessment of Predictions of Protein-Binding Sites for Biologically Relevant Organic Compounds. *Structure*. 19 (5), 613-621.
- Chen, T., Wardill, T. J., Sun, Y., Pulver, S. R., Renninger, S. L., Baohan, A., Schreiter, E. R., Kerr, R. A., Orger, M. B., Jayaraman, V., Looger, L. L., Svoboda, K. & Kim, D. S. (2013) Ultra-sensitive fluorescent proteins for imaging neuronal activity. *Nature*. 499 (7458), 295-300.
- Cobb, R. E., Chao, R. & Zhao, H. (2013) Directed evolution: Past, present, and future. *American Institute of Chemical Engineers Journal*. 59 (5), 1432-1440.
- Conway, K. E. & Cotten, J. F. (2012) Covalent Modification of a Volatile Anesthetic Regulatory Site Activates TASK-3 (KCNK9) Tandem-Pore Potassium Channels. *Molecular Pharmacology*. 81 (3), 393-400.
- Curtis, D. R.; Duggan, A. W.; Felix, D. & Johnston, G. A. R. (1970) GABA, Bicuculline and Central Inhibition. *Nature*. 226 (5252), 1222-1224.
- Colquhoun, D.; Dreyer, F.; Sheridan, R. E. (1979) The actions of tubocurarine at the frog neuromuscular junction. *Journal of Physiology*. 293, 247-84.
- Dale, H. H. & Wellcome Physiological Research Laboratories. (1914) The action of certain esters and ethers of choline and their relation to muscarine. Available from: <http://hdl.handle.net/2027/iau.31858047932276> .
- Dingledine, R., Dodd, J. & Kelly, J. S. (1980) The in vitro brain slice as a useful neurophysiological preparation for intracellular recording. *Netherlands, Elsevier B.V.* Available from: <https://www.sciencedirect.com/science/article/pii/0165027080900023>.
- Doyle, D. A., Cabral, J. M., Pfuetzner, R. A., Kuo, A., Gulbis, J. M., Cohen, S. L., Chait, B. T. & MacKinnon, R. (1998) The Structure of the Potassium Channel: Molecular Basis of K<sup>+</sup> Conduction and Selectivity. *Science*. 280 (5360), 69-77.

- Eban-rothschild, A.; Rothschild, G.; Giardino, W. J.; Jones, J. R. & De Lecea, L. (2016) VTA dopaminergic neurons regulate ethologically relevant sleep-wake behaviors. *Nature Neuroscience*. 19 (10)
- Ells, R., Kock, J. L. F., Van Wyk, Pieter W. J, Botes, P. J. & Pohl, C. H. (2009) Arachidonic acid increases antifungal susceptibility of *Candida albicans* and *Candida dubliniensis*. *Journal of Antimicrobial Chemotherapy*. 63 (1), 124-128.
- Ells, R., Kock, J. L., Albertyn, J. & Pohl, C. H. (2012) Arachidonic acid metabolites in pathogenic yeasts. *Lipids in Health and Disease*. 11 (1), 100.
- Engqvist, M. K. M., Mclsaac, R. S., Dollinger, P., Flytzanis, N. C., Abrams, M., Schor, S. & Arnold, F. H. (2015) Directed Evolution of *Gloeobacter violaceus* Rhodopsin Spectral Properties. *Journal of Molecular Biology*. 427 (1), 205-220.
- Fan, J., Lindemann, P., Feuilloley, M. G. & Papadopoulos, V. (2012) Structural and functional evolution of the translocator protein (18 kDa). *Current Molecular Medicine*. 12 (4), 369-386.
- Fenno, L., Yizhar, O. & Deisseroth, K. (2011) The Development and Application of Optogenetics. *Annual Review of Neuroscience*. 34 (1), 389-412.
- Frangaj, A. & Fan, Q. R. (2018). Structural biology of GABAB receptor. *Neuropharmacology*, 136(Pt A), pp.68-79.
- Gerngross, T. U. & Wildt, S. (2005) The humanization of N -glycosylation pathways in yeast. *Nature Reviews Microbiology*. 3 (2), 119-128.
- Flytzanis, N. C.; Bedbrook, C. N.; Chiu, H.; Engqvist, M. K. M.; Xiao, C.; Chan, K. Y.; Sternberg, P. W.; Arnold, F. H. & Gradinaru, V. (2014) Archaerhodopsin variants with enhanced voltage-sensitive fluorescence in mammalian and *Caenorhabditis elegans* neurons. *Nature Communications*. 5 (1), 4894.
- Ginsburg, H. (2016) <http://mpmp.huji.ac.il/maps/14-3-3prot.html> [Accessed 19th October 2016].
- Govorunova, E. G., Sineshchekov, O. A., Janz, R., Liu, X. & Spudich, J. L. (2015) *Neuroscience*. Natural light-gated anion channels: A family of microbial rhodopsins for advanced optogenetics. *Science* (New York, N.Y.). 349 (6248), 647.
- Govorunova, E. G., Sineshchekov, O. A. & Spudich, J. L. (2016) *Proteomonas sulcata* ACR1: A Fast Anion Channelrhodopsin. *Photochemistry and Photobiology*. 92 (2), 257-263.
- Govorunova, E. G., Sineshchekov, O. A., Rodarte, E. M., Janz, R., Morelle, O., Melkonian, M., Wong, G. K. & Spudich, J. L. (2017) The Expanding Family of Natural Anion Channelrhodopsins Reveals Large Variations in Kinetics, Conductance and Spectral Sensitivity. *Scientific Reports*. 7 (1), 43358.
- Govorunova, E. G., Sineshchekov, O. A., Hemmati, R., Janz, R., Morelle, O., Melkonian, M., Wong, G. K. & Spudich, J. L. (2018) Extending the Time Domain of Neuronal Silencing with Cryptophyte Anion Channelrhodopsins. *eNeuro*. 5 (3), 18.2018.
- Gray, A. T., Winegar, B. D., Leonoudakis, D. J., Forsayeth, J. R. & Yos, S. C. (1988) TOK1 is a volatile anesthetic stimulated K<sup>+</sup> channel. *Anesthesiology*. 88 (4)
- Grózer, Z., Tóth, A., Tóth, R., Kecskeméti, A., Vágvölgyi, C., Nosanchuk, J. D., Szekeres, A. & Gácsér, A. (2015) *Candida parapsilosis* produces prostaglandins from exogenous arachidonic acid and OLE2 is not required for their synthesis. *Virulence*. 6 (1), 85-92.
- Gruss, M., Bushell, T. J., Bright, D. P., Lieb, W. R., Mathie, A. & Franks, N. P. 2004. Two-pore-domain K<sup>+</sup> channels are a novel target for the anesthetic gases xenon, nitrous oxide, and cyclopropane. *Molecular pharmacology*, 65, 443-452.
- Guo, Y., Kalathur, R. C., Liu, Q., Kloss, B., Bruni, R., Ginter, C., Kloppmann, E., Rost, B. & Hendrickson, W. A. (2015) Protein structure. Structure and activity of tryptophan-rich TSPO proteins. *Science* (New York, N.Y.). 347 (6221), 551.
- Haass, F. A.; Jonikas, M.; Walter, P.; Weissman, J. S.; Jan, Y. N.; Jan, L. Y. & Schuldiner, M. (2007) Identification of Yeast Proteins Necessary for Cell-Surface Function of a Potassium Channel. *Proceedings of the National Academy of Sciences of the United States of America*. 104 (46), 18079-18084.

- Hochbaum, D. R., Zhao, Y., Farhi, S. L., Klapoetke, N., Werley, C. A., Kapoor, V., Zou, P., Kralj, J. M., Maclaurin, D., Smedemark-Margulies, N., Saulnier, J. L., Boulting, G. L., Straub, C., Cho, Y. K., Melkonian, M., Wong, G. K., Harrison, D. J., Murthy, V. N., Sabatini, B. L., Boyden, E. S., Campbell, R. E. & Cohen, A. E. (2014) All-optical electrophysiology in mammalian neurons using engineered microbial rhodopsins. *Nature Methods*. 11 (8), 825-833.
- Hodgkin, A. L.; Huxley, A. F. (1945) Resting and action potentials in single nerve fibres. *Journal of Physiology*. 104, 176-195
- Hodgkin, A. L.; Huxley, A. F. (1952) A quantitative description of membrane current, its application to conduction, excitation in nerve. *Journal of Physiology* 117, 500-544.
- Hollmann, M. & Heinemann, S. Cloned Glutamate Receptors. Molecular Neurobiology Laboratory.
- Honoré, T., Lauridsen, J. & Krosggaard-Larsen, P. (1982) The Binding of [3H]AMPA, a Structural Analogue of Glutamic Acid, to Rat Brain Membranes. *Journal of Neurochemistry*. 38 (1), 173-178.
- Honoré, E. (2007) The neuronal background K<sub>2</sub>P channels: focus on TREK1. *Nature Reviews Neuroscience*. 8 (4), 251-261
- Huang, Y. & Thathiah, A. (2015) Regulation of neuronal communication by G protein-coupled receptors. *FEBS Letters*. 589 (14), 1607-1619
- Iatmanen-Harbi, S., Senicourt, L., Papadopoulos, V., Lequin, O. & Lacapere, J. (2019) Characterization of the High-Affinity Drug Ligand Binding Site of Mouse Recombinant TSPO. *International Journal of Molecular Sciences*. 20 (6), 1444.
- Ikemura, T. (1982) Correlation between the abundance of yeast transfer RNAs and the occurrence of the respective codons in protein genes. *Journal of Molecular Biology*. 158 (4), 573-597.
- Jaremko, L.; Jaremko, M.; Giller, K.; Becker, S. & Zweckstetter, M. (2014) Structure of the Mitochondrial Translocator Protein in Complex with a Diagnostic Ligand. *Science*. 343 (6177), 1363-1366.
- Jendryka, M., Palchadhuri, M., Ursu, D., van der Veen, B., Liss, B., Kätzel, D., Nissen, W. & Pekcec, A. (2019) Pharmacokinetic and pharmacodynamic actions of clozapine-N-oxide, clozapine, and compound 21 in DREADD-based chemogenetics in mice. *Scientific Reports*. 9 (1), 1-14.
- Jiang, Y., Lee, A., Cadene, M., Chen, J., Chait, B. T. & MacKinnon, R. (2002) Crystal structure and mechanism of a calcium-gated potassium channel. *Nature*. 417 (6888), 515-522.
- Jin, L., Han, Z., Platasa, J., Woollorton, J. A., Cohen, L. & Pieribone, V. (2012) Single Action Potentials and Subthreshold Electrical Events Imaged in Neurons with a Fluorescent Protein Voltage Probe. *Neuron*. 75 (5), 779-785.
- Johansson, I. & Blatt, M. R. (2005) Interactive domains between pore loops of the yeast K<sup>+</sup> channel TOK1 associate with extracellular K<sup>+</sup> sensitivity. *Portland Press Ltd*.
- The Journal of Neuroscience (2018). Recommendations for the Design and Analysis of *In Vivo* Electrophysiology Studies. *Journal of Neuroscience*. 38(26), p. 5837.
- Karschin, C., Karschin, A., Wischmeyer, E., Preisig-Müller, R., Rajan, S., Derst, C., Grzeschik, K. & Daut, J. (2001) Expression Pattern in Brain of TASK-1, TASK-3, and a Tandem Pore Domain K<sup>+</sup> Channel Subunit, TASK-5, Associated with the Central Auditory Nervous System. *Molecular and Cellular Neuroscience*. 18 (6), 632-648.
- Keil, R. L.; Wolfe, D.; Reiner, T.; Peterson, C. J. & Riley, J. L. (1996) Molecular genetic analysis of volatile-anesthetic action. *Molecular and Cellular Biology*. 16 (7), 3446-3453.
- Kilisch, M., Lytovchenko, O., Schwappach, B., Renigunta, V. & Daut, J. (2015) The role of protein-protein interactions in the intracellular traffic of the potassium channels TASK-1 and TASK-3. *Pflügers Archiv - European Journal of Physiology*. 467 (5), 1105-1120.
- Klapoetke, N. C., Murata, Y., Kim, S. S., Pulver, S. R., Birdsey-Benson, A., Cho, Y. K., Morimoto, T. K., Chuong, A. S., Carpenter, E. J., Tian, Z., Wang, J., Xie, Y., Yan, Z., Zhang, Y., Chow, B. Y., Surek, B., Melkonian, M., Jayaraman, V., Constantine-Paton, M., Wong, G. K. & Boyden, E. S. (2014) Independent optical excitation of distinct neural populations. *Nature Methods*. 11 (9), 972.
- Kleinlogel, S.; Feldbauer, K.; Dempski, R. D.; Fotis, H.; Wood, P. G.; Bamann, C. & Bamberg, E. (2011) Ultra light-sensitive and fast neuronal activation with the Ca<sup>2+</sup>-permeable channelrhodopsin CatCh. *Nature Neuroscience*. 14 (4), 513-518.

- Kollwe, A., Lau, A. Y., Sullivan, A., Roux, B. & Goldstein, S. A. N. (2009) A structural model for K2P potassium channels based on 23 pairs of interacting sites and continuum electrostatics. *The Journal of General Physiology*. 134 (1), 53-68.
- Konc, J. & Janežič, D. (2014) Binding site comparison for function prediction and pharmaceutical discovery. *Current Opinion in Structural Biology*. 25 34-39.
- Kouprina, N. & Larionov, V. (2016) Transformation-associated recombination (TAR) cloning for genomics studies and synthetic biology. *Chromosoma*. 125 (4), 621-632.
- Kuang, Q., Purhonen, P. & Hebert, H. (2015) Structure of potassium channels. *Cellular and Molecular Life Sciences*. 72 (19), 3677-3693.
- Laurent, J. M., Young, J. H., Kachroo, A. H. & Marcotte, E. M. (2016) Efforts to make and apply humanized yeast. *Briefings in Functional Genomics*. 15 (2), 155-163.
- Lee, M. E., Deloache, W. C., Cervantes, B. & Dueber, J. E. 2015. A Highly Characterized Yeast Toolkit for Modular, Multipart Assembly. *American Chemistry Society Synthetic Biology*, 4, 975-86.
- Lewis, M. J. & Pelham, H. R. B. (2002) A New Yeast Endosomal SNARE Related to Mammalian Syntaxin 8. *Traffic*. 3 (12), 922-929.
- Li, F.; Liu, J.; Zheng, Y.; Garavito, R. M. & Ferguson-Miller, S. (2015) Crystal structures of translocator protein (TSPO) and mutant mimic of a human polymorphism. *Science*. 347 (6221), 555-558.
- Lin, J. Y. (2010) A user's guide to channelrhodopsin variants: features, limitations and future developments. *Experimental Physiology*. 96 (1), 19-25.
- Liu, Y. P.; Russell, S. P.; Ayala-Breton, C.; Russell, S. J. & Peng, K. W. (2014) Ablation of Nectin4 Binding Compromises CD46 Usage by a Hybrid Vesicular Stomatitis Virus/Measles Virus. *Journal of Virology*. 88 (4), 2195-2204.
- Long, S. B., Campbell, E. B. & MacKinnon, R. (2005) Voltage Sensor of Kv1.2: Structural Basis of Electromechanical Coupling. *Science*. 309 (5736), 903-908.
- Loukin, S. H. & Saimi, Y. (1999) K<sup>+</sup>-Dependent Composite Gating of the Yeast K<sup>+</sup> Channel, Tok1. *Biophysical Journal*. 77 (6), 3060-3070.
- Magnus, C. J., Lee, P. H., Atasoy, D., Su, H. H., Looger, L. L. & Sternson, S. M. (2011) Chemical and genetic engineering of selective ligand-ion channel interactions. Available from: [https://www.openaire.eu/search/publication?articleId=od\\_\\_\\_\\_\\_267::3602194a6d076a269847cb1cf6764dcb](https://www.openaire.eu/search/publication?articleId=od_____267::3602194a6d076a269847cb1cf6764dcb).
- Manvich, D. F., Webster, K. A., Foster, S. L., Farrell, M. S., Ritchie, J. C., Porter, J. H. & Weinschenker, D. (2018) The DREADD agonist clozapine N-oxide (CNO) is reverse-metabolized to clozapine and produces clozapine-like interoceptive stimulus effects in rats and mice. *Scientific Reports*. 8 (1), 3840-10.
- Manville, R. W., Povreslo, F. S., Corran, A. & Lewis, A. (2016) Pharmacology and Regulation of Fungal K2P Channels. *Biophysical Journal*. 110 (3), 449a.
- Mardinly, A. R.; Oldenburg, I. O.; Pégard, N. C.; Sridharan, S.; Lyall, E. H.; Chesnov, K.; Brohawn, S. G.; Waller, L. & Adesnik, H. (2018) Precise multimodal optical control of neural ensemble activity. *Nature Neuroscience*. 21 (6), 881-893.
- Mattis, J.; Tye, K. M.; Ferenczi, E. A.; Ramakrishnan, C.; O'shea, D. J.; Prakash, R.; Gunaydin, L. A.; Hyun, M.; Fenno, L. E.; Gradinaru, V.; Yizhar, O. & Deisseroth, K. (2012) Principles for applying optogenetic tools derived from direct comparative analysis of microbial opsins. *Nature Methods*. 9 (2), 159-172.
- Mauss, A. S., Busch, C. & Borst, A. (2017) Optogenetic Neuronal Silencing in Drosophila during Visual Processing. *Scientific Reports*. 7 (1), 13823-12.
- Miyawaki, A.; Llopis, J.; Heim, R. & McCaffery, J. M. (1997) Fluorescent indicators for Ca<sup>2+</sup>-based on green fluorescent proteins and calmodulin. *Nature*. 388 (6645), 882-887.
- Mohammad, F.; Stewart, J. C.; Ott, S.; Chlebikova, K.; Chua, J. Y.; Koh, T. W.; Ho, J. & Claridge-chang, A. (2017) Optogenetic inhibition of behavior with anion channelrhodopsins. *Nature Methods*. 14 (3), 271-274.
- Mochida, S. (1990) Acetylcholine elicits metabolically mediated M2-muscarinic hyperpolarization in isolated rabbit sympathetic neurons. *Japanese Journal of Physiology*.

- Nagai, T., Sawano, A., Park, E. S. & Miyawaki, A. (2001) Circularly permuted green fluorescent proteins engineered to sense [Ca<sup>2+</sup>]. *Proceedings of the National Academy of Sciences of the United States*. 98 (6), 3197.
- Nagel, G.; Szellas, T.; Huhn, W.; Kateriya, S.; Adeishvili, N.; Berthold, P.; Ollig, D.; Hegemann, P. & Bamberg, E. (2003) Channelrhodopsin-2, a Directly Light-Gated Cation-Selective Membrane Channel. *Proceedings of the National Academy of Sciences of the United States of America*. 100 (24), 13940-13945.
- Nestler, E. J. & Carlezon, W. A. (2006) The Mesolimbic Dopamine Reward Circuit in Depression. *Biological Psychiatry*. 59 (12), 1151-1159.
- NewEngland Biolabs Inc. (2019) *NEBioCalculator*. [Accessed 16th June 2019].
- O'Donnell, A. (2012) *Anaesthesia: A Very Short Introduction*. Oxford University Press.
- Patel, A. J., Honoré, E., Lesage, F., Romey, G., Lazdunski, M. & Fink, M. (1999) Inhalational anesthetics activate two-pore-domain background K<sup>+</sup> channels. *Nature Neuroscience*. 2 (5), 422-426.
- Piatkevich, K. D.; Jung, E. E.; Straub, C.; Linghu, C.; Park, D.; Suk, H. J.; Hochbaum, D. R.; Goodwin, D.; Pnevmatikakis, E.; Pak, N.; Kawashima, T.; Yang, C. Y.; Rhoades, J. L.; Shemesh, O.; Asano S.; Yoon, Y. G.; Freifeld, L.; Saulnier, J. L.; Riegler, C.; Engert, F.; Hughes, T.; Drobizhev, M.; Szabo, B.; Ahrens, M. B.; Flavell, S. W.; Sabatini, B. L. & Boyden, E. S. (2018) A robotic multidimensional directed evolution approach applied to fluorescent voltage reporters. *Nature Chemical Biology*. 14 (4), 352-360.
- Platasa, J.; Vasan, G.; Yang, A.; & Pieribone, V. A. (2017) Directed Evolution of Key Residues in Fluorescent Protein Inverses the Polarity of Voltage Sensitivity in the Genetically Encoded Indicator ArcLight. *American Chemical Society Chemical Neuroscience*. 8 (3), 513-523.
- Pologruto, T. A., Yasuda, R. & Svoboda, K. (2004) Monitoring Neural Activity and [Ca<sup>2+</sup>] with Genetically Encoded Ca<sup>2+</sup> Indicators. *Journal of Neuroscience*. 24 (43), 9572-9579.
- Rajan, S., Preisig-Müller, R., Wischmeyer, E., Nehring, R., Hanley, P. J., Renigunta, V., Musset, B., Schlichthörl, G., Derst, C., Karschin, A. & Daut, J. 2002. Interaction with 14-3-3 proteins promotes functional expression of the potassium channels TASK-1 and TASK-3. *Journal of Physiology*, 545, 13-26.
- Reiner, A. & Levitz, J. (2018) Glutamatergic Signaling in the Central Nervous System: Ionotropic and Metabotropic Receptors in Concert. *Neuron*. 98 (6), 1080-1098
- Renigunta, V., Yuan, H., Zuzarte, M., Rinné, S., Koch, A., Wischmeyer, E., Schlichthörl, G., Gao, Y., Karschin, A., Jacob, R., Schwappach, B., Daut, J. & Preisig-Müller, R. (2006) The Retention Factor p11 Confers an Endoplasmic Reticulum-Localization Signal to the Potassium Channel TASK-1. *Traffic*. 7 (2), 168-181.
- Renigunta, V., Fischer, T., Zuzarte, M., Kling, S., Zou, X., Siebert, K., Limberg, M. M., Rinné, S., Decher, N., Schlichthörl, G. & Daut, J. (2014) Cooperative endocytosis of the endosomal SNARE protein syntaxin-8 and the potassium channel TASK-1. *Molecular Biology of the Cell*. 25 (12), 1877-1891.
- Rhoads, A. & Au, K. F. (2015) PacBio Sequencing and Its Applications. 13 (5), 278-289. Available from: <http://lib.cqvip.com/qk/86775X/201505/667177821.html>.
- Roth, B. & Driscoll J., (2014) *NIMH Psychoactive Drug Screening Program Ki Database*.
- Roth, B. L. (2016) DREADDs for Neuroscientists. *Neuron*. 89 (4), 683-694.
- Routledge, S. J., Mikaliunaite, L., Patel, A., Clare, M., Cartwright, S. P., Bawa, Z., Wilks, M. D. B., Low, F., Hardy, D., Rothnie, A. J. & Bill, R. M. (2016) The synthesis of recombinant membrane proteins in yeast for structural studies. *Methods*. 95 26-37.
- Saldaña, C.; Naranjo, D.; Coria, R.; Peana, A & Vaca., L. (2002) Splitting the Two Pore Domains from TOK1 Results in Two Cationic Channels with Novel Functional Properties. *Journal of Biological Chemistry*. 277 (7), 4797-4805.
- Schwarzer, S., Kolacna, L., Lichtenberg-Fraté, H., Sychrova, H. & Ludwig, J. (2008) RESEARCH ARTICLE: Functional expression of the voltage-gated neuronal mammalian potassium channel rat ether à go-go1 in yeast. *FEMS Yeast Research*. 8 (3), 405-413.

- Sineshchekov, O.A.; Jung, K. H.; & Spudich, J. L. (2002) Two Rhodopsins Mediate Phototaxis to Low- and High-Intensity Light in *Chlamydomonas reinhardtii*. *Proceedings of the National Academy of Sciences of the United States of America*. 99 (13), 8689-8694.
- Steinberg, E., Wafford, K., Brickley, S., Franks, N. & Wisden, W. (2015) The role of K2P channels in anaesthesia and sleep. *Pflügers Archiv - European Journal of Physiology*. 467 (5), 907-916. Available from: <https://www.ncbi.nlm.nih.gov/pubmed/25482669>. Available from: doi: 10.1007/s00424-014-1654-4.
- Suzuki, T., Yamasaki, K., Fujita, S., Oda, K., Iseki, M., Yoshida, K., Watanabe, M., Daiyasu, H., Toh, H., Asamizu, E., Tabata, S., Miura, K., Fukuzawa, H., Nakamura, S. & Takahashi, T. (2003) Archaeal-type rhodopsins in *Chlamydomonas*: model structure and intracellular localization. *Biochemical and Biophysical Research Communications*. 301 (3), 711-717
- Suzuki, K. & Ohsumi, Y. (2010) Current knowledge of the pre-autophagosomal structure (PAS). *FEBS Letters*. 584 (7), 1280-1286.
- Svoboda, K. & Block, S. (1994) Biological applications of optical forces. *Annual Review of Biophysics and Biomolecular Structure*. 23, 247-85.
- Talley, E. M. & Bayliss, D. A. (2002) Modulation of TASK-1 (Kcnk3) and TASK-3 (Kcnk9) potassium channels: volatile anesthetics and neurotransmitters share a molecular site of action. *The Journal of Biological Chemistry*. 277 (20), 17733-17742.
- Tang, W., Ruknudin, A., Yang, W. P., Shaw, S. Y., Knickerbocker, A. & Kurtz, S. (1995) Functional expression of a vertebrate inwardly rectifying K<sup>+</sup> channel in yeast. *Molecular Biology of the Cell*. 6 (9), 1231-1240.
- Thestrup, T., Litzlbauer, J., Bartholomäus, I., Mues, M., Russo, L., Dana, H., Kovalchuk, Y., Liang, Y., Kalamakis, G., Laukat, Y., Becker, S., Witte, G., Geiger, A., Allen, T., Rome, L. C., Chen, T., Kim, D. S., Garaschuk, O., Griesinger, C. & Griesbeck, O. (2014) *Optimized Ratiometric Calcium Sensors For Functional In Vivo Imaging of Neurons and T-Lymphocytes*. Biological Magnetic Resonance Bank.
- Tinel, N., Lazdunski, M., Terrenoire, C., Romey, G., Borsotto, M. & Girard, C. (2002) p11, an annexin II subunit, an auxiliary protein associated with the background K<sup>+</sup> channel, TASK-1. *The EMBO Journal*. 21 (17), 4439-4448.
- Tsai, H., Zhang, F., Adamantidis, A., Stuber, G. D., Bonci, A., de Lecea, L. & Deisseroth, K. (2009) Phasic Firing in Dopaminergic Neurons Is Sufficient for Behavioral Conditioning. *Science*. 324 (5930), 1080-1084.
- U.S. National Library of Medicine. *Standard protein BLAST*. [Accessed June 2018].
- van Heusden, G. Paul H & Yde Steensma, H. (2006) Yeast 14-3-3 proteins. *Yeast*. 23 (3), 159-171.
- Vardy, E.; Mosier, P. D.; Frankowski, K. J.; Wu, H.; Katritch, V.; Westkaemper, R. B.; Aubé, J.; Stevens, R. C. & Roth, B. L. (2013) Chemotype-selective Modes of Action of  $\kappa$ -Opioid Receptor Agonists. *The Journal of Biological Chemistry*. 288 (48), 34470-34483.
- Vardy, E., Robinson, J., Li, C., Olsen, R. J., DiBerto, J., Giguere, P., Sassano, F., Huang, X., Zhu, H., Urban, D., White, K., Rittiner, J., Crowley, N., Pleil, K., Mazzone, C., Mosier, P., Song, J., Kash, T., Malanga, C. J., Krashes, M. & Roth, B. (2015) A New DREADD Facilitates the Multiplexed Chemogenetic Interrogation of Behavior. *Neuron*. 86 (4), 936-946.
- Veale, E. L., Kennard, L. E., Sutton, G. L., MacKenzie, G., Sandu, C. & Mathie, A. (2007) G<sub>q</sub>-Mediated Regulation of TASK3 Two-Pore Domain Potassium Channels: The Role of Protein Kinase C. *Molecular Pharmacology*. 71 (6), 1666-1675.
- Venner, A.; Todd, W. D.; Fraigne, J.; Bowrey, H.; Eban-Rothschild, A.; Kaur, S., Anaclet, C.. Newly identified sleep-wake and circadian circuits as potential therapeutic targets. *Sleep*. 2019;42(5)
- Wietek, J.; Wiegert, J. S.; Adeishvili, N.; Schneider, F.; Watanabe, H.; Tsunoda, S. P.; Vogt, A.; Elstner, M.; Oertner, T. G.; Hegemann, P. Conversion of channelrhodopsin into a light-gated chloride channel. *Science*. 2014;344(6182):409-12.
- World Health Organisation. (2015) *WHO Model List of Essential Medicines*.

- Wu, H., Wacker, D., Mileni, M., Katritch, V., Han, G. W., Vardy, E., Liu, W., Thompson, A. A., Huang, X., Carroll, F. I., Mascarella, S. W., Westkaemper, R. B., Mosier, P. D., Roth, B. L., Cherezov, V. & Stevens, R. C. (2012) Structure of the human  $\kappa$ -opioid receptor in complex with JDTic. *Nature*. 485 (7398), 327-332.
- Yang, Y.; Liu, N.; He, Y.; Liu, L.; Ge, L.; Zou, L.; Song, S. Xiong, W. & Liu, X. (2018) Improved calcium sensor GCaMP-X overcomes the calcium channel perturbations induced by the calmodulin in GCaMP. *Nature Communications*. 9 (1), 1-18.
- synaptic GABAA receptor. *Nature*. 559 (7712), 67-72.
- Yizhar, O.; Fenno, L. E.; Prigge, M.; Schneider, F.; Davidson, T. J.; O'Shea, D. J.; Sohal, V. S.; Goshen, I.; Finkelstein, J.; Paz, J. T.; Stehfest, K.; Fudim, R.; Ramakrishnan, C.; Huguenard, J. R.; Hegemann, P. & Deisseroth, K. (2011) Neocortical excitation/inhibition balance in information processing and social dysfunction. *Nature*. 477 (7363), 171-178.
- Zhang, F., Prigge, M., Beyrière, F., Tsunoda, S. P., Mattis, J., Yizhar, O., et al. (2008). *Red. Nature Neuroscience* 11(64(2)), p. 10-12.
- Zhang, Z., Ferretti, V., Güntan, i, Moro, A., Steinberg, E. A., Ye, Z., Zecharia, A. Y., Yu, X., Vyssotski, A. L., Brickley, S. G., Yustos, R., Pillidge, Z. E., Harding, E. C., Wisden, W. & Franks, N. P. (2015) Neuronal ensembles sufficient for recovery sleep and the sedative actions of  $\alpha$ 2 adrenergic agonists. *Nature Neuroscience*. 18 (4), 553-561
- Zhu, S., Noviello, C. M., Teng, J., Walsh, R. M., Kim, J. J. & Hibbs, R. E. (2018) Structure of a human synaptic GABAA receptor. *Nature*. 559 (7712), 67-72
- Zhu, S., Noviello, C. M., Teng, J., Walsh, R. M., Kim, J. J. & Hibbs, R. E. (2018) Structure of a human synaptic GABAA receptor. *Nature*. 559 (7712), 67-72.